

# A SURVEY OF SOILS FORMED ON SERPENTINITIC LANDSCAPES IN CALIFORNIA

by

**DONALD GREG M'GAHAN**

B.S. (University of California, Davis) 1997

M.S. (University of California, Davis) 2001

A DISSERTATION

submitted in partial satisfaction of the requirements for the degree of

DOCTOR OF PHILOSOPHY

in

SOILS and BIOGEOCHEMISTRY

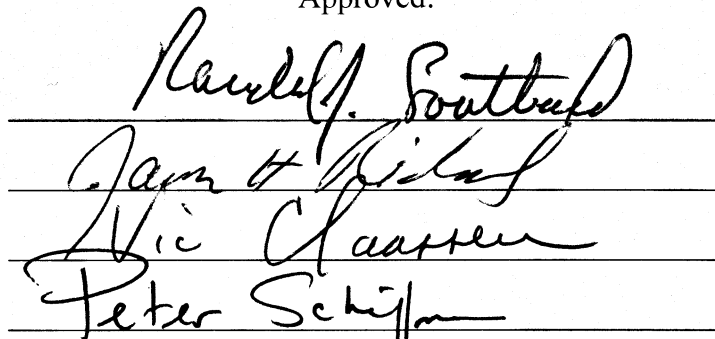
in the

GRADUATE DIVISION

of the

UNIVERSITY of CALIFORNIA, DAVIS

Approved:



Committee in charge

2007

# ACKNOWLEDGEMENTS

Maurice (Mac) McGahan and Nelva McGahan (mom and dad).

Support and encouragement were received in generous proportions from my wife Kathleen R. McGahan. Her enthusiasm in my work was inspiring and her belief in me enabling. She was also a great help during many field sampling expeditions.

I would like to acknowledge Dr. Randy J. Southard, Craig Rasmussen, Masha Murashkina, and Julie Baker for help and intellectual stimulation during sampling expeditions and hand digging soil pits. Labmates Rebecca Domingo-Neumann, Craig Rasmussen, Masha Murashkina, Julie Baker, and Chris B. Voit were patient and kind listeners as I rambled on about the latest data set. These labmates were positive and energizing workmates. Norm Winters helped guide me in the art and science of thin section mounting, but our conversations went far beyond the task and I enjoyed working while chewing the fat with Norm. Rebecca Domingo-Neumann was kind, helpful, and instructive in discussions of optical mineralogy.

I would like to especially thank committee members Dr. Vic P. Claassen and Dr. Randy J. Southard for financial support for the project and allowing me academic freedom. I would like to thank my committee members, Dr. Jim Richards and Dr. Peter Schiffman, for their thoughtful consideration of this work. I also would like to acknowledge the committee of researchers at McLaughlin (CRAM) for financial support.

Dr. Peter Schiffman and Dr. Sarah Roeske were very helpful and supportive while working with the microprobe and I am grateful for the support and for lively conversations.

# ABSTRACT

Serpentinite derived soils give rise to botanically distinct systems primarily as a result of inadequate Ca content of the parent material. I sampled 11 parent materials and soils across California at the soil survey modal location of the Henneke soil series (Clayey-skeletal, magnesian, thermic Lithic Argixerolls). I hypothesized that soils formed on serpentinitic landscapes have a range in extractable Ca, and total Ca and was correlated to vegetation Ca concentration. Total elemental analyses of the rocks underlying the soils showed CaO% varied from 0.01% to 23%, and CaO:MgO varied from <0.001 to 4. Rock at Napa and Tehama Counties, were xenolithic inclusions in the serpentinite landscape and contained no serpentine minerals (not serpentinites). The Napa County rocks contained almost no Ca-bearing minerals and probably would be identified as a serpentinite if relying upon elemental analysis and CaO:MgO alone.

Extractable soil Ca:Mg varied from 0.1 to 1.5, and total elemental Ca:Mg varied from <0.01 to 1.9. Soil extractable Ca was influenced by parent material mineralogy, where soils with a Ca:Mg of 0.2 or less were derived from serpentinite parent materials with only trace Ca-bearing minerals; soils with a Ca:Mg > 1 were derived from non-serpentinite parent materials, and soils with a Ca:Mg > 0.2 but < 1 were derived from serpentinite parent material that had minor amounts of accessory Ca-bearing minerals. In a greenhouse study, the grass *Vulpia microstachys* concentration of above ground biomass Ca correlated better with soil extractable Ca ( $R^2 = 0.89$ ;  $P < 0.01$ ) than with total elemental analysis Ca ( $R^2 = 0.64$ ;  $P < 0.01$ ). Extractable Ca was the best determinant of plant performance.

Zr, Ti, Y, or Nb were tested for use as an immobile element for mass balance strain calculation. Any would be acceptable for the Tehama County soil (non-serpentinic rodingite), but Zr was not immobile in the Colusa County (serpentinic) soil suggesting that the relative mobility of elements must be evaluated for each pedon on serpentinic landscapes in order to identify suitable conservative elements for strain analysis.

Three profiles were compared and had quite different mass flux (1 to 11 g cm<sup>-2</sup>) of the major soil elements (Si, Al, Fe, Mg and Ca) illustrating that soil formation on serpentinic landscapes can have quite different elemental fluxes. When the Ca content of the parent material is low the soil profile had mass transfer fraction gains. When the parent material Ca is higher (Tehama County) the Ca mass transfer fraction losses occurred.

# TABLE OF CONTENTS

## **Chapter 1: Site Descriptions**

1.1	Colusa County site profile description . . . . .	1
1.2	Glenn County site profile description . . . . .	3
1.3	Kings County site profile description . . . . .	4
1.4	Napa County site profile description. . . . .	6
1.5	San Benito County site profile description . . . . .	7
1.6	Shasta County site profile description. . . . .	8
1.7	Tehama County site profile description . . . . .	9
1.8	Mariposa County site profile description . . . . .	11
1.9	Mendocino County site profile description. . . . .	12
1.10	Shasta-Trinity National Forest site profile description . . . . .	14
1.11	Los Padres National Forest site profile description. . . . .	16

## **2: Xenoliths in Serpentinite Landscapes Contribute Ca as a Plant Nutrient**

2.1	Abstract . . . . .	18
2.2	Introduction . . . . .	19
2.3	Materials and Methods . . . . .	22
2.3.1	Field . . . . .	22
2.3.2	Laboratory . . . . .	22
2.4	Results and Discussion . . . . .	23
2.4.1	Non-serpentinites with bastites . . . . .	23
2.4.1.1	Tehama County. . . . .	23
2.4.1.2	Napa County. . . . .	26
2.4.2	Serpentinites with bastites . . . . .	27
2.4.2.1	Shasta County . . . . .	27
2.4.2.2	Glenn County . . . . .	27
2.4.3	Serpentinites without bastites. . . . .	28
2.4.3.1	Kings County . . . . .	28
2.4.3.2	San Benito County . . . . .	29
2.5	Implications for Ca supply and Plant Growth. . . . .	29
2.6	Reference. . . . .	31
2.7	Appendix A . . . . .	46

## **Chapter 3: Plant-available Calcium Varies Widely in Soils on Serpentinite Landscapes**

3.1	Abstract	47
3.2	Introduction	48
3.3	Materials and Methods	52
3.3.1	Field	52
3.3.2	Laboratory	53
3.4	Results and Discussion	54
3.4.1	Profile Morphologies	54
3.4.2	Parent Material Influences on Ca:Mg	56
3.4.3	Extractable Ca Pools	56
3.4.4	Plant Response to Varied Extractable Ca, Mg, or Ca:Mg	58
3.5	Summary/Conclusion	61
3.6	References	62
3.7	Appendix A	82

#### **Chapter 4: Determining Immobile Element Suitable for Mass Balance Calculations for Soils Formed on Serpentinic Landscapes**

4.1	Introduction	86
4.2	Materials and Methods	88
4.2.1	Field	88
4.2.2	Laboratory	89
4.2.2.1	Basic conservation equations	90
4.3	Results and Discussion	91
4.3.1	Colusa County	92
4.3.2	Tehama County	96
4.4	Conclusion	96
4.5	References	98
4.6	Figures	102
4.7	Appendix A	113
4.8	Appendix B	126
4.9	Appendix C	139
4.10	Appendix D	152

#### **Chapter 5: Flux of Elements by Mass Balance in Soils From Three Serpentinic Landscapes**

5.1	Introduction	166
5.2	Materials and Methods	168
5.2.1	Field	168
5.2.2	Laboratory	169
5.2.3	Mass Balance Construction	170
5.2.3.1	Basic conservation equations	170
5.2.3.2	Calculation of open-system mass transport	171

5.2.3.3	Determination of Strain	172
5.2.3.4	Calculation of gains and losses.	173
5.2.3.5	Contributions to chemical enrichment	174
5.3	Results and Discussion	175
5.3.1	Tehama County	176
5.3.2	Colusa County	180
5.3.3	Napa County	183
5.4	Summary	185
5.5	References	186
5.6	Figures	191
5.7	Appendix A	208

# LIST OF TABLES

## Chapter 1: Site Descriptions

### 2: Xenoliths in Serpentine Landscapes Contribute Ca as a Plant Nutrient

Table 2-1.	Content of selected elements in serpentinite parent material rocks beneath the 6 pedons. ....	34
Table 2-2.	Chemical composition of garnets. Reproduced after Hurlbut and Klein, 1977. ....	34
Table 2-3.	Chemical composition of pyroxenes and amphiboles. Reproduced after Hurlbut and Klein, 1977. ....	34
Table 2-4.	Appendix A. Content of elements in serpentinite parent material rocks beneath the 5 pedons not discussed. ....	46

### Chapter 3: Plant-available Calcium Varies Widely in Soils on Serpentine Landscapes

Table 3-1.	Selected morphological properties of soils sampled on serpentinitic landscapes. ....	66
Table 3-2.	Soil site classification determined from site pedon morphology. ....	69
Table 3-3.	Selected chemical properties and particle size distribution of soils from serpentinite derived landscapes. † ....	70
Table 3-4.	Soil density, coarse fraction volume, extractable Ca displaced with 1M NH <sub>4</sub> OAc at pH 7, and fine earth fraction (< 2mm) total Ca and Mg for each survey area. ....	72
Table 3-5.	Ca and Mg contents of soils and plants, <i>Vulpia microstachys</i> (Nutt.) Munro, grown in 500 cm <sup>3</sup> container filled with soil material from Henneke soil series map units. ....	74

### Chapter 4: Determining Immobile Element Suitable for Mass Balance Calculations for Soils Formed on Serpentinic Landscapes

### Chapter 5: Flux of Elements by Mass Balance in Soils From Three Serpentinic Landscapes

Table 5-1.	Colusa, Tehama, and Napa County mass flux, $m_{j,\text{flux}}$ , in g cm <sup>-2</sup> of the fine earth volume when strain is calculated with Y. ....	190
Table 5-2.	Colusa, Tehama, and Napa County minor and trace element mass flux, $m_{j,\text{flux}}$ , in g cm <sup>-2</sup> of the fine earth volume when strain is calculated with Y. ....	208



# LIST OF FIGURES

## Chapter 1: Site Descriptions

### 2: Xenoliths in Serpentinite Landscapes Contribute Ca as a Plant Nutrient

- Figure 2-1. Pedon sampling locations from 11 California soil survey areas within Henneke soil series (Clayey-skeletal, magnesian, thermic Lithic Argixerolls) map units. ....35
- Figure 2-2. X-ray diffractograms of serpentinite parent materials. **A.** Tehama County: hydroxy-interlayered-material, grossularite, diopside, and pumpellyite. **B.** Kings County: serpentine, andradite, and magnetite. **C.** Shasta County: serpentine, talc, and chlorite. **D.** Glenn County: serpentine and magnetite. **E.** Napa County: vermiculite and albite plagioclase. **F.** San Benito: serpentine.....36
- Figure 2-3. Energy dispersive x-ray spectra (EDX) of Tehama County parent material minerals A. Grossularite demonstrating some inclusion of Ti. B. Diopside. C. Pumpellyite D. Titanite. E. Ilmenite. F. Hydroxy-interlayered-material (HIM). ....37
- Figure 2-4. **A.** Photomicrograph of Tehama County parent material plane-polarized light, tightly packed small interlocking euhedral crystals of grossularite garnet (GN) appear as a large cinnamon-brown mass, the nearly opaque dark brown minerals are ilmenite (IL). **B.** Photomicrograph of Tehama County parent material with crossed polars. The garnets (GN) are isotropic dark purplish black and the ilmenite (IL) brown. **C.** Photomicrograph of Tehama County parent material; diopside, vertically aligned, with crossed polars. **D.** Photomicrograph of Tehama County parent material; diopside demonstrating inclined extinction; crossed polars. **E.** BSE micrograph of Tehama County parent material. Di = diopside; Tt = titanite; IL = ilmenite; GN = garnet (grossularite). **F.** BSE micrograph of Tehama County parent material. Lighter grey pumpellyite (PU) inter-grown into darker grey hydroxy-interlayered-material (HIM) upper left and center. Smaller masses of euhedral grossularite garnet crystals (GN) are lower center but are predominantly tightly packed and interlocked into larger masses (lower right). ....38
- Figure 2-5. **A.** Photomicrograph of Napa County parent material: crossed polars. clinopyroxene (cpx) surrounded by plagioclase feldspar (P) some expressing carlsbad twining and vermiculite (VR). **B.** Photomicrograph of Napa County parent material: crossed polars. Diopside (cpx) expressing extinction at inclined position surrounded by plagioclase feldspar (P) some expressing carlsbad twining and vermiculite (VR). **C.** BSE micrograph Napa County parent material. CPX = diopside; P = plagioclase feldspar VR = vermiculite. **D.** Energy

	dispersive x-ray spectra (EDX) Napa County parent material plagioclase. <b>E.</b> EDX Napa County parent material diopside. <b>F.</b> EDX Napa County parent material vermiculite. ....	39
Figure 2-6.	<b>A.</b> Photomicrograph of Shasta County parent material shown in plane-polarized light. Masses of radiating columnar crystals: CCA = tremolite, SY = serpentine. <b>B.</b> Photomicrograph of Shasta County parent material: crossed polars. Masses of radiating columnar crystals: CCA = tremolite, SY = serpentine. <b>C.</b> BSE micrograph Shasta County parent material. CCA = tremolite, SY = serpentine, white areas are iron oxides. <b>D.</b> EDX Shasta County parent material calcic clin amphibole.....	40
Figure 2-7.	<b>A.</b> Photomicrograph Glenn County parent material: plane polarized light. Enstatite (OPX) set in matrix of serpentine (SY). Field of view = 5 mm. <b>B.</b> Photomicrograph Glenn County parent material: crossed-polars. Enstatite (OPX) set in matrix of serpentine (SY). Field of view = 5 mm. <b>C.</b> Photomicrograph Glenn County parent material: crossed-polars. Parallel extinction of enstatite (OPX) in matrix of serpentine (SY). Field of view = 5 mm. <b>D.</b> BSE micrograph Glenn County parent material orthopyroxene with iron intergrowth (white) surrounded by serpentine. ....	41
Figure 2-8.	EDX Glenn County parent material enstatite. ....	42
Figure 2-9.	<b>A.</b> BSE micrograph Kings County parent material; talc (TA) amongst serpentine (SY) of varying shades of grey. Bright white spots are either magnetite or andradite garnet. <b>B.</b> Photomicrograph of Kings County parent material shown in plane-polarized light. A mass of talc (TA), dark magnetite (MG) and individual dodecahedral crystals of andradite garnet (GN) in a serpentine (SY) matrix. <b>C.</b> BSE micrograph Kings County parent material with bright white magnetite and andradite garnet amongst serpentine. <b>D.</b> BSE micrograph C with brightness and contrast adjusted to differentiate between bright white magnetite and grey andradite garnet. All the serpentine is black and indistinguishable from the epoxy voids of the thin section. ....	43
Figure 2-10.	Energy dispersive x-ray spectra (EDX) of Kings County parent material minerals A. Talc. B. Serpentine. C. Andradite garnet. D. Magnetite. ....	44
Figure 2-11.	<b>A.</b> Photomicrograph San Benito County parent material plane-polarized light. Serpentine (SY) with opaque inclusions. <b>B.</b> Photomicrograph San Benito County parent material crossed-polarized light. Serpentine (SY) with opaque inclusions. <b>C.</b> BSE micrograph of San Benito County parent material increased contrast and lowered brightness eliminates outlines of serpentine (SY) crystals that dominate the parent material but distinguishes between chromite spinel (SP) at center surrounded by chrome rich andradite garnet (GN). Lightest grey is magnetite (MT). <b>D.</b> Energy dispersive x-ray spectra (EDX) of San Benito County parent material chromite spinel. <b>E.</b> EDX	

of San Benito County parent material chrome rich andradite. F. EDX  
of San Benito County parent material magnetite.....45

**Chapter 3: Plant-available Calcium Varies Widely in Soils on Serpentinite Landscapes**

Figure 3-1. Serpentine soil sites by soil survey. ....75

Figure 3-2. Correlations of soil extractable Ca:Mg to Ca:Mg in *Vulpia microstachys* (Nutt.) Munro leaf.....76

Figure 3-3. Total fine earth fraction elemental analysis Ca:Mg to Ca:Mg in *Vulpia microstachys* (Nutt.) Munro leaf.....77

Figure 3-4. Total elemental analysis Ca to Ca in *Vulpia microstachys* (Nutt.) Munro leaf.....78

Figure 3-5. Total elemental analysis Mg to Ca in *Vulpia microstachys* (Nutt.) Munro leaf.....79

Figure 3-6. Soil extractable Mg to Ca in *Vulpia microstachys* (Nutt.) Munro leaf. 80

Figure 3-7. Correlation of soil extractable Ca to Ca in *Vulpia microstachys* (Nutt.) Munro leaf.....81

Figure 3-8. Total elemental analysis Mg to Mg in *Vulpia microstachys* (Nutt.) Munro leaf.....82

Figure 3-9. Correlation of soil extractable Mg to Mg in *Vulpia microstachys* (Nutt.) Munro leaf.....83

Figure 3-10. Total elemental analysis Ca to Mg in *Vulpia microstachys* (Nutt.) Munro leaf.....84

Figure 3-11. Soil extractable Ca to Mg in *Vulpia microstachys* (Nutt.) Munro leaf. 85

**Chapter 4: Determining Immobile Element Suitable for Mass Balance Calculations for Soils Formed on Serpentinic Landscapes**

Figure 4-1. Depth plots of bulk density ( $\rho_b$ ), and density ratio (bulk density of parent material  $\rho_p$  to the bulk density of each horizon  $\rho_w$ . Dotted vertical line is visual indicator for parent material. ....102

Figure 4-2. Colusa depth plots (A) weight percent Zr, Ti, Y, or Nb; (B) the enrichment factor is the ratio of concentration  $j$  in each horizon ( $C_{j,w}$ ) to parent material ( $C_{j,p}$ ) where  $j$  is Zr, Ti, Y, or Nb. Together the weight percent and enrichment factor are used to calculate (C) strain,  $\epsilon$ , for element Zr, Ti Y or Nb. Dotted vertical line is visual indicator for parent material value. ....103

Figure 4-3. Colusa County transported mass fraction,  $\tau_{Ti}$ ,  $\tau_Y$ , and  $\tau_{Nb}$ , with strain corrected by Zr,  $\epsilon_{Zr}$ . Dotted vertical line is visual indicator for parent material value.....104

Figure 4-4. Colusa County transported mass fraction,  $\tau_{Zr}$ ,  $\tau_Y$ , and  $\tau_{Nb}$ , with strain corrected by Ti,  $\epsilon_{Ti}$ . Dotted vertical line is visual indicator for parent material value.....104

Figure 4-5. Colusa County transported mass fraction,  $\tau_{Ti}$ ,  $\tau_{Zr}$ , and  $\tau_{Nb}$ , with strain corrected by Y,  $\epsilon_Y$ . Dotted vertical line is visual indicator for parent material value..... 105

Figure 4-6. Colusa County transported mass fraction,  $\tau_{Zr}$ ,  $\tau_Y$ , and  $\tau_{Ti}$ , with strain corrected by Nb,  $\epsilon_{Nb}$ . Dotted vertical line is visual indicator for parent material value..... 105

Figure 4-7. Colusa County contributions of the components of closed system mass movement of the element Zr, across the sample volume boundaries (soil horizons) using Ti ( $\epsilon_{Ti,w}$ ), Y ( $\epsilon_{Y,w}$ ) and Nb ( $\epsilon_{Nb,w}$ ) as the strain correcting element. Dotted lines represent  $\tau$ , the mass fraction added or subtracted from each sample at 0, 50 and 100%..... 106

Figure 4-8. Colusa County contributions of the components of closed system mass movement of the element Ti, Y or Nb across the sample volume boundaries (soil horizons) using Zr as the strain correcting element ( $\epsilon_{Zr,w}$ ). Dotted lines represent  $\tau$ , the mass fraction added or subtracted from each sample at 0, 50 and 100%..... 107

Figure 4-9. Colusa County contributions of the components of closed system mass movement across the sample volume boundaries (soil horizons). Dotted lines represent  $\tau$ , the mass fraction added or subtracted from each sample at 0, 50 and 100%..... 108

Figure 4-10. Tehama County depth plots (A) weight percent Zr, Ti, Y, or Nb; (B) the enrichment factor is the ratio of concentration  $j$  in each horizon ( $C_{j,w}$ ) to parent material ( $C_{j,p}$ ) where  $j$  is Zr, Ti, Y, or Nb. Together the weight percent and enrichment factor are used to calculate (C) strain,  $\epsilon$ , for element Zr, Ti Y or Nb. Dotted vertical line is visual indicator for parent material value. .... 109

Figure 4-11. Tehama County transported mass fraction,  $\tau_{Zr}$ ,  $\tau_{Ti}$ ,  $\tau_Y$ , or  $\tau_{Nb}$ , grouped by strain correcting element,  $\epsilon_{Zr}$ ,  $\epsilon_{Ti}$ ,  $\epsilon_Y$ , or  $\epsilon_{Nb}$ . Dotted vertical line is visual indicator for parent material value..... 110

Figure 4-12. Tehama County plots of density ratio  $\rho_p/\rho_w$  representing the residual enrichment contribution vs. enrichment corrected by strain using Zr, Ti, Y and Nb as the immobile element. Dotted lines represent  $\tau$ , the mass fraction added or subtracted from each sample at 0, 50 and 100%. .... 111

Figure 4-13. Depth plots of (A) weighted percent La, (B) enrichment factor, and (C) the transported mass fraction of La. (D) Plot of density ratio  $\rho_p/\rho_w$  representing the residual enrichment contribution vs. enrichment corrected by strain using Y as the immobile element. Dotted vertical line (A, B & C) is visual indicator for parent material value. Dotted lines (D) represent  $\tau$ , the mass fraction added or subtracted from each sample at 0, 50 and 100%. .... 114

Figure 4-14. Depth plots of (A) weighted percent Ce, (B) enrichment factor, and (C) the transported mass fraction of Ce. (D) Plot of density ratio  $\rho_p/\rho_w$  representing the residual enrichment contribution vs. enrichment corrected by strain using Y as the immobile element. Dotted vertical

	line (A, B & C) is visual indicator for parent material value. Dotted lines (D) represent $\tau$ , the mass fraction added or subtracted from each sample at 0, 50 and 100%. .....	115
Figure 4-15.	Depth plots of (A) weighted percent Pr, (B) enrichment factor, and (C) the transported mass fraction of Pr. (D) Plot of density ratio $\rho_p/\rho_w$ representing the residual enrichment contribution vs. enrichment corrected by strain using Y as the immobile element. Dotted vertical line (A, B & C) is visual indicator for parent material value. Dotted lines (D) represent $\tau$ , the mass fraction added or subtracted from each sample at 0, 50 and 100%. .....	116
Figure 4-16.	Depth plots of (A) weighted percent Sm, (B) enrichment factor, and (C) the transported mass fraction of Sm. (D) Plot of density ratio $\rho_p/\rho_w$ representing the residual enrichment contribution vs. enrichment corrected by strain using Y as the immobile element. Dotted vertical line (A, B & C) is visual indicator for parent material value. Dotted lines (D) represent $\tau$ , the mass fraction added or subtracted from each sample at 0, 50 and 100%. .....	117
Figure 4-17.	Depth plots of (A) weighted percent Eu, (B) enrichment factor, and (C) the transported mass fraction of Eu. (D) Plot of density ratio $\rho_p/\rho_w$ representing the residual enrichment contribution vs. enrichment corrected by strain using Y as the immobile element. Dotted vertical line (A, B & C) is visual indicator for parent material value. Dotted lines (D) represent $\tau$ , the mass fraction added or subtracted from each sample at 0, 50 and 100%. .....	118
Figure 4-18.	Depth plots of (A) weighted percent Gd, (B) enrichment factor, and (C) the transported mass fraction of Gd. (D) Plot of density ratio $\rho_p/\rho_w$ representing the residual enrichment contribution vs. enrichment corrected by strain using Y as the immobile element. Dotted vertical line (A, B & C) is visual indicator for parent material value. Dotted lines (D) represent $\tau$ , the mass fraction added or subtracted from each sample at 0, 50 and 100%. .....	119
Figure 4-19.	Depth plots of (A) weighted percent Tb, (B) enrichment factor, and (C) the transported mass fraction of Tb. (D) Plot of density ratio $\rho_p/\rho_w$ representing the residual enrichment contribution vs. enrichment corrected by strain using Y as the immobile element. Dotted vertical line (A, B & C) is visual indicator for parent material value. Dotted lines (D) represent $\tau$ , the mass fraction added or subtracted from each sample at 0, 50 and 100%. .....	120
Figure 4-20.	Depth plots of (A) weighted percent Dy, (B) enrichment factor, and (C) the transported mass fraction of Dy. (D) Plot of density ratio $\rho_p/\rho_w$ representing the residual enrichment contribution vs. enrichment corrected by strain using Y as the immobile element. Dotted vertical line (A, B & C) is visual indicator for parent material value. Dotted lines (D) represent $\tau$ , the mass fraction added or subtracted from each sample at 0, 50 and 100%. .....	121

- Figure 4-21. Depth plots of (A) weighted percent Ho, (B) enrichment factor, and (C) the transported mass fraction of Ho. (D) Plot of density ratio  $\rho_p/\rho_w$  representing the residual enrichment contribution vs. enrichment corrected by strain using Y as the immobile element. Dotted vertical line (A, B & C) is visual indicator for parent material value. Dotted lines (D) represent  $\tau$ , the mass fraction added or subtracted from each sample at 0, 50 and 100%. ..... 122
- Figure 4-22. Depth plots of (A) weighted percent Er, (B) enrichment factor, and (C) the transported mass fraction of Er. (D) Plot of density ratio  $\rho_p/\rho_w$  representing the residual enrichment contribution vs. enrichment corrected by strain using Y as the immobile element. Dotted vertical line (A, B & C) is visual indicator for parent material value. Dotted lines (D) represent  $\tau$ , the mass fraction added or subtracted from each sample at 0, 50 and 100%. ..... 123
- Figure 4-23. Depth plots of (A) weighted percent Yb, (B) enrichment factor, and (C) the transported mass fraction of Yb. (D) Plot of density ratio  $\rho_p/\rho_w$  representing the residual enrichment contribution vs. enrichment corrected by strain using Y as the immobile element. Dotted vertical line (A, B & C) is visual indicator for parent material value. Dotted lines (D) represent  $\tau$ , the mass fraction added or subtracted from each sample at 0, 50 and 100%. ..... 124
- Figure 4-24. Depth plots of (A) weighted percent Lu, (B) enrichment factor, and (C) the transported mass fraction of Lu. (D) Plot of density ratio  $\rho_p/\rho_w$  representing the residual enrichment contribution vs. enrichment corrected by strain using Y as the immobile element. Dotted vertical line (A, B & C) is visual indicator for parent material value. Dotted lines (D) represent  $\tau$ , the mass fraction added or subtracted from each sample at 0, 50 and 100%. ..... 125
- Figure 4-25. Depth plots of (A) weighted percent Sc, (B) enrichment factor, and (C) the transported mass fraction of Sc. (D) Plot of density ratio  $\rho_p/\rho_w$  representing the residual enrichment contribution vs. enrichment corrected by strain using Ti as the immobile element. Dotted vertical line (A, B & C) is visual indicator for parent material value. Dotted lines (D) represent  $\tau$ , the mass fraction added or subtracted from each sample at 0, 50 and 100%. ..... 126
- Figure 4-26. Depth plots of (A) weighted percent La, (B) enrichment factor, and (C) the transported mass fraction of La. (D) Plot of density ratio  $\rho_p/\rho_w$  representing the residual enrichment contribution vs. enrichment corrected by strain using Ti as the immobile element. Dotted vertical line (A, B & C) is visual indicator for parent material value. Dotted lines (D) represent  $\tau$ , the mass fraction added or subtracted from each sample at 0, 50 and 100%. ..... 127
- Figure 4-27. Depth plots of (A) weighted percent Ce, (B) enrichment factor, and (C) the transported mass fraction of Ce. (D) Plot of density ratio  $\rho_p/\rho_w$  representing the residual enrichment contribution vs. enrichment

- corrected by strain using Ti as the immobile element. Dotted vertical line (A, B & C) is visual indicator for parent material value. Dotted lines (D) represent  $\tau$ , the mass fraction added or subtracted from each sample at 0, 50 and 100%. ..... 128
- Figure 4-28. Depth plots of (A) weighted percent Pr, (B) enrichment factor, and (C) the transported mass fraction of Pr. (D) Plot of density ratio  $\rho_p/\rho_w$  representing the residual enrichment contribution vs. enrichment corrected by strain using Ti as the immobile element. Dotted vertical line (A, B & C) is visual indicator for parent material value. Dotted lines (D) represent  $\tau$ , the mass fraction added or subtracted from each sample at 0, 50 and 100%. ..... 129
- Figure 4-29. Depth plots of (A) weighted percent Sm, (B) enrichment factor, and (C) the transported mass fraction of Sm. (D) Plot of density ratio  $\rho_p/\rho_w$  representing the residual enrichment contribution vs. enrichment corrected by strain using Ti as the immobile element. Dotted vertical line (A, B & C) is visual indicator for parent material value. Dotted lines (D) represent  $\tau$ , the mass fraction added or subtracted from each sample at 0, 50 and 100%. ..... 130
- Figure 4-30. Depth plots of (A) weighted percent Eu, (B) enrichment factor, and (C) the transported mass fraction of Eu. (D) Plot of density ratio  $\rho_p/\rho_w$  representing the residual enrichment contribution vs. enrichment corrected by strain using Ti as the immobile element. Dotted vertical line (A, B & C) is visual indicator for parent material value. Dotted lines (D) represent  $\tau$ , the mass fraction added or subtracted from each sample at 0, 50 and 100%. ..... 131
- Figure 4-31. Depth plots of (A) weighted percent Gd, (B) enrichment factor, and (C) the transported mass fraction of Gd. (D) Plot of density ratio  $\rho_p/\rho_w$  representing the residual enrichment contribution vs. enrichment corrected by strain using Ti as the immobile element. Dotted vertical line (A, B & C) is visual indicator for parent material value. Dotted lines (D) represent  $\tau$ , the mass fraction added or subtracted from each sample at 0, 50 and 100%. ..... 132
- Figure 4-32. Depth plots of (A) weighted percent Tb, (B) enrichment factor, and (C) the transported mass fraction of Tb. (D) Plot of density ratio  $\rho_p/\rho_w$  representing the residual enrichment contribution vs. enrichment corrected by strain using Ti as the immobile element. Dotted vertical line (A, B & C) is visual indicator for parent material value. Dotted lines (D) represent  $\tau$ , the mass fraction added or subtracted from each sample at 0, 50 and 100%. ..... 133
- Figure 4-33. Depth plots of (A) weighted percent Dy, (B) enrichment factor, and (C) the transported mass fraction of Dy. (D) Plot of density ratio  $\rho_p/\rho_w$  representing the residual enrichment contribution vs. enrichment corrected by strain using Ti as the immobile element. Dotted vertical line (A, B & C) is visual indicator for parent material value. Dotted

	lines (D) represent $\tau$ , the mass fraction added or subtracted from each sample at 0, 50 and 100% . . . . .	134
Figure 4-34.	Depth plots of (A) weighted percent Ho, (B) enrichment factor, and (C) the transported mass fraction of Ho. (D) Plot of density ratio $\rho_p/\rho_w$ representing the residual enrichment contribution vs. enrichment corrected by strain using Ti as the immobile element. Dotted vertical line (A, B & C) is visual indicator for parent material value. Dotted lines (D) represent $\tau$ , the mass fraction added or subtracted from each sample at 0, 50 and 100% . . . . .	135
Figure 4-35.	Depth plots of (A) weighted percent Er, (B) enrichment factor, and (C) the transported mass fraction of Er. (D) Plot of density ratio $\rho_p/\rho_w$ representing the residual enrichment contribution vs. enrichment corrected by strain using Ti as the immobile element. Dotted vertical line (A, B & C) is visual indicator for parent material value. Dotted lines (D) represent $\tau$ , the mass fraction added or subtracted from each sample at 0, 50 and 100% . . . . .	136
Figure 4-36.	Depth plots of (A) weighted percent Yb, (B) enrichment factor, and (C) the transported mass fraction of Yb. (D) Plot of density ratio $\rho_p/\rho_w$ representing the residual enrichment contribution vs. enrichment corrected by strain using Ti as the immobile element. Dotted vertical line (A, B & C) is visual indicator for parent material value. Dotted lines (D) represent $\tau$ , the mass fraction added or subtracted from each sample at 0, 50 and 100% . . . . .	137
Figure 4-37.	Depth plots of (A) weighted percent Lu, (B) enrichment factor, and (C) the transported mass fraction of Lu. (D) Plot of density ratio $\rho_p/\rho_w$ representing the residual enrichment contribution vs. enrichment corrected by strain using Ti as the immobile element. Dotted vertical line (A, B & C) is visual indicator for parent material value. Dotted lines (D) represent $\tau$ , the mass fraction added or subtracted from each sample at 0, 50 and 100% . . . . .	138
Figure 4-38.	Depth plots of (A) weighted percent Sc, (B) enrichment factor, and (C) the transported mass fraction of Sc. (D) Plot of density ratio $\rho_p/\rho_w$ representing the residual enrichment contribution vs. enrichment corrected by strain using Nb as the immobile element. Dotted vertical line (A, B & C) is visual indicator for parent material value. Dotted lines (D) represent $\tau$ , the mass fraction added or subtracted from each sample at 0, 50 and 100% . . . . .	139
Figure 4-39.	Depth plots of (A) weighted percent La, (B) enrichment factor, and (C) the transported mass fraction of La. (D) Plot of density ratio $\rho_p/\rho_w$ representing the residual enrichment contribution vs. enrichment corrected by strain using Nb as the immobile element. Dotted vertical line (A, B & C) is visual indicator for parent material value. Dotted lines (D) represent $\tau$ , the mass fraction added or subtracted from each sample at 0, 50 and 100% . . . . .	140



- Figure 4-40. Depth plots of (A) weighted percent Ce, (B) enrichment factor, and (C) the transported mass fraction of Ce. (D) Plot of density ratio  $\rho_p/\rho_w$  representing the residual enrichment contribution vs. enrichment corrected by strain using Nb as the immobile element. Dotted vertical line (A, B & C) is visual indicator for parent material value. Dotted lines (D) represent  $\tau$ , the mass fraction added or subtracted from each sample at 0, 50 and 100%. ..... 141
- Figure 4-41. Depth plots of (A) weighted percent Pr, (B) enrichment factor, and (C) the transported mass fraction of Pr. (D) Plot of density ratio  $\rho_p/\rho_w$  representing the residual enrichment contribution vs. enrichment corrected by strain using Nb as the immobile element. Dotted vertical line (A, B & C) is visual indicator for parent material value. Dotted lines (D) represent  $\tau$ , the mass fraction added or subtracted from each sample at 0, 50 and 100%. ..... 142
- Figure 4-42. Depth plots of (A) weighted percent Sm, (B) enrichment factor, and (C) the transported mass fraction of Sm. (D) Plot of density ratio  $\rho_p/\rho_w$  representing the residual enrichment contribution vs. enrichment corrected by strain using Nb as the immobile element. Dotted vertical line (A, B & C) is visual indicator for parent material value. Dotted lines (D) represent  $\tau$ , the mass fraction added or subtracted from each sample at 0, 50 and 100%. ..... 143
- Figure 4-43. Depth plots of (A) weighted percent Eu, (B) enrichment factor, and (C) the transported mass fraction of Eu. (D) Plot of density ratio  $\rho_p/\rho_w$  representing the residual enrichment contribution vs. enrichment corrected by strain using Nb as the immobile element. Dotted vertical line (A, B & C) is visual indicator for parent material value. Dotted lines (D) represent  $\tau$ , the mass fraction added or subtracted from each sample at 0, 50 and 100%. ..... 144
- Figure 4-44. Depth plots of (A) weighted percent Gd, (B) enrichment factor, and (C) the transported mass fraction of Gd. (D) Plot of density ratio  $\rho_p/\rho_w$  representing the residual enrichment contribution vs. enrichment corrected by strain using Nd as the immobile element. Dotted vertical line (A, B & C) is visual indicator for parent material value. Dotted lines (D) represent  $\tau$ , the mass fraction added or subtracted from each sample at 0, 50 and 100%. ..... 145
- Figure 4-45. Depth plots of (A) weighted percent Tb, (B) enrichment factor, and (C) the transported mass fraction of Tb. (D) Plot of density ratio  $\rho_p/\rho_w$  representing the residual enrichment contribution vs. enrichment corrected by strain using Nb as the immobile element. Dotted vertical line (A, B & C) is visual indicator for parent material value. Dotted lines (D) represent  $\tau$ , the mass fraction added or subtracted from each sample at 0, 50 and 100%. ..... 146
- Figure 4-46. Depth plots of (A) weighted percent Dy, (B) enrichment factor, and (C) the transported mass fraction of Dy. (D) Plot of density ratio  $\rho_p/\rho_w$  representing the residual enrichment contribution vs. enrichment

	corrected by strain using Nb as the immobile element. Dotted vertical line (A, B & C) is visual indicator for parent material value. Dotted lines (D) represent $\tau$ , the mass fraction added or subtracted from each sample at 0, 50 and 100%. .....	147
Figure 4-47.	Depth plots of (A) weighted percent Ho, (B) enrichment factor, and (C) the transported mass fraction of Ho. (D) Plot of density ratio $\rho_p/\rho_w$ representing the residual enrichment contribution vs. enrichment corrected by strain using Nb as the immobile element. Dotted vertical line (A, B & C) is visual indicator for parent material value. Dotted lines (D) represent $\tau$ , the mass fraction added or subtracted from each sample at 0, 50 and 100%. .....	148
Figure 4-48.	Depth plots of (A) weighted percent Er, (B) enrichment factor, and (C) the transported mass fraction of Er. (D) Plot of density ratio $\rho_p/\rho_w$ representing the residual enrichment contribution vs. enrichment corrected by strain using Nb as the immobile element. Dotted vertical line (A, B & C) is visual indicator for parent material value. Dotted lines (D) represent $\tau$ , the mass fraction added or subtracted from each sample at 0, 50 and 100%. .....	149
Figure 4-49.	Depth plots of (A) weighted percent Yb, (B) enrichment factor, and (C) the transported mass fraction of Yb. (D) Plot of density ratio $\rho_p/\rho_w$ representing the residual enrichment contribution vs. enrichment corrected by strain using Nb as the immobile element. Dotted vertical line (A, B & C) is visual indicator for parent material value. Dotted lines (D) represent $\tau$ , the mass fraction added or subtracted from each sample at 0, 50 and 100%. .....	150
Figure 4-50.	Depth plots of (A) weighted percent Lu, (B) enrichment factor, and (C) the transported mass fraction of Lu. (D) Plot of density ratio $\rho_p/\rho_w$ representing the residual enrichment contribution vs. enrichment corrected by strain using Nd as the immobile element. Dotted vertical line (A, B & C) is visual indicator for parent material value. Dotted lines (D) represent $\tau$ , the mass fraction added or subtracted from each sample at 0, 50 and 100%. .....	151
Figure 4-51.	Depth plots of (A) weighted percent Sc, (B) enrichment factor, and (C) the transported mass fraction of Sc. (D) Plot of density ratio $\rho_p/\rho_w$ representing the residual enrichment contribution vs. enrichment corrected by strain using Zr as the immobile element. Dotted vertical line (A, B & C) is visual indicator for parent material value. Dotted lines (D) represent $\tau$ , the mass fraction added or subtracted from each sample at 0, 50 and 100%. .....	153
Figure 4-52.	Depth plots of (A) weighted percent La, (B) enrichment factor, and (C) the transported mass fraction of La. (D) Plot of density ratio $\rho_p/\rho_w$ representing the residual enrichment contribution vs. enrichment corrected by strain using Zr as the immobile element. Dotted vertical line (A, B & C) is visual indicator for parent material value. Dotted	

	lines (D) represent $\tau$ , the mass fraction added or subtracted from each sample at 0, 50 and 100% . . . . .	154
Figure 4-53.	Depth plots of (A) weighted percent Ce, (B) enrichment factor, and (C) the transported mass fraction of Ce. (D) Plot of density ratio $\rho_p/\rho_w$ representing the residual enrichment contribution vs. enrichment corrected by strain using Zr as the immobile element. Dotted vertical line (A, B & C) is visual indicator for parent material value. Dotted lines (D) represent $\tau$ , the mass fraction added or subtracted from each sample at 0, 50 and 100% . . . . .	155
Figure 4-54.	Depth plots of (A) weighted percent Pr, (B) enrichment factor, and (C) the transported mass fraction of Pr. (D) Plot of density ratio $\rho_p/\rho_w$ representing the residual enrichment contribution vs. enrichment corrected by strain using Zr as the immobile element. Dotted vertical line (A, B & C) is visual indicator for parent material value. Dotted lines (D) represent $\tau$ , the mass fraction added or subtracted from each sample at 0, 50 and 100% . . . . .	156
Figure 4-55.	Depth plots of (A) weighted percent Sm, (B) enrichment factor, and (C) the transported mass fraction of Sm. (D) Plot of density ratio $\rho_p/\rho_w$ representing the residual enrichment contribution vs. enrichment corrected by strain using Zr as the immobile element. Dotted vertical line (A, B & C) is visual indicator for parent material value. Dotted lines (D) represent $\tau$ , the mass fraction added or subtracted from each sample at 0, 50 and 100% . . . . .	157
Figure 4-56.	Depth plots of (A) weighted percent Eu, (B) enrichment factor, and (C) the transported mass fraction of Eu. (D) Plot of density ratio $\rho_p/\rho_w$ representing the residual enrichment contribution vs. enrichment corrected by strain using Zr as the immobile element. Dotted vertical line (A, B & C) is visual indicator for parent material value. Dotted lines (D) represent $\tau$ , the mass fraction added or subtracted from each sample at 0, 50 and 100% . . . . .	158
Figure 4-57.	Depth plots of (A) weighted percent Gd, (B) enrichment factor, and (C) the transported mass fraction of Gd. (D) Plot of density ratio $\rho_p/\rho_w$ representing the residual enrichment contribution vs. enrichment corrected by strain using Zr as the immobile element. Dotted vertical line (A, B & C) is visual indicator for parent material value. Dotted lines (D) represent $\tau$ , the mass fraction added or subtracted from each sample at 0, 50 and 100% . . . . .	159
Figure 4-58.	Depth plots of (A) weighted percent Tb, (B) enrichment factor, and (C) the transported mass fraction of Tb. (D) Plot of density ratio $\rho_p/\rho_w$ representing the residual enrichment contribution vs. enrichment corrected by strain using Zr as the immobile element. Dotted vertical line (A, B & C) is visual indicator for parent material value. Dotted lines (D) represent $\tau$ , the mass fraction added or subtracted from each sample at 0, 50 and 100% . . . . .	160

- Figure 4-59. Depth plots of (A) weighted percent Dy, (B) enrichment factor, and (C) the transported mass fraction of Dy. (D) Plot of density ratio  $\rho_p/\rho_w$  representing the residual enrichment contribution vs. enrichment corrected by strain using Zr as the immobile element. Dotted vertical line (A, B & C) is visual indicator for parent material value. Dotted lines (D) represent  $\tau$ , the mass fraction added or subtracted from each sample at 0, 50 and 100%. ..... 161
- Figure 4-60. Depth plots of (A) weighted percent Ho, (B) enrichment factor, and (C) the transported mass fraction of Ho. (D) Plot of density ratio  $\rho_p/\rho_w$  representing the residual enrichment contribution vs. enrichment corrected by strain using Zr as the immobile element. Dotted vertical line (A, B & C) is visual indicator for parent material value. Dotted lines (D) represent  $\tau$ , the mass fraction added or subtracted from each sample at 0, 50 and 100%. ..... 162
- Figure 4-61. Depth plots of (A) weighted percent Er, (B) enrichment factor, and (C) the transported mass fraction of Er. (D) Plot of density ratio  $\rho_p/\rho_w$  representing the residual enrichment contribution vs. enrichment corrected by strain using Zr as the immobile element. Dotted vertical line (A, B & C) is visual indicator for parent material value. Dotted lines (D) represent  $\tau$ , the mass fraction added or subtracted from each sample at 0, 50 and 100%. ..... 163
- Figure 4-62. Depth plots of (A) weighted percent Yb, (B) enrichment factor, and (C) the transported mass fraction of Yb. (D) Plot of density ratio  $\rho_p/\rho_w$  representing the residual enrichment contribution vs. enrichment corrected by strain using Zr as the immobile element. Dotted vertical line (A, B & C) is visual indicator for parent material value. Dotted lines (D) represent  $\tau$ , the mass fraction added or subtracted from each sample at 0, 50 and 100%. ..... 164
- Figure 4-63. Depth plots of (A) weighted percent Lu, (B) enrichment factor, and (C) the transported mass fraction of Lu. (D) Plot of density ratio  $\rho_p/\rho_w$  representing the residual enrichment contribution vs. enrichment corrected by strain using Zr as the immobile element. Dotted vertical line (A, B & C) is visual indicator for parent material value. Dotted lines (D) represent  $\tau$ , the mass fraction added or subtracted from each sample at 0, 50 and 100%. ..... 165

**Chapter 5: Flux of Elements by Mass Balance in Soils From Three Serpentinic Landscapes**

- Figure 5-1. Depth plots of A) bulk density ( $\rho_b$ ), and B) density ratio (bulk density of parent material ( $\rho_p$ ) to bulk density of each horizon ( $\rho_w$ ). Dotted vertical line is visual indicator for parent material value..... 191
- Figure 5-2. Tehama County depth plots (A) weight percent Y (B) the enrichment factor is the ratio of concentration Y in each horizon ( $C_{Y,w}$ ) to parent material ( $C_{Y,p}$ ). Together the weight percent and enrichment factor are

- used to calculate (C) strain,  $\epsilon_Y$ . Dotted vertical line is visual indicator for parent material value. .... 192
- Figure 5-3. Si: Tehama County depth plots of (A) weight percent (B) enrichment factor, and (C) the transported mass fraction. (D) Plot of density ratio  $\rho_p/\rho_w$  representing the residual enrichment contribution vs. enrichment corrected by strain using Y as the immobile element. Dotted vertical lines in A, B and C are visual indicator for parent material value. Sloped dotted lines (D) represent  $\tau$ , the mass fraction added or subtracted from each sample at 0, 50 and 100% ..... 192
- Figure 5-4. Tehama County Cr crushed rock and silt x-ray diffractograms. Hydroxy-interlayered-material (HIM) the 1.4 nm Mg-saturated peak that collapses incompletely to 1.0 nm with K-saturation and heating together with the reduction of a 0.355 nm (004) peak with K-saturation and heating; grossularite peaks at 0.299 & 0.266 nm; diopside 0.32 nm peak; pumpellyite 0.290 nm peak. .... 193
- Figure 5-5. Tehama County clay x-ray diffractograms. Hydroxy-interlayered-material (HIM) the 1.4 nm Mg-saturated peak that collapses incompletely to 1.0 nm with K-saturation and heating together with the reduction of a 0.355 nm (004) peak with K-saturation and heating; grossularite peaks at 0.299 & 0.266 nm. .... 194
- Figure 5-6. Mg: Tehama County depth plots of (A) weight percent (B) enrichment factor, and (C) the transported mass fraction. (D) Plot of density ratio  $\rho_p/\rho_w$  representing the residual enrichment contribution vs. enrichment corrected by strain using Y as the immobile element. Dotted vertical lines in A, B and C are visual indicator for parent material value. Sloped dotted lines, D, represent  $\tau$ , the mass fraction added or subtracted from each sample at 0, 50 and 100% ..... 195
- Figure 5-7. Al: Tehama County depth plots of (A) weight percent (B) enrichment factor, and (C) the transported mass fraction. (D) Plot of density ratio  $\rho_p/\rho_w$  representing the residual enrichment contribution vs. enrichment corrected by strain using Y as the immobile element. Dotted vertical lines in A, B and C are visual indicator for parent material value. Sloped dotted lines, D, represent  $t$ , the mass fraction added or subtracted from each sample at 0, 50 and 100% ..... 195
- Figure 5-8. Fe: Tehama County depth plots of (A) weight percent (B) enrichment factor, and (C) the transported mass fraction. (D) Plot of density ratio  $\rho_p/\rho_w$  representing the residual enrichment contribution vs. enrichment corrected by strain using Y as the immobile element. Dotted vertical lines in A, B and C are visual indicator for parent material value. Sloped dotted lines, D, represent  $\tau$ , the mass fraction added or subtracted from each sample at 0, 50 and 100% ..... 196
- Figure 5-9. Ca: Tehama County depth plots of (A) weight percent (B) enrichment factor, and (C) the transported mass fraction. (D) Plot of density ratio  $\rho_p/\rho_w$  representing the residual enrichment contribution vs. enrichment corrected by strain using Y as the immobile element. Dotted vertical

	lines in A, B and C are visual indicator for parent material value. Sloped dotted lines, D, represent $\tau$ , the mass fraction added or subtracted from each sample at 0, 50 and 100%.....	196
Figure 5-10.	Colusa County depth plots (A) weight percent Y (B) the enrichment factor is the ratio of concentration Y in each horizon ( $C_{Y,w}$ ) to parent material ( $C_{Y,p}$ ). Together the weight percent and enrichment factor are used to calculate (C) strain, $\epsilon_Y$ . Dotted vertical line is visual indicator for parent material value. ....	197
Figure 5-11.	Si: Colusa County depth plots of (A) weight percent (B) enrichment factor, and (C) the transported mass fraction. (D) Plot of density ratio $\rho_p/\rho_w$ representing the residual enrichment contribution vs. enrichment corrected by strain using Y as the immobile element. Dotted vertical lines in A, B and C are visual indicator for parent material value. Sloped dotted lines (D) represent $\tau$ , the mass fraction added or subtracted from each sample at 0, 50 and 100%.....	197
Figure 5-12.	Colusa County Cr horizon rock x-ray diffractograms. Serpentine (0.72 nm and 0.36 nm peaks) with a minor component of chlorite (1.4 nm and 0.475 nm peaks that persist with heating and do not expand with glycerol solvation). ....	198
Figure 5-13.	Colusa County silt x-ray diffractograms. Serpentine (0.72 nm and 0.36 nm peaks) with a minor component of chlorite (1.4 nm and 0.475 nm peaks that persist with heating and do not expand with glycerol solvation). ....	199
Figure 5-14.	Colusa County clay x-ray diffractograms. Serpentine (0.72 nm and 0.36 nm peaks), chlorite (1.4 nm and 0.475 nm peaks that persist with heating and do not expand with glycerol solvation), vermiculite (1.4 nm peak that collapses to 1.0 nm with K-saturation and heating), and smectite (1.4 nm peak that expands to ~1.8 nm with Mg-saturation and glycerol solvation). ....	200
Figure 5-15.	Mg: Colusa County depth plots of (A) weight percent (B) enrichment factor, and (C) the transported mass fraction. (D) Plot of density ratio $\rho_p/\rho_w$ representing the residual enrichment contribution vs. enrichment corrected by strain using Y as the immobile element. Dotted vertical lines in A, B and C are visual indicator for parent material value. Sloped dotted lines, D, represent $\tau$ , the mass fraction added or subtracted from each sample at 0, 50 and 100%.....	201
Figure 5-16.	Al: Colusa County depth plots of (A) weight percent (B) enrichment factor, and (C) the transported mass fraction. (D) Plot of density ratio $\rho_p/\rho_w$ representing the residual enrichment contribution vs. enrichment corrected by strain using Y as the immobile element. Dotted vertical lines in A, B and C are visual indicator for parent material value. Sloped dotted lines, D, represent $\tau$ , the mass fraction added or subtracted from each sample at 0, 50 and 100%.....	201
Figure 5-17.	Fe: Colusa County depth plots of (A) weighted percent; (B) enrichment factor, and (C) the transported mass fraction (D) Plot of	

- density ratio  $\rho_p/\rho_w$  representing the residual enrichment contribution vs. enrichment corrected by strain using Y as the immobile element. Dotted vertical lines in A, B and C are visual indicator for parent material value. Sloped dotted lines, D, represent  $\tau$ , the mass fraction added or subtracted from each sample at 0, 50 and 100%.....202
- Figure 5-18. Ca: Colusa County depth plots of (A) weight percent (B) enrichment factor, and (C) the transported mass fraction. (D) Plot of density ratio  $\rho_p/\rho_w$  representing the residual enrichment contribution vs. enrichment corrected by strain using Y as the immobile element. Dotted vertical lines in A, B and C are visual indicator for parent material value. Sloped dotted lines, D, represent  $\tau$ , the mass fraction added or subtracted from each sample at 0, 50 and 100%.....202
- Figure 5-19. Napa County depth plots (A) weight percent Y (B) the enrichment factor is the ratio of concentration Y in each horizon ( $C_{Y,w}$ ) to parent material ( $C_{Y,p}$ ). Together the weight percent and enrichment factor are used to calculate (C) strain,  $\epsilon_Y$ . Dotted vertical line is visual indicator for parent material value. ....203
- Figure 5-20. Si: Napa County depth plots of (A) weight percent (B) enrichment factor, and (C) the transported mass fraction. (D) Plot of density ratio  $\rho_p/\rho_w$  representing the residual enrichment contribution vs. enrichment corrected by strain using Y as the immobile element. Dotted vertical lines in A, B and C are visual indicator for parent material value. Sloped dotted lines (D) represent  $\tau$ , the mass fraction added or subtracted from each sample at 0, 50 and 100%.....203
- Figure 5-21. Napa County parent material x-ray diffractogram. Vermiculite 1.4 nm peak with Mg treatment collapsed to 1.0 nm with K-saturation treatment and heat; vermiculite peak also at 0.289. Plagioclase feldspar peaks at 0.630, 0.401, 0.374, 0.365, 0.336, 0.318, 0.293 nm. ....204
- Figure 5-22. Napa County clay and silt x-ray diffractograms. Vermiculite 1.4 nm peak with Mg treatment collapsed to 1.0 nm with K-saturation treatment and heat; vermiculite peak also at 0.289. Plagioclase feldspar peaks at 0.630, 0.401, 0.374, 0.365, 0.336, 0.318, 0.293 nm. Clay x-ray diffractograms similar to crushed rock and silt with the addition of smectite 1.8 nm peak with Mg-treatment and glycerol solvation. Maximum peak intensity shift from vermiculite in the Bt horizon to smectite in the A horizon. Plagioclase peaks diminished respective to rock or silt fraction.....205
- Figure 5-23. Mg: Napa County depth plots of (A) weight percent (B) enrichment factor, and (C) the transported mass fraction. (D) Plot of density ratio  $\rho_p/\rho_w$  representing the residual enrichment contribution vs. enrichment corrected by strain using Y as the immobile element. Dotted vertical lines in A, B and C are visual indicator for parent material value. Sloped dotted lines, D, represent  $\tau$ , the mass fraction added or subtracted from each sample at 0, 50 and 100%.....206

Figure 5-24. Al: Napa County depth plots of (A) weight percent (B) enrichment factor, and (C) the transported mass fraction. (D) Plot of density ratio  $\rho_p/\rho_w$  representing the residual enrichment contribution vs. enrichment corrected by strain using Y as the immobile element. Dotted vertical lines in A, B and C are visual indicator for parent material value. Sloped dotted lines, D, represent  $t$ , the mass fraction added or subtracted from each sample at 0, 50 and 100% .....206

Figure 5-25. Fe: Napa County depth plots of (A) weight percent (B) enrichment factor, and (C) the transported mass fraction. (D) Plot of density ratio  $\rho_p/\rho_w$  representing the residual enrichment contribution vs. enrichment corrected by strain using Y as the immobile element. Dotted vertical lines in A, B and C are visual indicator for parent material value. Sloped dotted lines, D, represent  $\tau$ , the mass fraction added or subtracted from each sample at 0, 50 and 100% .....207

Figure 5-26. Ca: Napa County depth plots of (A) weight percent (B) enrichment factor, and (C) the transported mass fraction. (D) Plot of density ratio  $\rho_p/\rho_w$  representing the residual enrichment contribution vs. enrichment corrected by strain using Y as the immobile element. Dotted vertical lines in A, B and C are visual indicator for parent material value. Sloped dotted lines, D, represent  $\tau$ , the mass fraction added or subtracted from each sample at 0, 50 and 100% .....207



# CHAPTER 1: SITE

## DESCRIPTIONS

The soil profiles described and sampled in this study were mapped as having a thermic soil temperature regime. The altitude of some profiles (>3000 feet) would normally indicate that these soils would probably fall into a mesic soil temperature regime. The serpentinite soil sites here are all on summit positions and have low percentage of vegetation cover, and therefore, are subject to greater insolation than soils not on serpentinitic landscapes due to greater vegetative cover. An example of the aspect effect on mesic/thermic regime was Shasta-Trinity National Forest where the soil survey indicates a thermic soil map (southwest aspect) unit in juxtaposition with a mesic soil map unit (northeast aspect). All sites sampled for this study were summit positions. No annual seasonal measurements were taken to confirm that the sites are thermic or mesic, so mesic was applied here where the altitude warranted it (>3000 feet).

### **1.1 Colusa County site profile description**

Sampled July 2, 2003 by Donald Greg McGahan and Randy Southard. The summit position (<3% slope); N aspect; convex, convex; covered by 50 percent serpentinite rock fragments mostly less than 5 cm in diameter; well drained; slow permeability; medium runoff poten-

tial; 2991 feet elevation; 2800 feet east and 380 feet south of the northwest corner of Section 26 T. 15 N, R. 6 W. MDB&M; Wilbur Springs California topographic quadrangle, 1991; WGS NAD83, 39° 7' 27.6" north latitude, 122° 29' 37.7" west longitude.

**TAXONOMIC CLASS:** Clayey, magnesian, mesic, shallow Typic Argixeroll

**A** – 0 to 3 cm; brown (7.5YR 4/3) loam, dark brown (5YR 3/2) moist; moderate medium subangular blocky parting to moderate coarse granular structure; moderately hard, slightly sticky, very plastic; common fine roots throughout; 12 percent gravel; slightly acid (pH 6.1); clear smooth boundary.

**ABt** – 3 to 8 cm; brown (7.5YR 4/3) gravelly clay loam, dark reddish brown (5YR 3/3) moist; moderate coarse subangular blocky parting to moderate fine and medium subangular blocky structure; moderately hard, slightly sticky, moderately plastic; common fine and medium roots throughout; many distinct clay films on sides and bottom of ped faces; 27 percent serpentinized peridotite gravel; moderately acid (pH 6.0); clear wavy boundary.

**Bt1** – 8 to 30 cm; brown (7.5YR 4/3) gravelly clay loam; dark reddish brown (5YR 3/3) moist; moderate coarse to medium angular blocky and moderate fine subangular blocky structure; moderately hard, moderately sticky, very plastic; common fine and few coarse roots; very many distinct dark stained clay films on all surfaces of peds and rock fragments; 27 percent serpentinized peridotite gravel; slightly acid (pH 6.2); clear wavy boundary.

**Bt2**– 30 to 42 cm; brown (7.5YR 4/3) gravelly clay, dark brown (7.5YR 3/3) moist; moderate medium prismatic parting to very weak medium wedge structure; very

hard, very sticky, very plastic; few fine and coarse roots; very many distinct clay films and pressure faces on all ped faces; 16 percent serpentinized peridotite gravel; neutral (pH 7.1); abrupt irregular boundary.

**Cr** – 42 to 72 cm; variegated, 30 percent brown (7.5YR 4/3), dark reddish brown (5YR 3/3) moist, 20 percent pale yellow (5Y 7/3), olive (5Y 5/4) moist and 20 percent light greenish grey (10Y 8/1), dark greenish grey (5GY 4/1) moist friable saprolite that crushes to sandy clay loam, and 30 percent hard light greenish grey (10GY 7/1), greenish grey (5GY 4/1) moist serpentinized peridotite; red, dark reddish and dark reddish brown clay seams following few medium and fine root intrusions into rock.

**Diagnostic features:** mollic epipedon 0 to 42 cm; argillic 3 to 42 cm; particle size control section 3 to 42 cm.

## 1.2 Glenn County site profile description

Sampled August 8, 2003 by Donald Greg McGahan. The summit position (3% slope); ESE aspect; well drained; slow permeability; medium runoff potential; 3595 feet elevation; about 750 feet west of the southeast corner of Section 23 T. 22N, R. 6W. MDB&M; Chrome California topographic quadrangle, 1968; WGS NAD83 39° 44' 30.2" north latitude, 122° 36' 33.4 west longitude.

**TAXONOMIC CLASS:** Loamy-skeletal, magnesian, thermic Lithic Argixeroll

**A** – 0 to 9 cm; brown (7.5YR 4/4) very gravelly sandy clay loam, dark reddish brown (2.5YR 3/3) moist; weak fine angular blocky parting to weak fine and medium

granular structure; soft, non-sticky, slightly plastic; many very fine roots throughout; common faint discontinuous clay films on rock and ped faces; 40 percent gravel and 2 percent cobbles; slightly acid (pH 6.3); abrupt wavy boundary.

**Bt** – 9 to 34 cm; reddish brown (5YR 4/4) very gravelly sandy clay loam, dark reddish brown (2.5YR 2.5/3) moist; weak fine angular blocky parting to strong medium granular structure; very friable, moderately sticky, very plastic; few fine, common medium, and common very coarse roots between peds; few fine dendritic tubular pores; many discontinuous clay films on ped and rock faces; 40 percent gravel and 15 percent cobbles; slightly acid (pH 6.4); clear irregular boundary.

**R** – 34 to 55 cm; 80 percent greenish black (10Y 2.5/1), and 20 percent yellow (2.5Y 7/6) hard, serpentized peridotite; 90 percent strong brown (7.5YR 4/6) clay films on rock faces; some soil material and common coarse roots along cracks in the rock.

**Diagnostic features:** mollic epipedon 0-34 cm, argillic 9-34 cm, particle size control section 0-34 cm.

### **1.3 Kings County site profile description**

Sampled September 1, 2003 by Donald Greg McGahan. The summit position (<2% slope); SW aspect; well drained; slow permeability; medium runoff potential; 3460 feet elevation; about 150 feet north of the line between Section 19 and Section 30 and about 1,400 feet west of the line between Section 19 and Section 18 SE ¼ of SE ¼ of the SE ¼ of Section

19 T. 23S, R. 16E. MDB&M; The Dark Hole California topographic quadrangle, 1987; WGS NAD83 35° 54' 24.2" north latitude, 120° 16' 34.7 west longitude.

**TAXONOMIC CLASS:** Loamy-skeletal, magnesian, mesic Lithic Argixeroll

**A** – 0 to 4 cm; dark greyish brown (10YR 4/2) very gravelly silt loam, very dark brown (10YR 2/2) moist; moderate thick platy parting to moderate fine granular structure; slightly hard, non-sticky, non-plastic; many very fine roots throughout; common fine dendritic tubular pores; many faint continuous clay films on rock faces and along surfaces of pores; 48 percent gravel and 2 percent cobbles; slightly acid (pH 6.1); abrupt wavy boundary.

**Bt1** – 4 to 13 cm; brown (10YR 5/3) extremely gravelly loam, dark brown (7.5YR 3/2) moist; moderate medium prismatic parting to moderate very coarse subangular blocky structure; very hard to extremely hard, slightly sticky, moderately plastic; common very fine roots throughout; common medium and many fine dendritic tubular pores; many prominent continuous clay films on ped and rock faces and along surfaces of pores; 55 percent gravel, 20 percent cobbles; slightly acid (pH 6.2); abrupt wavy boundary.

**Bt2** – 13 to 40 cm; dark grayish brown (10YR 4/2) extremely gravelly clay loam, dark brown (7.5YR 3/2) moist; strong medium subangular blocky structure; very hard, moderately sticky, moderately plastic; common very fine roots throughout; common medium dendritic tubular pores; many prominent continuous clay films on rock and ped faces and along surfaces of pores; 10 percent cobbles, 57 percent gravels; slightly acid (pH 6.2); irregular boundary.

**R** – 40 to 50 cm. 70 percent light greenish grey (5GY 8/1), 20 percent light greenish grey (10GY 8/1), 10 percent bluish black (5B 2.5/1), hard serpentinite and some soil material and common coarse roots along cracks in the rock.

**Diagnostic features:** mollic epipedon 0-40 cm, argillic 4-40 cm, particle size control section 4-40 cm.

## 1.4 Napa County site profile description

Sampled July 10, 2003 by Donald Greg McGahan and Craig Rasmussen. Summit position (<1% slope); ESE aspect; well drained; slow permeability; medium runoff potential; 543 feet elevation; non-sectionalized 9N, 4W. MDB&M; Chiles Valley California topographic quadrangle; WGS NAD83 38° 37' 8.9" north latitude, 122° 17' 25.6" west longitude.

**TAXONOMIC CLASS:** Loamy, mixed, active, thermic Lithic Haploxerept

**A** – 0 to 6 cm; reddish brown (5YR 4/4) loam, dark reddish brown (5YR 3/3) moist; moderate thick platy parting to moderate fine subangular and strong medium subangular blocky structure; slightly hard, non-sticky, non-plastic; common very fine and few fine root throughout; common fine tubular pores throughout; 2 percent gravel; slightly acid (pH 6.4); abrupt smooth boundary.

**Bt** – 6 to 20 cm; yellowish red (5YR 4/6) loam, dark reddish brown (5YR 3/4) moist; moderate coarse subangular blocky structure parting to strong medium subangular blocky structure; hard, slightly sticky, slightly plastic; common fine and medium roots and many coarse roots matted at top of horizon; common fine dendritic tubular pores throughout; very many distinct continuous clay films on vertical

faces of peds and lining pores; 7 percent gravel; neutral (pH 6.6); abrupt irregular boundary.

**R** – 20 to 52 cm; variegated, pale yellow 60 percent pale yellow (2.5Y 7/4) and 40 percent pale yellow (5Y 7/4) dry hard metamorphosed gabbro; rock surfaces in cracks variegated, 45 percent bluish black (5BP 2.5/1), 40 percent reddish brown (5YR 4/4), and 15 percent strong brown (7.5YR).

**Diagnostic features:** ochric epipedon 0-18 cm, cambic 6-20 cm, particle size control section 0-20 cm.

## 1.5 San Benito County site profile description

Sampled September 9, 2004 by Donald Greg McGahan. The summit position (<3% slope); convex, convex; covered by 80 percent serpentinite gravel rock fragments; well drained; moderately rapid permeability; medium runoff potential; moderate to high erosion potential; 4326 feet elevation; NE ¼ Section 7 T.18S, R.12E MDB&M; Idria California topographic quadrangle; WGS NAD83 36° 23' 16.6" north latitude, 120° 4' 32.6" west longitude.

**TAXONOMIC CLASS:** Loamy-skeletal, magnesian, mesic, shallow Typic Haploxeralfs

**A** – 0 to 8 cm, pale brown (10YR 6/3) very gravelly coarse sandy loam, brown (10YR 4/3) moist; weak, fine, subangular blocky structure; slightly hard, non-sticky and non-plastic; 43 percent gravel; neutral (pH 6.6), slightly effervescent with HCl; very abrupt, wavy boundary.

**Bt** – 8 to 20 cm, brown (10YR 5/3) extremely gravelly coarse sandy loam, very dark grey

(7.5YR 3/1) moist; moderate, medium, subangular blocky structure; soft, non-sticky and slightly plastic; many fine roots throughout; common, distinct, continuous clay films on rock fragments and between sand grains; 60 percent gravel; neutral (pH6.7), very slightly effervescent with HCl; clear, wavy boundary.

**Cr** – 20 to 50 cm, variegated, 60 percent gray (N 5/) and 40 percent light greenish grey (5GY 7/1) dry; highly fractured, hard, serpentinized peridotite; 30 percent of cracked rock faces lined with distinct prominent brownish yellow (10YR 6/6) clay films; common medium roots between rocks; fungal hyphae matted at top of horizon.

**R** – 50 to 70 cm, variegated, 70 percent light greenish grey (5GY 7/1) and 30 percent dark bluish grey (10B 4/1) slightly fractured, hard, serpentinized peridotite; 80 percent of cracks lined with distinct, prominent, brownish yellow (10YR 6/6) clay films.

**Diagnostic Features:** ochric epipedon 0-8 cm, Argillic horizon 8-20 cm, particle size control section 0-20 cm.

## 1.6 Shasta County site profile description

Sampled August 13, 2003 by Donald G. McGahan. Summit position (3 % slope); convex, convex; rock outcrops occupy 60 percent of area; 1973 feet elevation; WGS NADS83 40° 28' 36.4" north latitude, 122° 40' 38.3" west longitude.

**TAXONOMIC CLASS:** Loamy-skeletal, magnesian, thermic Lithic Haploxerept

**A** – 0 to 3 cm; yellowish brown (5YR 4/6), extremely stony loam, dark reddish brown (2.5YR 3/4) moist; moderate coarse subangular blocky parting to moderate coarse



granular structure; slightly hard, non-sticky, slightly plastic; many very fine roots throughout; common fine and medium dendritic tubular pores; 18 percent gravels and 60 percent stones; moderately acid (pH 5.7); abrupt smooth boundary.

**Bt** – 3 to 40 cm; yellowish red (5YR 4/6) extremely stony loam, dark reddish brown (2.5YR 3/4) moist; moderate coarse angular blocky structure; firm, slightly sticky, slightly plastic; common fine roots throughout; common fine dendritic tubular pores; many distinct discontinuous clay films on ped faces; 28 percent gravels and 60 percent stones; moderately acid (pH 5.9); abrupt irregular boundary.

**R** – 40 to 50 cm; 70 percent light grey (5Y 7/2), 30 percent greenish black (10Y 3/1) fractured, hard, serpentinized peridotite; cracks lined with dark grayish brown yellowish red (5YR 5/6) clay films.

**Diagnostic features:** ochric epipedon, 0-18 cm; cambic, 3-40 cm; particle size control section 25 to 40 cm.

## 1.7 Tehama County site profile description

Sampled August 10, 2004 by Donald Greg McGahan. Summit position (3% slope); NW aspect; convex, convex; covered by 90 percent serpentinite rock fragments (70% gravel, 20% cobble); well drained; slow permeability; medium runoff potential; 3042 feet elevation; NE1/4 of Section 33 T. 24 N, R. 7 W. MDB&M; Riley Ridge California quadrangle; NAD83, 39° 53' 53.8 north latitude, 122° 38' 55.0" west longitude.

**TAXONOMIC CLASS:** Loamy, mixed, mesic, shallow Typic Argixeroll

**A** – 0 to 3 cm, brown (7.5YR 4/3) very cobbly sandy clay loam, dark reddish brown (5YR

3/3) moist; moderate, medium, granular structure; slightly hard, slightly sticky, non-plastic; many very fine roots throughout; 25 percent cobbles, 18 percent gravel; slightly acid (pH 6.4); very abrupt wavy boundary.

**Bt1** – 3 to 7 cm, brown (7.5YR 4/4) sandy clay loam, very dark brown (5YR 3/2) moist; moderate, medium, subangular blocky structure; moderately hard, slightly sticky, moderately plastic; many very fine roots throughout; many very fine and medium dendritic tubular pores; many distinct reddish brown (5YR 4/4) clay films on sides and bottom of ped faces; 10 percent gravel; slightly acid (pH 6.1); abrupt wavy boundary.

**Bt2** – 7 to 16 cm, dark brown (7.5YR 3/3) gravelly sandy clay loam, dark brown (7.5YR 3/3) moist; moderate, coarse, angular blocky structure; hard, moderately sticky, very plastic; many fine roots throughout; many fine and medium dendritic tubular pores; many distinct dark reddish brown (5YR 3/2) clay films on all faces of peds and rock fragments; 34 percent (5Y 8/4) and (10Y 8/1) gravels; slightly acid (pH 6.3); very abrupt irregular boundary.

**Cr** – 16 to 60 cm, pink (5Y 8/4), pinkish white (5YR 8/2) and white (10Y 8/1) friable saprolite that crushes to sandy clay loam; common coarse and medium roots matted at top of horizon; many thin to thick distinct dark reddish brown (5YR 3/2) clay films on rocks and saprolite; 30 percent hard cobbles and stones that will not crush easily.

**Diagnostic features:** mollic epipedon 0-16 cm, argillic 3-16 cm, particle size control section 0-16 cm.

## 1.8 Mariposa County site profile description

Sampled July 29, 2003 by Donald Greg McGahan. Summit position (< 3% slope); convex, convex; well drained, moderately slow permeability, medium runoff potential; 2471 feet elevation; about 3 miles northwest of Bagby, above the road on State Route So. 49, SW1/4 of Section 19 T. 3S., R. 16E., MDB&M; Coulterville California topographic quadrangle; WGS NADS83 37° 39' 10" north latitude, 120° 8' 48.9"

**TAXONOMIC CLASS:** Loamy-skeletal, magnesian, thermic Lithic Argixeroll

**A** – 0 to 3 cm; brown (7.5YR 4/3) stony clay loam, very dark brown (7.5YR 2.5/2) moist; weak fine and medium angular blocky parting to weak fine and medium granular structure; medium hard, slightly sticky, very plastic; many very fine roots throughout; many very fine dendritic tubular pores throughout; 15 percent gravel and 10 percent stones; moderately acid (pH 5.9); very abrupt wavy boundary.

**Bt1** – 3 to 14 cm; brown (7.5YR 4/3) very gravelly loam, dark brown (7.5YR 3/2) moist; moderate coarse angular blocky parting to moderate fine angular blocky structure; moderately hard, slightly sticky, very plastic; common very fine roots throughout; common fine dendritic tubular pores; many, faint, continuous, brown (7.5YR 4/3) clay films on bottom of ped faces and on rocks; 23 percent gravels, 15 percent cobbles; moderately acid (pH 6.0); slightly effervescent with hydrogen peroxide, non-effervescent with hydrochloric acid; clear wavy boundary.

**Bt2** – 14 to 34 cm; brown (7.5YR 4/3) extremely gravelly clay loam, dark reddish brown (5YR 2.5/2) moist; moderate medium and fine angular blocky structure; friable, moderately sticky, very plastic; common medium and very fine roots matted

around rocks; common very fine dendritic tubular pores; many, prominent, continuous clay films on bottom of ped faces and on rocks; 36 percent gravels, 35 percent cobbles; slightly alkaline (pH 6.1); slightly effervescent with hydrogen peroxide, non-effervescent with hydrochloric acid; clear wavy boundary.

**Bt3** – 34 to 49 cm; brown (7.5YR 4/3) extremely cobbly clay loam, dark reddish brown (5YR 2.5/2) moist; strong coarse prismatic parting to strong coarse angular blocky structure; moderately sticky, very plastic; many very fine root throughout; common fine dendritic tubular pores; 32 percent gravels, 35 percent cobbles; moderately acid (pH 5.9); abrupt irregular boundary.

**R** – 49 to 60 cm; variegated, 35 percent very dark grey (5Y 3/1), 30 percent olive (5Y 4/3), 20 percent light olive gray (5Y 6/2) and 15 percent black (2.5Y 2/0) fractured, hard, serpentized peridotite; 20 percent pale yellow (5Y 7/3) and 80 percent of cracks lined with distinct, prominent, reddish brown (5YR 4/3) clay films.

**Diagnostic features:** mollic epipedon 0-49 cm, argillic 14-49 cm, particle size control section 14-49 cm.

## 1.9 Mendocino County site profile description

Sampled August 21, 2003 by Donald Greg McGahan. Summit position (3% slope); convex, convex; well drained, moderate permeability, medium runoff potential; 721 feet elevation; MDB&M, Purdys Garden California topographic quadrangle; WGS, NADS83 39° 2' 0.6" latitude north, 123° 6' 53.7" longitude west.

**TAXONOMIC CLASS:** Loamy-skeletal, magnesian, thermic Lithic Argixeroll

**A** – 0 to 2 cm; dark grayish brown (2.5Y 4/2) gravelly silt loam, very dark grayish brown (10YR 3/2) moist; moderate, thin, platy parting to weak fine and very fine, granular structure; soft, slightly sticky, moderately plastic; many very fine roots throughout; 16 percent gravels; non-effervescent with hydrogen peroxide; strongly acid (pH 5.5); very abrupt wavy boundary.

**Bt1** – 2 to 8 cm; dark grayish brown (2.5Y 4/2) gravelly silt loam, very dark gray (10YR 3/1) moist; strong, medium columnar structure; rigid, moderately sticky, very plastic; many very fine roots throughout and matted around rocks; few fine dendritic tubular pores; many, bridging clays between grains and very many prominent continuous clay films on vertical and bottom ped faces; 15 percent gravels; slightly effervescent with hydrogen peroxide; moderately acid (pH 6.0); abrupt wavy boundary.

**Bt2** – 8 to 30 cm; dark grayish brown (2.5Y 4/2) extremely stoney silt loam, black (7.5YR 2.5/1) moist; strong, coarse angular blocky structure; very friable, moderately sticky, moderately plastic; many fine roots matted around rocks; many fine dendritic tubular pores; many clays bridging between sand grains, prominent continuous clay films on rocks; 50 percent gravels, 30 percent stones, 10 percent cobbles; strongly effervescent with hydrogen peroxide; slightly acid (pH 6.2); clear wavy boundary.

**R** – 30 to 70 cm; variegated, 70 percent light greenish grey (5GY 7/1), 30 percent greenish black (10G 2.5/) slightly fractured, hard, serpentized peridotite; 90 percent of cracks lined with distinct, prominent, dark grayish brown (2.5Y 4/2) clay films.

**Diagnostic Features:** mollic epipedon 0-30 cm; argillic horizon 2-30 cm; particle size control section 0-30 cm.

## **1.10 Shasta-Trinity National Forest site profile description**

Sampled July 17, 2003 by Donald Greg McGahan and Julie Baker. Summit position (1 % slope); SW aspect; convex, convex; covered 90 percent by variegated 15 percent very dark gray (10YR 3/1), 35 percent gray (10YR 5/1), 15 percent pink (5YR 8/4), 25 percent light greenish gray (5GY 8/1) dry serpentinized peridotite rock fragments mostly less than 5 cm in diameter; well drained; slow permeability; medium runoff potential; 3795 feet elevation; about ¼ mile southeast on Forest Road 28N07 off of Forest Road 28N10; NE ¼ Section 5 T. 28 N., R. 10 W. MDB&M; Pony Buck Peak topographic quadrangle; WGS NAD83, 40° 18' 44.2" north latitude, 123° 0' 43.7" west longitude.

**TAXONOMIC CLASS:** Clayey, magnesian, mesic, shallow Typic Argixeroll

**A1** – 0 to 2 cm; reddish brown (5YR 4/3) gravelly loam, dark reddish brown (5YR 3/3) moist; moderate very fine granular structure; slightly sticky, slightly plastic; 17 percent gravel; very slightly effervescent with hydrogen peroxide; slightly acid (pH 6.1); very abrupt smooth boundary.

**A2** – 2 to 5 cm; dark reddish brown (2.5YR 3/3) loam, very dark grayish brown (2.5YR 3/2) moist; strong coarse angular blocky parting to very fine granular structure; slightly hard, slightly sticky, slightly plastic; many very fine and few fine roots throughout; many medium irregular pores; 3 percent gravel, 10 percent cobbles;

strongly effervescent with hydrogen peroxide; slightly acid (pH 6.2); clear wavy boundary.

**AB**– 5 to 12 cm; reddish brown (5YR 4/3) clay, dark reddish brown (5YR 3/2) moist; strong coarse subangular blocky parting to moderate medium angular blocky structure; hard, moderately sticky, very plastic; many medium roots throughout, common coarse and many fine roots matted at top of horizon; common fine dendritic tubular pores; many prominent continuous organic stained clay films on rock faces; 9 percent gravels; strongly effervescent with hydrogen peroxide; moderately acid (pH 5.8); abrupt wavy boundary.

**Bt1** – 12 to 23 cm; reddish brown (5YR 4/3) clay, dark brown (7.5YR 3/3) moist; moderate fine and medium angular blocky structure; firm, moderately sticky, very plastic; common very coarse roots matted at top of horizon, common medium roots throughout; common fine dendritic tubular pores; many distinct continuous clay films on ped faces; 5 percent gravels; very slightly effervescent with hydrogen peroxide; strongly acid (pH 5.5); clear wavy boundary.

**Bt2** – 23 to 40 cm; reddish brown (5YR 4/3) clay, dark brown (7.5YR 3/3) moist; strong medium prismatic parting to strong medium angular blocky structure; rigid, moderately sticky, very plastic; common coarse roots at top of horizon and common medium roots throughout; many prominent continuous clay films on ped faces, few distinct slickensides at bottoms of prisms; 5 percent gravel; very slightly effervescent with hydrogen peroxide; strongly acid (pH 5.3); clear irregular boundary.

**Cr** – 40 to 55 cm; variegated, 60 percent reddish brown (5YR 5/4) moist, 25 percent strong brown (7.5Y 4/6) moist, and 15 percent greenish gray (10Y 6/1) moist friable saprolite that crushes to sandy clay loam; common medium roots; clear irregular boundary.

**R** – 55 to 75 cm; hard serpentized peridotite. 85 percent light grey (2.5Y 7/2), 15 percent greenish black (10GY 2.5/1) fractured, hard, serpentized peridotite; cracks lined with clay films.

**Diagnostic Features:** mollic epipedon 0-40 cm, argillic horizon 5-40 cm, particle size control section 5-40 cm, Cr horizon is easily penetrated by roots at a frequency less than 10 cm excluding the top of the horizon.

## 1.11 Los Padres National Forest site profile description

Sampled September 10, 2003 by Donald Greg McGahan. Summit position (1% slope); NNW aspect; convex, convex; 4052 feet elevation; WGS, NAD83 34° 43' 21.4" north latitude, 119° 58' 1.4" west longitude.

**Taxonomic Class:** Loamy-skeletal, magnesian, mesic Lithic Haploxeroll

**A** – 0 to 18 cm; brown (10YR 4/3) very gravelly sandy clay loam, dark reddish brown (2.5YR 3/2) moist; moderate fine subangular blocky structure; soft, non-sticky, non-plastic; common fine roots matted around rock fragments; many, distinct, clay films on rock fragments; 46 percent gravels; slightly acid (pH 6.2); abrupt irregular boundary.

**R** – 18 to 25 cm; hard serpentized peridotite 80 percent greenish grey (5GY 6/1), 15



percent dark greenish grey (5GY 4/1), 5 percent dark greenish grey (5GY 3/1); fractured, hard, serpentinized peridotite; 35 percent of cracks lined with brown (10YR 4/3) clay films.

**Diagnostic Features:** Mollic epipedon 0-18 cm, particle size control section 0-18 cm.

# CHAPTER 2: XENOLITHS IN SERPENTINITE LANDSCAPES CONTRIBUTE CA AS A PLANT NUTRIENT

## 2.1 ABSTRACT

Serpentine derived soils give rise to botanically distinct systems primarily as a result of inadequate Ca content of the parent material. We hypothesized that Ca content varies widely in what is nominally referred to as serpentine. The Ca:Mg of  $<0.7$  is often used to relate the imbalance of these elements in serpentine derived soils, and frequently the ratio is reported without indicating if it is a measure of total or extractable Ca and Mg contents. We sampled 6 parent materials and soils across California in Henneke soil series (Clayey-skeletal, magnesian, thermic Lithic Argixerolls) map unit polygons, that contained the series modal location for each of the soil survey areas. Total elemental analyses of the rocks underlying the soils showed CaO% varied from 1.0 to 230 mg kg<sup>-1</sup>, and CaO:MgO varied from  $<0.1$  to 4. A combination of X-ray diffraction (XRD), polarized light microscopy (PLM), and electron microscopy was used to identify the Ca-bearing accessory minerals clinopyroxene (diopside), ugrandite garnets (grossularite and andradite), and calcic clinopyroxene (tremolite). Accessory mineral content was often too low to be detected by XRD, or minerals were too finely disseminated and difficult to detect in thin section by

PLM. Electron microscopy in concert with XRD and PLM were needed to fully characterize the mineral assemblage. Serpentinite parent material characterization should include screening for ugrandite garnets, as they were a common Ca-bearing accessory mineral in some of the serpentinites. Rock materials at two sites, Napa and Tehama Counties, were xenolithic inclusions in the serpentinite landscape and contained no serpentine minerals, and are therefore not serpentinites. The Napa County rocks contained almost no Ca-bearing minerals and probably would be identified as a serpentinite if relying upon elemental analysis and CaO:MgO alone. The inclusion of xenoliths in the landscape, and to a lesser extent Ca-bearing accessory minerals, has the potential of acting as landscape fertilizers of calcium.

## **2.2 INTRODUCTION**

Serpentinized ultramafic lithologies give rise to botanically distinct systems (Walker, 1948). Debates have abounded regarding edaphic influences for this effect, but the Ca:Mg has been used to relate the high Mg and low Ca condition that exists in these soils. Early researchers attributed Mg toxicity to the poor growth of vegetation on serpentine soils (Loew and May, 1901; Gorden and Lipman, 1926). Vlamis and Jenny (1948) demonstrated that calcium deficiency, rather than magnesium toxicity, was the primary cause of poor plant growth. Walker et al. (1955) demonstrated that non-native species yields were reduced when the exchangeable Ca was 20% or less, and had little or no growth or yield below 10% exchangeable Ca. Native plant species, however, were better able to extract Ca, and yield was only reduced 24% in the 5 to 3% exchangeable Ca range; non-native plant species had a 90% yield reduction. Soils dominated by Mg-silicates, with a potential Ca

deficiency and its resulting effects on plant growth in agriculture or native settings are recognized in Soil Taxonomy at the family mineralogical class as “magnesian” (Soil Survey Staff, 1999). Identification of magnesium silicates requires X-ray diffraction (XRD) and polarized light microscopy (PLM). Still, total or extractable Ca:Mg has been a sometimes useful indicator of serpentinite-derived soils. An extractable Ca:Mg of 0.7 or greater is generally desired for agricultural crop production (Brooks, 1987).

Serpentinite is a product of the low temperature and pressure metamorphism/metasomatism of ultramafic rocks. Metasomatism is a process of indefinite elemental replacement, loss and/or addition of elements as a result of percolating solutions (Merill, 1906). As a result, during metamorphism or metasomatism, the anhydrous peridotite minerals become more hydrous, and calcium content decreases relative to the original rocks, resulting in a relative enrichment of magnesium (Page, 1966, Page, 1967; Coleman and Keith, 1971). Olivine is the dominant mineral in peridotite, the idealized serpentinite precursor, and is readily altered to serpentine during metasomatism. Serpentinous pseudomorphs after the peridotite accessory chain and layer silicates pyroxene, talc, and amphibole are commonly identified in thin section studies of serpentinitized rocks. These pseudomorphs in serpentinites are called bastites (Merrill, 1906; Wicks and Whittaker, 1977; O’Hanley, 1996). Wicks and Whittaker (1977) assert that bastites should be considered a textural, rather than a mineralogical term because once serpentinitization is complete it is often impossible to distinguish a pyroxene bastite from a amphibole bastite. But, if distinguishable, bastites after clinopyroxene or calcic-clinoamphibole may indicate that, prior to metasomatism, the peridotite contained more Ca than if the bastites identified in the serpentinite were after orthopyroxene or orthoamphibole. Pyroxene and amphibole are less susceptible to

serpentinization than olivine, and it is feasible that not all the Ca in the clinopyroxene/clinoamphibole was completely removed from the lithologic unit during metasomatism. Together with metamorphic secondary minerals, such as garnets that may contain calcium, it is reasonable to assume that the Ca content of soils on serpentinitic landscape is variable and, therefore, influences plant nutrient supplying status as a result of serpentinite weathering.

Less mafic lithic inclusions in serpentinite landscapes can influence the total and extractable Ca:Mg contents of the bulk parent material and the soil. Rabenhorst and Foss (1981), attempted to predict mafic or ultramafic parent lithology while mapping soils of the eastern Piedmont of Maryland. Based on their study of 39 samples, if the exchangeable Ca:Mg ranged from 0.0 to 0.1, the probability that the soil was formed from serpentinite rather than a mafic lithology was 98%. A Ca:Mg of 0.2 to 0.3 yielded a probability of 53%, whereas a 0.6 to 0.7 Ca:Mg reduced the probability to 21%. Clearly at Ca:Mg ratios greater than 0.3 the likelihood that the soil is derived solely from ultramafic parent material is low.

A basic question is “Do some lithologies underlying serpentinitic landscapes contain Ca-bearing minerals that can significantly alter extractable Ca:Mg?” This paper reports on the variation in parent material mineralogy beneath magnesian pedons, nominally serpentinite, throughout California. This focus on bulk mineralogy and Ca-bearing accessory mineralogy of the parent material is necessary as a prerequisite to follow-on studies of soil morphology at these sites. We expect to find a variation in accessory minerals, specifically Ca-bearing minerals, in these nominally serpentine parent materials and that these accessory minerals have a profound influence on the total and extractable Ca:Mg ratios in the soils weathered from the serpentinites.

## **2.3 MATERIALS AND METHODS**

### **2.3.1 Field**

Sampling locations were from 6 California soil survey areas within Henneke soil series (Clayey-skeletal, magnesian, thermic Lithic Argixerolls) map units (Fig. 2-1). These are soils formed in material weathered from serpentine and rocks of similar mineralogy (Soil Survey Staff, 2005). We sampled pedons near the location of the modal pedon for the Henneke series for each soil survey. To minimize the impacts of colluviation we sampled pedons on summits above the modal pedon location and within the polygon containing the modal location. Pits were excavated by hand tools. Soils were described and sampled by horizon using conventional procedures, and rocks samples were collected within the Cr and/or R horizons (Soil Survey Division Staff, 1993).

### **2.3.2 Laboratory**

Three rocks from each parent material were ground with a agate mortar and pestle to pass a 140-mesh sieve. The rock powders were mounted on porous ceramic tiles, washed with  $MgCl_2$  or KCl salt solutions, rinsed with deionized water to remove excess salts, then reoriented by smoothing with a glass slide held at an angle to the sample. X-ray analyses were made with a Diano XRD 8000 diffractometer (Diano Corporation, Woburn, MA) producing Cu K radiation fitted with a nickel filter and curved graphite monochromator. After the initial diffraction analysis, the  $MgCl_2$  treated samples were treated with glycerol and reanalyzed. The KCl samples were reanalyzed after 350°C and 550°C heat treatments (Whittig and Allardice, 1986). Major oxide content of the rock powders was determined by ICP-

emission spectrometry following a  $\text{LiBO}_2$  fusion and dilute nitric acid digestion (Sawhney and Stilwell, 1994).

Three rock samples from each R or Cr horizon were impregnated with Petropoxy-154 resin (Palouse Petro Products, Palouse, WA). Thin sections of these samples were prepared and examined with a polarizing light microscope (PLM) (Drees and Ransom, 1994; Stoops, 2003). Selected thin-sections were polished, and analyzed using back scatter electron-microscopy (BSE) and energy dispersive x-ray spectroscopy (EDX) on a Cameca SX-100 electron probe microanalyzer (Cameca, Paris, France).

## **2.4 RESULTS AND DISCUSSION**

### **2.4.1 Non-serpentinites with bastites**

Napa and Tehama County parent materials were not dominated by serpentine minerals and, therefore, not serpentinites. The Tehama and Napa County parent materials contained bastites after a calcic clinopyroxene, but were quite different in the amounts of the remainder of the parent material mineral suite.

#### **2.4.1.1 Tehama County**

The Tehama County parent material contained garnet (0.299 and 0.266 nm peaks), clinopyroxene (0.32 nm peak), hydroxy-interlayered-material (HIM) (1.4nm peak), and pumpellyite (0.29 nm peak). The HIM was characterized by a 1.4 nm Mg-saturated peak, that collapses with K-saturation and heating treatments leaving a plateau of peaks between 1.4 nm and 1.0 nm (Fig. 2-2 A).

Garnets have the idealized formula of  $X_3Y_2(SiO_4)_3$  and are further divided into the pyralspite and grandite (or ugrandite) groups where Y is Al, X is Ca in the grandite group, and X is not Ca in the pyralspite group (Table 2-2). EDX of the Tehama County garnet corroborated XRD results indicating that the garnet was grossularite of the ugrandite group (Fig. 2-3 A).

In thin-sections with plane-polarized light at lower magnifications, the small euhedral interlocking grains of grossularite were nearly indistinguishable and formed large cinnamon-brown, somewhat granular masses (Fig. 2-4 A). The masses were isotropic under crossed polarizers (Fig. 2-4 B).

Pyroxene is a common inclusion in ultramafic serpentinite protoliths and is more resistant to alteration than is olivine, the most common mineral in the ultramafic protolith. The idealized formula for pyroxene is  $XYSi_2O_6$ . Clinopyroxene is distinguished optically from orthopyroxene by inclined, rather than parallel, extinction and by its higher interference colors as viewed in cross polarized light. For orthopyroxene, X is Mg and/or Fe, but for clinopyroxene X is Ca, Na, Li, and therefore, a potential calcium source upon weathering (Table 2-3).

The clinopyroxene diopside was identified in thin-sections by inclined extinction (Fig. 2-4 C and D). The clinopyroxene was determined by EDX to be a member of the diopside-hedenbergite series with considerably greater Ca than Fe and therefore may be referred to as diopside (Fig. 2-3 B).

Pumpellyite, a sorosilicate, (idealized formula  $Ca_2MgAl_2(SiO_4)(Si_2O_7)(OH)_2 \cdot (H_2O)$ ) could be easily missed in the x-ray diffractogram and was not identified in thin-section, but



EDX confirmed the presence of the pumpellyite (Fig. 2-3 C). The BSE micrograph clearly shows that it was inter-grown with the HIM (Fig. 2-4 F), and HIM chemistry was confirmed by EDX (Fig. 2-3 F).

Among the six parent materials, the Ti and Al contents were highest in the Tehama County parent material, while Si content was the lowest (Table 2-1). The Ti was a trace element in grossularite (Fig. 2-3 A), but was a major element in ilmenite and titanite (Fig. 2-3 D and E). Titanite (sphene) was finely disseminated and associated with the diopside (Fig. 2-2 E).

Grandite garnets are characteristic of rodingites (Coleman, 1979, 1980). Rodingites are the result of small-scale, localized metasomatism of non-peridotites in association with the metasomatic alteration of peridotites to serpentinite. These rodingites can be xenoliths within the serpentinite mass, or can occur at metasomatic contacts with the country rock. The replacement or invasion by calcsilicate minerals, such as Ca-garnets, into the protomineralogy of the xenolith is coupled with the calcium lost from the peridotite during metasomatism. Chlorite and calcic clinopyroxenes are commonly associated with grandite garnets in rodingites (Coleman, 1979, 1980). This mineral suite fits well with the observed mineralogy of the Tehama County parent material, which was dominated by grossularite, and also contained calcic clinopyroxene. The HIM in the parent materials is probably the result of interlayer stripping from a precursor chlorite in the hard rock underlying the Cr layer we analyzed.

Rodingites are not serpentinites, but probably occur frequently enough in serpentinitic landscapes to supply significant amounts of calcium to the soil solution upon weathering. The calcium resulting from rodingite xenolith weathering clearly could have a significant

impact on plant growth and plant community composition. Ca-bearing xenoliths, especially at topographically higher locations, may have a large impact on down-slope soil solution Ca content and may provide colluvium that has mineralogy significantly different from the underlying rock.

#### **2.4.1.2 Napa County**

Napa County parent material was dominantly vermiculite (1.4 nm peak with Mg treatment collapsed to 1.0 nm with K treatment and heat) and plagioclase feldspar (0.630, 0.374, 0.365, 0.318, 0.293 nm peaks) (Fig. 2-2 E). EDX confirms that the plagioclase was albite (Fig. 2-5 D).

A pyroxene XRD peak is not evident, but a pyroxene with inclined extension was clearly identified by PLM (Fig. 2-5 A and B). The clinopyroxene, like the clinopyroxene in Tehama County parent material, contained more Ca than Fe, and had a small amount of Al (Fig. 2-5 E). The vermiculite contained more Al and less O (Fig. 2-5 F) than the Tehama County HIM (Fig. 2-3 F). The dominant source of Ca was most likely the diopside identified by PLM and electron microscopy (Fig. 2-5 E). This mineral was not identified by XRD, and therefore, only a minor component of the parent material (Fig. 2-2 E). Low abundance of diopside, together with high vermiculite content, was likely responsible for a  $\text{CaO}:\text{MgO} < 0.1$  (Table 2-1). Napa County parent material contains no detectable serpentine. It was, therefore, not a serpentinite. It did not have Ca-garnets and was not a rodingite. It was an example of a mafic xenolithic inclusion in the serpentinitic terrain. Weathering of this parent material resulted in soil Ca enrichment (extractable and total Ca:Mg of 1.3),

likely as a result of rapid weathering of the plagioclase feldspar and biocycling of the Ca as the diopside weathered (McGahan, 2007).

## **2.4.2 Serpentinites with bastites**

### **2.4.2.1 Shasta County**

Shasta County parent material was dominated by serpentine (XRD peaks at 0.724, 0.455, 0.362 nm) and talc (0.93, 0.466, 0.31 nm peaks) with a sub dominant component of chlorite (persistent 1.425 nm peak and 0.475, 0.71, 0.355 and 0.284 nm peaks) (Fig. 2-2 C). Not identified by XRD, but clearly distinguishable in thin sections by PLM and BSE, was calcic clin amphibole (Fig. 2-6 A, B and C) probably tremolite, as confirmed by EDX (Fig. 2-6 D).

Tremolite contains Ca, and yet the CaO% content of the parent material was very low (Table 2-1), and therefore, the tremolite was probably not an abundant accessory component of the rock.

### **2.4.2.2 Glenn County**

Glenn County parent material was dominated by serpentine (0.731, 0.457, 0.363 and 0.250 nm peaks) with a trace of magnetite (0.253 nm peak) (Fig. 2-2 D). Enstatite was not identified by XRD, but was clearly identified by PLM by its parallel extinction (Fig. 2-7 A, B and C). The enstatite was intergrown with iron oxide (Fig. 2-7 D). EDX confirmed it contained no Ca (Fig. 2-8).

The CaO% content of Glenn County parent material was similar to the CaO% content of Shasta County parent material (Table 2-1), and no Ca containing minerals were identified in the Glenn County parent materials in this study.

### **2.4.3 Serpentinites without bastites**

#### **2.4.3.1 Kings County**

Kings County parent material was dominated by serpentine (0.724, 0.455, 0.363 and 0.250 nm) (Fig. 2-2 B). There were also traces of andradite garnet (0.302, 0.271 and 0.246 nm), and magnetite (0.297 and 0.253 nm XRD peaks) detected by XRD (Fig. 2-2 B). The andradite XRD peaks were very weak and could easily be missed. PLM clearly shows garnet amongst the serpentine and was interspersed with magnetite (Fig. 2-9 B & D). The iron content of andradite increases back-scattered electron fluorescence, and therefore, may easily be mistaken for magnetite in BSE images (Fig. 2-9 C). Andradite could be easily distinguished from magnetite by PLM, EDX analysis or by adjusting the contrast of the BSE image (Fig. 2-9 D).

The serpentine EDX was representative of serpentine in all parent materials where it was identified (Fig. 2-10 B). The talc (idealized formula  $Mg_3Si_4O_{10}(OH)_2$ ) was not identified by XRD, but could be seen in thin-section by PLM and in BSE images (Fig. 2-9 A and B). The talc chemistry was confirmed by EDX (Fig. 2-10 A). Magnetite chemistry was also confirmed by EDX (Fig. 2-10 D). The garnet was confirmed as andradite by EDX and had more Fe than grossularite (Fig. 2-10 C; Table 2-1). Unlike the grossularite in the Tehama county parent material, the andradite garnet in Kings County occurred as individual crystals or in small clusters in the dominantly serpentine Kings County parent material (Fig. 2-9 B).

Talc does not contribute to soil calcium (Fig. 2-10 A), nor does serpentine (Fig. 2-10 B), but the andradite would contribute to the soil solution Ca upon weathering (Fig. 2-10 C). The total Ca content was far less ( $3.2 \text{ mg kg}^{-1}$ ) in the Kings County parent material than in the Tehama County parent material ( $229 \text{ mg kg}^{-1}$ ), and the CaO:MgO is markedly lower ( $<0.1$ ) than for Tehama County parent material (4.0) (Table 2-1).

#### **2.4.3.2 San Benito County**

San Benito County parent material is dominated by serpentine (0.73, 0.45, 0.36 0.27 nm peaks) (Fig. 2-2 F). No accessory chain silicates were identified. PLM clearly identifies opaque inclusions (Fig. 2-11 A and B). The opaque minerals seen in PLM are resolved by BSE and EDX to be magnetite, chromite spinel, and chromium-rich andradite garnet (Fig. 2-11).

The XRD of San Benito County showed only serpentine and spinels, and no pyroxene basaltites were identified by PLM (Fig. 2-2 F). With EDX, however, we were able to determine that the chromium rich andradite garnet was contributing to a CaO% content of  $14 \text{ mg kg}^{-1}$  (Table 2-1, Fig. 2-11 E).

## **2.5 IMPLICATIONS FOR CA SUPPLY AND PLANT GROWTH**

We asked, how do you know if a soil is derived from serpentinite? The simple answer is to characterize the parent material and insure it is dominated by serpentine minerals. If a parent material is dominated by serpentine minerals, and therefore a serpentinite, could it still contain calcium-bearing minerals? Do accessory minerals influence the Ca:Mg?

Elemental analysis clearly demonstrated that Ca content was variable on nominally serpentinite landscapes. The parent material of two out of six pedons contained no serpentine minerals. One parent material, Tehama County, had abundant Ca-bearing minerals and the other, Napa County, contained very few Ca-bearing minerals.

It is clear that reliance solely on CaO:MgO from parent material analysis would have incorrectly identified the Napa County parent material as serpentinite. It was not a serpentinite and despite the low parent material total CaO:MgO ( $< 0.01$ ), the soils derived from it had relatively high (1.3) extractable Ca:Mg.

Further complicating interpretation of the CaO:MgO is the fact that serpentinite parent materials can contain Ca-bearing minerals. XRD was not able to identify Ca-bearing trace accessory minerals in many of the parent materials. Kings, Shasta, and San Benito Counties parent materials were examples of serpentinites that had no obvious accessory minerals, other than magnetite, as detected by XRD. They did have trace accessory minerals detected by PLM and/or BSE and EDX. Weathering of these parent materials, like the non-serpentinite xenoliths such as rodingites and mafics, could result in down-slope Ca enrichment. Their impact would be further varied based on slope dynamics down-slope e.g., water gathering versus water spreading landscape positions.

With other supporting analysis such as PLM and electron microscopy we identified the minerals contributing to calcium fertilization: clinopyroxene (diopside), ugrandite garnets (grossularite and andradite), and calcic clinoamphibole (tremolite). Ugrandite garnets were a common Ca source in serpentinites and rodingites. Identification of these Ca-bearing accessory minerals by a screening process could be especially beneficial to researchers

investigating “serpentine soil” to avoid anomalous results arising from xenolith inclusions on serpentinitic landscapes, or calcic accessory minerals in serpentinites. The inclusion of xenoliths in the landscape, and to a lesser extent Ca-bearing accessory minerals, has the potential of acting as landscape fertilizers of calcium. Landscape managers or revegetation efforts may also benefit from identification of site sources of calcium, as it may help to adjust practices of managing amendment application rates.

## 2.6 REFERENCE

- Brooks, R.R. 1987. *Serpentine and its vegetation: a multidisciplinary approach*. Dioscorides Press, Portland, Or.
- Coleman, R.G., and T.C. Keith. 1971. A chemical study of serpentization: Burro Mountain, California. *Journal of Petrology* 12:311-328.
- Coleman, R.G. 1979. Tectonic inclusions in serpentinites. p. 89-102. *In* J. Bertrand and J. Deferne (eds.), *Proceedings symposium on tectonic inclusions and associated rocks in serpentines*. Swiss National Science Foundation, Geneva. September 17-29 1979.
- Coleman, R.G. 1980. Ophiolite tectonics and metamorphism. p. 167-184. *In* J. Aubouin and C.J. Allegre (ed.), *Colloques internationaux du centre national de la recherche scientifique; No. 272; orogenic mafic ultra mafic association*. Grenoble June 6-11 1977, Paris, France.
- Drees, L.R., and M.D. Ransom. 1994. Light microscope techniques in quantitative soil mineralogy. p. 137-176. *In* J. E. Amonette and L. W. Zelazny, (ed.) *Quantitative methods in soil mineralogy* SSSA Miscellaneous Publication. Soil Science Society of America, Madison, WI., USA.

- Gordon, A., and C.B. Lipman. 1926. Why are serpentine and other magnesian soils infertile? *Soil Science* 22:291-302.
- Hurlbut, C.S., and C. Klein. 1977. *Manual of mineralogy* (after James D. Dana). John Wiley and Sons, New York.
- Loew, O., and D.W. May. 1901. The relation of lime and magnesia to plant growth. I. Liming of soils from a physiological standpoint. II Experimental study of the relation of lime and magnesia to plant growth. U.S. Dept. Arg., Plant Indus. Bull. 1, 53.
- McGahan, Donald G. 2007. A survey of soils formed on serpentinitic landscapes in California. Ph.D. diss. University of California Davis.
- Merrill, G.P. 1906. *A treatise on rocks, rock-weathering and soils*. New ed. Macmillan, New York, London.
- O'Hanley, D.S. 1996. *Serpentinites: records of tectonic and petrological history*. Oxford University Press, New York.
- Page, N.J. 1966. Mineralogy and chemistry of the serpentine group minerals and the serpentinization process. Ph.D. diss. University of California Berkeley.
- Page, N.J. 1967. Serpentinization considered as a constant volume metasomatic process: a discussion. *The American Mineralogist* 52:545-549.
- Rabenhorst, M.C., and J.E. Foss. 1981. Soil and geologic mapping over mafic and ultramafic parent materials in Maryland. *Soil Science Society of America Journal* 45:1156-1160.
- Sawhney, B.L., and D.E. Stilwell. 1994. Dissolution and elemental analysis of minerals, soils and environmental samples, p. 49-82, *In* J. E. Amonette and L. W. Zelazny, (ed.)



- Quantitative methods in soil mineralogy SSSA Miscellaneous Publication. Soil Science Society of America, Madison, WI., USA.
- Soil Survey Division Staff. 1993. Soil survey manual - agriculture handbook No. 18. U.S. Dept. of Agriculture: Supt. of Docs. U.S. G.P.O., Washington, DC.
- Soil Survey Staff. 2005. Official soil series descriptions [Online WWW]. Available URL: “<http://soils.usda.gov/technical/classification/osd/index.html>” [Accessed 10 February 2005].
- Soil Survey Staff. 1999. Soil Taxonomy, a basic system of soil classification of making and interpreting soil surveys. USDA-NRCS, Washington D.C.
- Stoops, G. 2003. Guidelines for analysis and description of soil and regolith thin sections. Soil Science Society of America, Madison, Wisconsin.
- Vlams, J., and H. Jenny. 1948. Calcium deficiency in serpentine soils as revealed by absorbent technique. *Science* 107:549.
- Walker, R.B. 1948. A study of serpentine soil infertility with special reference to edaphic endemism. Ph.D. diss. University of California, Berkeley.
- Walker, R.B., H.M. Walker, and P.R. Ashworth. 1955. Calcium-magnesium nutrition with special reference to serpentine soils. *Plant Physiology* 30:214-221.
- Whittig, L.D., and W.R. Allardice. 1986. X-ray diffraction techniques. In: A. Klute (Ed.), *Methods of soil analysis: part 1 physical and mineralogical methods*. American Society Agronomy, Madison, WI., pp. 331-362.
- Wicks, F.J. and E.J Whittaker. 1977. Serpentine textures and serpentinization. *Canadian Mineralogist*. 459-488.

**Table 2-1.** Content of selected elements in serpentinite parent material rocks beneath the 6 pedons.

Survey Area						
	Tehama County 16 to 60 cm	Kings County 40 to 50 cm	Shasta County 40 to 50 cm	Glenn County 34 to 55 cm	Napa County 20 to 52 cm	San Benito County 50 to 70 cm
	mg kg <sup>-1</sup>					
SiO <sub>2</sub>	363	498	423	387	390	394
Al <sub>2</sub> O <sub>3</sub>	151	11	9.0	3.8	23	5.4
Fe <sub>2</sub> O <sub>3</sub>	84	95	84	110	101	91
MgO	57	248	331	325	319	352
CaO	229	3.2	1.0	1.4	0.2	4.4
Na <sub>2</sub> O	<0.1	0.1	0.3	0.2	0.1	<0.1
K <sub>2</sub> O	<0.2	0.3	<0.2	<0.2	<0.2	<0.2
TiO <sub>2</sub>	15	0.2	0.2	<0.1	0.2	<0.1
P <sub>2</sub> O <sub>5</sub>	2.6	0.5	0.6	0.6	0.8	0.4
MnO	1.3	1.3	0.8	1.5	1.4	1.0
Cr <sub>2</sub> O <sub>3</sub>	0.3	4.5	3.7	4.5	5.3	4.2
CaO:MgO	4.0	<0.1	<0.1	<0.1	<0.1	<0.1
LOI	95	135	142	160	149	134

LOI = loss on ignition

**Table 2-2.** Chemical composition of garnets. Reproduced after Hurlbut and Klein, 1977.

Pyralspite Group	
Pyrope	Mg <sub>3</sub> Al <sub>2</sub> Si <sub>3</sub> O <sub>12</sub>
Almandite	Fe <sub>3</sub> Al <sub>2</sub> Si <sub>3</sub> O <sub>12</sub>
Spessartite	Mn <sub>3</sub> Al <sub>2</sub> Si <sub>3</sub> O <sub>12</sub>
Ugrandite Group	
Grossularite	Ca <sub>3</sub> Al <sub>2</sub> Si <sub>3</sub> O <sub>12</sub>
Andradite	Ca <sub>3</sub> Fe <sub>2</sub> Si <sub>3</sub> O <sub>12</sub>
Uvarovite	Ca <sub>3</sub> Cr <sub>2</sub> Si <sub>3</sub> O <sub>12</sub>
Hydrogrossularite	Ca <sub>3</sub> Al <sub>2</sub> Si <sub>3</sub> O <sub>8</sub> (SiO <sub>4</sub> ) <sub>1-m</sub> (OH) <sub>4m</sub> m = 0-1

**Table 2-3.** Chemical composition of pyroxenes and amphiboles. Reproduced after Hurlbut and Klein, 1977.

	W	X	Y	Examples
Orthopyroxene XYSi <sub>2</sub> O <sub>6</sub>		Mg, Fe	Mg, Fe	Enstatite
Clinopyroxene XYSi <sub>2</sub> O <sub>6</sub>		Ca, Na, Li	Mg, Fe, Al	Diopside
Orthoamphibole W <sub>0-1</sub> X <sub>2</sub> Y <sub>5</sub> Si <sub>8</sub> O <sub>22</sub> (OH) <sub>2</sub>		Mg, Fe	Mg, Fe, Al	Anthophyllite
Clinoamphibole W <sub>0-1</sub> X <sub>2</sub> Y <sub>5</sub> Si <sub>8</sub> O <sub>22</sub> (OH) <sub>2</sub>	Na, K	Ca, Na	Mg, Fe, Al, Ti	Tremolite

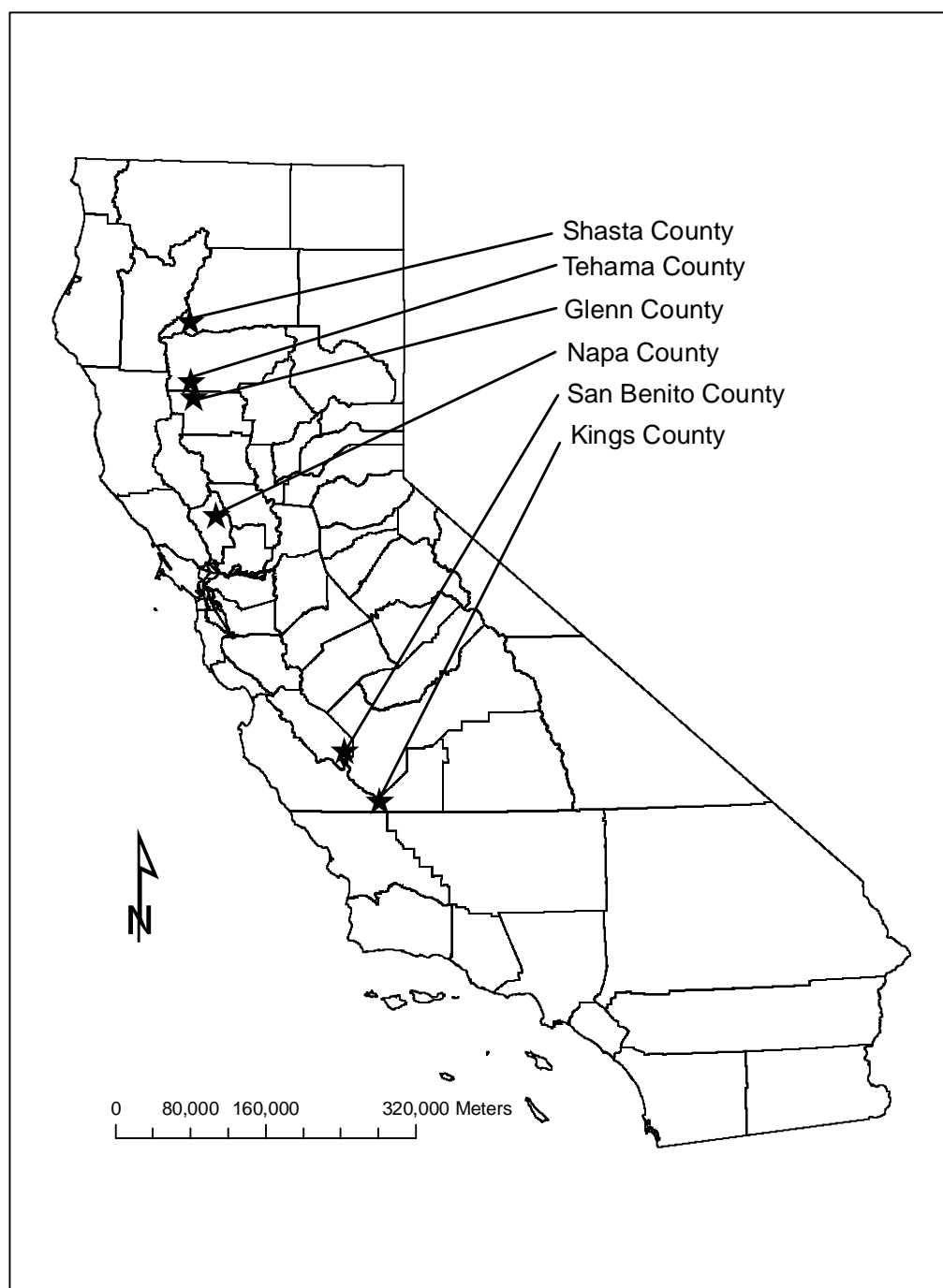


**Figure 2-1.** Pedon sampling locations from 11 California soil survey areas within Henneke soil series (Clayey-skeletal, magnesian, thermic Lithic Argixerolls) map units.

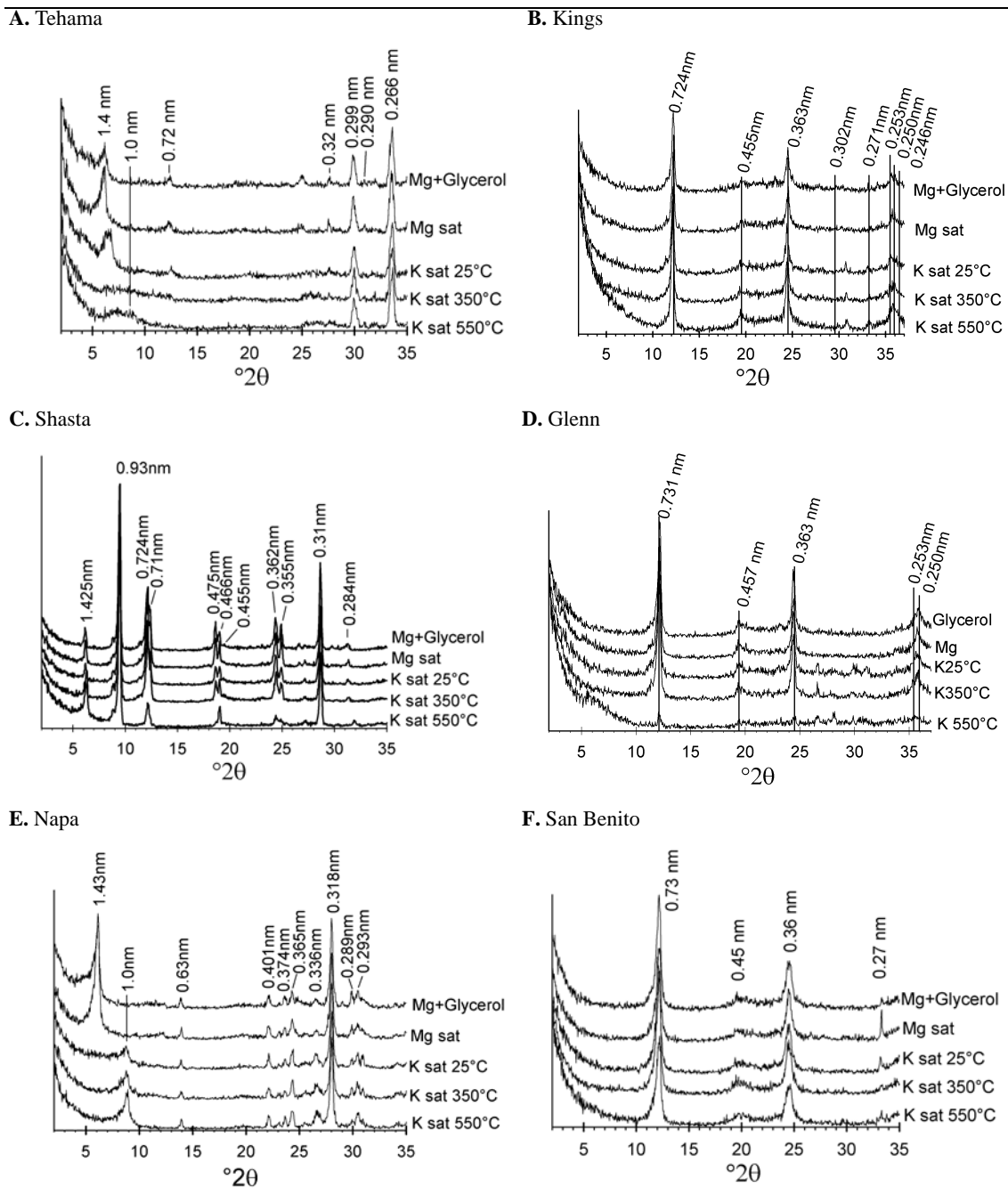


**Figure 2-2.** X-ray diffractograms of serpentine parent materials. **A.** Tehama County: hydroxy-interlayered-material, grossularite, diopside, and pumpellyite. **B.** Kings County: serpentine, andradite, and magnetite. **C.** Shasta County: serpentine, talc, and chlorite. **D.** Glenn County: serpentine and magnetite. **E.** Napa County: vermiculite and albite plagioclase. **F.** San Benito: serpentine.

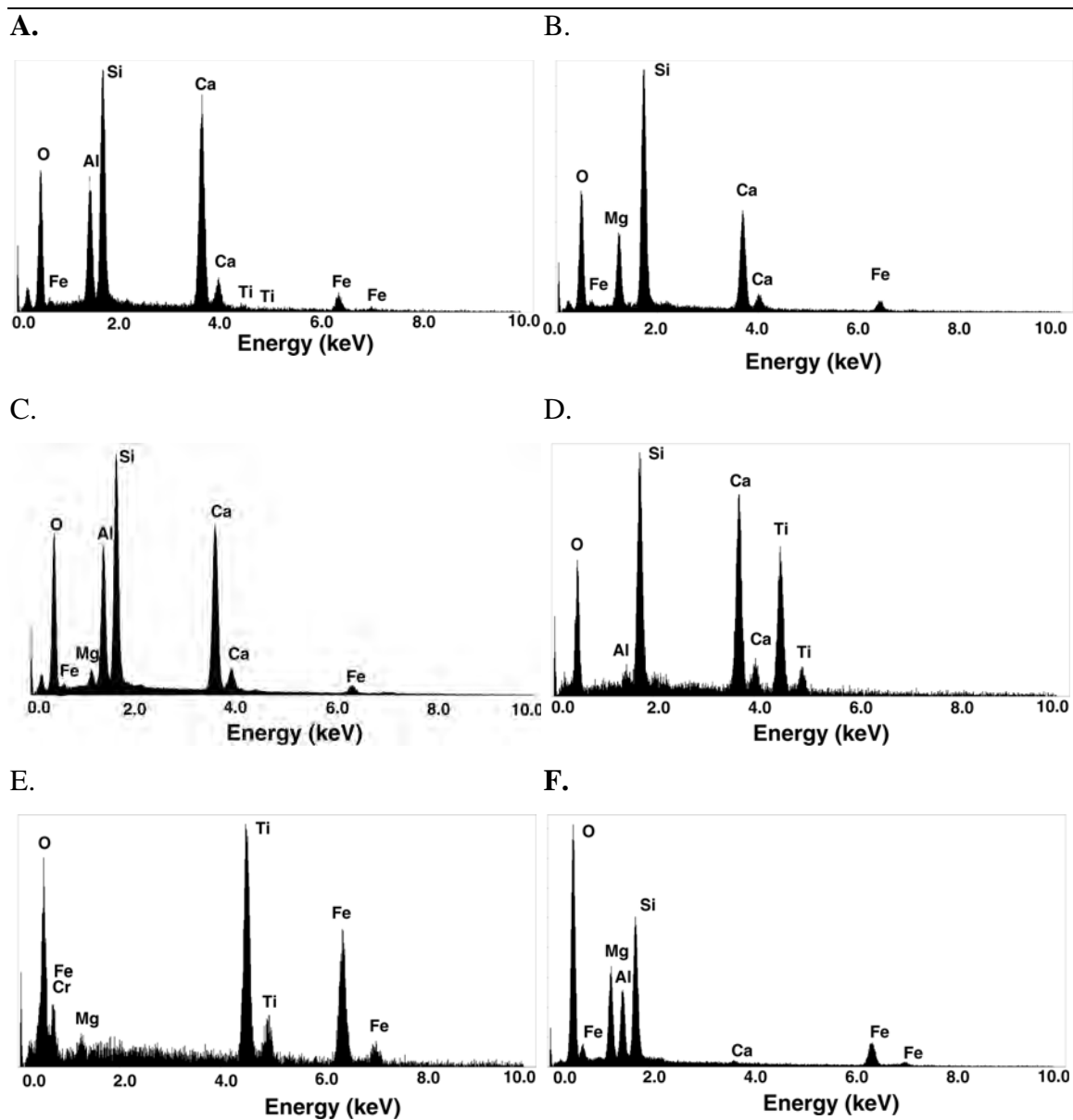


**Figure 2-3.** Energy dispersive x-ray spectra (EDX) of Tehama County parent material minerals **A.** Grossularite demonstrating some inclusion of Ti. **B.** Diopside. **C.** Pumpellyite **D.** Titanite. **E.** Ilmenite. **F.** Hydroxy-interlayered-material (HIM).

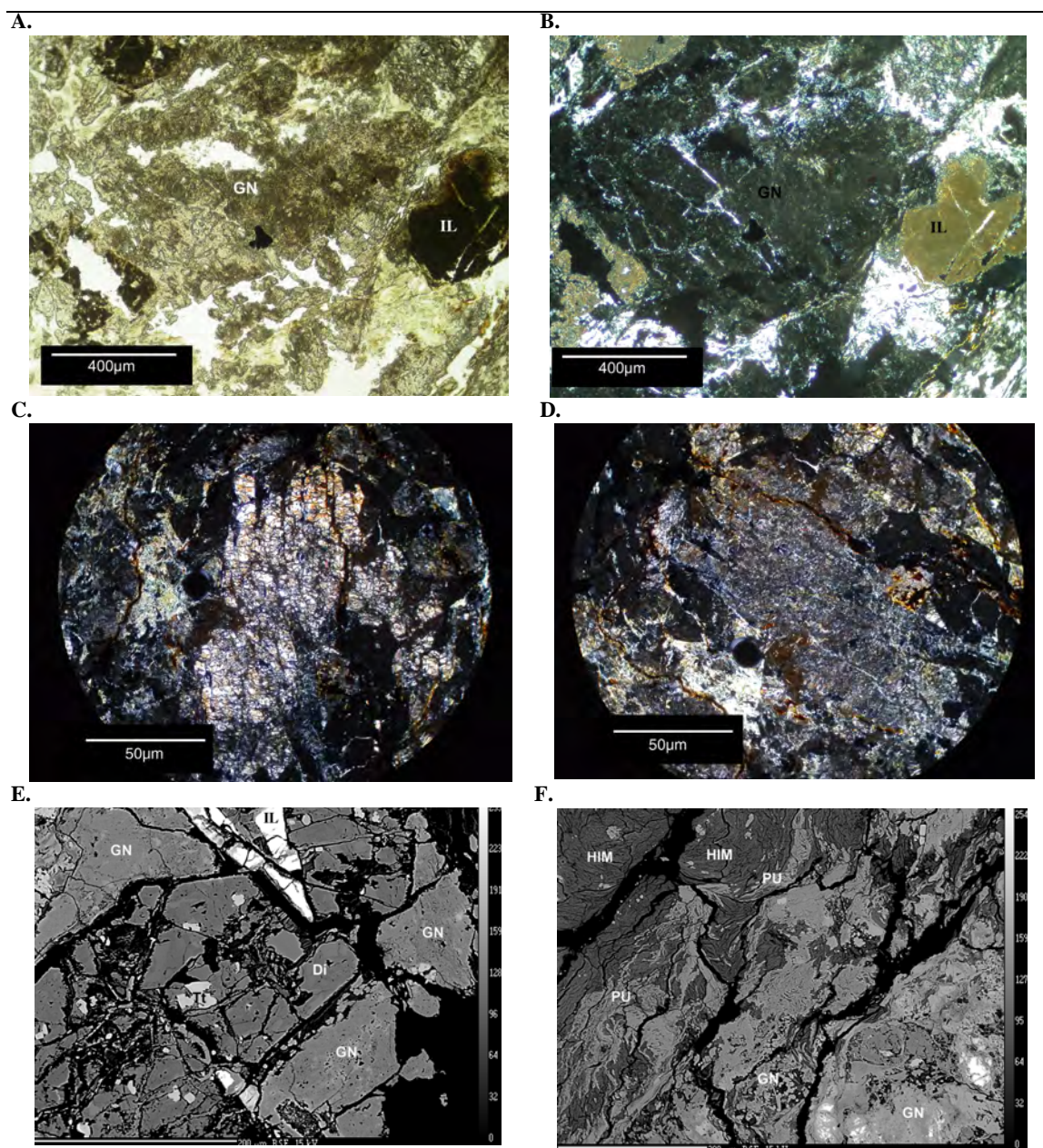


**Figure 2-4.** **A.** Photomicrograph of Tehama County parent material plane-polarized light, tightly packed small interlocking euhedral crystals of grossularite garnet (GN) appear as a large cinnamon-brown mass, the nearly opaque dark brown minerals are ilmenite (IL). **B.** Photomicrograph of Tehama County parent material with crossed polars. The garnets (GN) are isotropic dark purplish black and the ilmenite (IL) brown. **C.** Photomicrograph of Tehama County parent material; diopside, vertically aligned, with crossed polars. **D.** Photomicrograph of Tehama County parent material; diopside demonstrating inclined extinction; crossed polars. **E.** BSE micrograph of Tehama County parent material. Di = diopside; Tt = titanite; IL = ilmenite; GN = garnet (grossularite). **F.** BSE micrograph of Tehama County parent material. Lighter grey pumpellyite (PU) inter-grown into darker grey hydroxy-interlayered-material (HIM) upper left and center. Smaller masses of euhedral grossularite garnet crystals (GN) are lower center but are predominantly tightly packed and interlocked into larger masses (lower right).

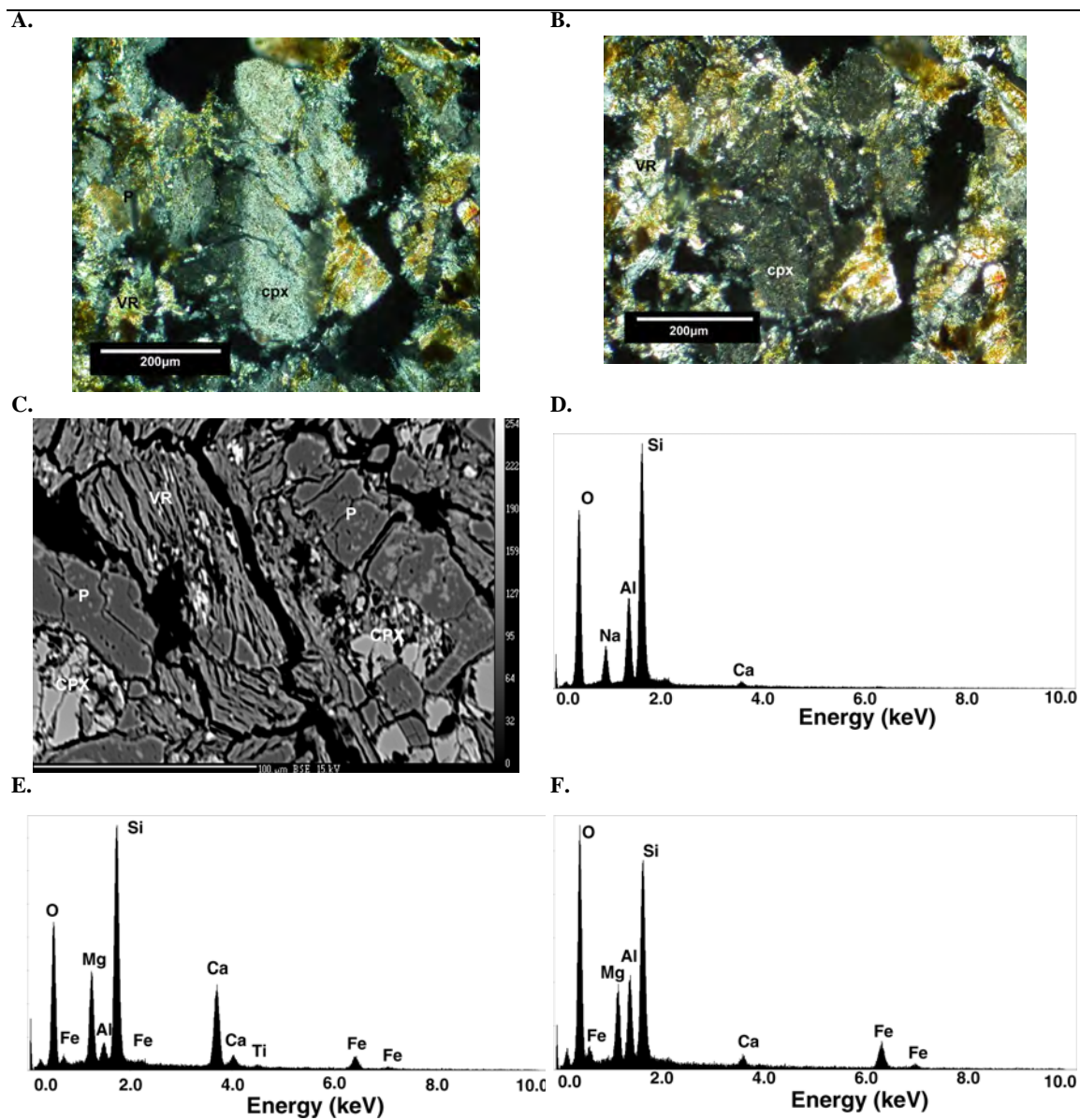


**Figure 2-5.** A. Photomicrograph of Napa County parent material: crossed polars. clinopyroxene (cpx) surrounded by plagioclase feldspar (P) some expressing carlsbad twinning and vermiculite (VR). B. Photomicrograph of Napa County parent material: crossed polars. Diopside (cpx) expressing extinction at inclined position surrounded by plagioclase feldspar (P) some expressing carlsbad twinning and vermiculite (VR). C. BSE micrograph Napa County parent material. CPX = diopside; P = plagioclase feldspar VR = vermiculite. D. Energy dispersive x-ray spectra (EDX) Napa County parent material plagioclase. E. EDX Napa County parent material diopside. F. EDX Napa County parent material vermiculite.

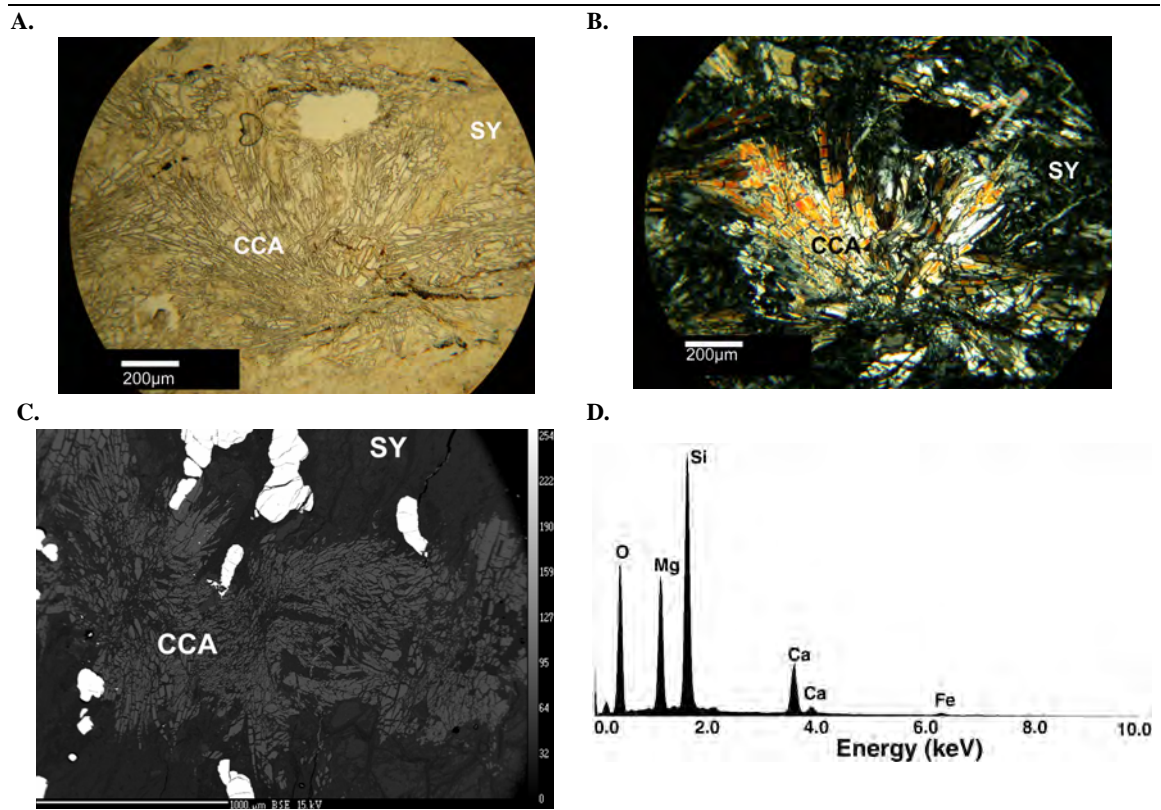


**Figure 2-6.** **A.** Photomicrograph of Shasta County parent material shown in plane-polarized light. Masses of radiating columnar crystals: CCA = tremolite, SY = serpentine. **B.** Photomicrograph of Shasta County parent material: crossed polars. Masses of radiating columnar crystals: CCA = tremolite, SY = serpentine. **C.** BSE micrograph Shasta County parent material. CCA = tremolite, SY = serpentine, white areas are iron oxides. **D.** EDX Shasta County parent material calcic clinoamphibole.



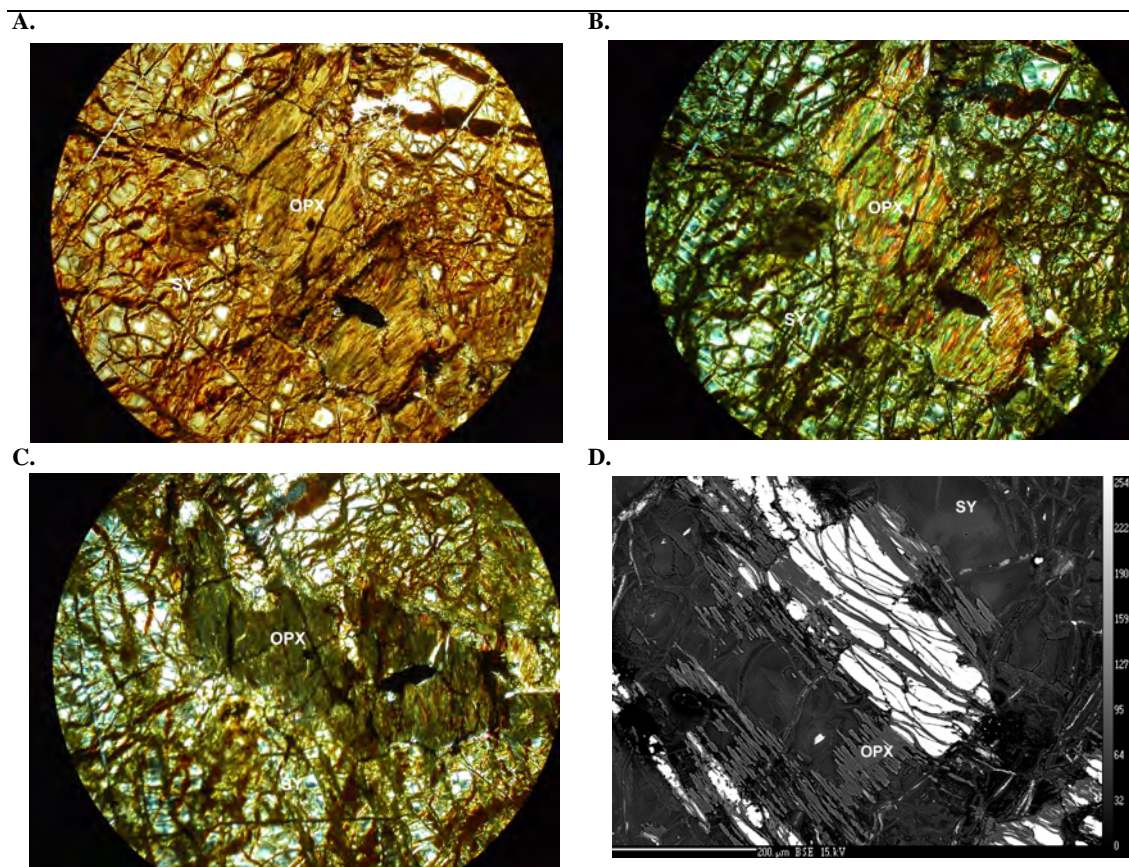


**Figure 2-7.** **A.** Photomicrograph Glenn County parent material: plane polarized light. Enstatite (OPX) set in matrix of serpentine (SY). Field of view = 5 mm. **B.** Photomicrograph Glenn County parent material: crossed-polars. Enstatite (OPX) set in matrix of serpentine (SY). Field of view = 5 mm. **C.** Photomicrograph Glenn County parent material: crossed-polars. Parallel extinction of enstatite (OPX) in matrix of serpentine (SY). Field of view = 5 mm. **D.** BSE micrograph Glenn County parent material orthopyroxene with iron intergrowth (white) surrounded by serpentine.

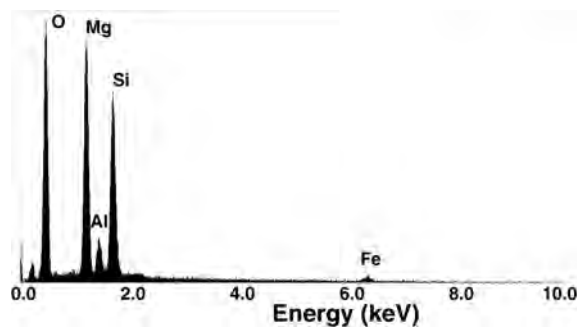


**Figure 2-8.** EDX Glenn County parent material enstatite.

---

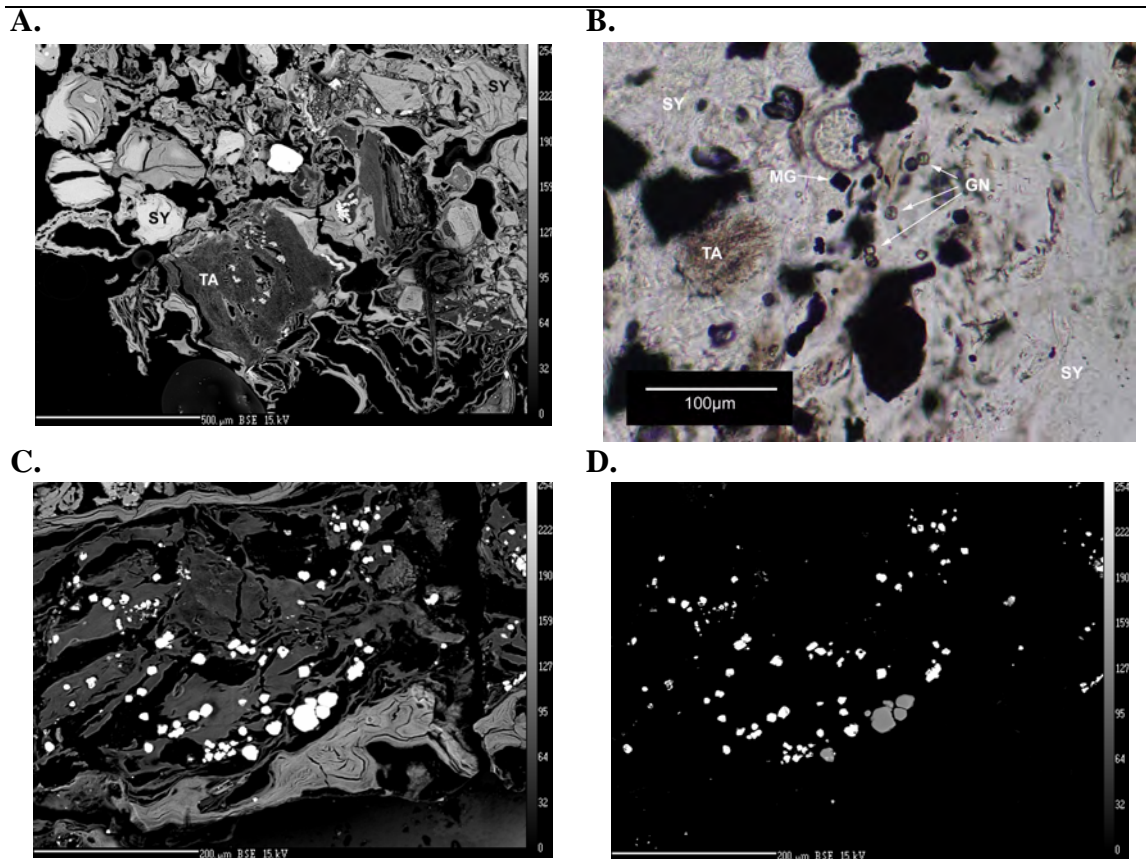


**Figure 2-9.** **A.** BSE micrograph Kings County parent material; talc (TA) amongst serpentine (SY) of varying shades of grey. Bright white spots are either magnetite or andradite garnet. **B.** Photomicrograph of Kings County parent material shown in plane-polarized light. A mass of talc (TA), dark magnetite (MG) and individual dodecahedral crystals of andradite garnet (GN) in a serpentine (SY) matrix. **C.** BSE micrograph Kings County parent material with bright white magnetite and andradite garnet amongst serpentine. **D.** BSE micrograph C with brightness and contrast adjusted to differentiate between bright white magnetite and grey andradite garnet. All the serpentine is black and indistinguishable from the epoxy voids of the thin section.

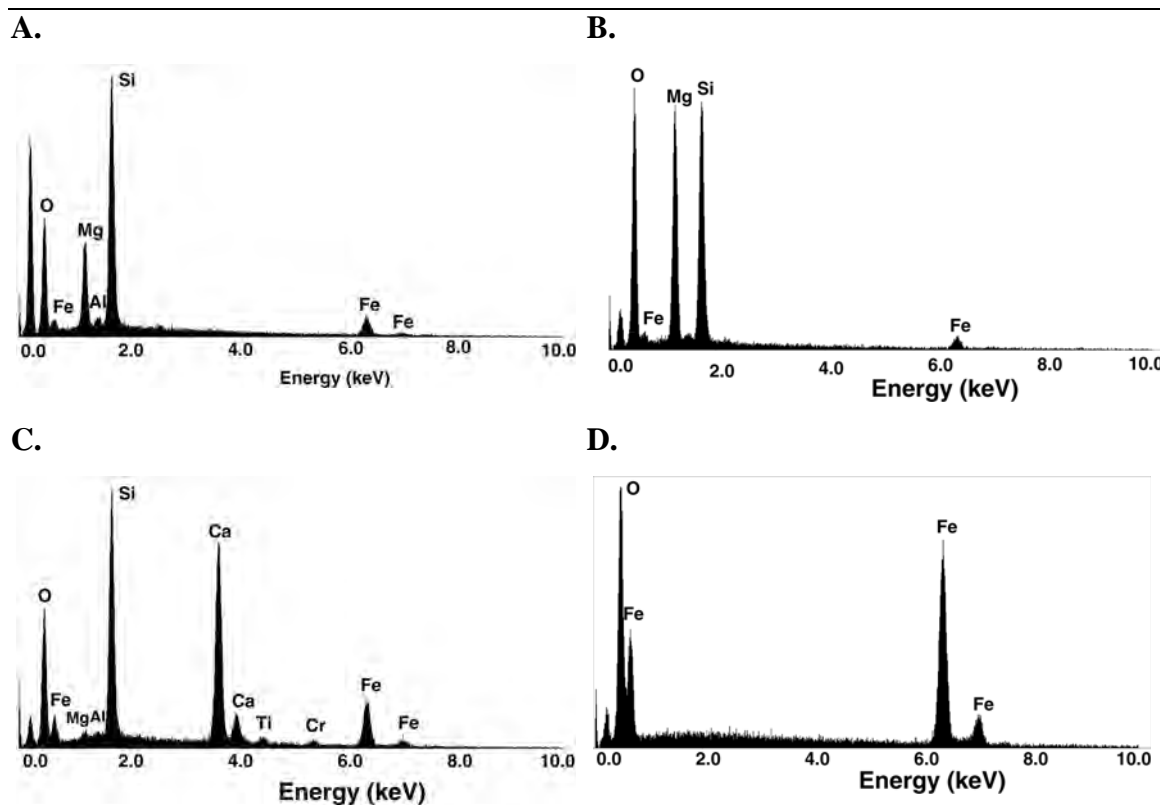


**Figure 2-10.** Energy dispersive x-ray spectra (EDX) of Kings County parent material minerals **A.** Talc. **B.** Serpentine. **C.** Andradite garnet. **D.** Magnetite.

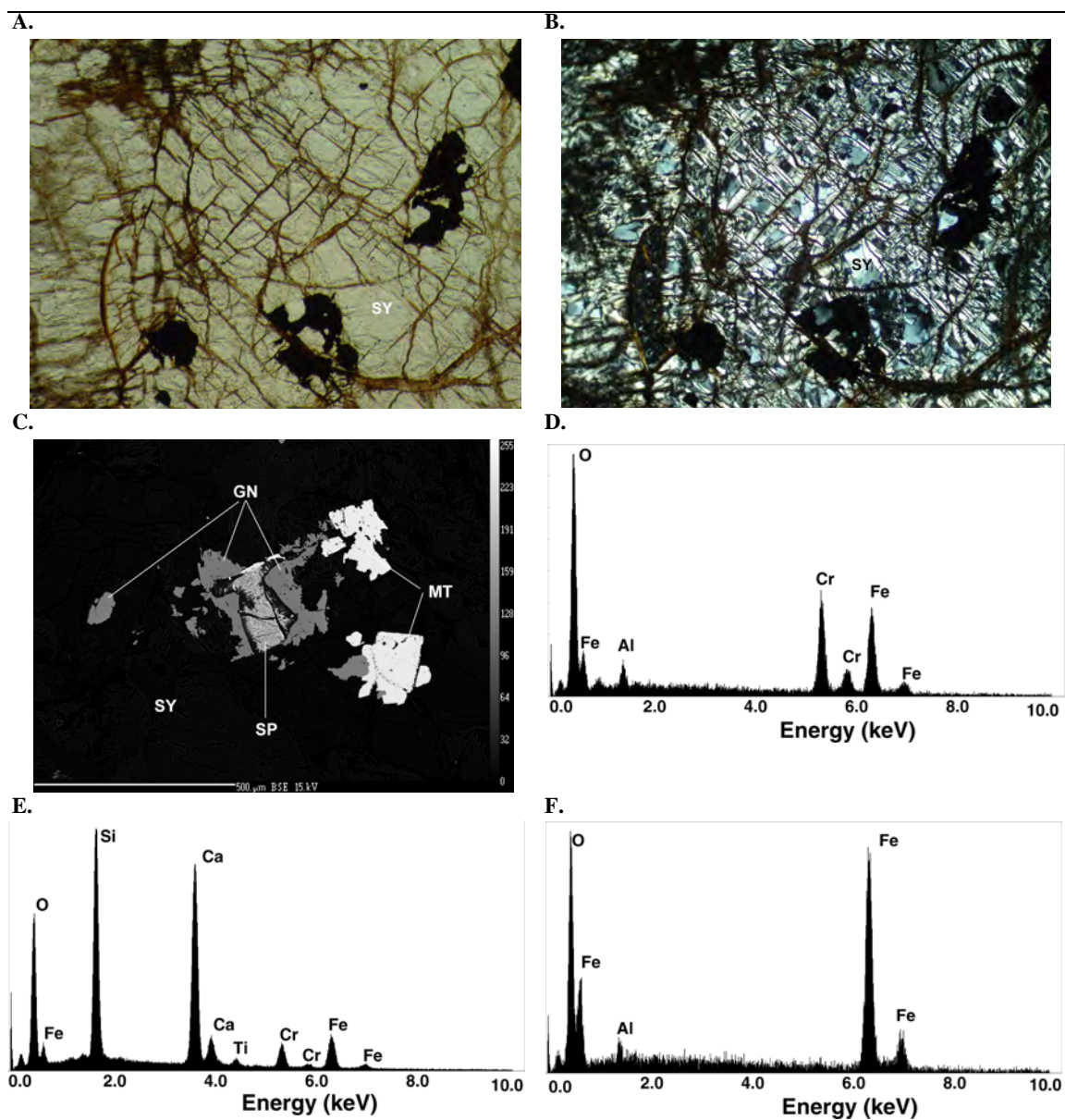


**Figure 2-11.** **A.** Photomicrograph San Benito County parent material plane-polarized light. Serpentine (SY) with opaque inclusions. **B.** Photomicrograph San Benito County parent material crossed-polarized light. Serpentine (SY) with opaque inclusions. **C.** BSE micrograph of San Benito County parent material increased contrast and lowered brightness eliminates outlines of serpentine (SY) crystals that dominate the parent material but distinguishes between chromite spinel (SP) at center surrounded by chrome rich andradite garnet (GN). Lightest grey is magnetite (MT). **D.** Energy dispersive x-ray spectra (EDX) of San Benito County parent material chromite spinel. **E.** EDX of San Benito County parent material chrome rich andradite. **F.** EDX of San Benito County parent material magnetite.

## 2.7 APPENDIX A

**Table 2-4.** Appendix A. Content of elements in serpentinite parent material rocks beneath the 5 pedons not discussed.

	Survey Area				
	Shasta-Trinity National Forest	Mariposa County 49 to 55 cm	Colusa County 42 to 72 cm	Mendocino County 30 to 70 cm	Los Padres National Forest 18 to 25 cm
	mg kg <sup>-1</sup>				
SiO <sub>2</sub>	421	402	392	380	41
Al <sub>2</sub> O <sub>3</sub>	4.0	12.7	56	87	2.8
Fe <sub>2</sub> O <sub>3</sub>	91	76	196	99	77
MgO	312	367	141	256	37
CaO	0.1	0.6	8.1	13.2	0.2
Na <sub>2</sub> O	<0.1	0.6	0.2	0.1	0.8
K <sub>2</sub> O	<0.2	<0.2	0.3	<0.2	<0.2
TiO <sub>2</sub>	<0.1	0.2	1.3	5.7	<0.1
P <sub>2</sub> O <sub>5</sub>	0.4	0.8	0.7	1.2	0.7
MnO	1.0	0.8	2.0	1.3	0.5
Cr <sub>2</sub> O <sub>3</sub>	2.8	3.9	6.1	2.2	2.0
CaO:MgO	<0.1	<0.1	<0.1	<0.1	<0.1
LOI	163	132	190	152	132

LOI = loss on ignition

# CHAPTER 3: PLANT-AVAILABLE CALCIUM VARIES WIDELY IN SOILS ON SERPENTINITE LANDSCAPES

## 3.1 ABSTRACT

Serpentinitic landscapes are recognized as having vegetation patchiness. Since it is well established that low Ca availability is a primary limitation to vegetative vigor it is possible that a relationship exists between vegetation and soil Ca availability. We hypothesized that soils formed on serpentinitic landscapes, and nominally called “serpentine soils,” have a range in properties (morphological, chemical, and parent material mineralogy) and that these soil properties are linked to variable extractable Ca:Mg, extractable Ca, and total Ca. Furthermore, we hypothesized that the variable Ca content is correlated to vegetation Ca concentration. Eleven pedons from California were sampled and described; all were within the soil survey mapping polygon containing the modal location for a classic “serpentine soil” Henneke soil series (Clayey-skeletal, magnesian, thermic Lithic Argixerolls). Extractable Ca:Mg varied from 0.1 to 1.5, and total elemental Ca:Mg varied from <0.01 to 1.9, in the soils. Soil extractable Ca was influenced by parent material mineralogy, where soils with a Ca:Mg of 0.2 or less were derived from serpentinite parent materials with only trace Ca-bearing minerals; soils with a Ca:Mg > 1 were derived from non-serpentinite parent

materials, and soils with a Ca:Mg > 0.2 but < 1 were derived from serpentinite parent material that had minor amounts of accessory Ca-bearing minerals. The grass *Vulpia microstachys* was grown in the soils in a greenhouse pot study and the concentration of Ca measured in the above ground biomass correlated better with soil extractable Ca ( $R^2 = 0.89$ ;  $P = < 0.01$ ) than with total elemental analysis Ca ( $R^2 = 0.64$ ;  $P < 0.01$ ). The shallow soil depth of the profiles, together with the generally high coarse fragment fraction, limit the soil volume available to roots. Profiles with the highest extractable Ca:Mg, in Napa and Tehama Counties, also had the greatest extractable Ca pool, 1169 and 394 g m<sup>-2</sup>. The extractable Ca:Mg, the Ca extractable pool, and the distribution of the Ca pool all varied across soil formed on serpentinite landscapes and these were important determinants of plant performance, determined by leaf Ca content, in these soils. Extractable Ca was the best determinant of plant performance.

### 3.2 INTRODUCTION

Ultramafic rocks, of which serpentinite is a member, occupy <1% of the land surface of the earth, but they have long been the study of botanists, plant physiologists, phytochemists, plant geographers and scientists from other disciplines. Serpentinite derived soils often support vegetation that stands in stark contrast (reduced vigor, reduced numbers, and more endemic species) to vegetation adjacent to non-serpentinite derived soils. The perceived difference has often been termed the “serpentine factor,” and botanists often refer to “serpentine flora” (Brooks, 1987; Kruckeberg, 1985).

We hypothesized that soils formed on serpentinitic landscapes, and nominally called “serpentine soils,” have a range in properties (morphological, chemical, and parent material



mineralogy) and that these soil properties are linked to variable extractable Ca:Mg, extractable Ca, and total Ca. We also hypothesized that the variable Ca content is correlated to vegetation Ca concentration. “Serpentine soils” is a misnomer. Serpentine is the name of a class of minerals of which antigorite, chrysotile and lizardite are the most recognized members (Deer et al., 1979). Serpentine minerals are 1:1 minerals with the general formula  $Mg_3Si_2O_5(OH)_4$  and are trioctahedral analogs to the dioctahedral kaolinite ( $Al_2Si_2O_5(OH)_4$ ). Serpentine minerals are not formed in soils. They are products of metamorphism (serpentinization) of ultramafic rocks such as dunites, pyroxenites, and peridotites (O’Hanley, 1996). Ultramafic rocks with abundant serpentine are defined as serpentinite. These serpentinite rocks usually also contain minor amounts of the minerals magnetite, brucite, talc, and various carbonates. Many other accessory minerals may occur in serpentinites as trace components including pyroxenes, amphiboles, garnets, chlorite, vermiculite, chromite spinel, ilmenite, and titanite. A preferable term to “serpentine soils” might therefore be “serpentinite-derived soils.”

The perceived differences between soils on what we nominally call serpentinite and those adjacent to them, and perceived to be non-serpentinite derived, have perhaps led to a perception that the soils formed on serpentinite landscapes are relatively homogenous with respect to the “serpentine factor.”

Metasomatism is a process of indefinite elemental replacement, loss and/or addition of elements as a result of percolating solutions (Merrill, 1906). As a result, during metamorphism or metasomatism, the anhydrous minerals of the protolith dunite, pyroxenite, or peridotite become more hydrous, and calcium content decreases from the original rocks resulting in a relative enrichment of magnesium (Coleman and Keith, 1971; Page, 1966; Page, 1967).

The Ca:Mg has been used to relate the high Mg and low Ca condition that exists in these soils. Early researchers attributed poor growth to Mg toxicity on serpentinite-derived soils (Loew and May, 1901; Gordon and Lipman, 1926). Vlamis and Jenny (1948) demonstrated that Ca deficiency, rather than Mg toxicity, was the primary cause of poor plant growth despite high exchangeable Mg content. Walker et al. (1955) emphasized the importance of Ca to vegetation and demonstrated that non-native species yields were reduced about 50% when exchangeable Ca was 20% or less of the CEC, and the plants had little or no growth or yield below 10% exchangeable Ca. Native plant species, however, were better able to extract Ca, and yield was only reduced 24% in the 5 to 3% exchangeable Ca range.

It is often presumed that soils formed on “serpentinite landscapes” suffer from low Ca content and an abundance of Mg. Researchers guided by existing soil or geologic maps to locate serpentinite landscapes need to consider the scale and purpose of those maps.

A Ca:Mg of 0.7 is often adopted as a quotient to separate serpentinite parent material from non-serpentinite parent material (Brooks, 1987). In light of the work by Walker et al. (1955) and Vlamis and Jenny (1948), this value may not be particularly useful when working with “native” serpentinite vegetation. Proctor and Woodell (1971) found a wide range in the Ca:Mg quotient (0.03 to 2.37) in “serpentine” soils from Scotland and England. Rabenhorst and Foss (1981), in an effort to predict mafic or ultramafic parent lithology while mapping soils of the eastern Piedmont of Maryland, found that from a population of 39 pedons, that if the exchangeable Ca:Mg was  $< 0.1$  the probability that the soil was formed from serpentinite rather than a mafic lithology was 98%, a Ca:Mg of 0.2 to 0.3 yielded a serpentinite probability of 53%, and at 0.6 to 0.7 Ca:Mg, the probability was only

21%. Clearly at Ca:Mg ratios greater than 0.2 the confidence that the soil is derived from ultramafic parent material is low.

The literature is replete with Ca:Mg ratios often without stating the method of determining the elemental concentrations, e.g., whole rock elemental analysis vs. extractable Ca and Mg. Investigators of the “serpentine effect” are warned by Proctor and Woodell (1971) to not rely on whole rock analysis as representative of the pool of soil nutrients available to plants. Complicating the determination of the “serpentine effect” is the occurrence of non-serpentinite parent materials on the serpentinitic landscape (Page, 1966; Page, 1967; Coleman and Keith, 1971). While extractable Ca and Mg contents give a better representation of the pool of soil nutrients available to plants than total elemental analysis, parent material rock elemental analysis, fine earth fraction elemental analysis, polarized light microscopy (PLM), X-ray diffraction (XRD), and electron dispersive X-ray analysis (EDX) should be employed to augment the assertion that a site is truly serpentinite derived (McGahan, 2007). Upslope xenolithic inclusions could influence Ca fertility via porewaters from upslope weathering of Ca-containing minerals or from colluvium containing Ca-bearing minerals. Eolian influences are also a possibility not fully explored by researchers investigating the “serpentine effect.”

We present morphology of soils formed on serpentinitic landscapes to support our hypothesis that soils formed on serpentinitic landscapes, and nominally called “serpentine soils,” have a range in properties (morphological, chemical, and parent material mineralogy) and that these soil properties are linked to variable extractable Ca:Mg, extractable Ca, and total Ca contents. Furthermore, we hypothesize that the variable Ca content is correlated to vegetation Ca concentration. The parent materials of the soils used in this study have been

examined for mineralogical composition in another study so that meaningful relationships can be drawn from morphological observations (McGahan, 2007). Finally, a grass, *Vulpia microstachys* (Nutt.) Munro (hereafter referred to as *Vulpia*), was grown in the soils, in a greenhouse pot study. Above-ground biomass Ca and Mg contents were measured and compared to soil extractable Ca:Mg and total soil CaO%:MgO% to understand how rock and soil composition affects bioaccumulation of Ca and Mg.

### **3.3 MATERIALS AND METHODS**

#### **3.3.1 Field**

We choose to use soils mapped as the Henneke soil series (Clayey-skeletal, magnesian, thermic Lithic Argixerolls) and soil survey modal locations as a basis for sampling locations (Soil Survey Staff, 1999). Henneke soils are widely mapped, and are “soils formed in material weathered from serpentine and rocks of similar mineralogy” (Soil Survey Staff, 2005). The sampling sites encompassed a wide range of serpentinite landscape lithology. All soil pits were on summits above modal locations, to eliminate colluvial and alluvial influences, and were within the mapping polygon containing the Henneke series modal location for each soil survey area. Eleven sites were sampled across California (Fig. 3-1). The use of Henneke survey modal locations generally constrained the soil climate to be xeric/thermic. Pits were excavated by hand tools. Soils were described and sampled using conventional procedures (Soil Survey Division Staff, 1993). Volume of cobbles and stones was estimated in the field. The fine earth fraction and gravels were sampled in conjunction with compliant cavity bulk density measurements (Soil Survey Staff, 2004).

### 3.3.2 Laboratory

Soils were air dried, sieved to pass through a 2-mm sieve, and this fine earth fraction analyzed for particle size distribution by the pipette method as described by Gee and Bauder (1986). Fine earth fraction extractable cations were measured by displacement with pH 7.0, 1M NH<sub>4</sub>OAc, and concentrations of Na, Ca, Mg, and K in the leachate were measured with flame atomic absorption, or emission, spectrometry. Cation exchange capacity was measured by saturating samples with 1M NH<sub>4</sub>OAc, at pH 7, washing with 95% ethanol, extracting with 2M KCl to remove adsorbed NH<sub>4</sub>, and determining the NH<sub>4</sub> concentration in the leachate conductimetrically (Carlson, 1978). The pH of the fine earth fraction was determined at 1:1, soil:water, on a mass basis (Soil Survey Staff, 2004).

Volume of gravels was determined directly by volume displacement in water. Displacement was performed after sieving compliant cavity bulk density samples to separate the gravels, then soaking the gravels for 15 h in deionized water, washing to remove slaked soil material, and drying at 105°C for 15 h (Soil Survey Staff, 2004).

We blended fine earth fraction soil materials from A and B horizons for our greenhouse pot studies. These soils were used to fill 500 cm<sup>3</sup> pots and planted with approximately three dozen seeds of *Vulpia* per pot. *Vulpia* was observed to grow at many serpentinite sites surveyed, and the seed used was collected from serpentinite landscapes. After three weeks of growth the plants were fertilized with 0.5 L of solution equivalent to 1/4 Hoaglands solution of the elements N and P (4,000 and 500 μmol L<sup>-1</sup>) each week to remove potential effects of deficiencies of these elements. After 16 weeks growth and prior to the plants setting seed, the above ground plant material, hereafter referred to as leaf, produced in each

pot was clipped, rinsed in de-ionized water, dried at 45°C for 72 h, ground, weighed, ashed by heating in a muffle furnace at 500°C for 4 hours, the ash digested in hot 1 N HCl, and the digest analyzed for Mg and Ca by flame atomic absorption spectrometry (Gavlak, et al., 1994). Content of Ca in leaf was used as indicator of plant performance.

Approximately 10 g sub-sample of the fine earth fraction soil from each horizon, and the blended fine earth fraction that was used for the container experiment were ground and sieved until all passed a No. 140 sieve (100 µm). Elemental analysis of most elements was performed by ICP-emission spectrometry following a lithium metaborate (LiBO<sub>2</sub>) fusion and dilute nitric acid digestion. The precious and base metals, Au, Ag, As, Bi, Cd, Cu, Hg, Mo, Ni, Pb, Sb, Se, Tl, and Zn were analyzed ICP-emission spectrometry from a leachate of hot (95°C) Aqua Regia (Sawhney and Stilwell, 1994).

## **3.4 RESULTS AND DISCUSSION**

### **3.4.1 Profile Morphologies**

The variation of morphologies (Table 3-1) and the resultant differences in classification serve to demonstrate that soils formed on serpentinitic landscapes result in varying soil individuals, even when constraining the soil sampling sites to polygons containing the modal location of the same soil series (Henneke).

All the pedons sampled were Lithic at the subgroup level or were in shallow families (Table 3-1). Textures were generally loamy (loams, sandy loams, sandy clay loams, and clay loams), with the exception of a clay texture at the base of the Colusa County profile (Bt<sub>2</sub>) and the B horizons of the Shasta-Trinity National Forest profile (Table 3-3). Four

pedons, Shasta-Trinity National Forest, Napa, Colusa, and Tehama Counties, were not skeletal (Table 3-3). These textural deviations result in loamy or clayey family textural classes. Other departures in soil properties that resulted in alternate classification of the soils were presence of an ochric epipedon (rather than mollic) in the Napa, Shasta and San Benito Counties sites and absence of an argillic horizon in the Napa and Shasta County pedons. Therefore, the San Benito County site was classified as an Alfisol, and the Napa and Shasta County sites as Inceptisols (Table 3-2) (Soil Survey Staff, 1999).

The shallow soils, and high coarse fraction percentage leave limited soil volume from which vegetative communities can assimilate nutrients. Since it is well established that low Ca availability is a primary limitation to vegetative vigor we focus on the distribution of Ca in the extractable fraction in relation to the total pool of these elements.

Our sampling strategy excluded sites that could be influenced by colluvium, alluvium, or from Ca dissolved in pore water as a result of up-slope weathering of Ca enriched parent materials. Differences in the extractable Ca:Mg were attributed to the differences in the Ca and Mg in the parent material or to the relative weathering of the Mg- and Ca-bearing minerals that comprised the parent material.

For seven of the 11 profiles Mg was the dominant extractable cation, and those soils had an extractable Ca:Mg of  $< 0.2$  (Table 3-3). Four profiles, from Napa, Tehama, Kings and Shasta Counties, were in contrast to the dominance of extractable Mg and had an extractable Ca:Mg of  $> 0.2$  in most of the profile, which was consistent with our hypothesis that soils formed on serpentinitic landscapes would have variability in extractable Ca:Mg (Table 3-3).

### **3.4.2 Parent Material Influences on Ca:Mg**

There was a link to parent material mineralogical composition, or rock type. We examined the parent material from the R or Cr horizon from each site by total elemental analysis, polarizing light microscopy, back scatter electron microscopy, energy dispersive electron microscopy, and x-ray diffraction to document the variability of the lithology. More detailed descriptions are reported elsewhere (McGahan, 2007).

Nine of the 11 parent materials were serpentinites. The Napa and Tehama County parent materials were quite different from each other and from the other sites. Neither parent rock contained serpentine minerals and were therefore not serpentinites. Napa County was dominantly vermiculite and albite, but contained minor amounts of Ca-bearing clino-pyroxene. Tehama County parent material was dominated by the calcsilicate ugrandite garnet grossularite and with sub-dominant amounts of Ca-bearing sorosilicate pumpellyite, and Ca-bearing clinopyroxene. The rock from the Shasta and Kings County sites were serpentinite, dominated by serpentine minerals, but had minor amounts of Ca-bearing accessory minerals (calcic clinoamphibole (tremolite) and the calcsilicate ugrandite garnet (andradite) respectively). The seven other parent materials were serpentinites and exhibited, at best, trace amounts of Ca-bearing minerals.

### **3.4.3 Extractable Ca Pools**

Soil extractable Ca:Mg followed parent material Ca-bearing mineral content. Extractable Ca:Mg for Napa County were the greatest (1.3 to 1.5), followed by Tehama County (0.5 to 1.3). Shasta (0.3 to 0.4) and Kings (0.3 to 0.6) Counties extractable Ca:Mg were intermediate, and the balance of the sites generally had a Ca:Mg less than 0.2 (Table 3-3).



The total extractable Ca pool, calculated from soil extractable Ca of the fine earth fraction, in Napa County was nearly three times greater ( $1169 \text{ g m}^{-2}$ ) than the next largest Ca pool in Tehama County ( $394 \text{ g m}^{-2}$ ) (Table 3-4). The variations in the extractable Ca:Mg were further reinforced by increased pool size of extractable Ca where the extractable Ca:Mg is  $>1$  in Napa County, and the Tehama County Bt2 horizon. The fraction of extractable Ca as a proportion of the total fine earth Ca was also five times greater in the Napa County profile than in the Tehama County profile (Table 3-4). This likely reflects the relative weathering of the minerals present in the parent material. A great portion of the Ca-bearing minerals in the Tehama County parent material was in the form of garnets, and garnets have greater resistance to weathering than the Ca-bearing clino-pyroxene of the Napa County parent material (Pettijohn, 1941).

We noted that the Shasta and Kings Counties parent materials had minor inclusions of Ca-bearing minerals. The Shasta County total fine earth fraction Ca:Mg (Table 3-4) was lower than the extractable Ca:Mg (Table 3-3), and this is likely a result of aggressive biocycling of Ca in the very limited fine earth fraction volume of this profile. Kings County had more fine earth fraction volume (0.25 to 0.50) than Shasta County (0.12 to 0.22), and the Kings County fine earth fraction total Ca:Mg is similar to the extractable Ca:Mg.

The Mariposa County site stands out amongst the other profiles because the extractable Ca pools were also large, but the larger extractable Ca pool was accompanied by larger extractable Mg pool resulting in low extractable Ca:Mg, and low fine earth fraction total Ca:Mg similar to the other profiles.

These pools of Ca probably vary as a function of parent material composition differences, mineral weathering differences, and biocycling. A number of processes can be inferred by inspection of the total and extractable Ca pools. If the extractable Ca fraction of the total Ca increases toward the surface, this may reflect biocycling, via litter deposition and decomposition, and Ca retention in the profile. If the ratio increases with depth this may indicate Ca-bearing mineral weathering or preferential leaching of Ca vs. Mg, and biocycling did not significantly retain the Ca in surface horizons. A roughly static ratio throughout the profile may indicate weathering equals leaching.

As we hypothesized, the total extractable Ca pool varies across the eleven pedons, but the distribution pattern of the extractable Ca pool within the pedons also varies with depth. Parent material variation across serpentinitic landscapes was a factor in Ca pool variations laterally across the landscape and perhaps to some degree horizontally within the profile (Table 3-4).

#### **3.4.4 Plant Response to Varied Extractable Ca, Mg, or Ca:Mg**

Total elemental contents of the container soils (all fine earth fraction) for Napa and Tehama County yielded Ca:Mg > 1 in agreement with the total elemental analysis by horizon for each profile. The soil extractable Ca:Mg for the other container soils followed the same general trends, and were also in agreement with the soil profiles extractable cations (Table 3-5; Table 3-3).

We recognized that the parent material mineralogy was variable in soils formed on serpentinitic landscapes, and that parent material mineral content variability influenced the extractable Ca pool. Three groupings of soils based on parent material were made. The first

comprised seven serpentinite derived soils that had no more than trace amounts of Ca-bearing minerals. The second was the two profiles (Napa and Tehama Counties) that were derived from parent materials that were not serpentinite, and the third, the two profiles (Kings and Shasta Counties) that had minor amounts of Ca-bearing minerals. We wished to know if the Ca:Mg or Ca of the leaf was influenced by the total or exchangeable Ca:Mg, Ca, or Mg of the fine earth fraction.

Extractable Ca:Mg to leaf Ca:Mg had a moderately strong positive significant correlation ( $R^2 = 0.55$ ;  $P < 0.01$ ) and could be used to separate non-serpentinite from serpentinite derived soil. Examining serpentinite derived soil alone showed that extractable Ca:Mg to leaf Ca:Mg correlation was weak ( $R^2=0.07$ ;  $P = 0.23$ ) and not significant. Removing serpentinite sites that contained a minor amount of Ca-bearing minerals improved the relationship, but it was not significant ( $R^2=0.27$ ;  $P = 0.50$ ) (Fig. 3-2).

Fine earth fraction total elemental analysis Ca:Mg had a very strong correlation ( $R^2 = 0.81$ ;  $P < 0.01$ ). It was a stronger relationship than leaf Ca:Mg to extractable Ca:Mg. Similar to extractable Ca:Mg, the total Ca:Mg to leaf Ca:Mg the relationship to leaf Ca:Mg for serpentinite only sites was not significant ( $R^2 = 0.03$ ;  $P = 0.66$ ). For serpentinites without minor Ca-bearing minerals, the total Ca:Mg to leaf Ca:Mg correlation was not significant ( $R^2 = 0.04$ ;  $P = 0.69$ ) (Fig. 3-3).

So Ca:Mg, whether extractable or total has some usefulness because it separates non-serpentinite from serpentinite parent materials, but fails in any predictive power to relate leaf Ca:Mg for serpentinites. Because low Ca availability is a primary limitation to vegetative vigor, leaf Ca content relationships are perhaps of more usefulness.

Total Ca was a moderately strong correlation to leaf Ca ( $R^2 = 0.64$ ;  $P < 0.01$ ), but removing the non-serpentinite sites weakened the relationship to a moderate correlation ( $R^2 = 0.40$ ;  $P = 0.07$ ). Removing serpentinites without Ca-bearing minerals resulted in a similar relationship, but was no longer significant ( $R^2 = 0.40$ ;  $P = 0.13$ ) (Fig. 3-4).

Total Mg was very strongly negatively correlated to leaf Ca ( $R^2 = 0.72$ ;  $P < 0.01$ ), and removing non-serpentinite sites strengthened the relationship ( $R^2 = 0.90$ ;  $P < 0.01$ ). Unlike the total Ca, removing serpentinite sites without minor Ca-bearing minerals weakened the relationship to leaf Ca, but it remained significant ( $R^2 = 0.85$ ;  $P < 0.01$ ) (Fig. 3-5).

While these are helpful relationships, total elemental analysis is not a routine analysis, and the exchangeable pool is more readily available to plants. Unlike total Mg, extractable Mg was not correlated to leaf Ca ( $R^2 = 0.02$ ;  $P = 0.68$ ) for all sites. When the non-serpentinite sites were removed extractable Mg had a moderately strong correlation to leaf Ca ( $R^2 = 0.45$ ;  $P = 0.05$ ). When the serpentinites without Ca-bearing minerals were removed, extractable Mg had a very strong correlation to leaf Ca ( $R^2 = 0.72$ ;  $P < 0.02$ ) (Fig. 3-6).

Extractable Ca was very strongly correlated to leaf Ca with all sites ( $R^2 = 0.89$ ;  $P < 0.01$ ). When non-serpentinites were removed extractable Ca remained very strongly correlated to leaf Ca ( $R^2 = 0.69$ ;  $P < 0.01$ ). Removing serpentinites without minor amounts of Ca-bearing minerals the correlation remained significant ( $R^2 = 0.66$ ;  $P < 0.03$ ) (Fig. 3-7).

Correlations of *Vulpia* leaf Ca content was strongest to soil exchangeable Ca and negatively to total Mg. We expected a negative correlation with extractable Mg similar to total Mg. From our data, we cannot deduce a cause for why there would be positive correlations with increasing extractable Mg. We could speculate that the increased pool size of extractable

cations allowed the plants to exploit a larger exchangeable Ca pool. We noted that extractable Ca:Mg was greater than total Ca:Mg for profiles with a low Ca:Mg. This leads us to speculate that biocycling plays some roll in Ca retention in the soil. Ca:Mg correlations to *Vulpia* leaf did not support this idea. We amended for N and P, but it is possible another nutrient increased in availability with increased extractable pool size that enhanced *Vulpia* uptake of Ca over Mg.

The plants responded to Ca-differences in the soils sampled across serpentinitic landscapes. Parent material Ca content clearly contributed to the soil fine earth fraction Ca content, and to the soil extractable Ca. The soil extractable Ca is presumed to be the pool that plants can utilize and this study confirms that the soil extractable Ca was the only viable Ca measurement correlated to leaf Ca on the serpentinitic landscape.

### **3.5 SUMMARY/CONCLUSION**

We hypothesized that soils formed on serpentinitic landscapes, and nominally called “serpentine soils,” have a range in properties (morphological, chemical, and parent material mineralogy) and that these soil properties are linked to variable extractable Ca:Mg, extractable Ca, and total Ca. We hypothesized that the variable Ca is correlated to vegetation Ca concentration.

The extractable Ca:Mg, the Ca extractable pool, and the distribution of the Ca pool all varied across soil formed on serpentinite landscapes. Extractable Ca was the most important determinants of plant performance on these soils. Soil extractable Ca was influenced by parent material mineralogy, where soils with a Ca:Mg of 0.2 or less were derived from

serpentinite parent materials with only trace Ca-bearing minerals; soils with a Ca:Mg > 1 were derived from non-serpentinite parent materials, and soils with a Ca:Mg > 0.2 but < 1 were derived from serpentinite parent material that had minor amounts of accessory Ca-bearing minerals.

### **3.6 REFERENCES**

- Brooks, R.R. 1987. *Serpentine and its vegetation: a multidisciplinary approach*. Dioscorides Press, Portland, OR.
- Carlson, R.M. 1978. Automated separation and conductimetric determination of ammonia and dissolved carbon dioxide. *Analytical Chemistry*. 50:1528-1531.
- Coleman, R.G., and T.C. Keith. 1971. A chemical study of serpentinization: Burro Mountain, California. *Journal of Petrology* 12:311-328.
- Coleman, R.G. 1979. Tectonic inclusions in serpentinites. p. 89-102. In J. Bertrand and J. Deferne (eds.), *Proceedings symposium on tectonic inclusions and associated rocks in serpentines*. Swiss National Science Foundation, Geneva. September 17-29 1979.
- Coleman, R.G. 1980. Ophiolite Tectonics and Metamorphism. p. 167-184. In J. Aubouin and C.J. Allegre (ed.), *Colloques Internationaux du Centre national de la recherche scientifique*; No. 272; Orogenic Mafic Ultra Mafic Association. Grenoble June 6-11 1977, Paris, France.
- Deer, W.A., R.A. Howie, and J. Zussman. 1997. *Rock-forming minerals*. 2nd ed. Geological Society, London.

- Gavlak, R.G., D.A. Horneck, and R.O. Miller. 1994. Plant, soil, and water reference methods for the western region / produced in cooperation with the Far West Fertilizer and Agrichemical Association. Western Rural Development Center, Corvallis, OR.
- Gee, G.W. and J.W. Bauder. 1986. Particle size analysis. pp. 383-411 In: A. Klute (ed), Methods of soil analysis: Part 1 Physical and mineralogical methods. American Society of Agronomy, Madison, WI.
- Gordon, A., and C.B. Lipman. 1926. Why are serpentine and other magnesian soils infertile? *Soil Science* 22:291-302.
- Kruckeberg, A.R., 1985. California serpentines: flora, vegetation, geology, soils, and management problems. University of California Press, Berkeley.
- Loew, O., and D.W. May. 1901. The relation of lime and magnesia to plant growth. I. Liming of soils from a physiological standpoint. II Experimental study of the relation of lime and magnesia to plant growth. U.S. Dept. Ag., Plant Indus. Bull. 1, 53. Government Printing Office, Washington.
- McGahan, Donald G. 2007. A survey of soils formed on serpentinitic landscapes in California. Ph.D. diss. University of California Davis.
- Merrill, G.P. 1906. A treatise on rocks, rock-weathering and soils. New ed. Macmillan, New York, London.
- O'Hanley, D.S. 1996. Serpentinites: records of tectonic and petrological history. Oxford University Press, New York.
- Page, N.J. 1966. Mineralogy and chemistry of the serpentine group minerals and the serpentinization process. Ph.D. diss. University of California Berkeley.

- Page, N.J. 1967. Serpentinization considered as a constant volume metasomatic process: a discussion. *The American Mineralogist* 52:545-549.
- Pettijohn, F. J., 1941, Persistence of heavy minerals and geologic age: *Journal of Geology*, v. 79, p. 610–625.
- Proctor, J., and S.R.J. Woodell. 1971. The plant ecology of serpentine: I. Serpentine vegetation of England and Scotland. *The Journal of Ecology* 59:375-395.
- Rabenhorst, M.C., and J.E. Foss. 1981. Soil and geologic mapping over mafic and ultramafic parent materials in Maryland. *Soil Science Society of America Journal* 45:1156-1160.
- Sawhney, B.L., and D.E. Stilwell. 1994. Dissolution and elemental analysis of minerals, soils and environmental samples, p. 49-82, In J. E. Amonette and L. W. Zelazny, eds. *Quantitative methods in soil mineralogy* SSSA Miscellaneous Publication. Soil Science Society of America, Madison, Wis., USA.
- Soil Survey Division Staff. 1993. *Soil survey manual - agriculture handbook No. 18*. U.S. Dept. of Agriculture: Supt. of Docs. U.S. G.P.O., Washington, DC.
- Soil Survey Staff. 1999. *Soil Taxonomy: a basic system of soil classification for making and interpreting soil surveys*. 2nd ed. United States Department of Agriculture, Natural Resources Conservation Service, Washington, DC.
- Soil Survey Staff. 2004. *Soil Survey Laboratory Methods Manual - Soil Survey Investigations Report No. 42 Ver. 4.0*. USDA-NRCS. Lincoln, Nebraska, USA. [Online WWW] URL: "<http://soils.usda.gov/technical/lmm/>" [Accessed 24 August 2006].



Soil Survey Staff., 2005. Official soil series descriptions [Online WWW]. Available URL: “<http://soils.usda.gov/technical/classification/osd/index.html>” [Accessed 10 February 2005].

Vlaminis, J., and H. Jenny. 1948. Calcium deficiency in serpentine soils as revealed by absorbent technique. *Science* 107:549.

Walker, R.B., H.M. Walker, and P.R. Ashworth. 1955. Calcium-magnesium nutrition with special reference to serpentine soils. *Plant Physiology* 30:214-221.

**Table 3-1.** Selected morphological properties of soils sampled on serpentinitic landscapes.

Horizon Name	Depth cm	Boundary†	Color Dry	Color Moist	Structure‡	Structure PartsTo‡
<b>Colusa County</b>						
A	0-3	CS	5YR 3/2	7.5YR 4/3	2 M SBK	2 CO GR
ABt	3-8	CW	5YR 4/3	5YR 3/3	2 CO SBK	2 M SBK
Bt1	8-30	CW	7.5YR 4/3	5YR 3/3	2 CO SBK	2 F SBK
Bt2	30-42	AI	7.5YR 4/3	7.5YR 3/3	2 M PR	1 M WEG
Cr	42-72		30% 7.5YR 4/3, 30% 10GY 7/1, 20% 5Y 7/3, 20% 10Y 8/1	30% 5YR 3/3, 30% 5GY 4/1, 20% 5Y 5/4, 20% 5GY 4/1		
<b>Glenn County</b>						
A	0-9	AW	7.5YR 4/4	2.5YR 3/3	1 F ABK	2 M GR
Bt	9-34	CI	5YR 4/4	2.5YR 2.5/3	1 F ABK	3 M GR
R	34		80% 10Y 2.5/1, 20% 2.5Y 7/6	ND		
<b>Kings County</b>						
A	0-4	AW	10YR 4/2	10YR 2/2	2 VK PL	2 F GR
Bt1	4-13	AW	10YR 5/3	7.5YR 3/2	2 M PR	2 VC SBK
Bt2	13-40	AI	10YR 4/2	7.5YR 3/2	3 M SBK	–
R	40		70% 5GY 8/1, 20% 10GY 8/1, 10% 5B 2.5/1	ND		
<b>Napa County</b>						
A	0-6	AS	7.5YR 4/4	5YR 3/3	2 TK PL	2 F SBK
Bt	6-20	AI	5YR 4/6	5YR 3/3	2 CO SBK	3 M SBK
R	20		60% 2.5Y 7/4, 40% 5Y 7/4	ND		
<b>San Benito County</b>						
A	0-8	VW	10YR 6/3	10YR 4/3	1 F SBK	–
Bt	8-20	CW	10YR 5/3	7.5YR 3/1	2 M SBK	–
Cr	20-50		60% N 5/, 40% 5GY 7/1	ND		

Horizon Name	Depth cm	Boundary†	Color Dry	Color Moist	Structure‡	Structure PartsTo‡
R	50		70% 5GY 7/1, 30% 10B 4/1	ND		
<b>Shasta County</b>						
A	0-3	AS	5YR 4/6	2.5YR 3/4	2 CO SBK	2 CO GR
Bt	3-40	AI	5YR 4/6	2.5YR 3/4	2 CO ABK	–
R	40		70% 5Y 7/2, 30% 10Y 3/1	ND		
<b>Tehama County</b>						
A	0-3	VW	7.5YR 4/3	5YR 3/3	2 M GR	–
Bt1	3-7	AW	7.5YR 4/4	5YR 3/2	2 M SBK	–
Bt2	7-16	VI	7.5YR 3/3	7.5YR 3/3	2 CO ABK	–
Cr	16-60		75% 5Y 8/4, 15% 5YR 8/2, 10% 10Y 8/1	ND		
<b>Mariposa County</b>						
A	0-3	VW	7.5YR 4/3	7.5YR 2.5/2	3 M ABK	3 M GR
Bt1	3-14	CW	7.5YR 4/3	7.5YR 3/2	2 CO ABK	2 F ABK
Bt2	14-34	CW	7.5YR 4/3	5YR 2.5/2	2 M ABK	–
Bt3	34-49	AI	7.5YR 4/3	5YR 2.5/2	3 CO PR	3 CO ABK
R	49		35% 5Y 3/1, 30% 5Y 4/3, 20% 5Y 6/2, 15% 2.5Y 2/0	ND		
<b>Mendocino County</b>						
A	0-2	VW	2.5Y 4/2	10YR 3/2	2 TN PL	2 F GR
Bt1	2-8	AW	2.5Y 4/2	10YR 3/1	3 M COL	–
Bt2	8-30	CW	2.5Y 4/2	7.5YR 2.5/1	3 CO ABK	–
R	30		70% 5GY 7, 30% 10G 2.5	ND		
<b>Shasta-Trinity National Forest</b>						
A1	0-2	VS	5YR 4/3	5YR 3/3	2 VF GR	–
A2	2-5	CW	2.5YR 3/3	2.5YR 3/2	3 CO SBK	3 CO GR
AB	5-12	AW	5YR/ 4/3	5YR 3/2	3 CO SBK	2 M ABK
Bt1	12-23	CW	5YR 4/3	7.5YR 3/3	2 M ABK	–
Bt2	23-40	CI	5YR 4/3	7.5YR 3/3	3 M PR	3 M ABK

Horizon Name	Depth cm	Boundary†	Color Dry	Color Moist	Structure‡	Structure PartsTo‡
Cr	40-55		85% 5Y 7/2, 15% 10BG 2.5/1	60% 5YR 5/4, 25% 7.5YR 4/6, 15% 10YR 6/1		
R	55		ND	ND		
<b>Los Padres National Forest</b>						
A	0-18	AI	10YR 4/3	2.5YR 3/2	2 F SBK	–
R	18		80% 5GY 6/1, 15% 5GY 4/1, 5% 5GY 3/1	ND		

† Horizon Boundary: AI - abrupt irregular; AW abrupt wavy; CI – clear irregular; CW – clear wavy; VI – very irregular; VS – very abrupt smooth; VW-very abrupt wavy.

‡ Structure: 1 – weak; 2 – moderate; 3 – strong; VF – very fine; F – fine; M –medium; CO – coarse; TN – thin; TK – thick; VK – very thick; ABK – angular blocky; COL – columnar; GR – granular; PL – platy; PR – prismatic; SBK – subangular blocky.

ND – Not Determined

**Table 3-2.** Soil site classification determined from site pedon morphology.

<b>Soil Survey</b>	<b>Soil Taxonomy</b>
<b>Henneke Series</b>	Clayey-skeletal, magnesian, thermic Lithic Argixeroll
<b>Colusa County</b>	Clayey, magnesian, thermic, shallow Typic Argixeroll <sup>†</sup>
<b>Glenn County</b>	Loamy-skeletal, magnesian, mesic Lithic Argixeroll <sup>†</sup>
<b>Kings County</b>	Loamy-skeletal, magnesian, mesic Lithic Argixeroll <sup>†</sup>
<b>Napa County</b>	Loamy, mixed, active, thermic Lithic Haploxerept
<b>San Benito County</b>	Loamy-skeletal, magnesian, mesic, shallow Typic Haploxeralf <sup>†</sup>
<b>Shasta County</b>	Loamy-skeletal, magnesian, thermic Lithic Haploxerept <sup>†</sup>
<b>Tehama County</b>	Loamy, mixed, mesic, shallow Typic Argixeroll <sup>†</sup>
<b>Mariposa County</b>	Loamy-skeletal, magnesian, thermic Lithic Argixeroll <sup>†</sup>
<b>Mendocino County</b>	Loamy-skeletal, magnesian, thermic Lithic Argixeroll <sup>†</sup>
<b>Shasta-Trinity National Forest</b>	Clayey, magnesian, mesic, shallow Typic Argixeroll <sup>†</sup>
<b>Los Padres National Forest</b>	Loamy-skeletal, magnesian, mesic Lithic Haploxeroll <sup>†</sup>

<sup>†</sup>Elevation of the site (>3000 feet) suggested that the soil temperature regime was mesic but no seasonal temperature measurements were made. Soils were mapped as thermic soil temperature regime.

**Table 3-3.** Selected chemical properties and particle size distribution of soils from serpentinite derived landscapes.†

Horizon Name	Depth cm	K <sup>†</sup>	Mg <sup>†</sup>	Ca <sup>†</sup>	Na <sup>†</sup>	CEC- 7 <sup>††</sup>	BS	Ca:Mg †	pH	sand	silt	clay
		----- cmol(+)/kg -----						%			-----% -----	
		-										
<b>Colusa County</b>												
A	0-3	0.3	25.7	9.0	0.1	23.0	152	0.35	6.1	45.9	33.2	20.9
ABt	3-8	0.2	23.7	5.6	0.1	21.4	138	0.23	6.0	42.3	30.6	27.1
Bt1	8-30	0.1	23.2	1.9	<0.1	23.7	107	0.08	6.2	40.2	27.7	32.1
Bt2	30-42	0.1	44.3	0.3	<0.1	43.0	104	0.01	7.1	26.5	18.3	55.2
<b>Glenn County</b>												
A	0-9	0.2	21.9	4.4	<0.1	18.8	142	0.20	6.3	54.4	20.2	25.4
Bt	9-34	0.3	18.9	4.5	<0.1	27.5	92	0.20	6.3	48.6	17.9	33.5
<b>Kings County</b>												
A	0-4	0.2	12.1	1.4	0.1	23.7	83	0.58	6.1	42.8	54.5	2.7
Bt1	4-13	0.6	12.1	7.0	0.1	18.0	109	0.51	6.2	35.5	49.4	15.1
Bt2	13-40	0.8	17.7	4.4	0.1	20.0	115	0.25	6.2	27.3	45.4	27.3
<b>Napa County</b>												
A	0-6	0.4	16.4	24.1	0.1	31.1	132	1.47	5.8	43.2	42.3	14.5
Bt	6-20	0.1	16.2	21.5	0.1	27.9	136	1.32	5.7	53.8	29.2	17.0
<b>San Benito County</b>												
A	0-8	<0.1	3.0	0.7	<0.1	3.1	123	0.24	6.6	79.5	8.4	12.1
Bt	8-20	0.0	0.1	5.6	0.6	5.6	113	0.11	6.7	74.1	6.7	19.1
<b>Shasta County</b>												
A	0-3	0.3	9.7	3.5	0.1	13.2	103	0.36	5.7	36.7	49.0	14.3
Bt	3-40	0.2	10.1	2.0	<0.1	12.2	101	0.20	6.0	39.3	46.4	14.3
<b>Tehama County</b>												
A	0-3	0.4	12.4	16.3	<0.1	40.2	72	1.31	6.4	56.9	18.7	24.4
Bt1	3-7	0.5	20.2	16.5	<0.1	32.7	114	0.82	6.3	54.6	19.9	25.4
Bt2	7-16	0.2	27.7	13.7	0.1	30.0	139	0.50	6.1	50.9	16.7	32.4
<b>Mariposa County</b>												
A	0-3	0.6	28.3	5.8	0.1	29.3	119	0.20	5.9	42.1	25.9	32.0
Bt1	3-14	0.4	33.7	6.2	<0.1	27.9	144	0.18	6.0	40.6	34.0	25.4
Bt2	14-34	0.3	44.3	6.2	0.1	34.1	149	0.14	6.1	35.6	33.1	31.3
Bt3	34-49	0.1	78.2	4.4	0.1	43.6	190	0.06	5.9	35.9	30.8	33.3
<b>Mendocino County</b>												
A	0-2	0.5	12.8	2.2	0.1	19.3	80	0.18	5.5	56.6	30.3	13.1
Bt1	2-8	0.2	27.1	3.4	0.1	19.8	155	0.13	6.0	51.4	27.9	20.7
Bt2	8-30	0.2	30.5	3.7	0.1	22.9	150	0.12	6.2	50.7	26.2	23.2
<b>Shasta-Trinity National Forest</b>												
A1	0-2	0.2	18.8	6.6	0.0	23.0	112	0.35	6.1	34.6	43.9	21.6
A2	2-5	0.2	25.5	4.1	0.1	21.5	140	0.16	6.1	32.6	42.4	25.0
AB	5-12	0.3	29.3	3.5	<0.1	29.6	112	0.12	5.8	23.6	36.1	40.3

Horizon Name	Depth	K <sup>†</sup>	Mg <sup>†</sup>	Ca <sup>†</sup>	Na <sup>†</sup>	CEC-7 <sup>††</sup>	BS	Ca:Mg <sup>†</sup>	pH	sand	silt	clay
	cm	----- cmol(+)/kg -----					%			-----% -----		
		-										
Bt1	12-23	0.2	30.3	1.5	<0.1	26.5	121	0.05	5.5	19.7	28.7	51.6
Bt2	23-40	0.1	64.9	0.8	<0.1	48.7	135	0.01	5.3	11.1	21.5	67.4
<b>Los Padres National Forest</b>												
A	0-18	0.2	12.1	1.4	0.1	10.1	136	0.11	6.3	64.1	12.4	23.5

† Extracted by 1M NH<sub>4</sub>OAc at pH 7.

†† The CEC-7 underestimates the actual CEC as both the index cation (NH<sub>4</sub><sup>+</sup>) and the displacing cation (K<sup>+</sup>) can cause collapse of vermiculite and hydroxy-interlayered-materials, and these were present in most horizons.

**Table 3-4.** Soil density, coarse fraction volume, extractable Ca displaced with 1M NH<sub>4</sub>OAc at pH 7, and fine earth fraction (< 2mm) total Ca and Mg for each survey area.

	DB soil† g cm <sup>-3</sup>	CF††	Extractable Ca cmol(+) m <sup>-2</sup>	Extractable Ca g m <sup>-2</sup>	Fine Earth Total Ca g m <sup>-2</sup>	Fine Earth Total Mg g m <sup>-2</sup>	Extractable Ca Fine Earth Fraction Total Ca	Fine Earth Fraction Total Ca:Mg
<b>Colusa County</b>								
A	1.05 ± 0.08 (3)	0.12	249	50	610	2559	0.08	0.24
ABt	1.21 ± 0.02 (3)	0.27	247	50	833	4493	0.06	0.19
Bt1	1.33 ± 0.13 (3)	0.27	406	81	3740	22504	0.02	0.17
Bt2	1.05 ± 0.19 (2)	0.16	32	6	1755	10264	<0.01	0.17
	Σ		934	187	6939	39820	0.03	0.17
<b>Glenn County</b>								
A	1.09 ± 0.12 (3)	0.55	194	39	142	6669	0.27	0.02
Bt	1.14 ± 0.37 (3)	0.84	205	41	143	6454	0.29	0.02
	Σ		399	80	285	13123	0.28	0.02
<b>Kings County</b>								
A	0.80 ± 0.17 (3)	0.50	22	4	279	556	0.02	0.50
Bt1	1.15 ± 0.04 (3)	0.75	181	36	457	910	0.08	0.50
Bt2	1.06 ± 0.05 (3)	0.67	595	119	1444	3417	0.08	0.42
	Σ		799	160	2180	4883	0.07	0.45
<b>Napa County</b>								
A	1.51 ± 0.29 (3)	0.02	2140	429	2659	1879	0.16	1.41
Bt	1.32 ± 0.35 (4)	0.07	3695	740	5122	3907	0.15	1.31
	Σ		5835	1169	7781	5787	0.15	1.34
<b>San Benito County</b>								
A	1.51 ± 0.32 (3)	0.43	255	51	340	14650	0.15	0.02
Bt	1.16 ± 0.20 (3)	0.60	39	8	306	11769	0.03	0.03
	Σ		294	59	646	26419	0.09	0.02
<b>Shasta County</b>								
A	0.53 ± 0.33 (2)	0.78	48	10	53	393	0.18	0.14
Bt	0.94 ± 0.11 (2)	0.88	146	29	692	4749	0.04	0.15
	Σ		194	39	746	5143	0.05	0.14
<b>Tehama County</b>								
A	0.83 ± 0.04 (3)	0.43	58	12	1216	858	0.01	1.42
Bt1	1.18 ± 0.06 (3)	0.10	692	139	3862	2413	0.04	1.60
Bt2	1.24 ± 0.16 (2)	0.34	1215	244	7707	3478	0.03	2.22
	Σ		1966	394	12785	6750	0.03	1.89



	DB soil† g cm <sup>-3</sup>	CF††	Extractable Ca cmol(+) m <sup>-2</sup>	Extractable Ca g m <sup>-2</sup>	Fine Earth Total Ca g m <sup>-2</sup>	Fine Earth Total Mg g m <sup>-2</sup>	Extractable Ca Fine Earth Fraction Total Ca	Fine Earth Fraction Total Ca:Mg
<b>Mariposa County</b>								
A	1.07 ± 0.07 (3)	0.25	140	28	236	2793	0.12	0.08
Bt1	1.43 ± 0.05 (3)	0.38	605	121	990	12204	0.12	0.08
Bt2	1.63 ± 0.25 (2)	0.71	586	117	1061	10929	0.11	0.10
Bt3	1.51 ± 0.06 (2)	0.67	329	66	2169	5423	0.03	0.40
	Σ		1659	333	4455	31350	0.08	0.14
<b>Mendocino County</b>								
A	0.98 ± 0.15 (3)	0.16	33	7	202	2517	0.03	0.08
Bt1	1.46 ± 0.08 (3)	0.14	166	33	635	12753	0.05	0.05
Bt2	1.24 ± 0.46 (2)	0.80	186	37	456	9022	0.08	0.05
	Σ		384	77	1294	24292	0.06	0.05
<b>Shasta-Trinity National Forest</b>								
A1	0.93 ± 0.21 (3)	0.17	102	20	141	1539	0.15	0.09
A2	1.12 ± 0.13 (3)	0.13	120	24	280	2743	0.09	0.10
AB	1.06 ± 0.11 (3)	0.09	236	47	434	7159	0.11	0.06
Bt1	1.01 ± 0.01 (3)	0.05	158	32	392	11973	0.08	0.03
Bt2	1.05 ± 0.09 (3)	0.05	136	27	776	12354	0.04	0.06
	Σ		752	151	2023	35767	0.07	0.06
<b>Los Padres National Forest</b>								
A	1.18 ± 0.13 (3)	0.46	69	14	262	19132	0.05	0.01
	Σ		69	14	262	19132	0.05	0.01

† Density g cm<sup>-3</sup> ± standard deviation (number of samples).

†† Volume fraction Coarse Fraction (> 2mm) of horizon volume.

**Table 3-5.** Ca and Mg contents of soils and plants, *Vulpia microstachys* (Nutt.) Munro, grown in 500 cm<sup>3</sup> container filled with soil material from Henneke soil series map units.

Survey Area	Total†		Extractable††		Leaf†††		Ca:Mg Total	Ca:Mg Extractable	Ca:Mg Plant
	Mg	Ca	Mg	Ca	Mg	Ca			
	g kg <sup>-1</sup>	g kg <sup>-1</sup>	g kg <sup>-1</sup>	g kg <sup>-1</sup>	g kg <sup>-1</sup>	g kg <sup>-1</sup>			
<b>Colusa County</b>	92	14.7	2.0	0.5	2.4	2.4	0.16	0.24	1.02
<b>Glenn County</b>	133	2.6	3.0	0.8	2.1	1.9	0.02	0.26	0.92
<b>Kings County</b>	41.8	14.1	2.8	2.6	4.2	3.5	0.34	0.94	0.84
<b>Napa County</b>	22.1	27.9	1.5	3.9	1.4	6.5	1.26	2.56	4.67
<b>San Benito County</b>	211	4.9	0.6	0.2	0.6	0.7	0.02	0.26	1.19
<b>Shasta County</b>	114	15.2	1.4	0.6	2.2	2.0	0.13	0.42	0.92
<b>Tehama County</b>	54.8	90	2.7	3.0	1.3	6.6	1.64	1.15	5.01
<b>Mariposa County</b>	104	13.8	5.0	1.2	1.4	3.1	0.13	0.25	2.13
<b>Mendocino County</b>	163	9.6	2.6	0.7	6.1	1.5	0.06	0.26	2.49
<b>Shasta-Trinity National Forest</b>	100	6.0	3.0	0.7	4.5	2.3	0.06	0.22	0.50
<b>Los Padres National Forest</b>	167	2.3	1.5	0.4	1.2	1.6	0.01	0.24	1.34

† Total of fine earth fraction; †† extractable from fine earth fraction; ††† dry plant leaf and stem weight.

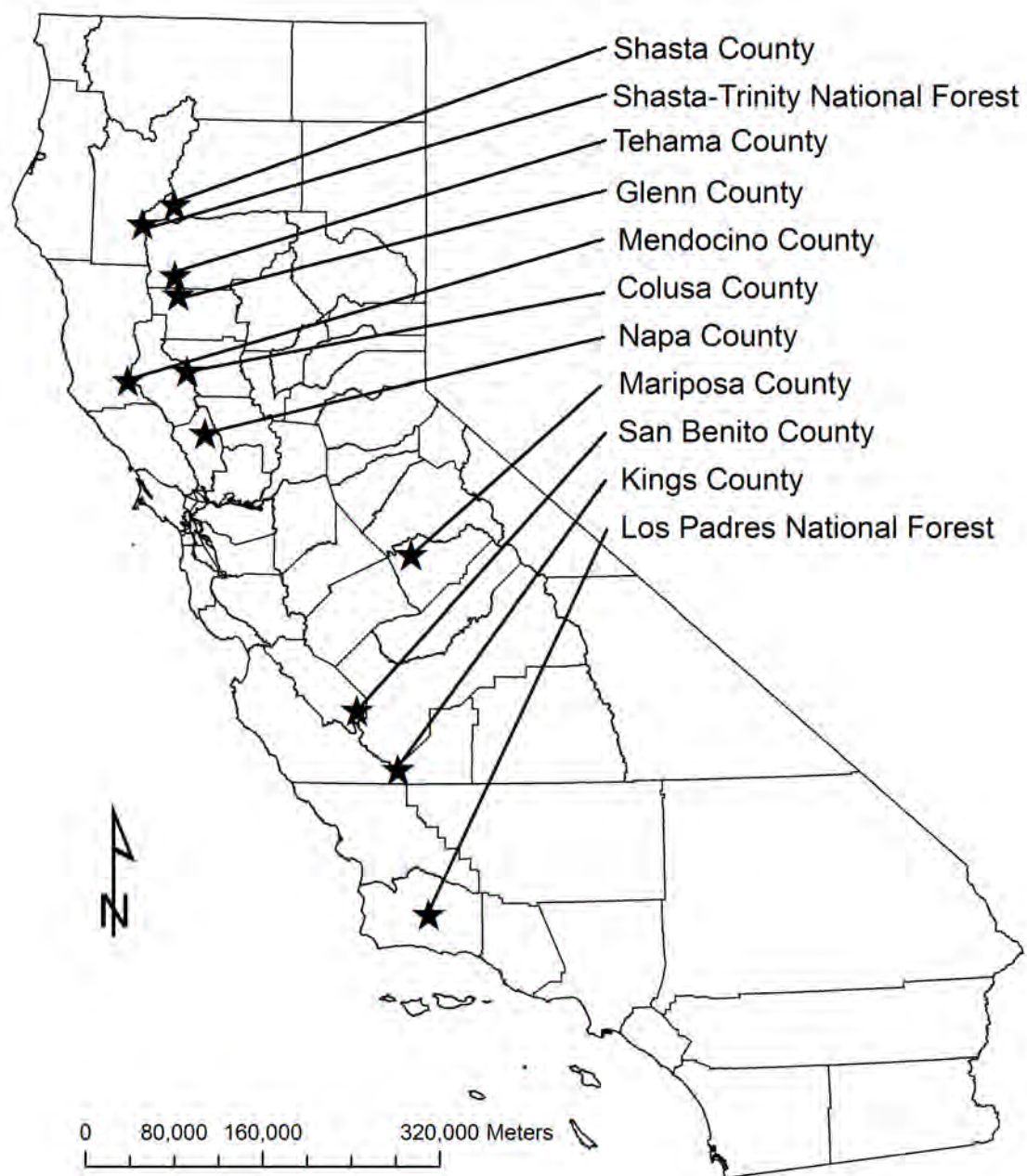


**Figure 3-1.** Serpentine soil sites by soil survey.

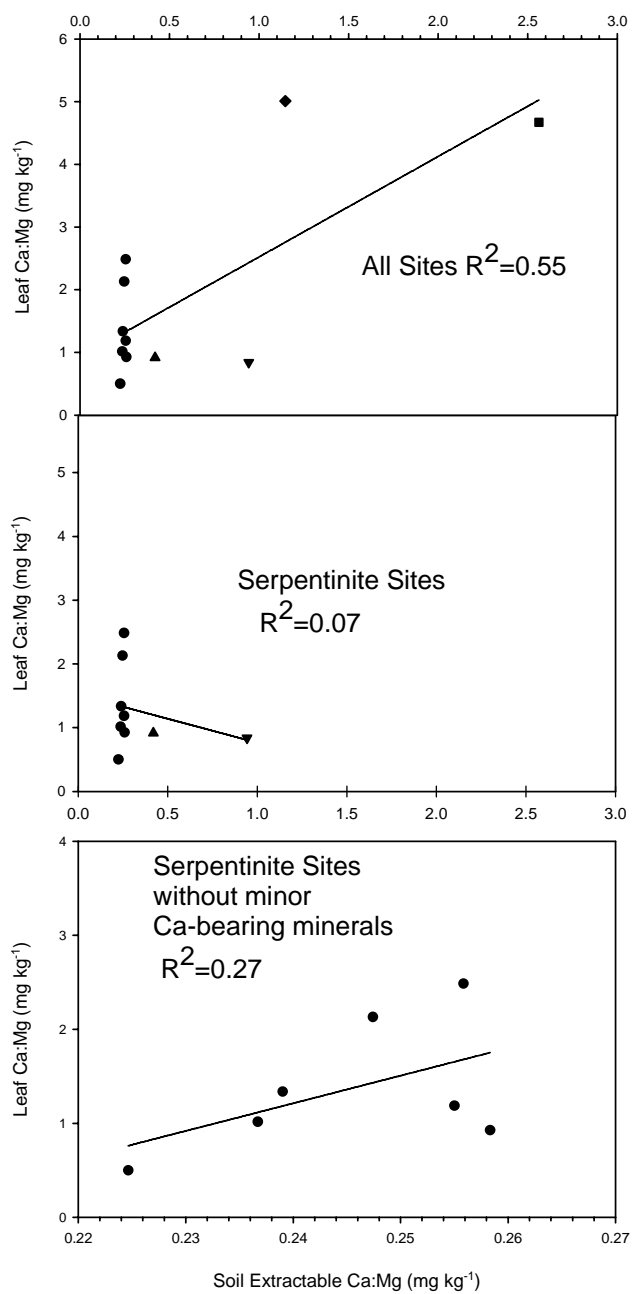


**Figure 3-2.** Correlations of soil extractable Ca:Mg to Ca:Mg in *Vulpia microstachys* (Nutt.) Munro leaf.

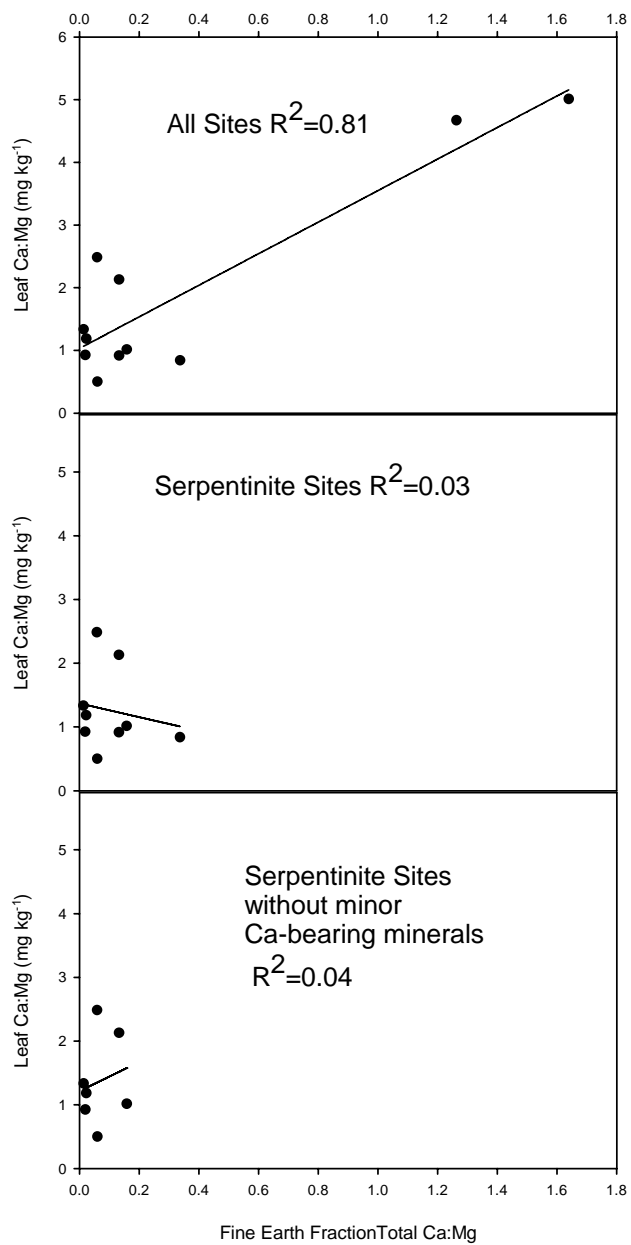


**Figure 3-3.** Total fine earth fraction elemental analysis Ca:Mg to Ca:Mg in *Vulpia microstachys* (Nutt.) Munro leaf.

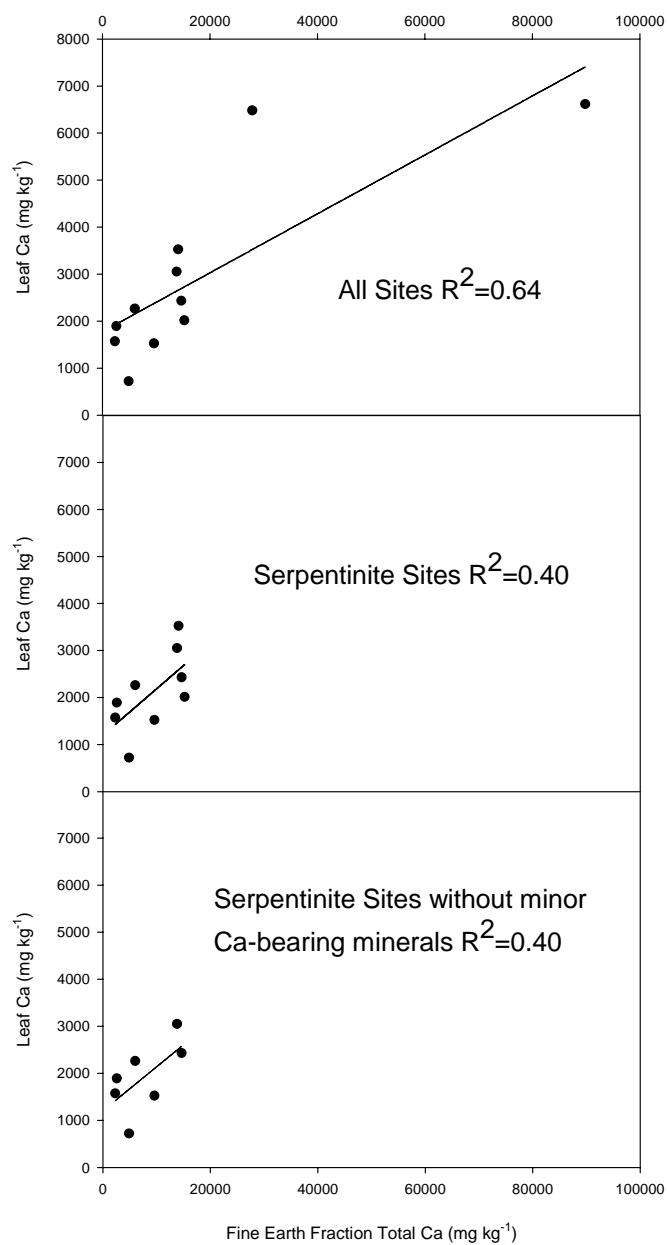


**Figure 3-4.** Total elemental analysis Ca to Ca in *Vulpia microstachys* (Nutt.) Munro leaf.

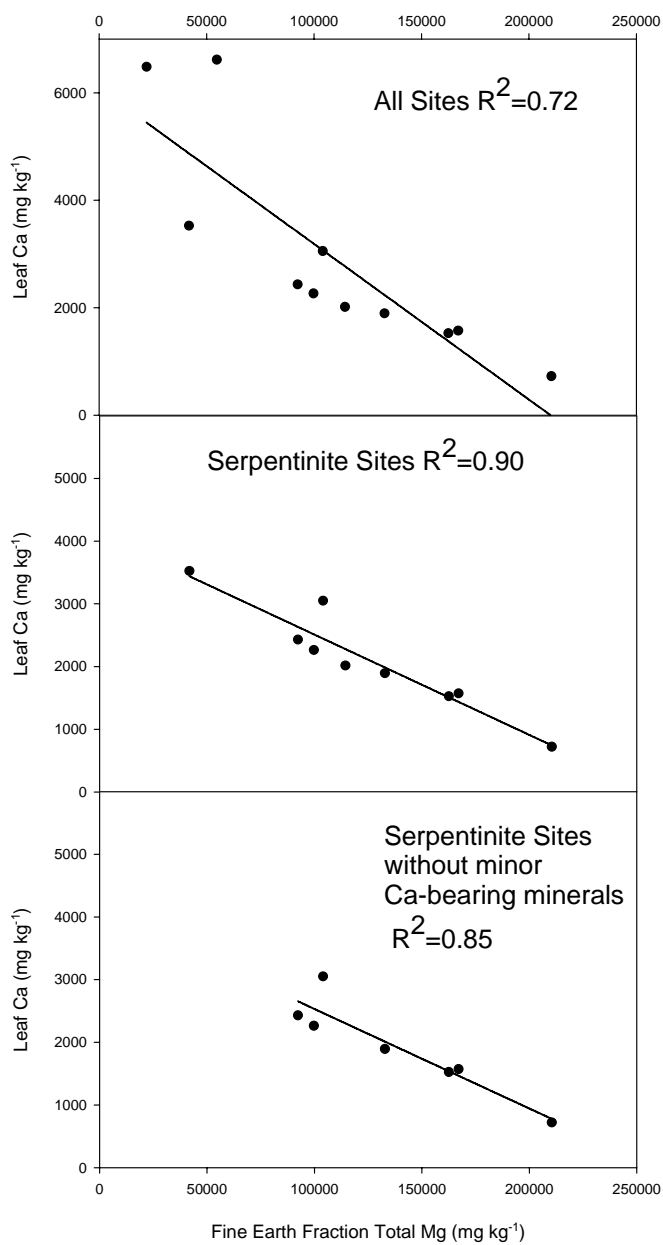


**Figure 3-5.** Total elemental analysis Mg to Ca in *Vulpia microstachys* (Nutt.) Munro leaf.

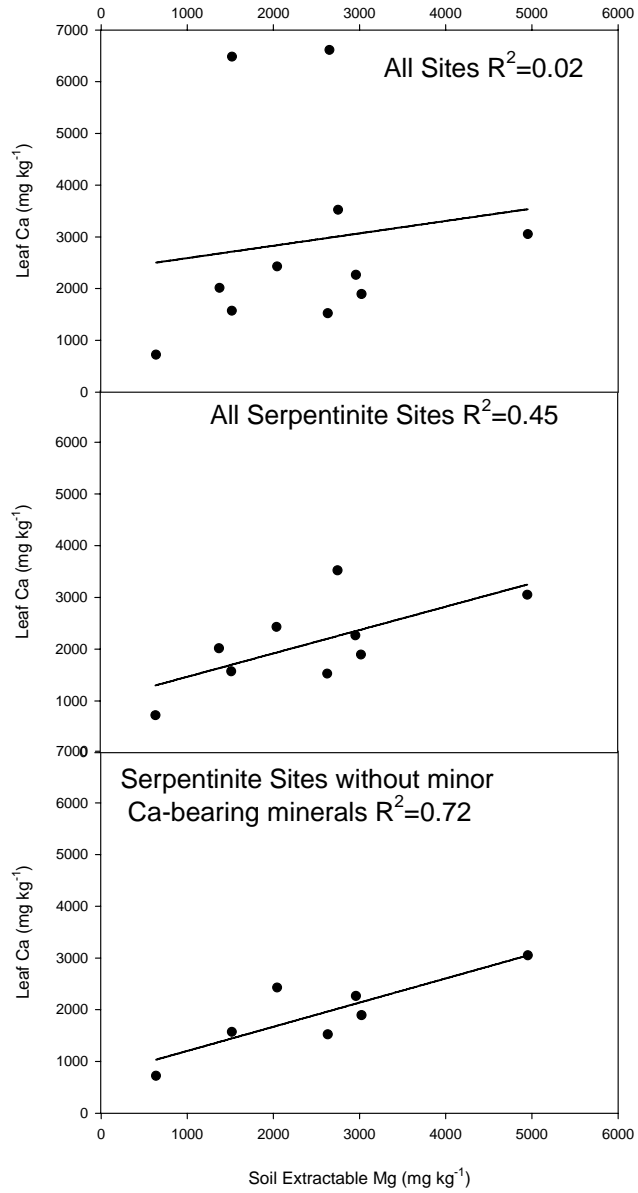


**Figure 3-6.** Soil extractable Mg to Ca in *Vulpia microstachys* (Nutt.) Munro leaf.



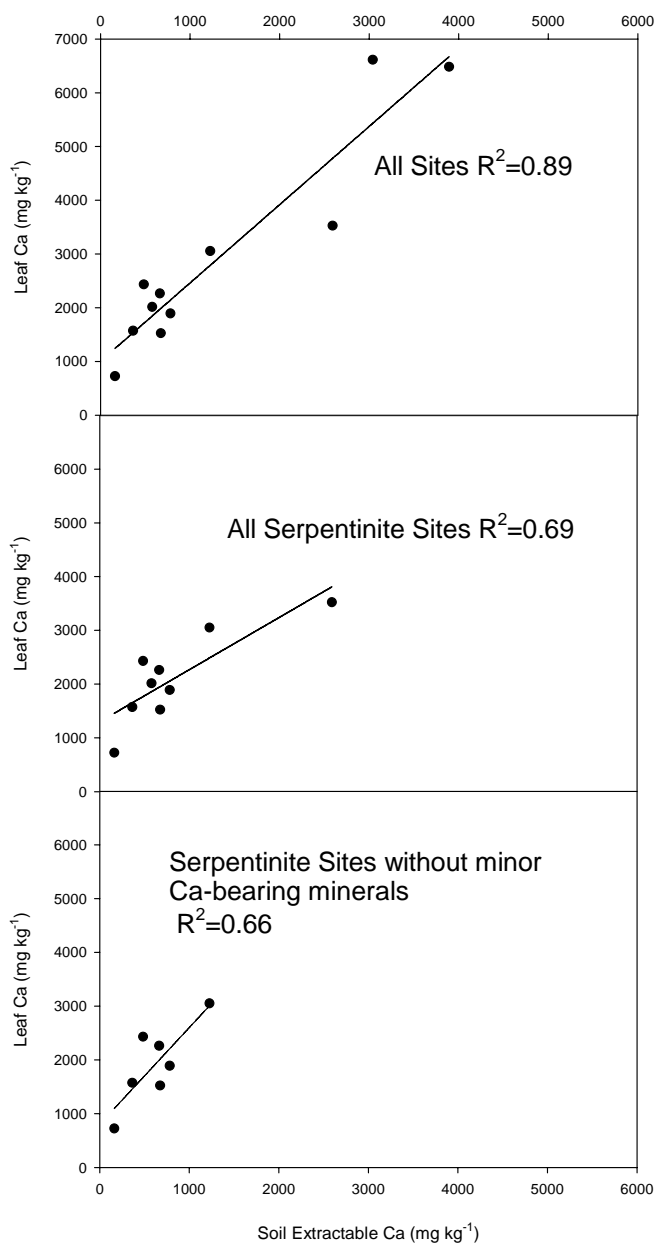


**Figure 3-7.** Correlation of soil extractable Ca to Ca in *Vulpia microstachys* (Nutt.) Munro leaf.

### 3.7 APPENDIX A

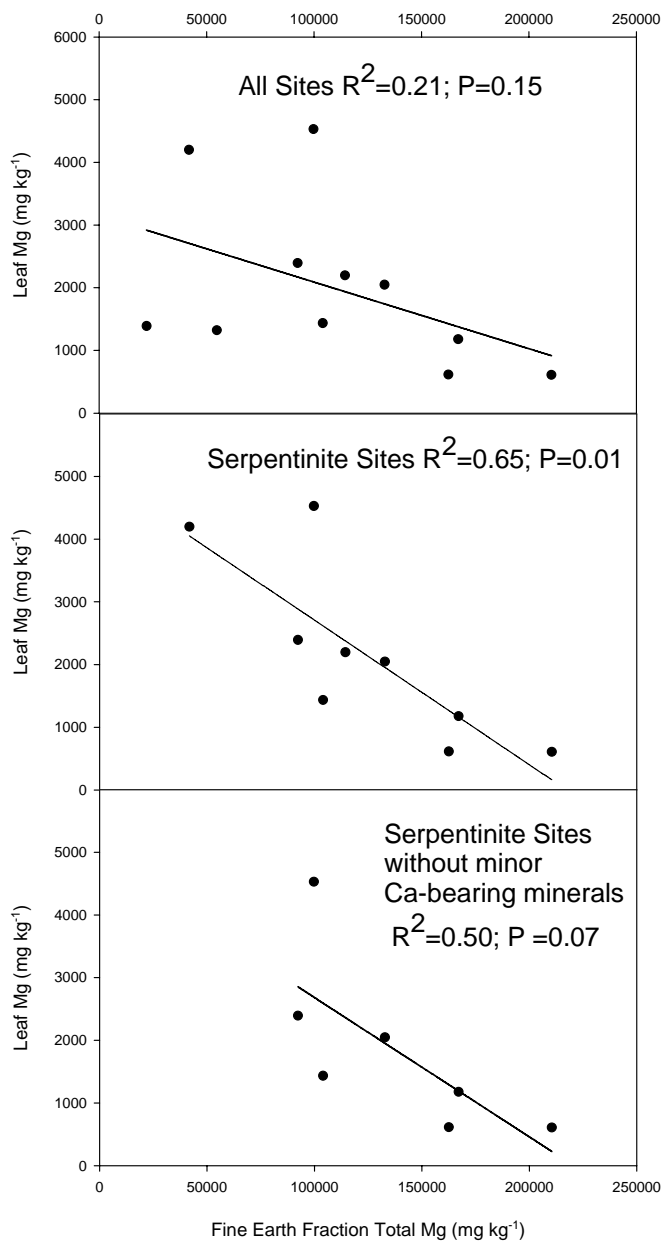


**Figure 3-8.** Total elemental analysis Mg to Mg in *Vulpia microstachys* (Nutt.) Munro leaf.

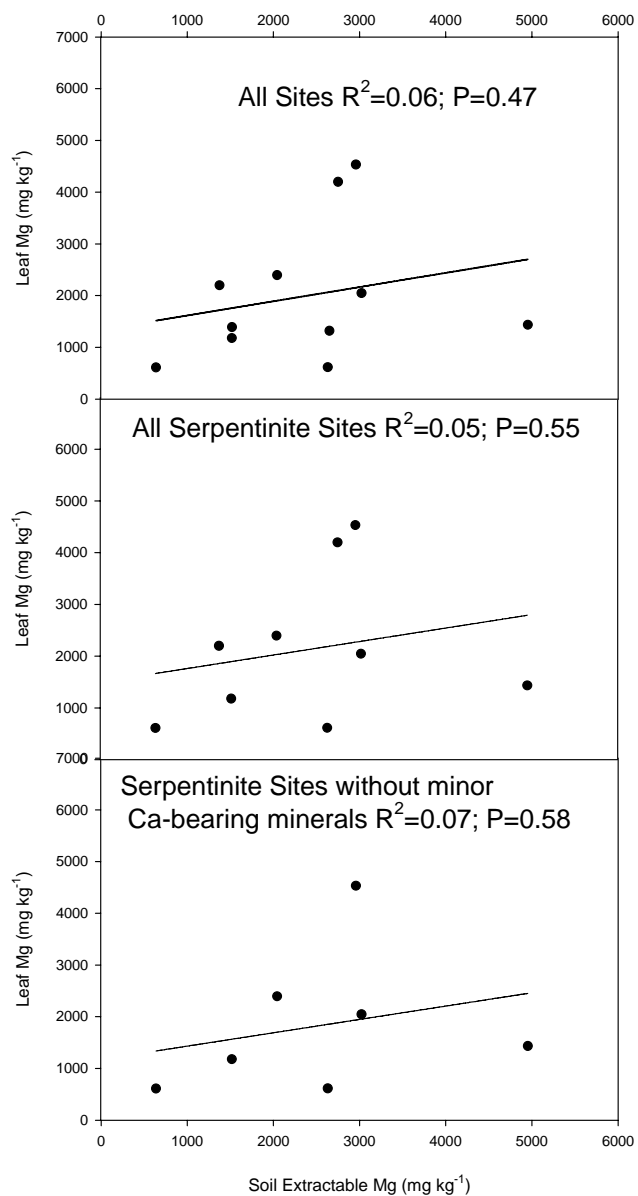


**Figure 3-9.** Correlation of soil extractable Mg to Mg in *Vulpia microstachys* (Nutt.) Munro leaf.

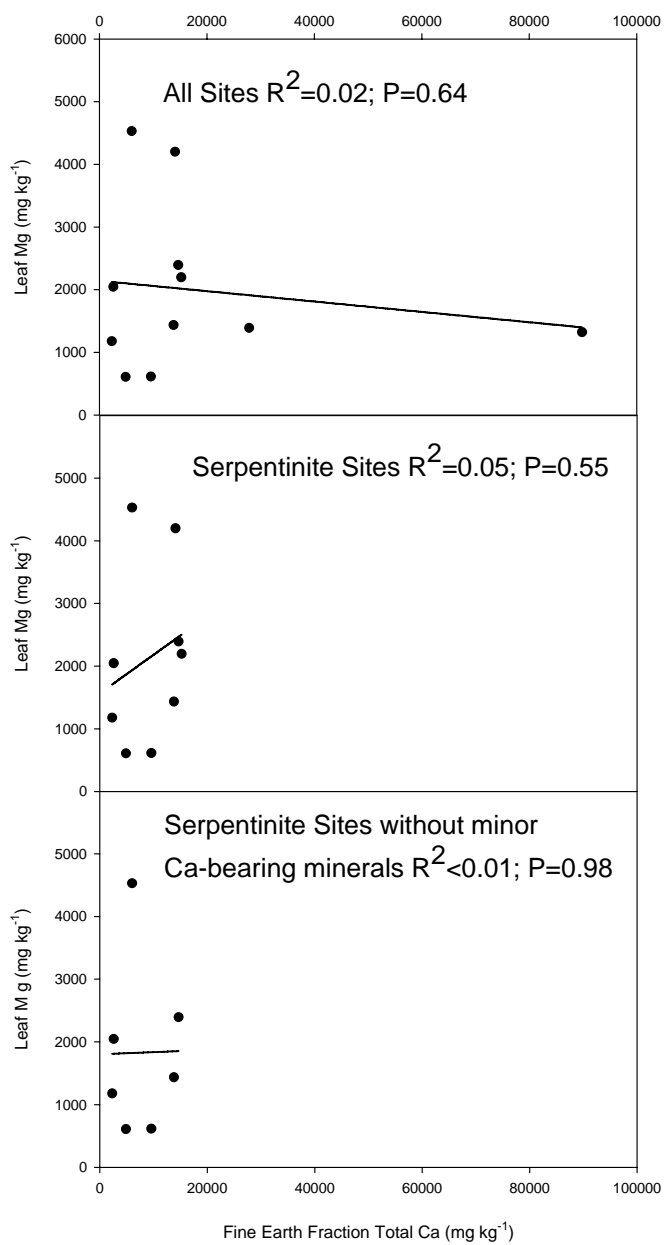


**Figure 3-10.** Total elemental analysis Ca to Mg in *Vulpia microstachys* (Nutt.) Munro leaf.

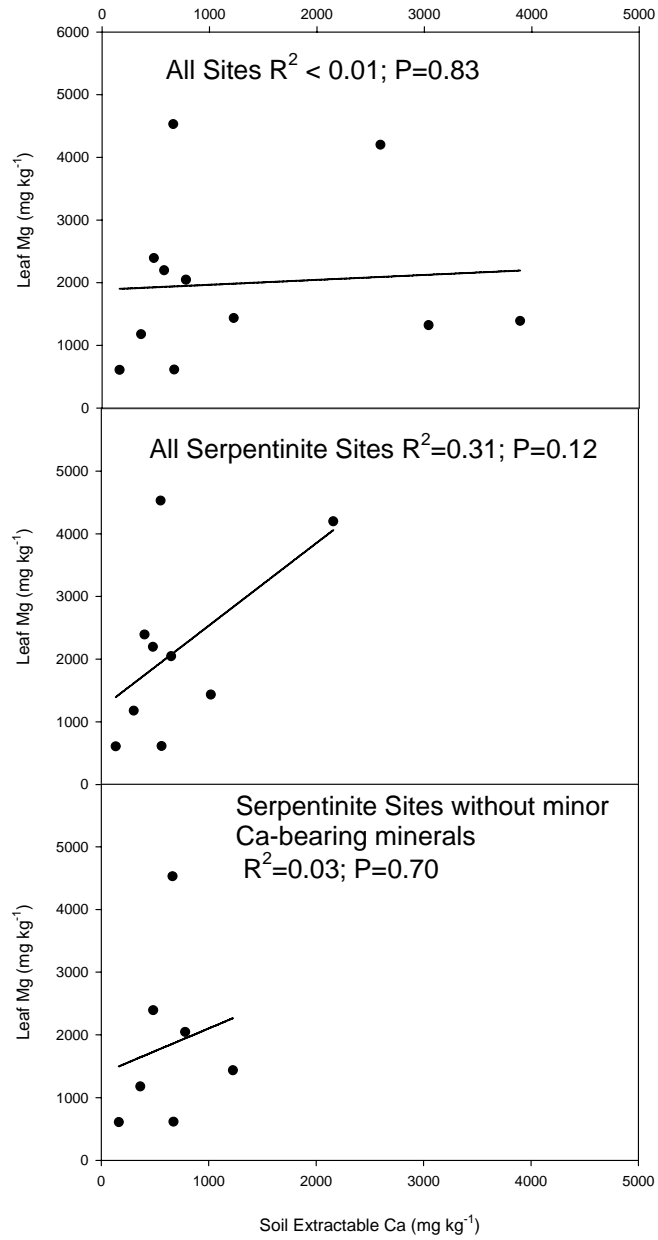


**Figure 3-11.** Soil extractable Ca to Mg in *Vulpia microstachys* (Nutt.) Munro leaf.

# **CHAPTER 4: DETERMINING IMMOBILE ELEMENT SUITABLE FOR MASS BALANCE CALCULATIONS FOR SOILS FORMED ON SERPENTINITIC LANDSCAPES**

## **4.1 INTRODUCTION**

The element Zr, as an immobile element, has been used as an independent calculation of strain (Jackson, 1985; Chadwick et al., 1990; Oh and Richter, 2005). Strain, or volume strain, results when a change in bulk density is not compensated by a change in the concentration of an immobile element (Chadwick et al., 1990). However, zirconium may be a problematic choice of an immobile element for strain computations in soils formed on serpentinitic landscapes, because the content of Zr is low in ultramafic rocks ( $20 \text{ mg kg}^{-1}$ ) and controlled by the silicate minerals olivine, pyroxenes, and amphiboles (Milnes and Fitzpatrick, 1989).

The ultramafic rock serpentinite is a product of the low temperature and pressure metamorphism/metasomatism of ultramafic rocks (Deer et al., 1979; O'Hanley, 1996). Metasomatism is a process of indefinite elemental replacement, loss and/or addition of elements as a

result of percolating solutions (Merill, 1906). As a result, during metamorphism or metasomatism, the anhydrous minerals of the idealized precursor rock peridotite become more hydrous (Page, 1966; Page, 1967; Coleman and Keith, 1971). Olivine is the dominant mineral in peridotite, the idealized serpentinite protolith, and is readily altered to serpentine during metasomatism. Serpentinite rocks usually also contain minor amounts of the minerals magnetite, brucite, talc, and various carbonates. Many other accessory minerals may be in serpentinites as trace components including pyroxenes, amphiboles, garnets, chlorite, vermiculite, chromite spinel, ilmenite, and titanite.

McGahan (2007) found that out of eleven parent materials sampled on serpentinitic landscapes only nine were serpentinites. The others were a rodingite and a meta-gabbro. Of the nine serpentinitic parent materials, no olivine remained. If identified at all, pyroxenes and amphiboles were only trace constituents of the serpentinitic parent materials.

Other elements commonly considered immobile are the rare earth elements (REEs) (Winchester and Floyd, 1977; Wood et al., 1979; Taylor and McLennan, 1985). REEs are the lanthanum series excluding Pm and including Y and Sc. The REEs are not immobile in all instances. Aide and Smith-Aide (2003) noted marked REE association with the clay fraction of soils. Movement of REEs with translocated clays would make them a poor choice for independent calculation of strain. Aide and Smith-Aide (2003) noted that the association of neodymium (Nd) and europium (Eu) with translocated clays was most the pronounced, but a general trend was that the heavy REEs, Eu to Lu, were more mobile than the light REEs, La to Sm. Niobium (Nb) has been used as an immobile element in ultramafic materials in investigations of Ni enrichment (Brimhall and Dietrich, 1987). But if niobium is associated with clay eluviation resulting in inter-horizon Nb redistribution, as Aide

and Smith-Aide (2003) found for Nd and Eu it would exclude niobium's use as an immobile element for intra-profile analysis.

Eleven profiles were sampled in conjunction with a survey of soils formed on serpentinitic landscapes across California (McGahan, 2007). Elemental analysis of the eleven parent materials revealed that many of the potentially immobile elements were below detectable limits.

Our basic question was, "Can zirconium be used as an immobile element for soils formed on serpentinitic landscapes?" Further, is there another element that can be used as an independent calculation of strain? We test Zr, Ti, Y and Nb to determine the suitability of each as immobile elements to calculate strain.

## **4.2 MATERIALS AND METHODS**

Two (Colusa and Tehama Counties) of the eleven sites used in this study are discussed in this paper because they differed in mineralogy (serpentinite and rodingite derived).

### **4.2.1 Field**

Pits were excavated by hand tools. Soils were described and sampled using conventional procedures (Soil Survey Division Staff, 1993). Henneke soil series (Clayey-skeletal, magnesian, thermic Lithic Argixerolls) survey modal locations were chosen as a basis of site locations (Soil Survey Staff, 1999) as it is a widely mapped soil series that is "soils formed in material weathered from serpentine and rocks of similar mineralogy" (Soil Survey Staff, 2005). The soil pits were excavated on summits above modal locations, in order to eliminate colluvial and alluvial influences, and were within the mapping polygon containing the



Henneke series modal location. The soils moisture regimes are xeric and the temperature regimes are mapped as thermic. Volume of cobbles and stones were estimated in the field. Soils and gravels were sampled in conjunction with compliant cavity bulk density measurements (Soil Survey Staff, 2004).

#### **4.2.2 Laboratory**

Soils were air dried, sieved to pass through a 2-mm sieve and analyzed for particle size distribution by pipette method as described by Gee and Bauder (1986). Volume of coarse fraction gravels was determined directly by displacement of water. Displacement was performed after sieving compliant cavity bulk density samples to separate the gravels, then soaking the gravels for 15 h in deionized water, washing to remove slaked soil material, and drying at 105°C for 15 h and weighed (Soil Survey Staff, 2004).

Three rocks from each parent material were ground with a quartz mortar and pestle to pass a 140-mesh sieve. An approximately 10 g sub-sample of the sieved < 2 mm soil from each horizon was ground and sieved to pass a No. 140 sieve. Major oxide percentages were determined by ICP-emission spectrometry following a LiBO<sub>2</sub> fusion and dilute nitric acid digestion or a leachate of hot (95°C) Aqua Regia for precious and base metals (Au, Ag, As, Bi, Cd, Cu, Hg, Mo, Ni, Pb, Sb, Se, Tl, Zn) (Sawhney and Stilwell, 1994).

The derivation and formulation of a mass balance model has been described in detail (Brimhall and Dietrich, 1987; Brimhall et al., 1988, 1991, 1992; Chadwick et al., 1990). Construction of the mass balance formulation is repeated here for clarity and follows that outlined by Chadwick et al (1990).

#### 4.2.2.1 Basic conservation equations

The equation relating a chemical element,  $j$ , contained in the parent material to a chemical element in the weathered soil is:

$$\left( \frac{(V_p \rho_p C(j, p))}{100} \right) + m_{(j, flux)} = \frac{(V_w \rho_w C(j, w))}{100} \quad \text{Equation 4-1.}$$

The left side of Equation 4-1 has two terms; the first term  $\left( \frac{(V_p \rho_p C(j, p))}{100} \right)$  is the mass, in grams, of the element,  $j$ , contained in the parent material prior to weathering, subscripted as  $p$ . The term  $V$  is the volume in  $\text{cm}^3$ ,  $\rho$  the dry bulk density in  $\text{g cm}^{-3}$ , and  $C$  the chemical element concentration in weight percent. The second term  $m_{j, flux}$  is mass of element  $j$  introduced into or removed from the parent material volume. The right hand side of the Equation 4-1 is the mass of the element  $j$  contained in the fine earth fraction of the weathered volume of interest, subscripted  $w$ , and is also given as the product of the volume, dry bulk density, and weight percent concentration of the horizon of interest.

Volumetric changes that occur during pedogenesis are determined by adopting the classical definition of strain,  $\varepsilon$ , the ratio of the volume change in a process to the initial volume:

$$\varepsilon(i, w) = \frac{(V_w - V_p)}{V_p} = \left( \frac{V_w}{V_p} - 1 \right) \quad \text{Equation 4-2.}$$

where the subscript  $i$  refers to the strain determined by use of an immobile strain index element, and subscript  $w$  refers to strain due to weathering.

The element mass fraction,  $m_{j,flux}$ , added or removed from the system relative to the mass of element  $j$  originally in the parent material  $C_{j,p}\rho_p V_p$  is the open-chemical-system transport function,  $\tau_{j,w}$ :

$$\tau_{(j, w)} = 100 \frac{m_{(j, flux)}}{(C_{(j, p)}\rho_p V_p)} \quad \text{Equation 4-3.}$$

### 4.3 RESULTS AND DISCUSSION

Of the eleven profiles sampled in conjunction with a survey of soils formed on serpentinitic landscapes across California (McGahan, 2007), Colusa and Tehama County survey area profiles had differed from each other in mineralogy (serpentinite and rodingite), had adequate concentrations of Zr, Ti, Y, and Nb to be detected by our analysis, and had multiple B horizons. Profiles with multiple B horizons were chosen to insure well developed soils. Additionally, B horizons have can have components of both eluviation and illuviation. Therefore, by choosing profiles with multiple B horizons we optimize conditions for possible movement of potential immobile elements Zr, Ti, Y and Nb between horizons as a result of pedogenesis.

Calculation of the transport function,  $\tau_{j,w}$ , for each element requires an estimate of strain (i.e., volume change). In soils, this can only be done by use of an immobile element. If we assume that an element like Zr, Ti, Y, or Nb has been immobile, it follows that the flux term  $m_{j,flux}$  in Equation 4-3 is zero, and hence the open-system mass transport term  $\tau_{j,w}$  is

assumed to be zero. Therefore, Equation 4-1, Equation 4-2, and Equation 4-3 can be used to give Equation 4-4 (Brimhall et al., 1988):

$$\varepsilon_{(i, w)} = \left( \frac{\rho_p C_{(j, p)}}{(\rho_w C_{(j, w)})} - 1 \right) \quad \text{Equation 4-4.}$$

Strain results ( $\varepsilon_{i,w}$ ) whenever a change in bulk density from the parent material,  $\rho_p$ , to the weathered soil,  $\rho_w$ , is not compensated by an inversely proportional change in the concentration of the immobile element in the weathered soil,  $C_{i,w}$ . Intense dissolution of minerals containing mobile elements leaves the weathered product enriched in immobile elements contained in chemically resistant minerals. Without a commensurate counteracting change in density, the calculated strain is negative, consistent with collapse, i.e., reduction of soil volume compared to the parent material volume. A greater-than-counteracting change in density results in dilation, i.e., increase in soil volume. Organic matter addition, faunal burrowing, and root dilation are among the mechanisms causing dilation (Chadwick et al, 1990; Brimhall et al, 1992).

### 4.3.1 Colusa County

The Colusa County fine earth fraction density generally decreased from the parent material with proximity to the surface, creating a large density ratio  $\rho_p/\rho_w$  (Fig. 4-1 A). The Colusa County Bt2 horizon was notable in that it had as low a bulk density as the A horizon.

Colusa County soils were Zr-, Ti-, Y-, and Nb-enriched with proximity to the surface on a weight % basis (Fig. 4-2 A) and based on the enrichment factor  $C_{j,w}/C_{j,p}$  (Fig. 4-2 B). The ratio of concentration of Zr, Ti, Y, and Nb in the parent material to the concentration in the weathered horizon,  $C_{j,p}/C_{j,w}$ , combine with the density ratio,  $\rho_p/\rho_w$ , to compute immobile

(i) strain values  $\varepsilon_{i,w}$  (Fig. 4-2 C). Strain profiles of the Colusa County soil had slight dilation in the Bt2 horizon and collapse in the overlying Bt1, ABt and A horizons (Fig. 4-2 C). Again this assumes that mass flux of the element in question,  $m_{Zr,flux}$ ,  $m_{Ti,flux}$ ,  $m_{Y,flux}$ , or  $m_{Nb,flux}$ , is zero, and therefore yields an open system chemical mass transport function,  $\tau_{j,w}$ , of zero in Equation 4-3.

The open-system-transport function,  $\tau_{j,w}$ , is the mass fraction added or subtracted from each sample. It is computed directly from density and chemical composition data in combination with volume change values derived from the strain calculations:

$$\tau_{(j, w)} = \left( \frac{\rho_w C(j, w)}{(\rho_p C(j, p))} (\varepsilon(i, w) + 1) - 1 \right) \quad \text{Equation 4-5.}$$

The open-system-transport function value of 0.0 indicates that the element has been immobile and it was affected only by internal closed-chemical-system processes. These are residual effects due to changes in bulk density, and strain effects due to changes in volume. A negative  $\tau_{j,w}$  value is a loss of element  $j$  mass, due to weathering, from that mass of element  $j$  originally present in the parent material. A positive value of  $\tau_{j,w}$  means that a mass of element  $j$  was added to the sample volume.

Assuming Zr immobility (i=Zr), the strain profile,  $\varepsilon_{Zr,w}$ , depicted in Figure 4-2 was used in Equation 4-5. The Colusa County Ti transported mass fraction,  $\tau_{Ti,w}$ ,  $\tau_{Y,w}$ , and  $\tau_{Nb,w}$ , showed losses in the A, ABt, and Bt1 horizons and a gain in the Bt2 horizon (Fig. 4-3). The strain correction reduces the gains that would be expected from weight % and enrichment factor inspection alone (Fig. 4-2) for an actual net loss for the profile when strain was cor-

rected using Zr. Zirconium enrichment in the ABt horizon (Fig. 4-2) was likely responsible for Ti, Y, and Nb calculated losses for the ABt horizon when strain was corrected using Zr. Correcting for strain with  $i=Ti$  for  $\varepsilon_{Ti,w}$  (Fig. 4-4),  $i=Y$  for  $\varepsilon_{Y,w}$  (Fig. 4-5), or  $i=Nb$  for  $\varepsilon_{Nb,w}$  (Fig. 4-6) resulted in less calculated mass transfer of Nb, Ti, and Y ( $\tau_{Ti,w}$ ,  $\tau_{Y,w}$ , or  $\tau_{Nb,w}$ ) than when correcting for strain with Zr. Mass transfer fraction of Zr ( $\tau_{Zr,w}$ ) in the ABt horizon was positive by a large fraction when Nb, Ti, or Y was used for strain correction computations (Fig. 4-4; Fig. 4-5; Fig. 4-6).

Pedogenic changes can be expressed by the ratio of the chemical concentration of an element in a soil horizon to its concentration in the parent material. This ratio, often called the enrichment factor,  $C_{j,w}/C_{j,p}$ , is derived from Figure 4-5.

The enrichment factor,  $C_{j,w}/C_{j,p}$ , of each sample volume is determined by three distinct processes: residual enrichment  $\rho_p/\rho_w$ , strain  $\frac{1}{(\varepsilon(i, w) + 1)}$ , and mass transport,  $1 + \tau_{j,w}$ :

$$\frac{C_{(j, w)}}{C_{(j, p)}} = \frac{\rho_p}{\rho_w} \times \frac{1}{(\varepsilon(i, w) + 1)} \times (1 + \tau_{(j, w)}) \quad \text{Equation 4-6.}$$

For a closed system the mass transport of an immobile element is zero, and therefore, the open-system transport term  $\tau_{j,w}$  of the immobile element is assumed to be zero. Substituting zero for the open-system transport term  $\tau_{j,w}$  and rearranging Equation 4-6 allows separation of the enrichment factor corrected for by strain from residual enrichment when  $\tau = 0$ :

$$\frac{C_{(j, w)}}{C_{(j, p)}} (\varepsilon(i, w) + 1) = \frac{\rho_p}{\rho_w} \quad \text{Equation 4-7.}$$

Residual enrichment of an element results from density changes due to dissolution and removal of mobile elements with a corresponding increase in porosity. The enrichment factor volume change may be associated with the density changes that are described by the strain term. Together, residual enrichment and enrichment corrected by strain describe “closed-system” contribution that results from mass movement of the element across the sample volume boundaries of soil horizons or pedons.

To graphically depict the open-system, transport Equation 4-6 is rearranged to Equation 4-8:

$$\frac{C_{(j,w)}}{C_{(j,p)}} (\varepsilon_{(i,w)} + 1) = \frac{\rho_p}{\rho_w} (1 + \tau_{(j,w)}) \quad \text{Equation 4-8.}$$

By substituting values of 0, 0.5, 1.0, -0.5, and -1.0 for the mass transport  $1 + \tau_{j,w}$  a series of lines are produced as guides to visualize the open-system transport.

The data for Zr ABt horizon do not plot along the  $\tau = 0$  of the open-system component graphic with strain corrected by Ti, Y and Nb, suggesting the transferred fraction was open system transport (Fig. 4-7). This fits with our assessment that Zr enrichment was responsible for apparent enrichment of Ti, Y, and Nb, when Zr was used to calculate strain. If Zr were used to calculate strain the ABt horizon would appear to have mass fraction loss of Ti, Y, and Nb (Fig. 4-8). However, when using Ti, Y and Nb for strain correction, the mass transfer fraction of Ti, Y, and Nb all plotted along the  $\tau = 0$  in the graphical depiction of the open-system and this indicated closed system transport (Fig. 4-9). Therefore, calculating strain using Ti, Y or Nb is acceptable, but Zr should not be used in strain correcting computations for this profile.

Analysis of the other REEs indicated that, for the Colusa County soil, La, Pr, Sm, Eu, Gd, and Er plotted along the  $\tau = 0$ , when strain was corrected with Ti, Y or Nb. The element Sc and REEs Ce, Tb, Dy, Ho, Yb, and Lu did not behave conservatively and would not be suitable for strain correction computations for the Colusa County soil.

### 4.3.2 Tehama County

Tehama County soils were Zr-, Ti-, Y-, Nb-depleted with proximity to the surface on a weight % basis and based on enrichment factor (Fig. 4-10 A and B). All strain profiles of the Tehama County soil had significant dilation that increased in magnitude with proximity to the surface (Fig. 4-10 C). Tehama County strain profiles also suggest that Zr, Ti, Y and Nb behaved similarly during soil genesis.

The Tehama County Ti transported mass fraction,  $\tau_{Zr,w}$ ,  $\tau_{Ti,w}$ ,  $\tau_{Y,w}$ , and  $\tau_{Nb,w}$ , corrected by strain,  $\varepsilon_{Zr,w}$ ,  $\varepsilon_{Ti,w}$ ,  $\varepsilon_{Y,w}$ , and  $\varepsilon_{Nb,w}$ , showed only minor gains or losses irrespective of the strain correcting element (Fig. 4-11). The  $\tau$  data points plotted near the  $\tau = 0$  line of the open-system component graphic (Fig. 4-12). This indicated closed system transport for Zr, Ti, Y, and Nb. For the Tehama County soil all of the REE's, and the element Sc, plotted along the closed-system transport line. Any of these elements would be suitable for strain correcting computations.

## 4.4 CONCLUSION

The question was asked: Can zirconium be used as an immobile element for soils formed on serpentinitic landscapes? The use of Zr as an independent calculation of strain for soils formed on serpentinitic landscapes was suspect. While it was acceptable to use Zr in the



Tehama County profile, it was not for the Colusa County profile. Our concern about the use of Zr in strain correction computations on serpentinitic landscapes appears to be warranted. Furthermore, we asked: Is there another element that can be used as an as an independent calculation of strain? Calculation of strain using the alternate elements we tested, Ti, Y, or Nb, would be possible for the Colusa County and Tehama County profiles. All of the REEs were effectively conservative in the Tehama County profile. The Colusa County soil had several REEs that were effectively conservative, but others were not.

The difference in element behavior in Colusa versus Tehama Counties is probably due to our choice of sites. While both sites are in serpentinitic landscapes, they are dissimilar in parent material composition. Content of Zr in the Tehama County (rodingite) parent material was greater than the Zr content of the Colusa County (serpentinite) parent material. We could speculate that this is not merely an analytical problem arising from low concentrations. In addition to being dissimilar in Zr content, the mineralogical suite of the Colusa County serpentinite is quite different from the Tehama County rodingite. Since no analysis was performed on a size fraction basis of the soil we cannot determine if Zr was included in a mineral in the Tehama County parent material that was more resistant to weathering than the minerals of the Colusa County parent material. Additionally, without analysis of size fractions we cannot determine if Zr was incorporated into clays and/or oxides that suffered differing translocation fates in the two profiles.

These results suggest that the relative mobility of elements must be evaluated for each pedon on serpentinitic landscapes in order to identify suitable conservative elements for strain analysis.

## 4.5 REFERENCES

- Aide, M., and C. Smith-Aide. 2003. Assessing soil genesis by rare-earth elemental analysis. *Soil Sci. Soc. Am. J.* 67:1470–1476.
- Brimhall, G.H. and W.E. Dietrich. 1987. Constitutive mass balance relations between chemical composition, volume, density, porosity, and strain in metasomatic hydrochemical systems: results on weathering and pedogenesis. *Geochimica et Cosmochimica Acta*, 51: 567-587.
- Brimhall, G.H., C.J. Lewis, J.J. Ague, W.E. Dietrich, J. Hampe and P. Rix. 1988. Metal enrichment in bauxites by deposition of chemically mature aeolian dust. *Nature*, 333: 819-824.
- Brimhall, G.H., C.J. Lewis, C. Ford, J. Bratt, G. Taylor and O. Warren. 1991. Quantitative geochemical approach to pedogenesis: importance of parent material reduction, Volumetric Expansion, and Eolian Influx in Laterization. *Geoderma*, 51: 51-91.
- Brimhall, G.H., O.A. Chadwick, C.J. Lewis, W. Compston, I.F. Williams, K.J. Danti, W.E. Dietrich, M.E. Power, D. Hendricks and J. Bratt. 1992. Deformational mass transport and invasive processes in soil evolution. *Science*, 255: 695-702.
- Chadwick, O.A., G.H. Brimhall, D.M.Hendricks. 1990. From a black box to a gray box -- a mass balance interpretation of pedogenesis. *Geomorphology*, 3: 369-390.

- Coleman, R.G. and T.C. Keith. 1971. A chemical study of serpentinization-Burro Mountain, California. *Journal of Petrology* 12:311-328.
- Deer, W.A., R.A. Howie, and J. Zussman. 1997. *Rock-forming minerals*. 2nd ed. Geological Society, London.
- Gee, G.W. and J.W. Bauder. 1986. Particle size analysis. In: A. Klute (Editor), *Methods of soil analysis: Part 1 Physical and mineralogical methods*. American Society of Agronomy, Madison, WI., pp. 383-411.
- Gouveia, M.A., M.I. Prudencio, M.O. Figueiredo, L.C.J. Pereira, J.C. Waerenborgh, I. Morgado, T. Pena and A. Lopes. 1993. Behaviour of REE and other trace and major elements during weathering of granite rocks, Evora, Portugal. *Chem. Geol.* 107:293–296.
- Jackson, M.L. 1985. *Soil chemical analysis - Advanced course*. Revised 2nd edition, Parallel Press, Madison Wisconsin.
- Marsh, J.S. 1991. REE fractionation and Ce anomalies in weathered Karoo dolerite. *Chem. Geol.* 90:189–194.
- McGahan, Donald G. 2007. *A survey of soils formed on serpentinitic landscapes in California*. Ph.D. diss. University of California Davis.
- Merrill, G.P. 1906. *A treatise on rocks, rock-weathering and soils*. New ed. Macmillan, New York, London.
- Milnes A. R. and Fitzpatrick R. W. (1989) Titanium and zirconium minerals, p. 1131–1205, *In* J. B. Dixon and S. B. Weed eds. *Minerals in the soil environment*. Soil Science Society of America., Madison, Wis., USA.

- O'Hanley, D.S. 1996. *Serpentinites: records of tectonic and petrological history*. Oxford University Press, New York.
- Oh, N. and D.D. Richter. 2005. Elemental translocation and loss from three highly weathered soil–bedrock profiles in the southeastern United States. *Geoderma*. 126:5-25.
- Page, N.J. 1966. *Mineralogy and chemistry of the serpentine group minerals and the serpentinization process*. Ph.D. diss. University of California Berkeley.
- Page, N.J. 1967. Serpentinization considered as a constant volume metasomatic process: a discussion. *The American Mineralogist* 52:545-549.
- Sawhney, B.L. and D.E. Stilwell. 1994. Dissolution and elemental analysis of minerals, soils and environmental samples, p. 49-82, *In* J. E. Amonette and L. W. Zelazny, eds. *Quantitative methods in soil mineralogy*, SSSA Miscellaneous Publication. Soil Science Society of America, Madison, Wis., USA.
- Soil Survey Division Staff. 1993. *Soil survey manual - Agriculture Handbook No. 18*. U.S. Dept. of Agriculture: Supt. of Docs. U.S. G.P.O., Washington, DC.
- Soil Survey Staff. 1999. *Soil taxonomy: a basic system of soil classification for making and interpreting soil surveys*. 2 ed. United States Department of Agriculture, Natural Resources Conservation Service, Washington, DC.
- Soil Survey Staff. 2004. *Soil survey laboratory methods manual - soil survey investigations report No. 42*. [Online WWW]. Available URL: <http://soils.usda.gov/technical/Imm/> [Accessed 7 February 2007]

Soil Survey Staff., 2005. Official soil series descriptions [Online WWW]. Available URL: “<http://soils.usda.gov/technical/classification/osd/index.html>” [Accessed 7 February 2007].

Taylor, S.R. and S.M. McLennan. 1985. The continental crust: its composition and evolution. Blackwell Scientific Publication, Oxford, England.

Winchester, J.A. and P.A. Floyd. 1977. Geochemical discrimination of different magma series and their differentiation products using immobile elements. *Chem. Geol.* 20, 325-343.

Wood, D.A., J.L. Joron and M. Treuil. 1979. A re-appraisal of the use of trace elements to classify and discriminate between magma series erupted in different tectonic settings. *Earth Planet. Sci. Letts.* 45, 326-336.

## 4.6 FIGURES

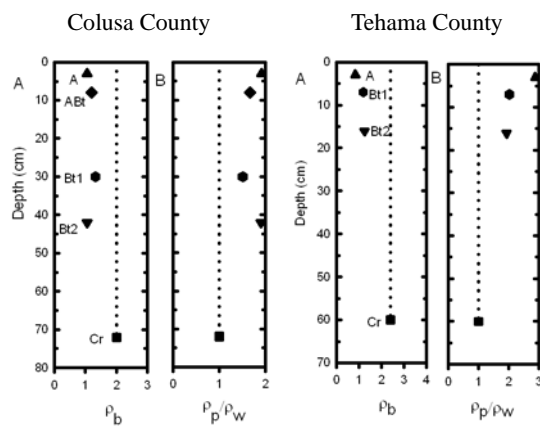


**Figure 4-1.** Depth plots of bulk density ( $\rho_b$ ), and density ratio (bulk density of parent material  $\rho_p$  to the bulk density of each horizon  $\rho_w$ ). Dotted vertical line is visual indicator for parent material.

Colusa County

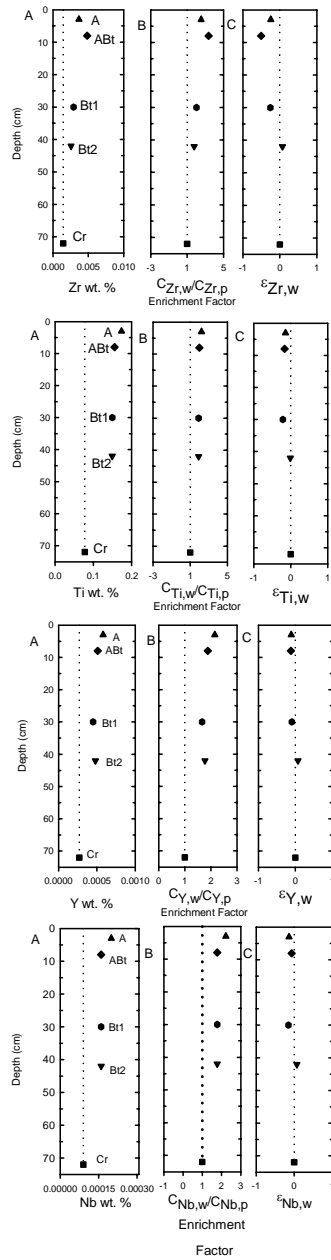


**Figure 4-2.** Colusa depth plots (A) weight percent Zr, Ti, Y, or Nb; (B) the enrichment factor is the ratio of concentration  $j$  in each horizon ( $C_{j,w}$ ) to parent material ( $C_{j,p}$ ) where  $j$  is Zr, Ti, Y, or Nb. Together the weight percent and enrichment factor are used to calculate (C) strain,  $\epsilon$ , for element Zr, Ti Y or Nb. Dotted vertical line is visual indicator for parent material value.

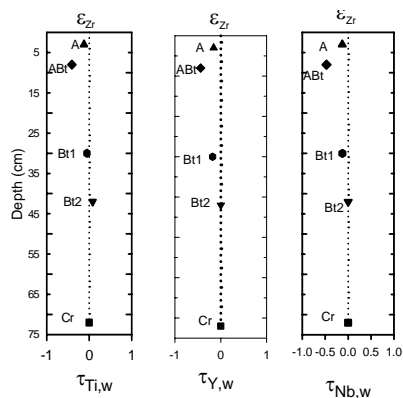


**Figure 4-3.** Colusa County transported mass fraction,  $\tau_{Ti}$ ,  $\tau_Y$ , and  $\tau_{Nb}$ , with strain corrected by  $Zr$ ,  $\epsilon_{Zr}$ . Dotted vertical line is visual indicator for parent material value.

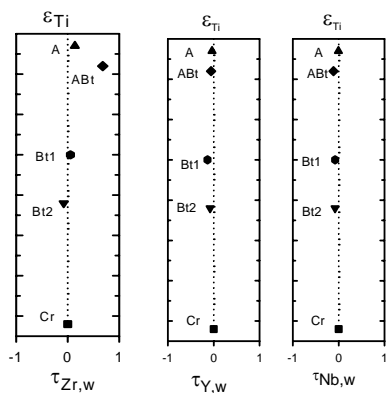


**Figure 4-4.** Colusa County transported mass fraction,  $\tau_{Zr}$ ,  $\tau_Y$ , and  $\tau_{Nb}$ , with strain corrected by  $Ti$ ,  $\epsilon_{Ti}$ . Dotted vertical line is visual indicator for parent material value.



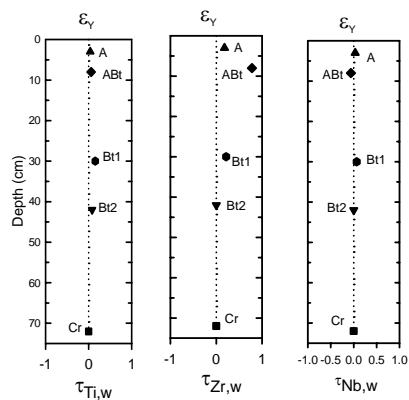


**Figure 4-5.** Colusa County

transported mass fraction,  $\tau_{Ti}$ ,  $\tau_{Zr}$ , and  $\tau_{Nb}$ , with strain corrected by Y,  $\epsilon_Y$ . Dotted vertical line is visual indicator for parent material value.

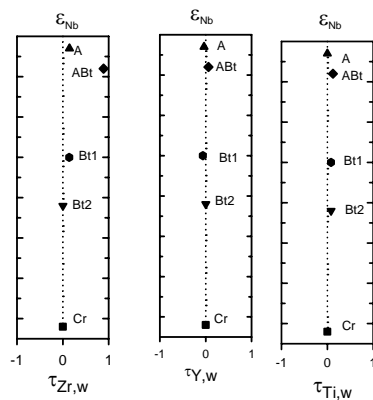


**Figure 4-6.** Colusa County

transported mass fraction,  $\tau_{Zr}$ ,  $\tau_Y$ , and  $\tau_{Ti}$ , with strain corrected by Nb,  $\epsilon_{Nb}$ . Dotted vertical line is visual indicator for parent material value.

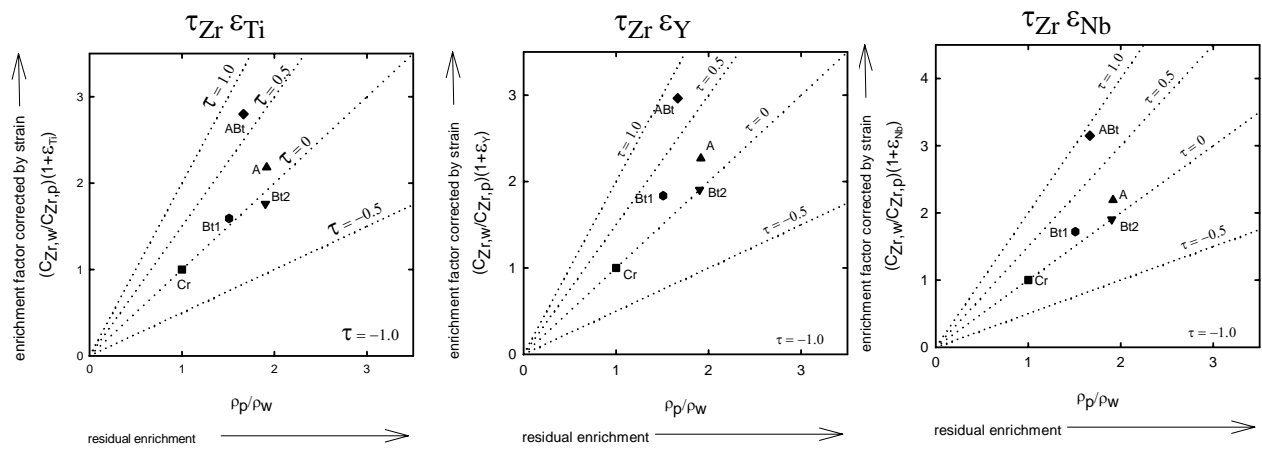


**Figure 4-7.** Colusa County contributions of the components of closed system mass movement of the element Zr, across the sample volume boundaries (soil horizons) using Ti ( $\epsilon_{Ti,w}$ ), Y ( $\epsilon_{Y,w}$ ) and Nb ( $\epsilon_{Nb,w}$ ) as the strain correcting element. Dotted lines represent  $\tau$ , the mass fraction added or subtracted from each sample at 0, 50 and 100%.

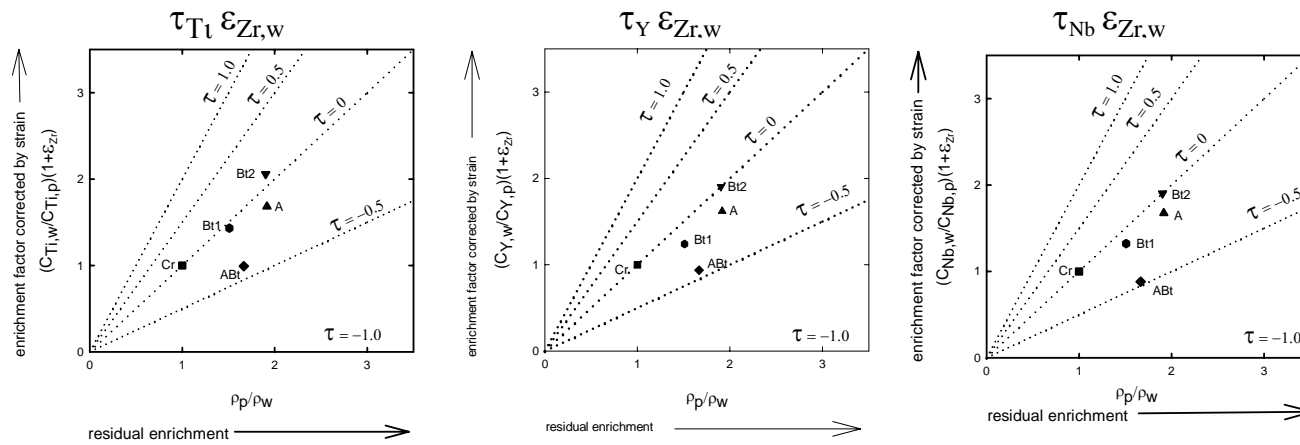


**Figure 4-8.** Colusa County contributions of the components of closed system mass movement of the element Ti, Y or Nb across the sample volume boundaries (soil horizons) using Zr as the strain correcting element ( $\epsilon_{Zr,w}$ ). Dotted lines represent  $\tau$ , the mass fraction added or subtracted from each sample at 0, 50 and 100%.

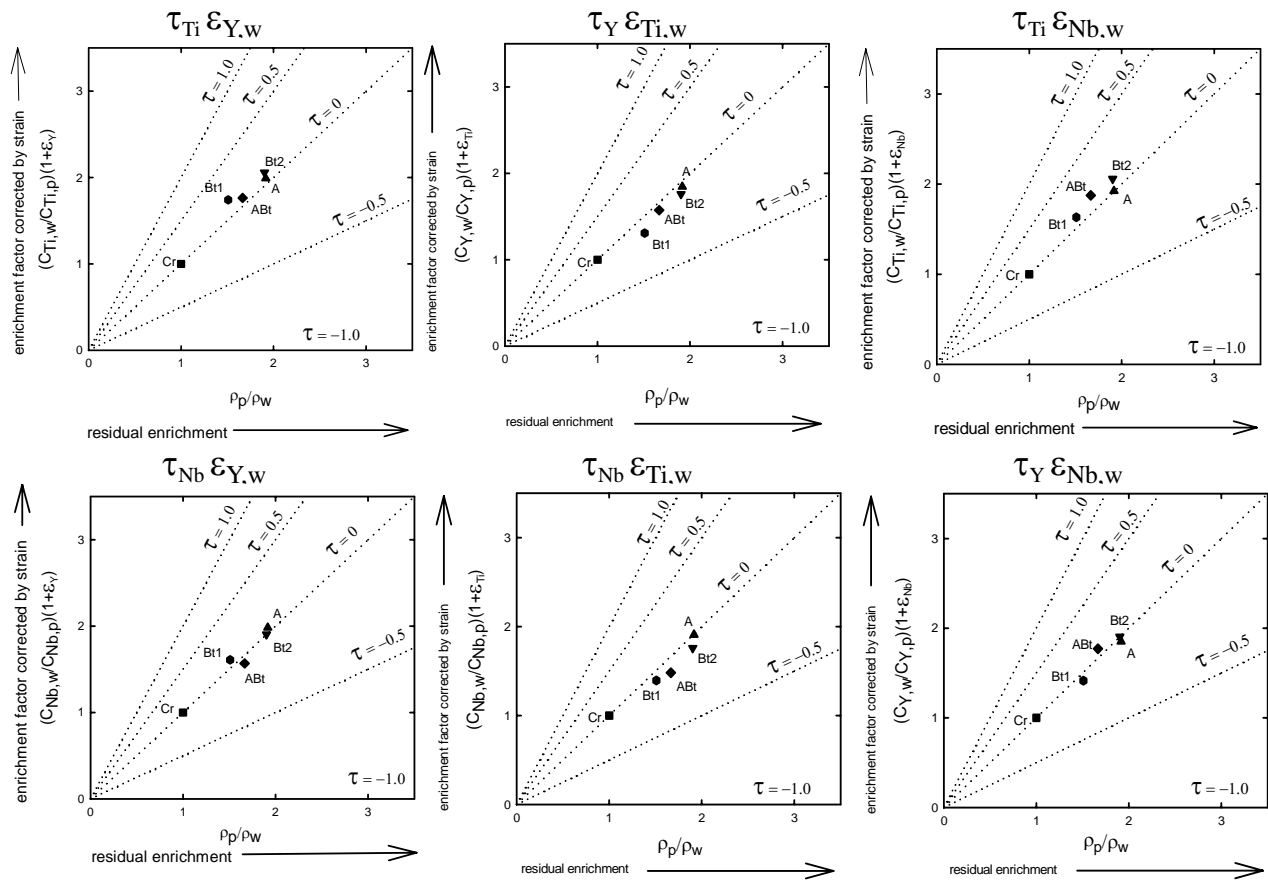


**Figure 4-9.** Colusa County contributions of the components of closed system mass movement across the sample volume boundaries (soil horizons). Dotted lines represent  $\tau$ , the mass fraction added or subtracted from each sample at 0, 50 and 100%.

## Tehama County

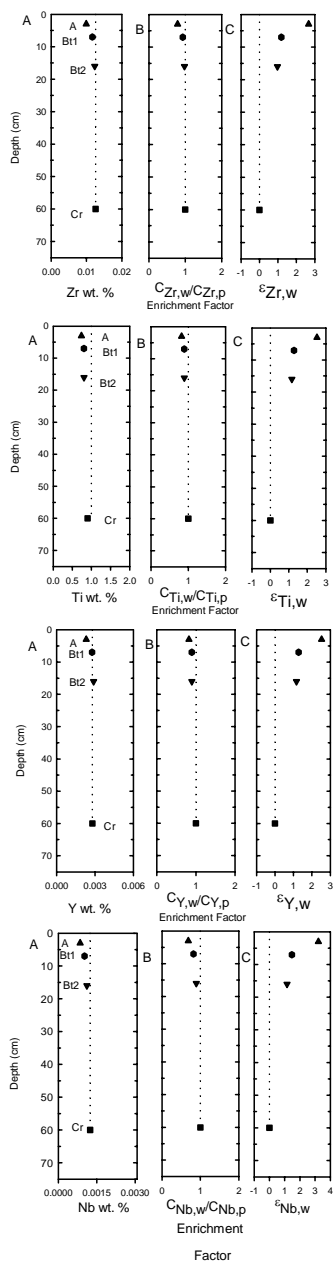


**Figure 4-10.** Tehama County depth plots (A) weight percent Zr, Ti, Y, or Nb; (B) the enrichment factor is the ratio of concentration  $j$  in each horizon ( $C_{j,w}$ ) to parent material ( $C_{j,p}$ ) where  $j$  is Zr, Ti, Y, or Nb. Together the weight percent and enrichment factor are used to calculate (C) strain,  $\epsilon$ , for element Zr, Ti Y or Nb. Dotted vertical line is visual indicator for parent material value.

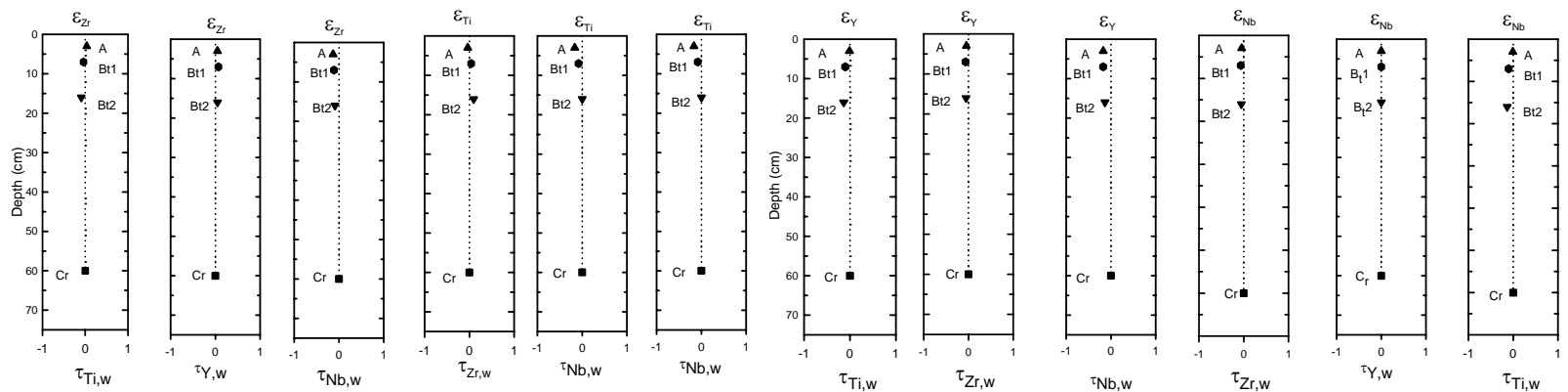


**Figure 4-11.** Tehama County transported mass fraction,  $\tau_{Zr}$ ,  $\tau_{Ti}$ ,  $\tau_Y$ , or  $\tau_{Nb}$ , grouped by strain correcting element,  $\epsilon_{Zr}$ ,  $\epsilon_{Ti}$ ,  $\epsilon_Y$ , or  $\epsilon_{Nb}$ . Dotted vertical line is visual indicator for parent material value.

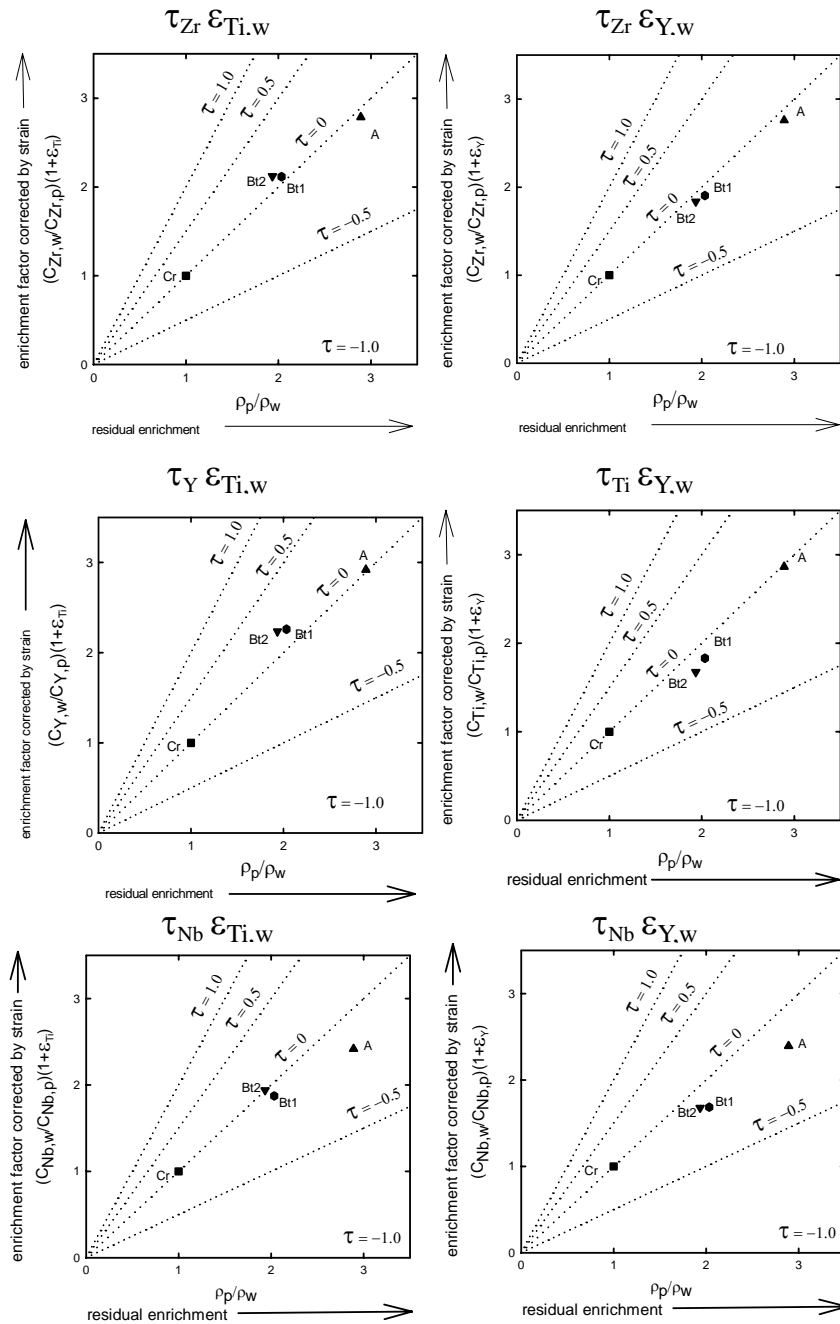


**Figure 4-12.** Tehama County plots of density ratio  $\rho_p/\rho_w$  representing the residual enrichment contribution vs. enrichment corrected by strain using Zr, Ti, Y and Nb as the immobile element. Dotted lines represent  $\tau$ , the mass fraction added or subtracted from each sample at 0, 50 and 100%.

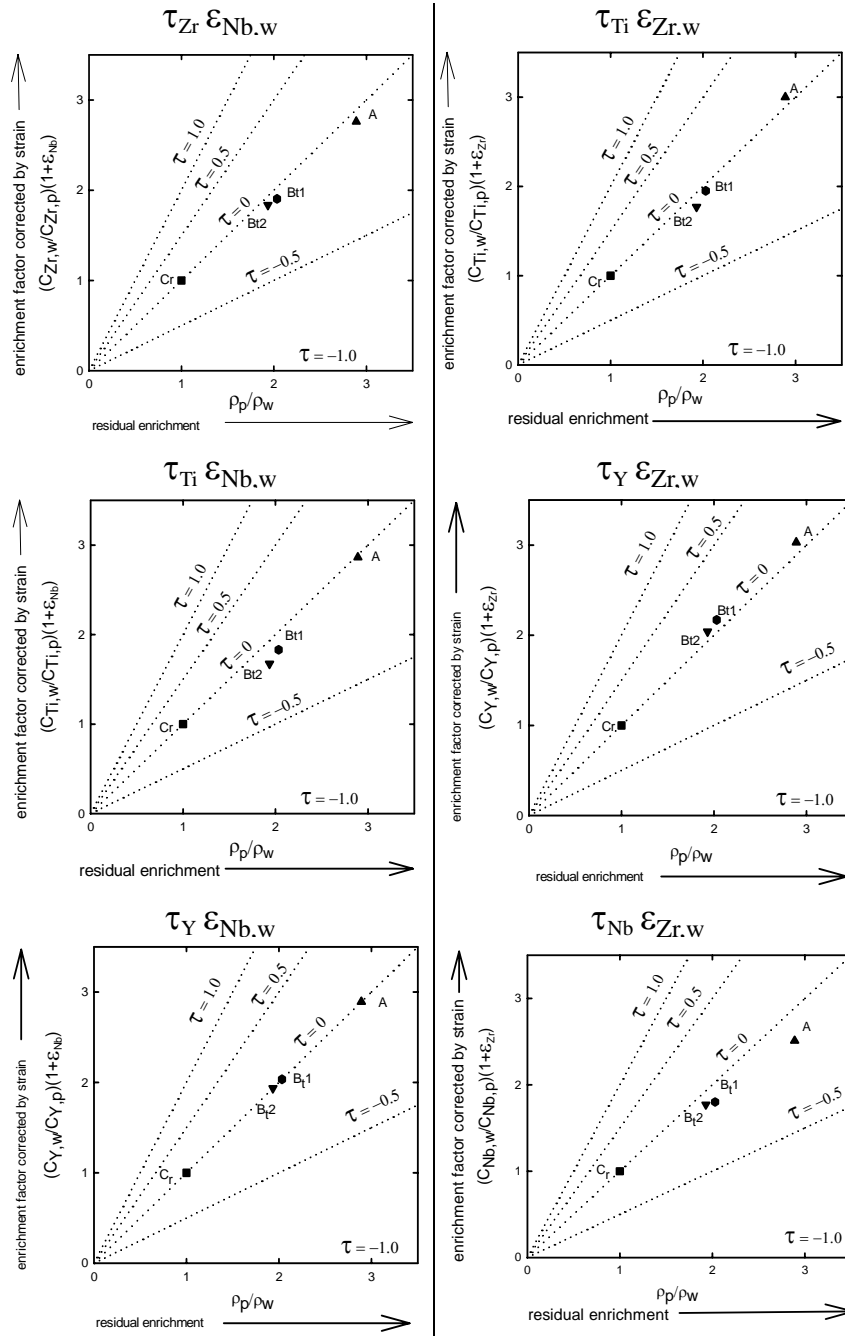


**Figure 4-12. (continued)** Tehama County plots of density ratio  $\rho_p/\rho_w$  representing the residual enrichment contribution vs. enrichment corrected by strain using Zr, Ti, Y and Nb as the immobile element. Dotted lines represent  $\tau$ , the mass fraction added or subtracted from each sample at 0, 50 and 100%.



## 4.7 APPENDIX A

The REE's, and the element Sc graphed as (A) weight percent, (B) enrichment factor and (C) transported mass fraction with strain corrected by Y. Dotted vertical lines in A to C serve as visual indicator for parent material value. (D) Graphic contributions of the components of closed system mass movement of the element across the sample volume boundaries (soil horizons) using Y ( $\epsilon_{Y,w}$ ) as the strain correcting element. Where dotted lines represent  $\tau$ , the mass fraction added or subtracted from each sample at 0, 50 and 100%.

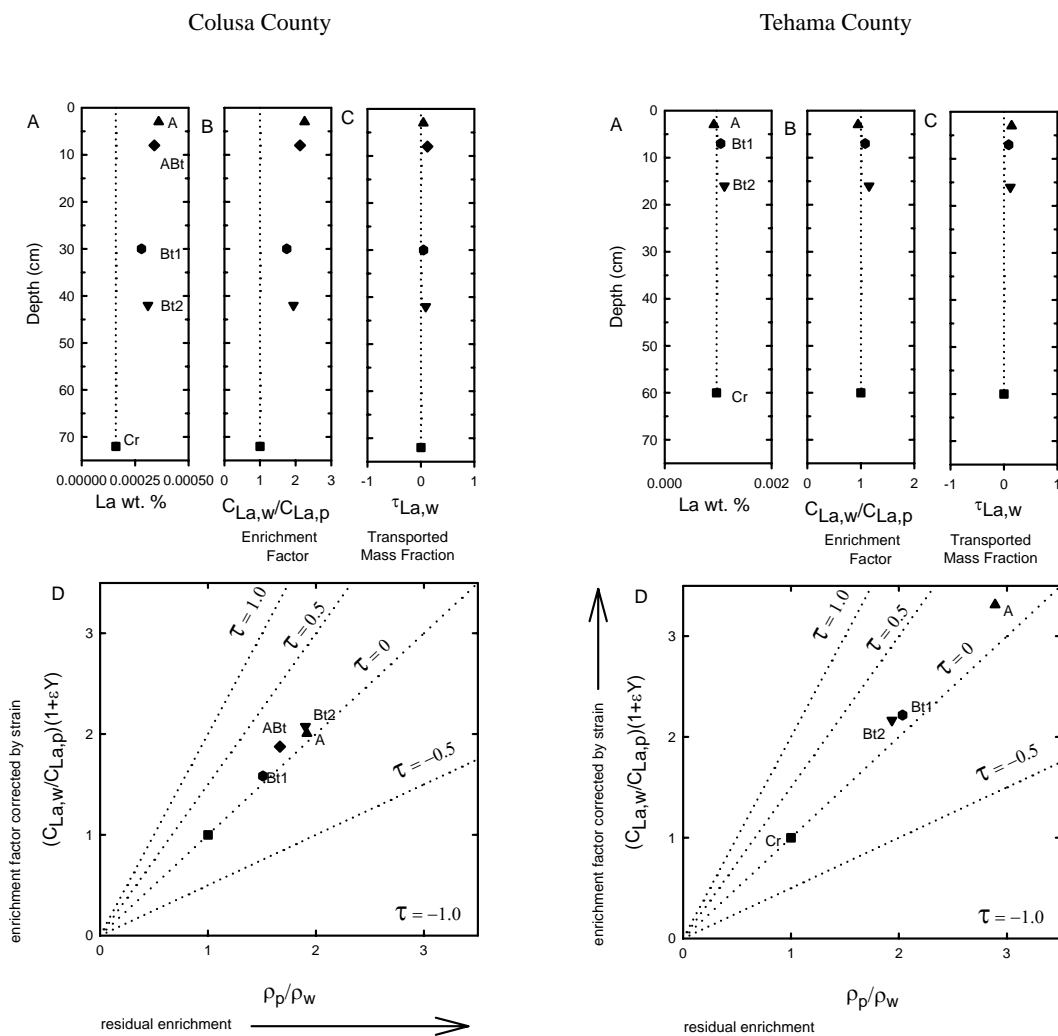


**Figure 4-13.** Depth plots of (A) weighted percent La, (B) enrichment factor, and (C) the transported mass fraction of La. (D) Plot of density ratio  $\rho_p/\rho_w$  representing the residual enrichment contribution vs. enrichment corrected by strain using Y as the immobile element. Dotted vertical line (A, B & C) is visual indicator for parent material value. Dotted lines (D) represent  $\tau$ , the mass fraction added or subtracted from each sample at 0, 50 and 100%.

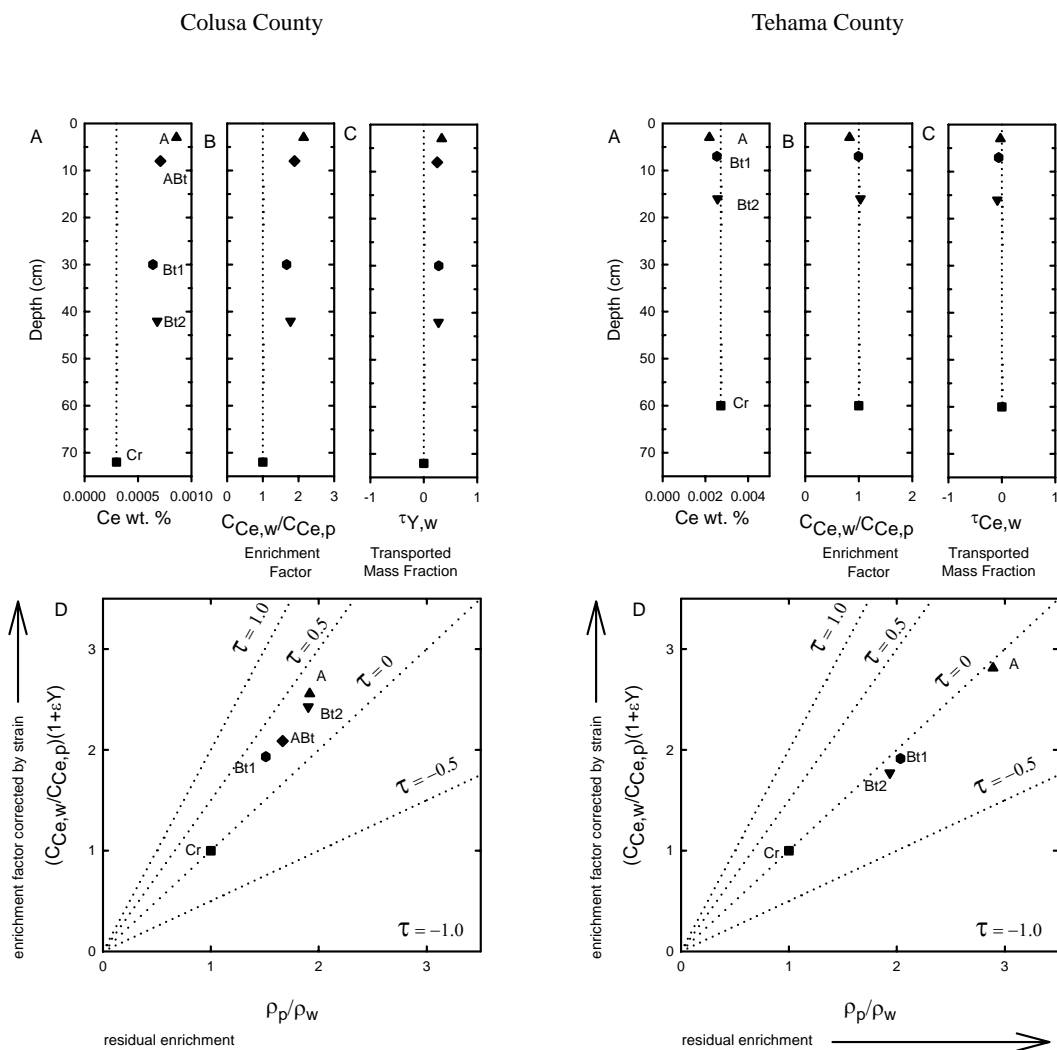


**Figure 4-14.** Depth plots of (A) weighted percent Ce, (B) enrichment factor, and (C) the transported mass fraction of Ce. (D) Plot of density ratio  $\rho_p/\rho_w$  representing the residual enrichment contribution vs. enrichment corrected by strain using Y as the immobile element. Dotted vertical line (A, B & C) is visual indicator for parent material value. Dotted lines (D) represent  $\tau$ , the mass fraction added or subtracted from each sample at 0, 50 and 100%.

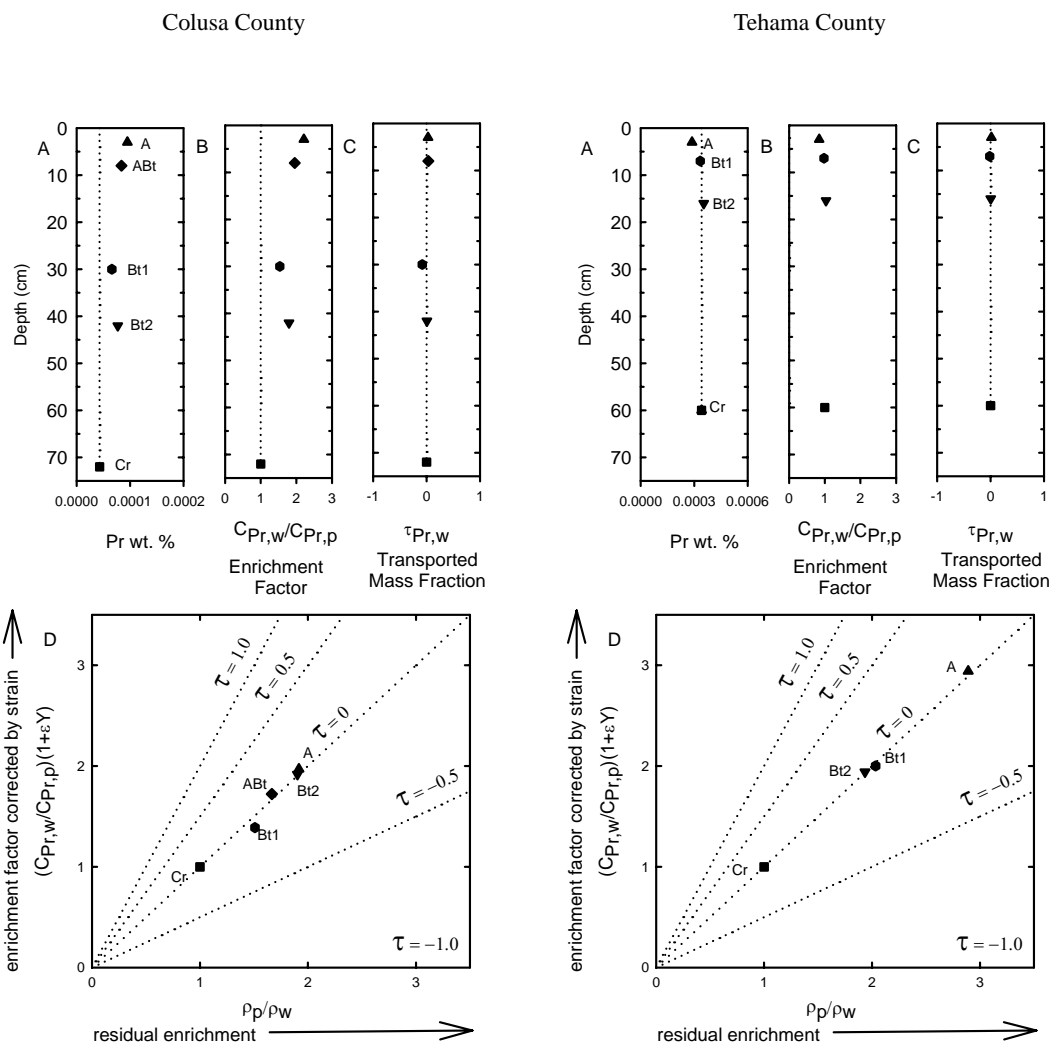


**Figure 4-15.** Depth plots of (A) weighted percent Pr, (B) enrichment factor, and (C) the transported mass fraction of Pr. (D) Plot of density ratio  $\rho_p/\rho_w$  representing the residual enrichment contribution vs. enrichment corrected by strain using Y as the immobile element. Dotted vertical line (A, B & C) is visual indicator for parent material value. Dotted lines (D) represent  $\tau$ , the mass fraction added or subtracted from each sample at 0, 50 and 100%.

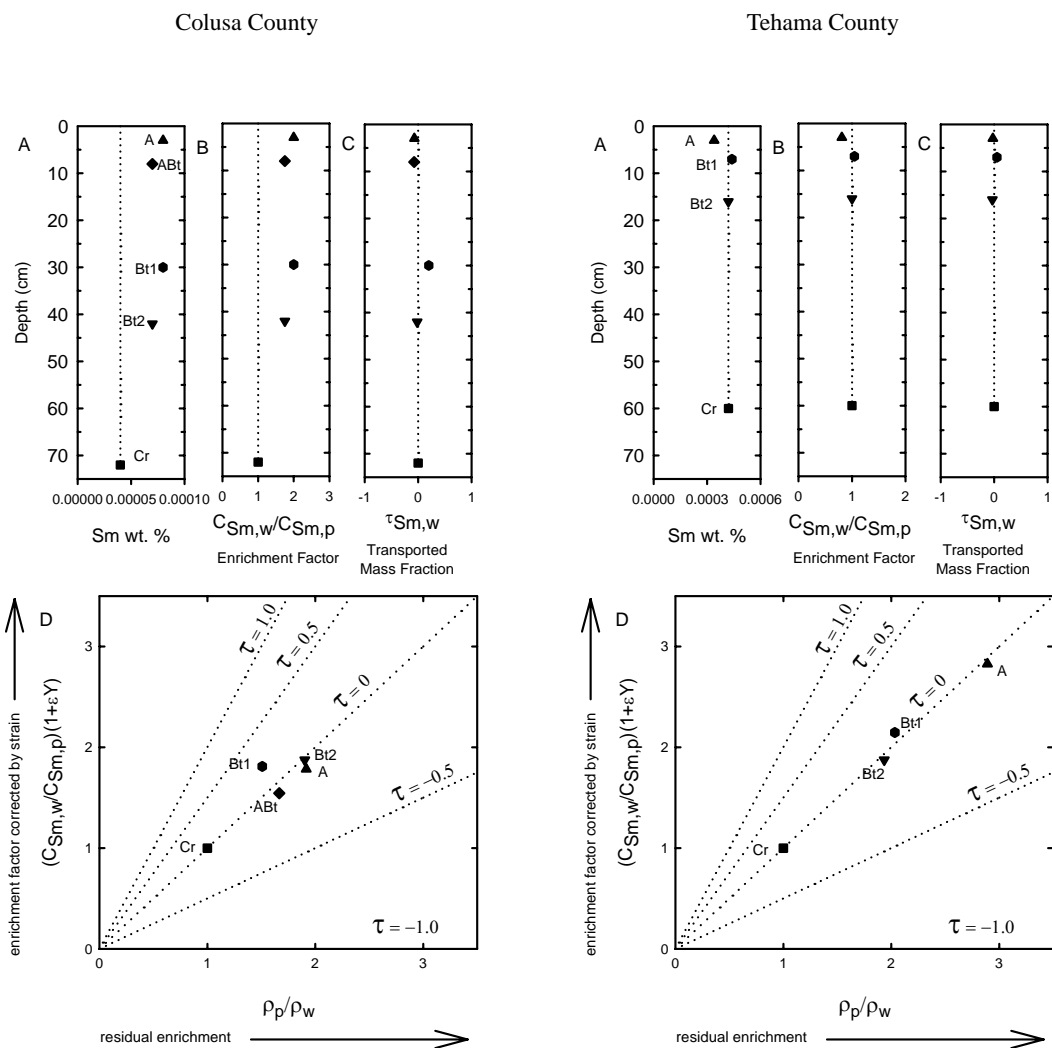


**Figure 4-16.** Depth plots of (A) weighted percent Sm, (B) enrichment factor, and (C) the transported mass fraction of Sm. (D) Plot of density ratio  $\rho_p/\rho_w$  representing the residual enrichment  $\tau$  contribution vs. enrichment corrected by strain using Y as the immobile element. Dotted vertical line (A, B & C) is visual indicator for parent material value. Dotted lines (D) represent  $\tau$ , the mass fraction added or subtracted from each sample at 0, 50 and 100%.

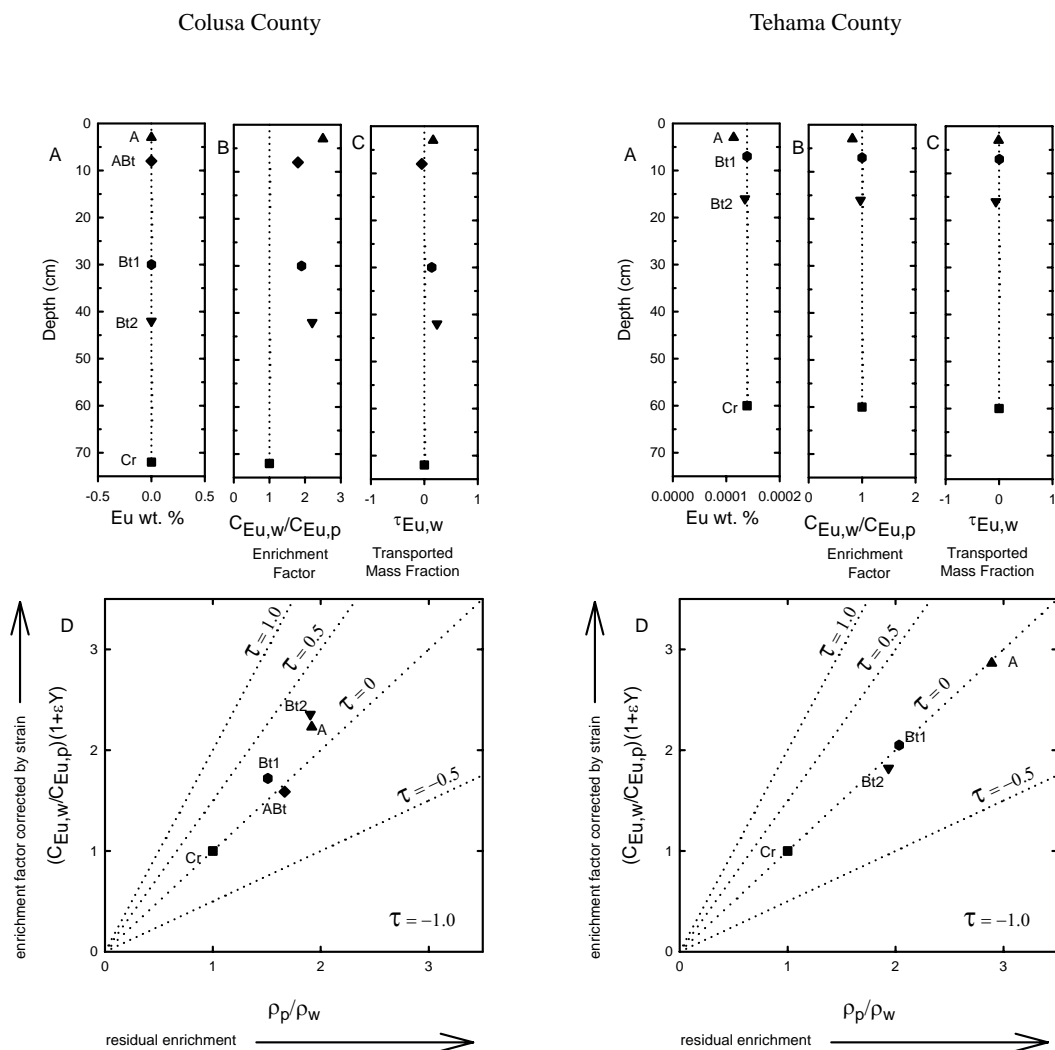


**Figure 4-17.** Depth plots of (A) weighted percent Eu, (B) enrichment factor, and (C) the transported mass fraction of Eu. (D) Plot of density ratio  $\rho_p/\rho_w$  representing the residual enrichment contribution vs. enrichment corrected by strain using Y as the immobile element. Dotted vertical line (A, B & C) is visual indicator for parent material value. Dotted lines (D) represent  $\tau$ , the mass fraction added or subtracted from each sample at 0, 50 and 100%.

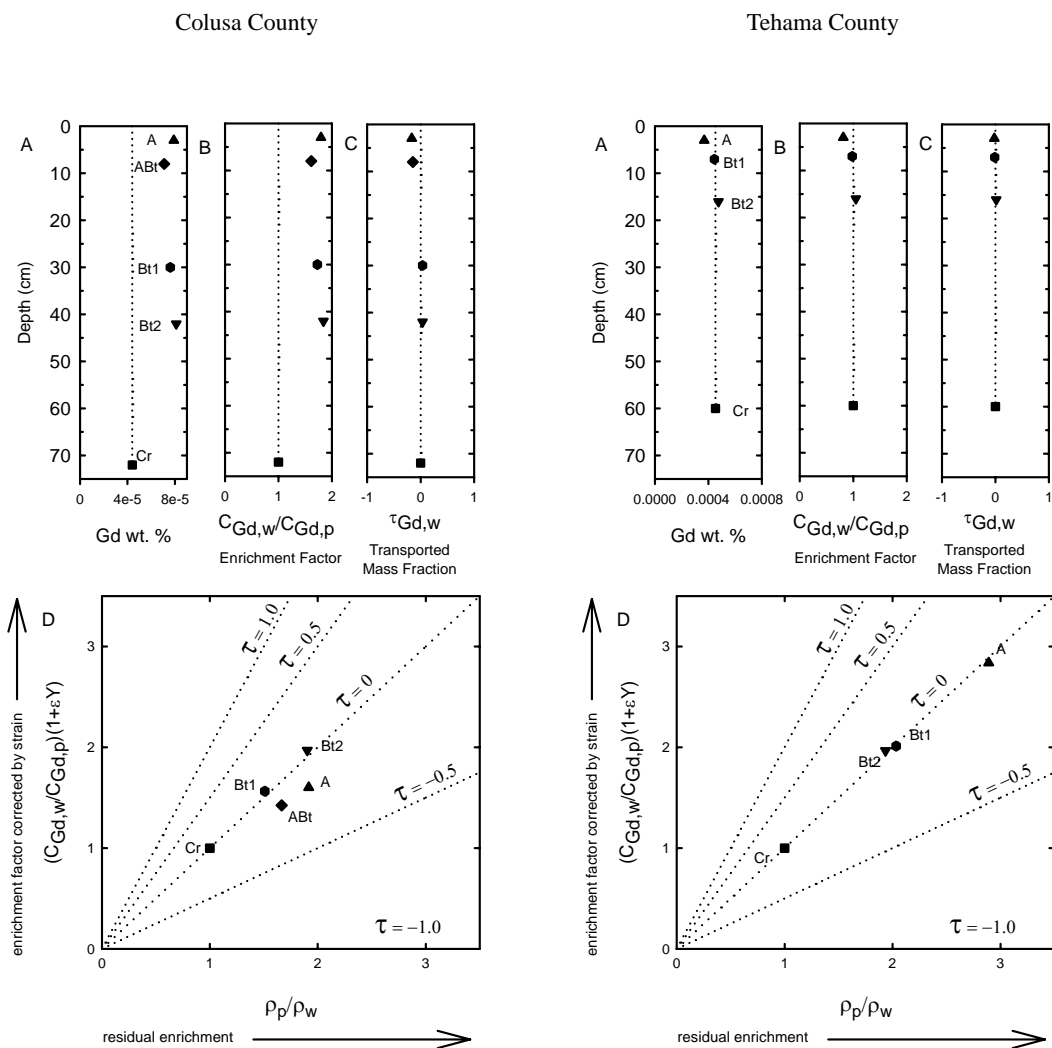


**Figure 4-18.** Depth plots of (A) weighted percent Gd, (B) enrichment factor, and (C) the transported mass fraction of Gd. (D) Plot of density ratio  $\rho_p/\rho_w$  representing the residual enrichment contribution vs. enrichment corrected by strain using Y as the immobile element. Dotted vertical line (A, B & C) is visual indicator for parent material value. Dotted lines (D) represent  $\tau$ , the mass fraction added or subtracted from each sample at 0, 50 and 100%.

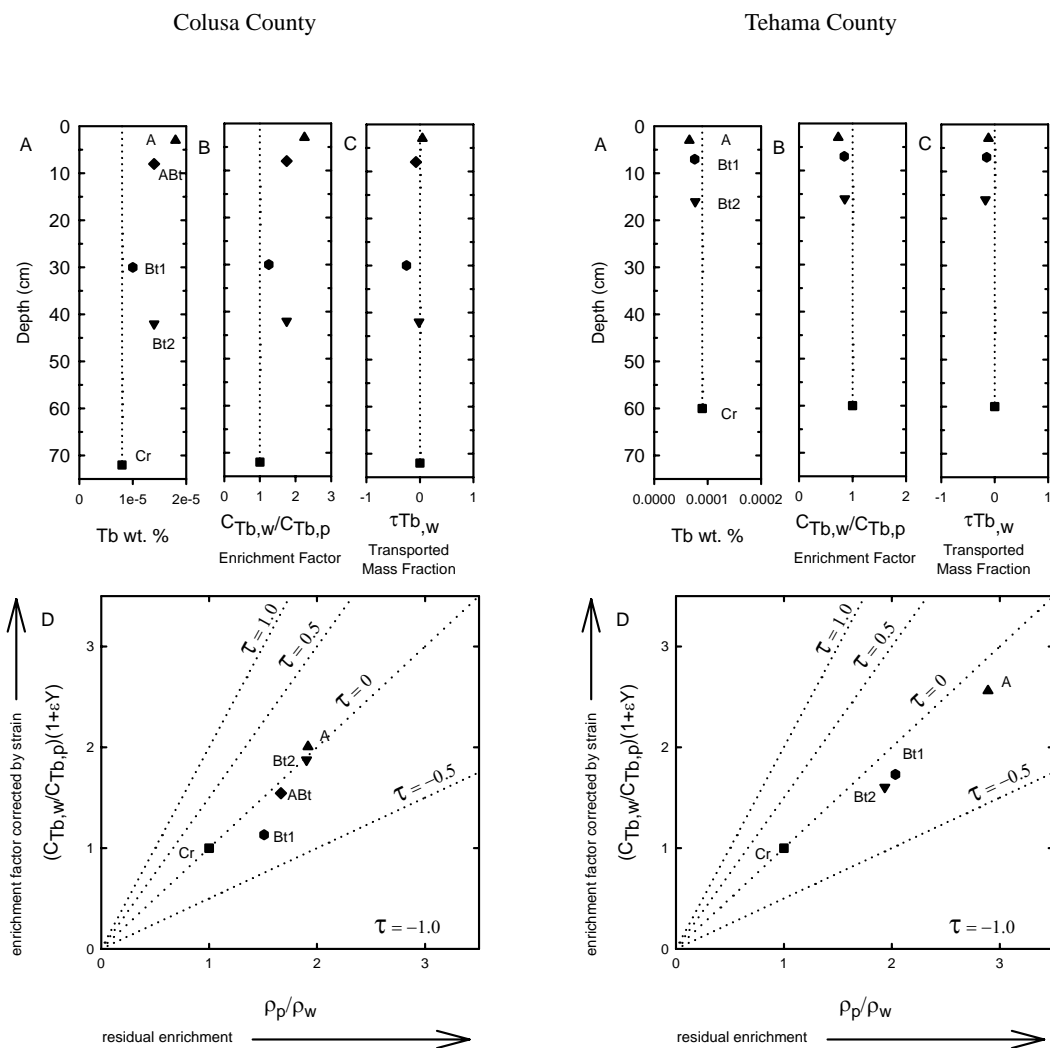


**Figure 4-19.** Depth plots of (A) weighted percent Tb, (B) enrichment factor, and (C) the transported mass fraction of Tb. (D) Plot of density ratio  $\rho_p/\rho_w$  representing the residual enrichment contribution vs. enrichment corrected by strain using Y as the immobile element. Dotted vertical line (A, B & C) is visual indicator for parent material value. Dotted lines (D) represent  $\tau$ , the mass fraction added or subtracted from each sample at 0, 50 and 100%.



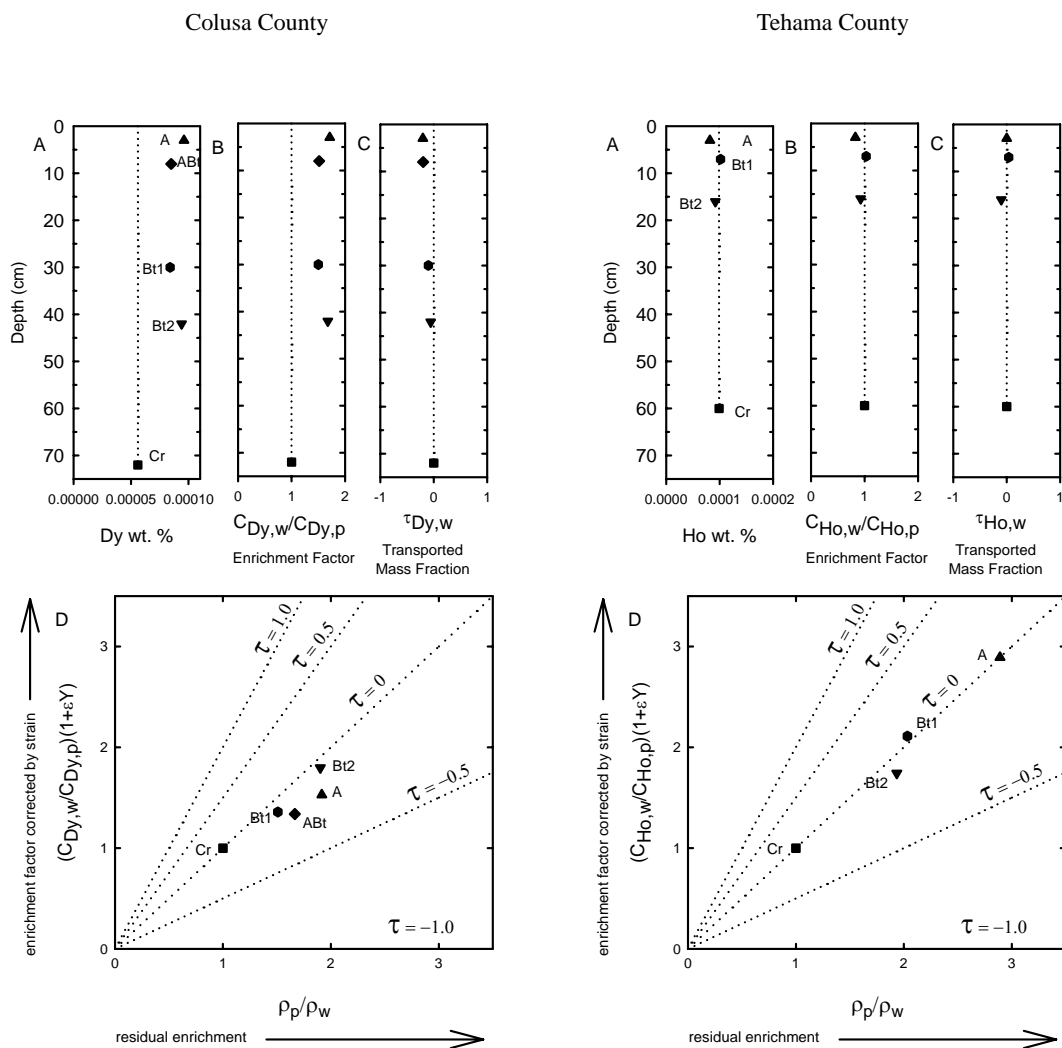


**Figure 4-20.** Depth plots of (A) weighted percent Dy, (B) enrichment factor, and (C) the transported mass fraction of Dy. (D) Plot of density ratio  $\rho_p/\rho_w$  representing the residual enrichment contribution vs. enrichment corrected by strain using Y as the immobile element. Dotted vertical line (A, B & C) is visual indicator for parent material value. Dotted lines (D) represent  $\tau$ , the mass fraction added or subtracted from each sample at 0, 50 and 100%.

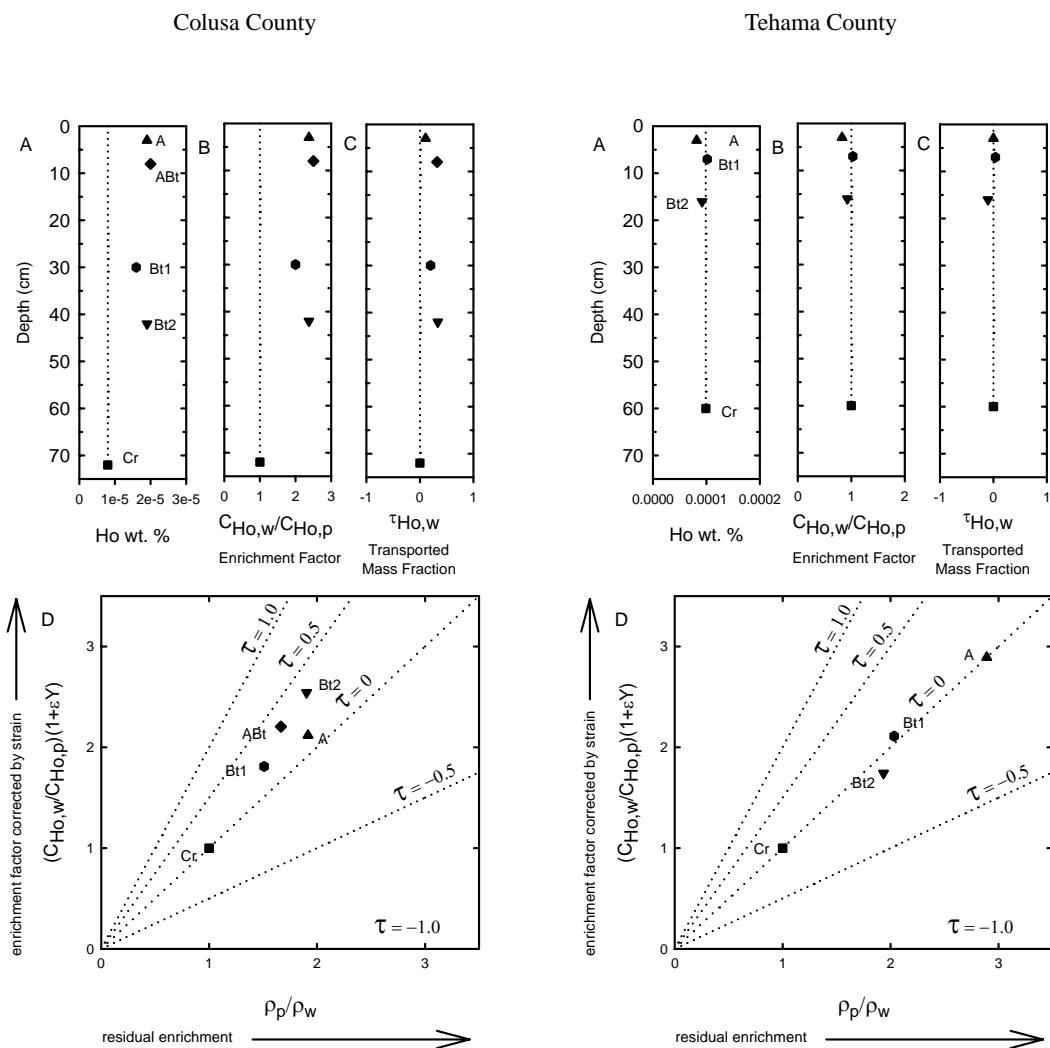


**Figure 4-21.** Depth plots of (A) weighted percent Ho, (B) enrichment factor, and (C) the transported mass fraction of Ho. (D) Plot of density ratio  $\rho_p/\rho_w$  representing the residual enrichment contribution vs. enrichment corrected by strain using Y as the immobile element. Dotted vertical line (A, B & C) is visual indicator for parent material value. Dotted lines (D) represent  $\tau$ , the mass fraction added or subtracted from each sample at 0, 50 and 100%.

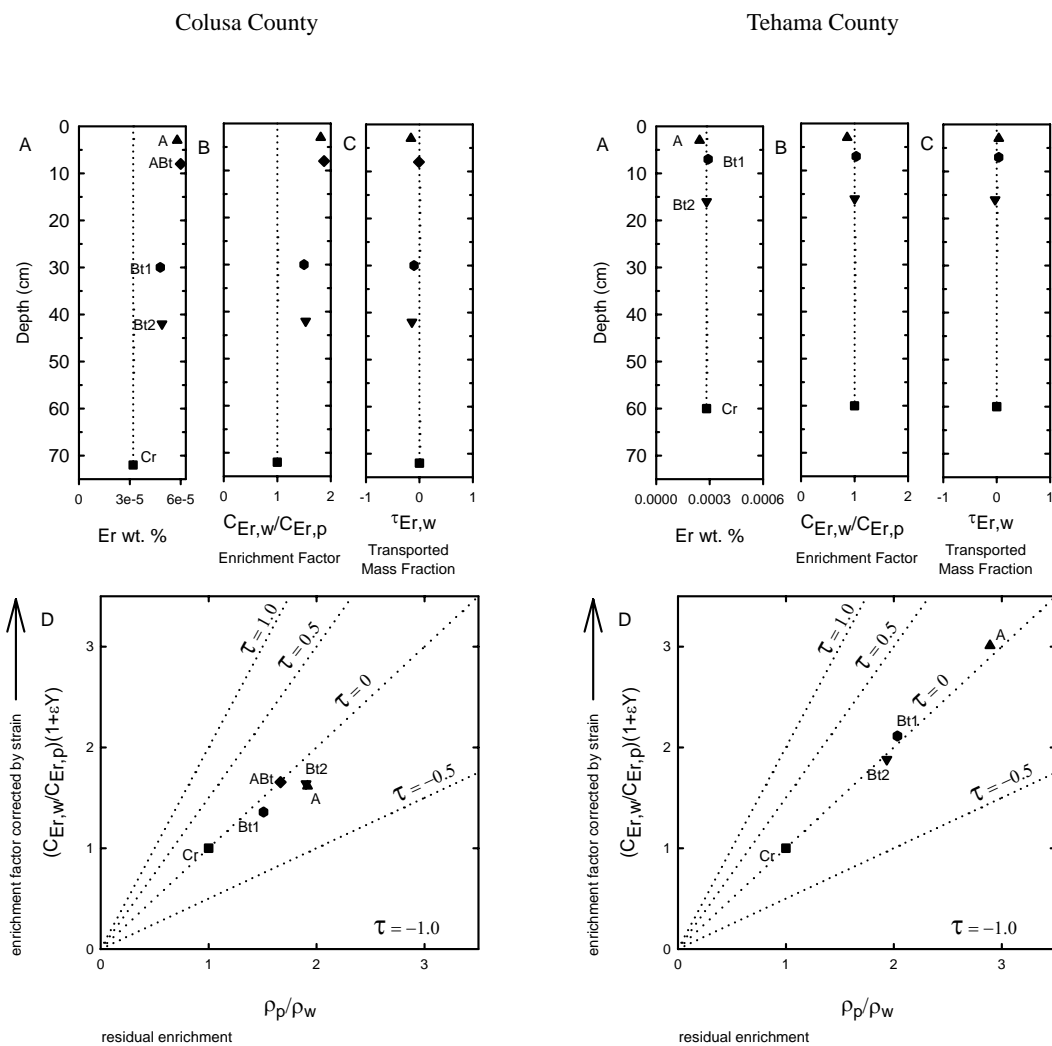


**Figure 4-22.** Depth plots of (A) weighted percent Er, (B) enrichment factor, and (C) the transported mass fraction of Er. (D) Plot of density ratio  $\rho_p/\rho_w$  representing the residual enrichment contribution vs. enrichment corrected by strain using Y as the immobile element. Dotted vertical line (A, B & C) is visual indicator for parent material value. Dotted lines (D) represent  $\tau$ , the mass fraction added or subtracted from each sample at 0, 50 and 100%.

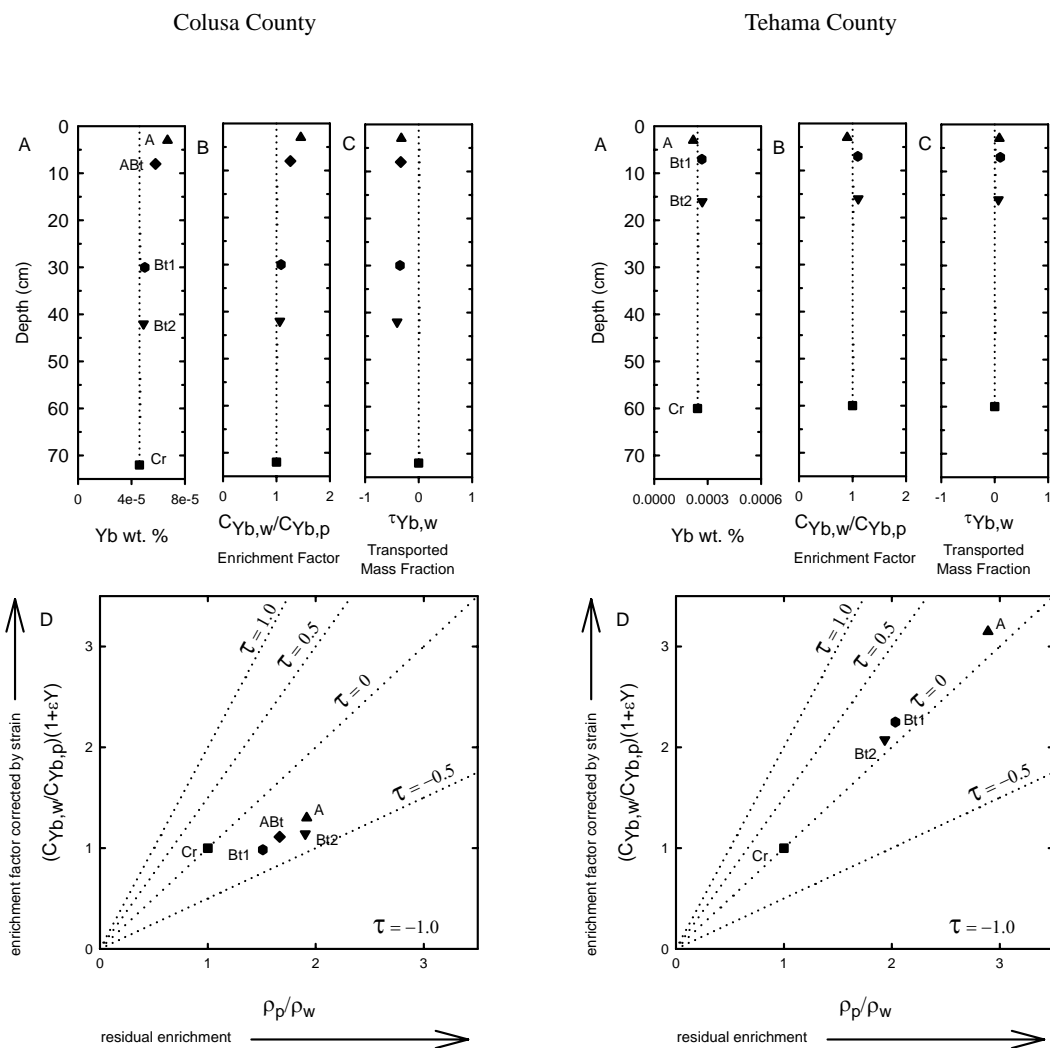


**Figure 4-23.** Depth plots of (A) weighted percent Yb, (B) enrichment factor, and (C) the transported mass fraction of Yb. (D) Plot of density ratio  $\rho_p/\rho_w$  representing the residual enrichment contribution vs. enrichment corrected by strain using Y as the immobile element. Dotted vertical line (A, B & C) is visual indicator for parent material value. Dotted lines (D) represent  $\tau$ , the mass fraction added or subtracted from each sample at 0, 50 and 100%.

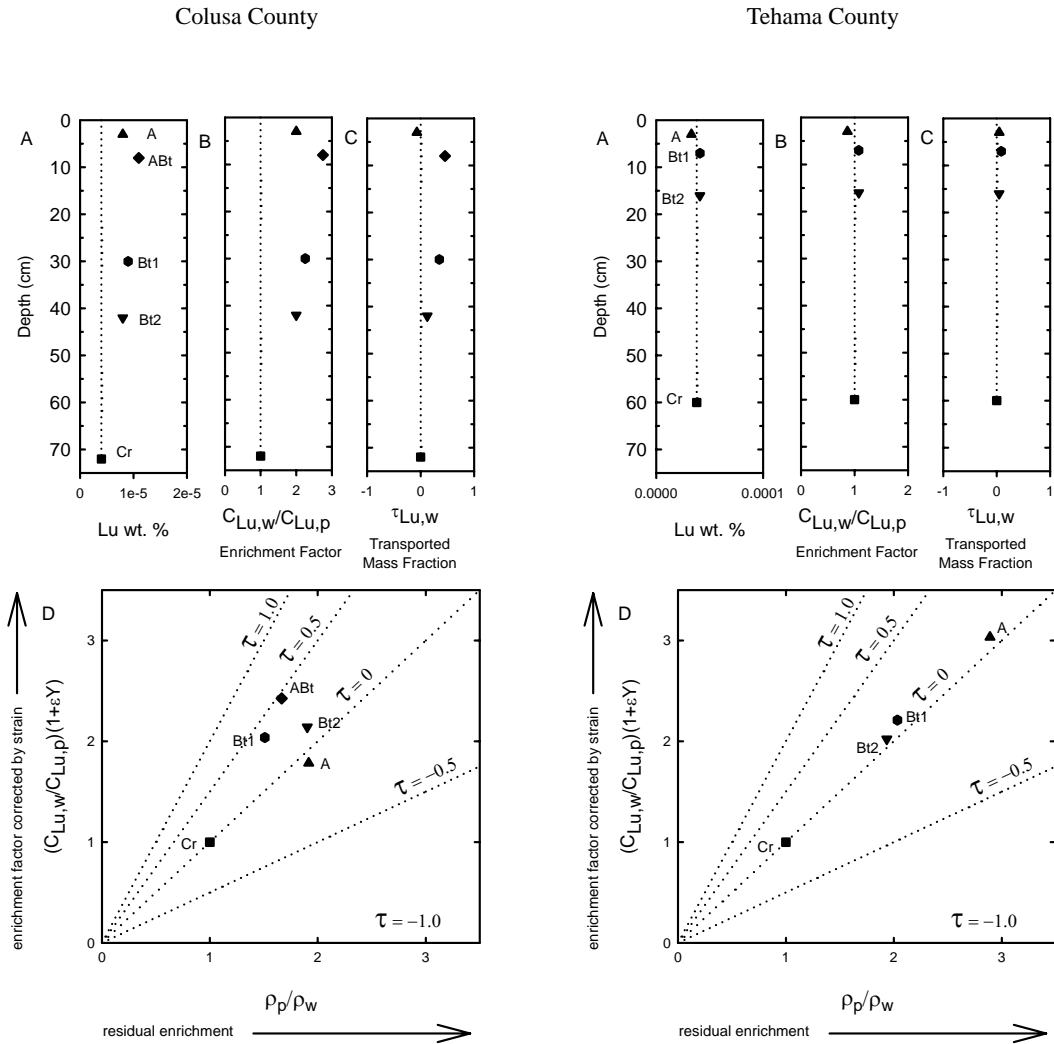


**Figure 4-24.** Depth plots of (A) weighted percent Lu, (B) enrichment factor, and (C) the transported mass fraction of Lu. (D) Plot of density ratio  $\rho_p/\rho_w$  representing the residual enrichment contribution vs. enrichment corrected by strain using Y as the immobile element. Dotted vertical line (A, B & C) is visual indicator for parent material value. Dotted lines (D) represent  $\tau$ , the mass fraction added or subtracted from each sample at 0, 50 and 100%.

## 4.8 APPENDIX B

All of the REE's, and the element Sc graphed as (A) weight percent, (B) enrichment factor and (C) transported mass fraction with strain corrected by Ti. Dotted vertical lines in A to C serve as visual indicator for parent material value. (D) Graphic contributions of the components of closed system mass movement of the element across the sample volume boundaries (soil horizons) using Ti ( $\epsilon_{Ti,w}$ ) as the strain correcting element. Where dotted lines represent  $\tau$ , the mass fraction added or subtracted from each sample at 0, 50 and 100%.

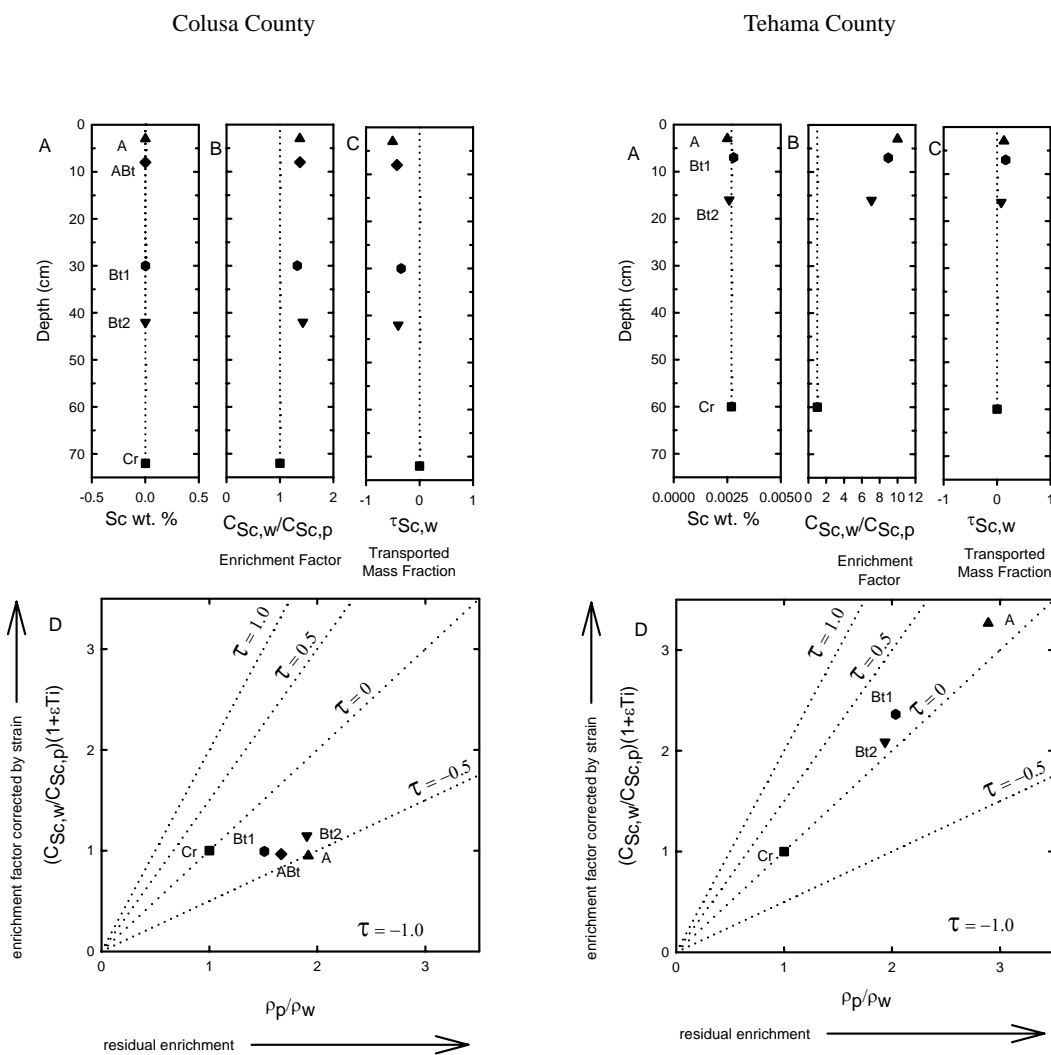


**Figure 4-25.** Depth plots of (A) weighted percent Sc, (B) enrichment factor, and (C) the transported mass fraction of Sc. (D) Plot of density ratio  $\rho_p/\rho_w$  representing the residual enrichment contribution vs. enrichment corrected by strain using Ti as the immobile element. Dotted vertical line (A, B & C) is visual indicator for parent material value. Dotted lines (D) represent  $\tau$ , the mass fraction added or subtracted from each sample at 0, 50 and 100%.

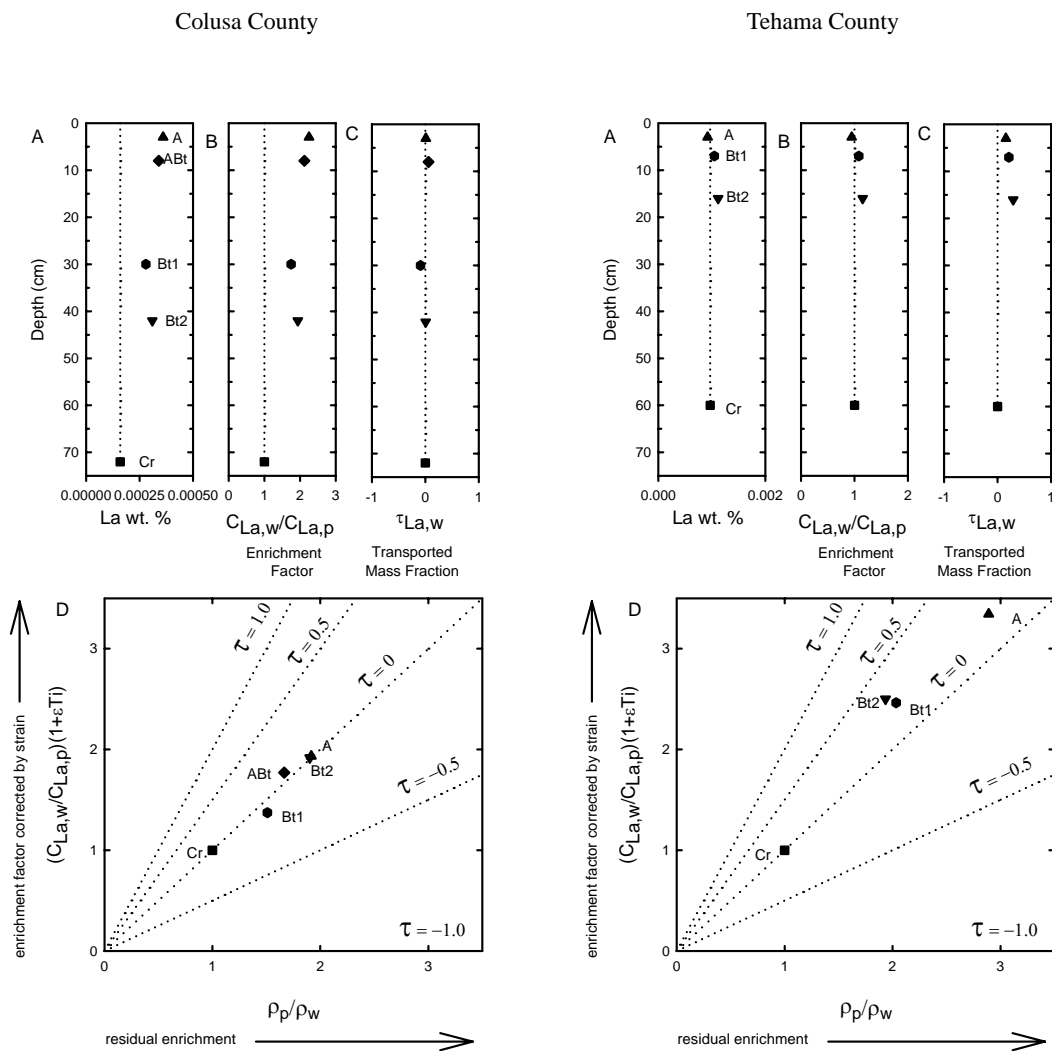


**Figure 4-26.** Depth plots of (A) weighted percent La, (B) enrichment factor, and (C) the transported mass fraction of La. (D) Plot of density ratio  $\rho_p/\rho_w$  representing the residual enrichment contribution vs. enrichment corrected by strain using Ti as the immobile element. Dotted vertical line (A, B & C) is visual indicator for parent material value. Dotted lines (D) represent  $\tau$ , the mass fraction added or subtracted from each sample at 0, 50 and 100%.

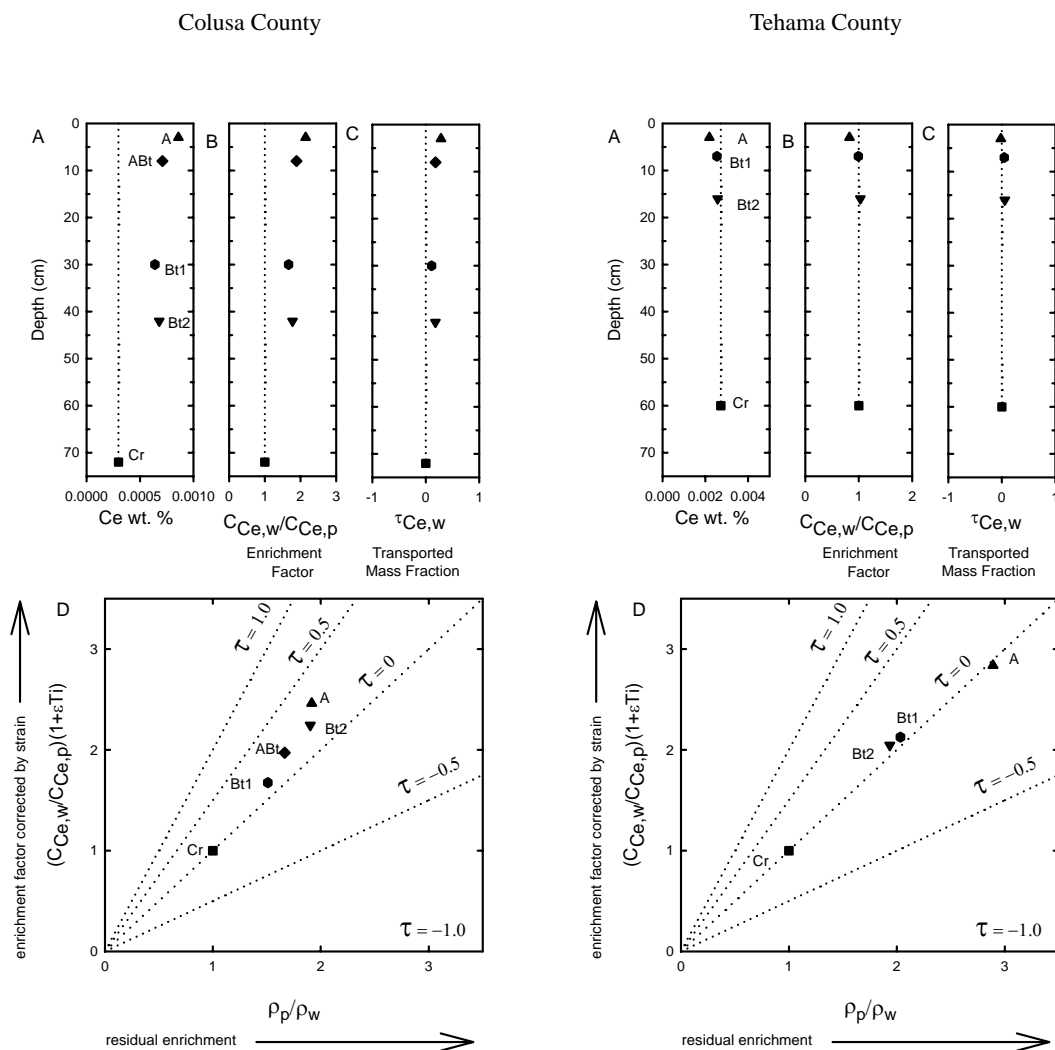


**Figure 4-27.** Depth plots of (A) weighted percent Ce, (B) enrichment factor, and (C) the transported mass fraction of Ce. (D) Plot of density ratio  $\rho_p/\rho_w$  representing the residual enrichment contribution vs. enrichment corrected by strain using Ti as the immobile element. Dotted vertical line (A, B & C) is visual indicator for parent material value. Dotted lines (D) represent  $\tau$ , the mass fraction added or subtracted from each sample at 0, 50 and 100%.



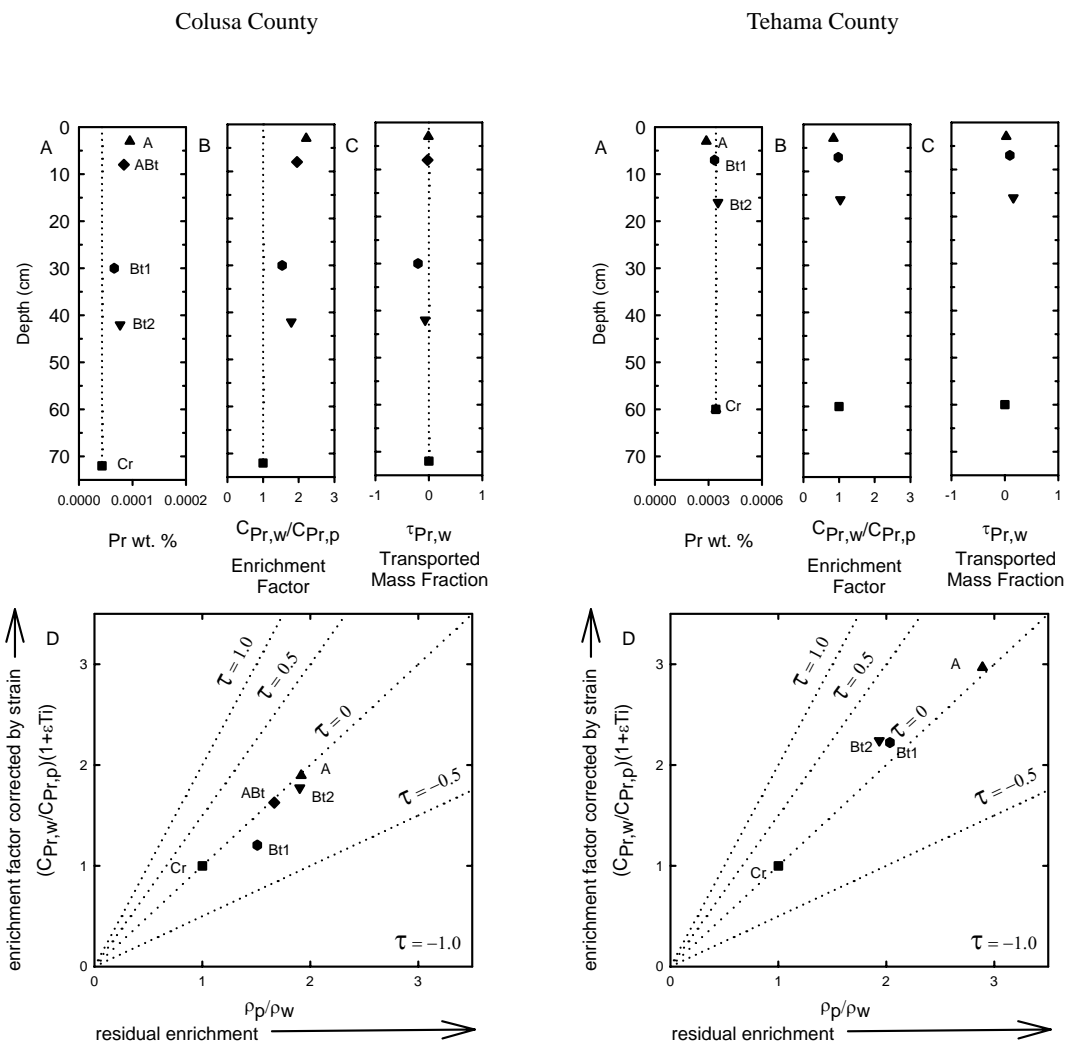


**Figure 4-28.** Depth plots of (A) weighted percent Pr, (B) enrichment factor, and (C) the transported mass fraction of Pr. (D) Plot of density ratio  $\rho_p/\rho_w$  representing the residual enrichment contribution vs. enrichment corrected by strain using Ti as the immobile element. Dotted vertical line (A, B & C) is visual indicator for parent material value. Dotted lines (D) represent  $\tau$ , the mass fraction added or subtracted from each sample at 0, 50 and 100%.

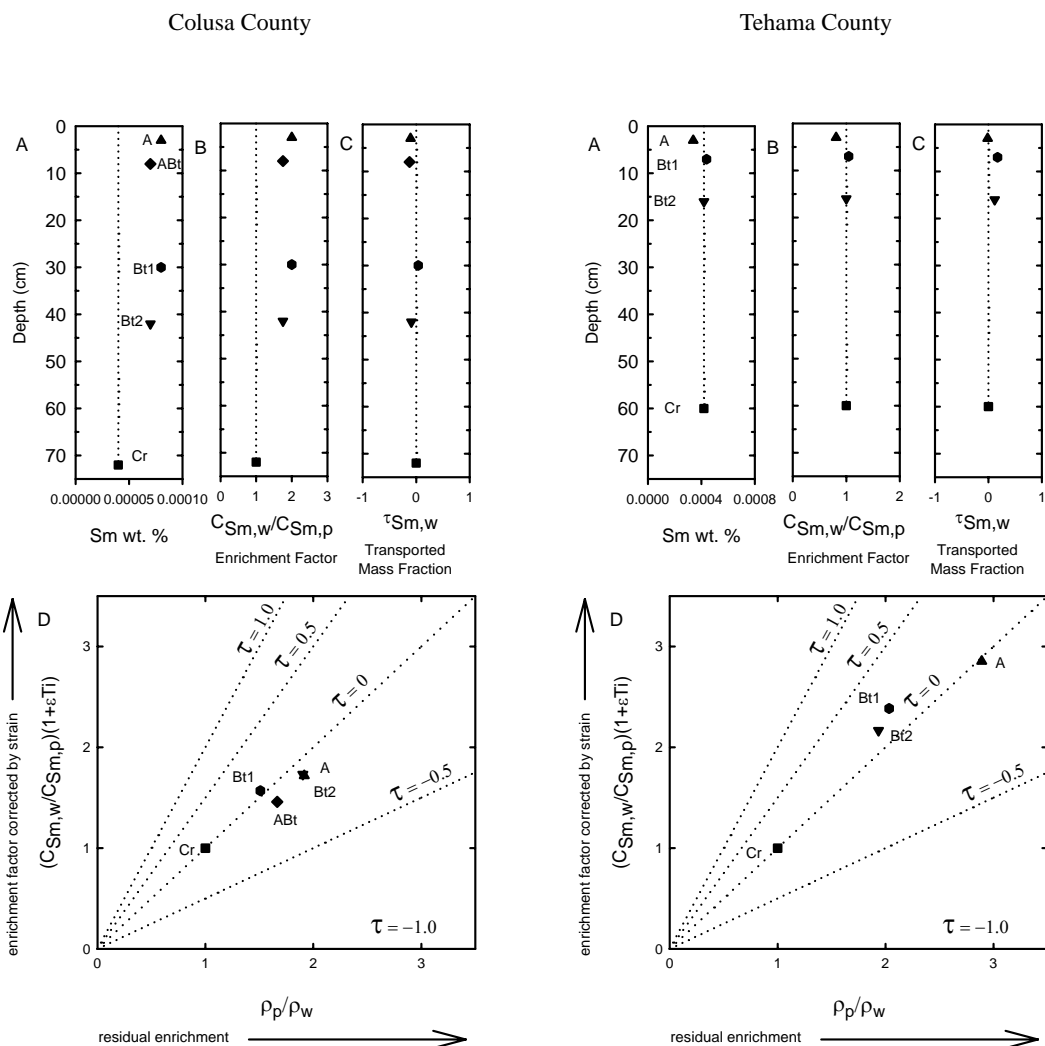


**Figure 4-29.** Depth plots of (A) weighted percent Sm, (B) enrichment factor, and (C) the transported mass fraction of Sm. (D) Plot of density ratio  $\rho_p/\rho_w$  representing the residual enrichment contribution vs. enrichment corrected by strain using Ti as the immobile element. Dotted vertical line (A, B & C) is visual indicator for parent material value. Dotted lines (D) represent  $\tau$ , the mass fraction added or subtracted from each sample at 0, 50 and 100%.

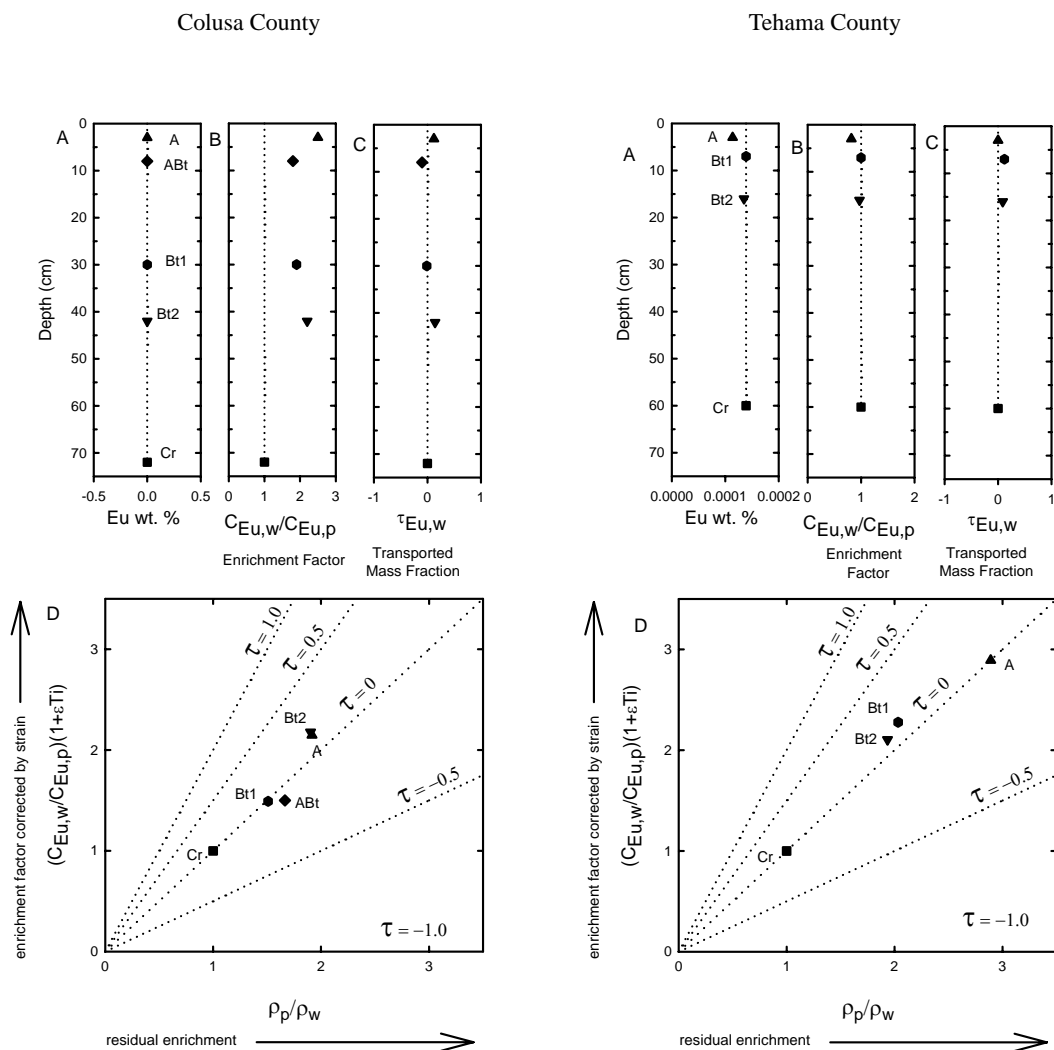


**Figure 4-30.** Depth plots of (A) weighted percent Eu, (B) enrichment factor, and (C) the transported mass fraction of Eu. (D) Plot of density ratio  $\rho_p/\rho_w$  representing the residual enrichment contribution vs. enrichment corrected by strain using Ti as the immobile element. Dotted vertical line (A, B & C) is visual indicator for parent material value. Dotted lines (D) represent  $\tau$ , the mass fraction added or subtracted from each sample at 0, 50 and 100%.

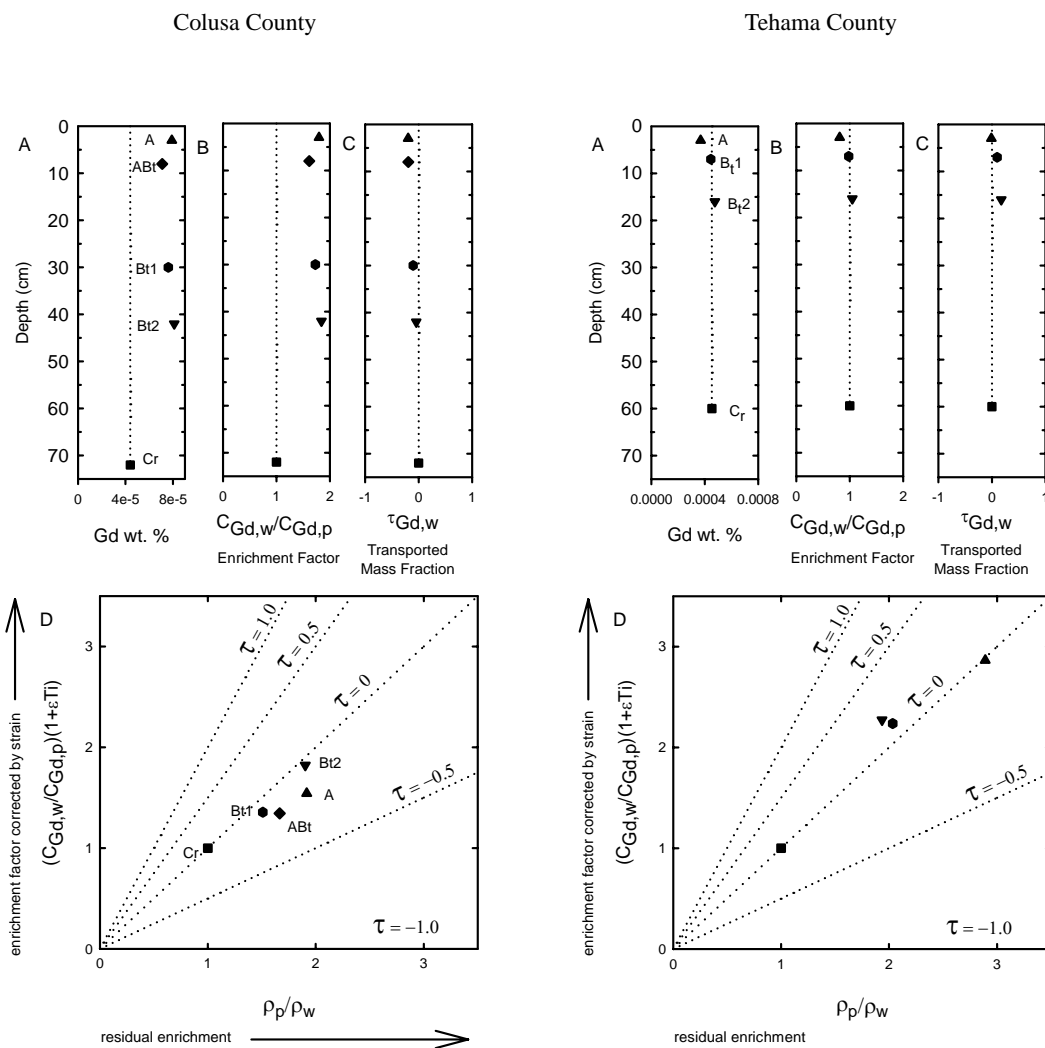


**Figure 4-31.** Depth plots of (A) weighted percent Gd, (B) enrichment factor, and (C) the transported mass fraction of Gd. (D) Plot of density ratio  $\rho_p/\rho_w$  representing the residual enrichment contribution vs. enrichment corrected by strain using Ti as the immobile element. Dotted vertical line (A, B & C) is visual indicator for parent material value. Dotted lines (D) represent  $\tau$ , the mass fraction added or subtracted from each sample at 0, 50 and 100%.

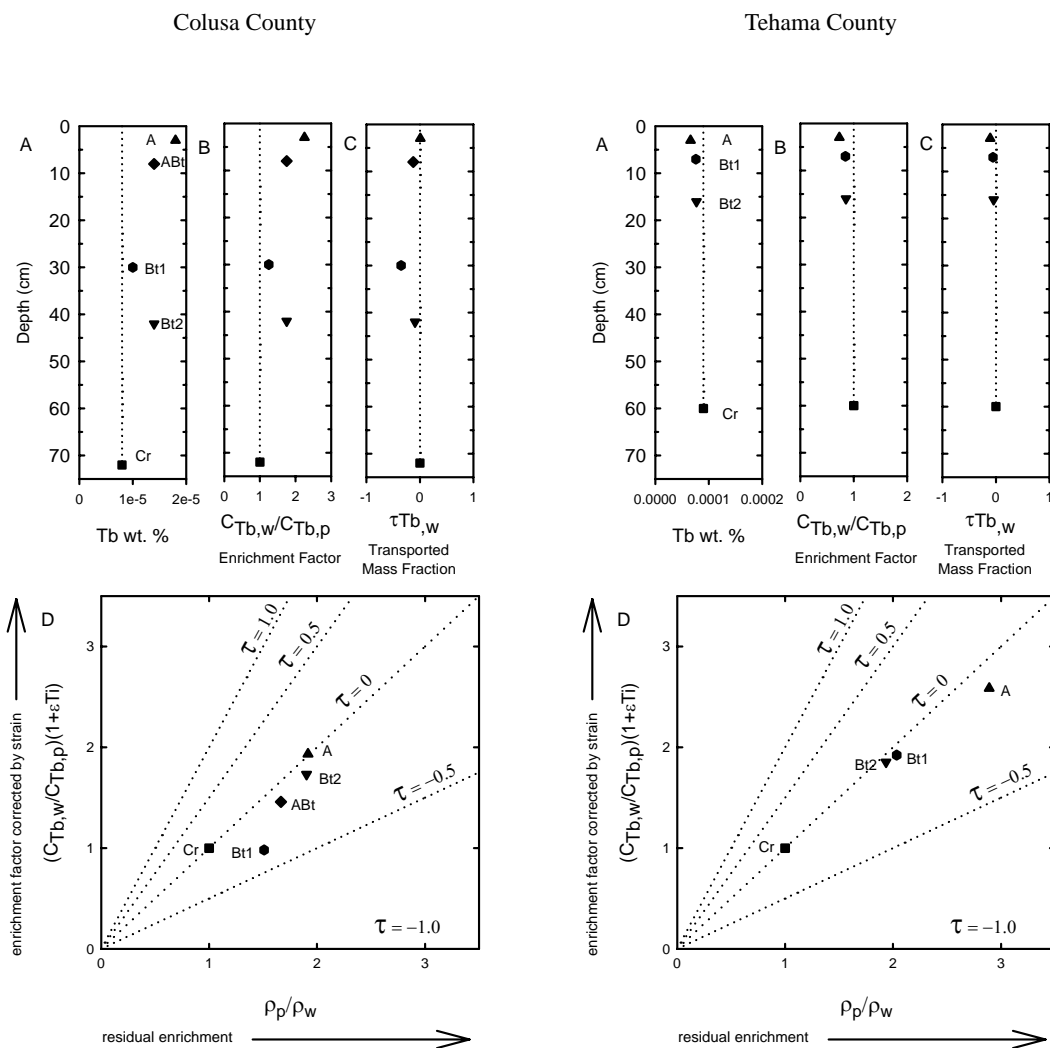


**Figure 4-32.** Depth plots of (A) weighted percent Tb, (B) enrichment factor, and (C) the transported mass fraction of Tb. (D) Plot of density ratio  $\rho_p/\rho_w$  representing the residual enrichment contribution vs. enrichment corrected by strain using Ti as the immobile element. Dotted vertical line (A, B & C) is visual indicator for parent material value. Dotted lines (D) represent  $\tau$ , the mass fraction added or subtracted from each sample at 0, 50 and 100%.

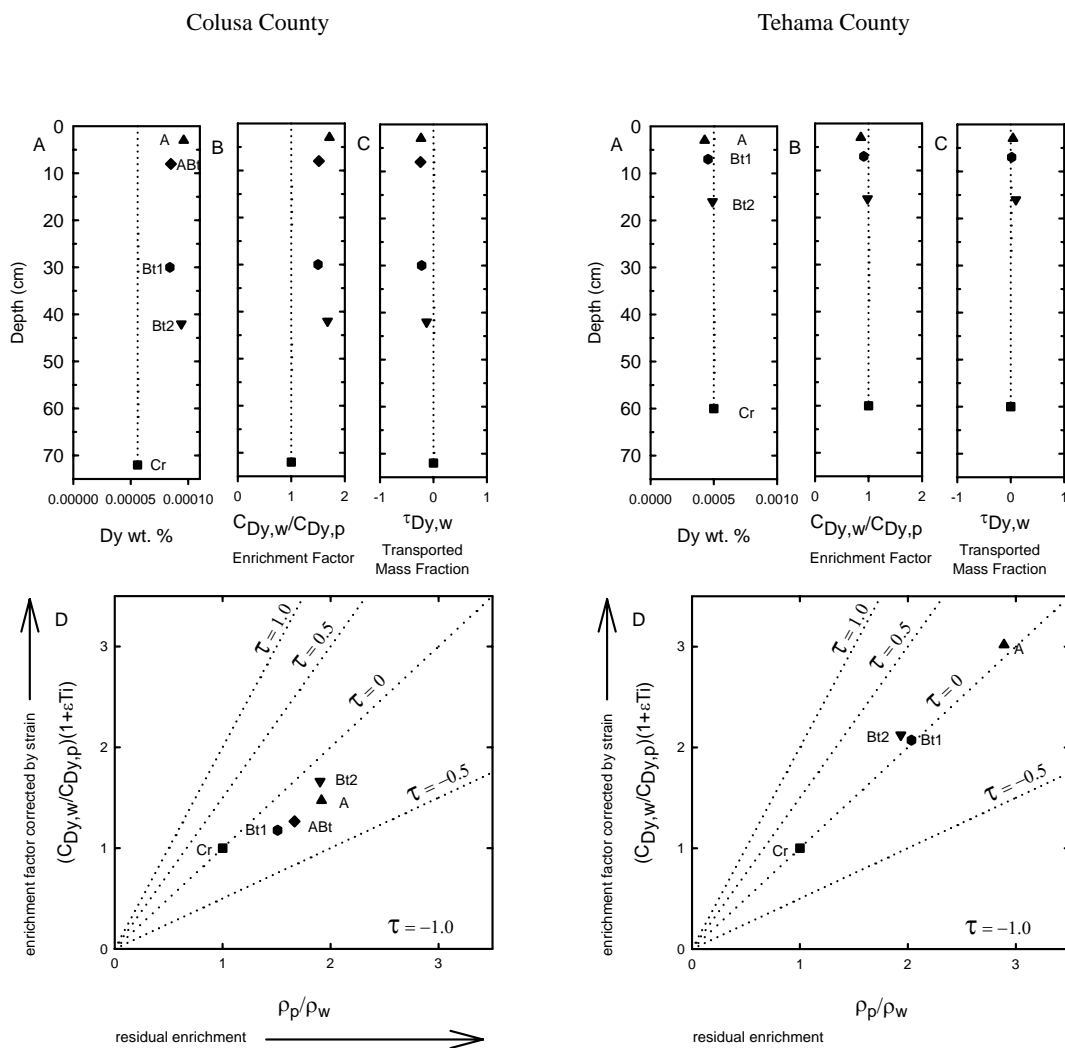


**Figure 4-33.** Depth plots of (A) weighted percent Dy, (B) enrichment factor, and (C) the transported mass fraction of Dy. (D) Plot of density ratio  $\rho_p/\rho_w$  representing the residual enrichment contribution vs. enrichment corrected by strain using Ti as the immobile element. Dotted vertical line (A, B & C) is visual indicator for parent material value. Dotted lines (D) represent  $\tau$ , the mass fraction added or subtracted from each sample at 0, 50 and 100%.

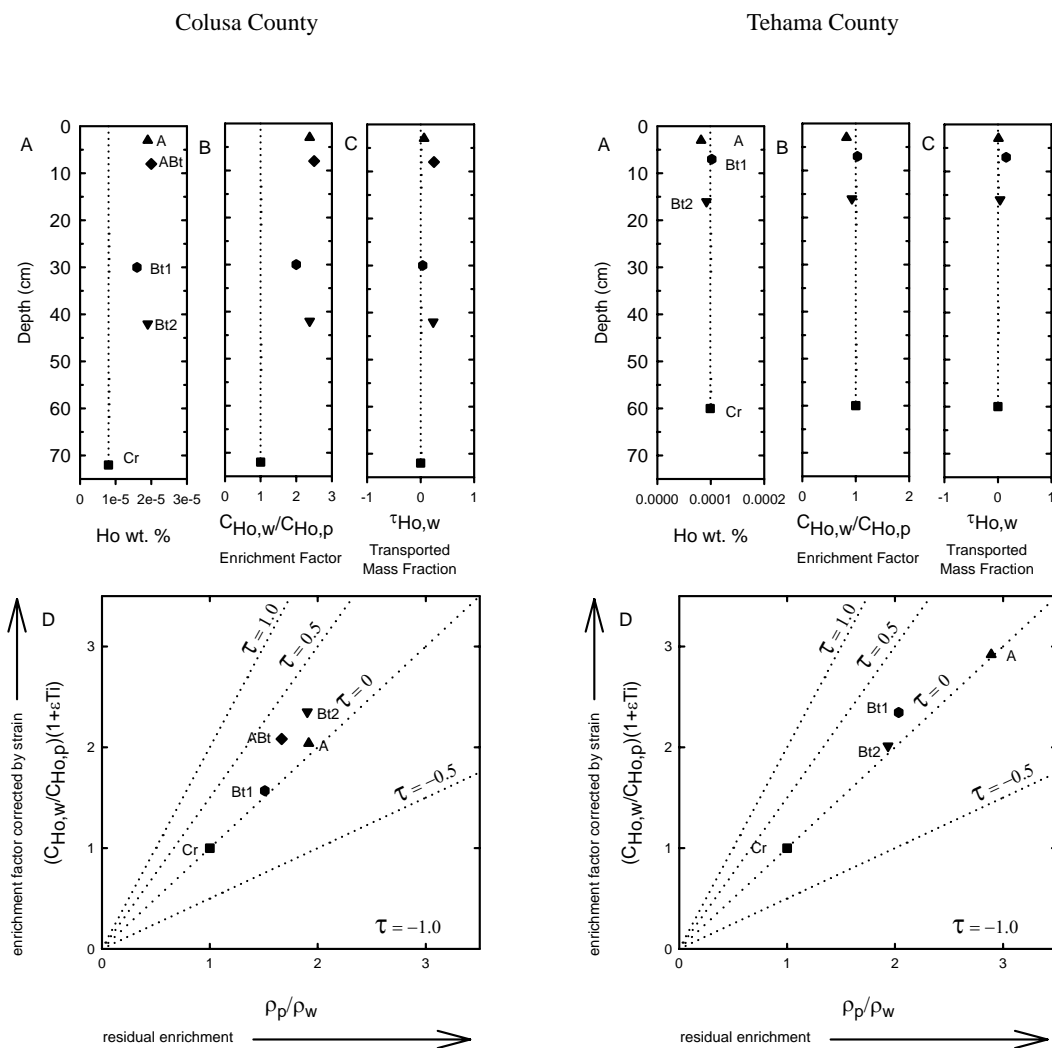


**Figure 4-34.** Depth plots of (A) weighted percent Ho, (B) enrichment factor, and (C) the transported mass fraction of Ho. (D) Plot of density ratio  $\rho_p/\rho_w$  representing the residual enrichment contribution vs. enrichment factor corrected by strain using Ti as the immobile element. Dotted vertical line (A, B & C) is visual indicator for parent material value. Dotted lines (D) represent  $\tau$ , the mass fraction added or subtracted from each sample at 0, 50 and 100%.

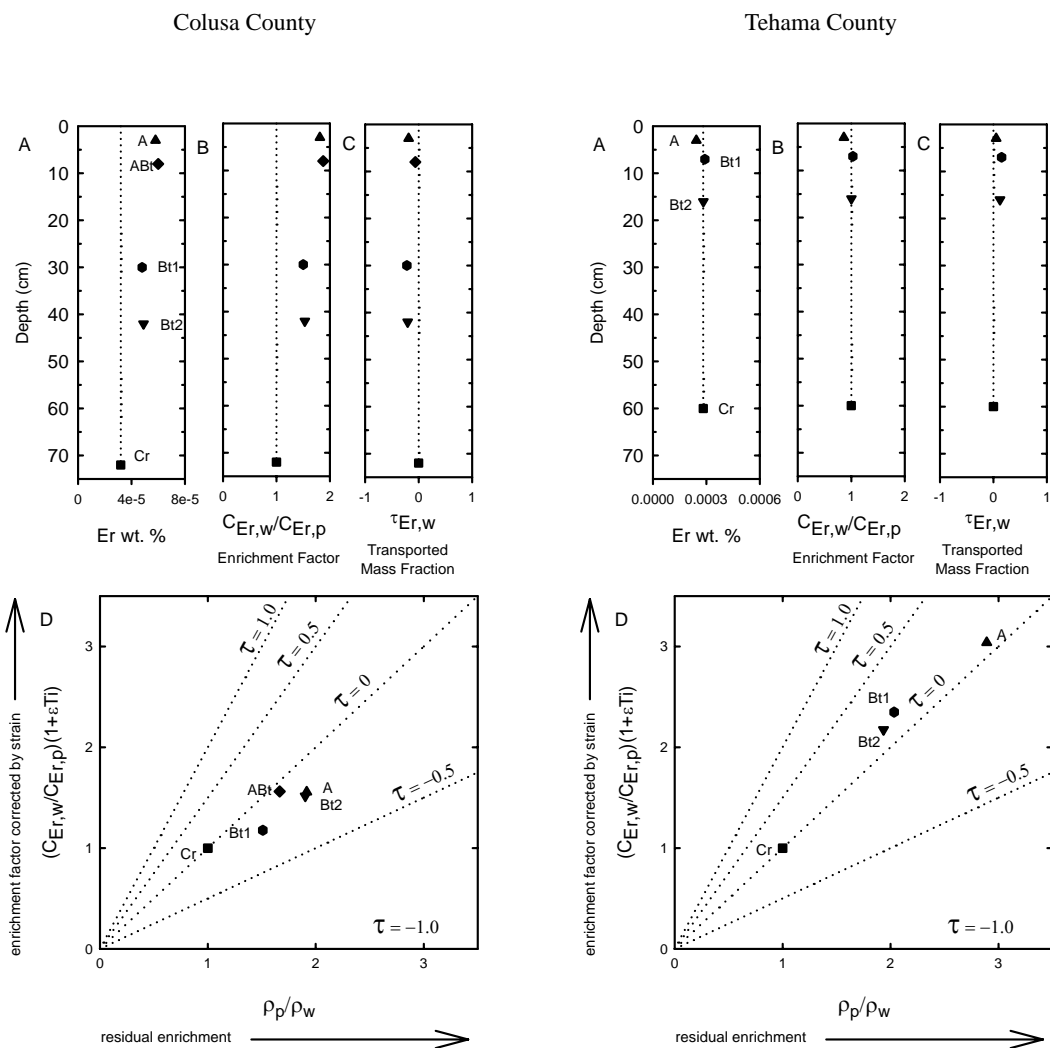


**Figure 4-35.** Depth plots of (A) weighted percent Er, (B) enrichment factor, and (C) the transported mass fraction of Er. (D) Plot of density ratio  $\rho_p/\rho_w$  representing the residual enrichment contribution vs. enrichment corrected by strain using Ti as the immobile element. Dotted vertical line (A, B & C) is visual indicator for parent material value. Dotted lines (D) represent  $\tau$ , the mass fraction added or subtracted from each sample at 0, 50 and 100%.



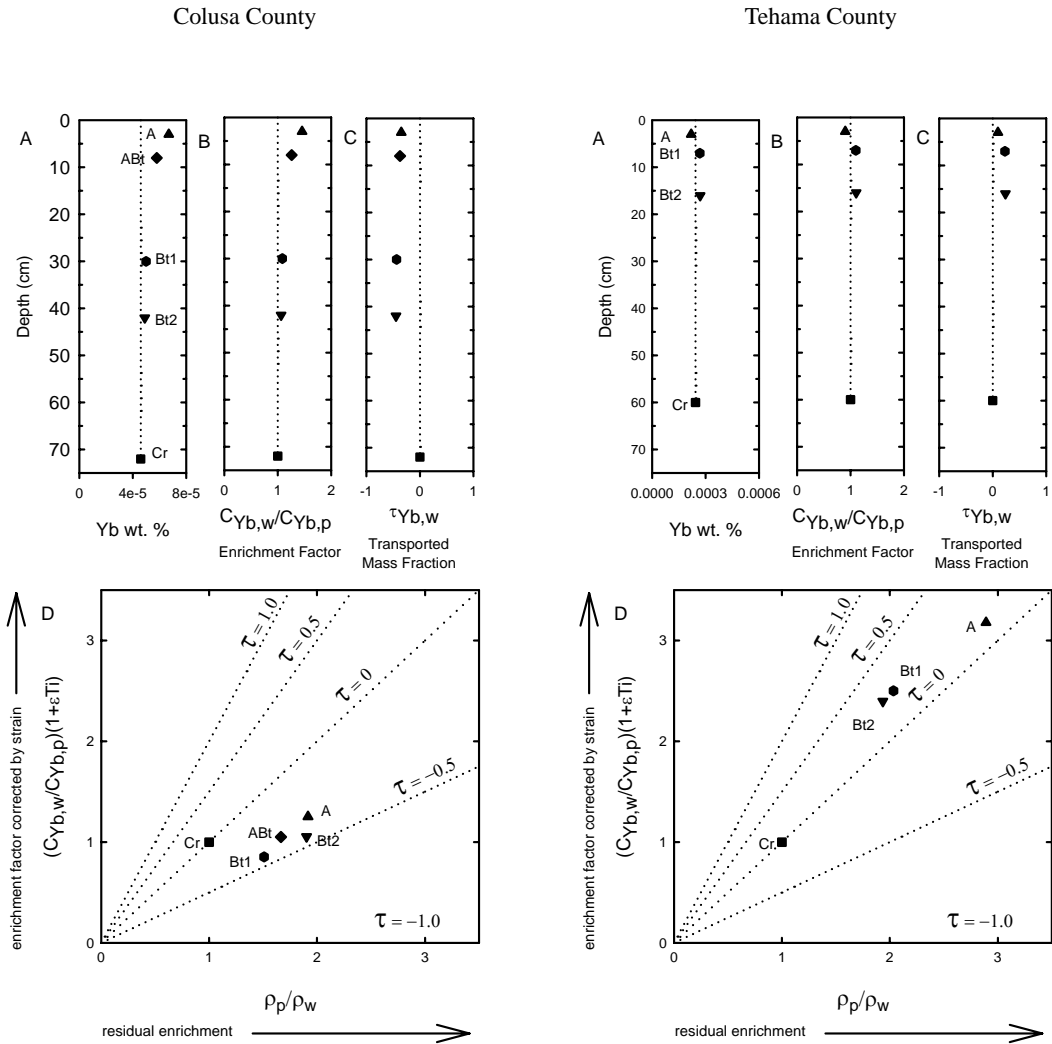


**Figure 4-36.** Depth plots of (A) weighted percent Yb, (B) enrichment factor, and (C) the transported mass fraction of Yb. (D) Plot of density ratio  $\rho_p/\rho_w$  representing the residual enrichment contribution vs. enrichment corrected by strain using Ti as the immobile element. Dotted vertical line (A, B & C) is visual indicator for parent material value. Dotted lines (D) represent  $\tau$ , the mass fraction added or subtracted from each sample at 0, 50 and 100%.

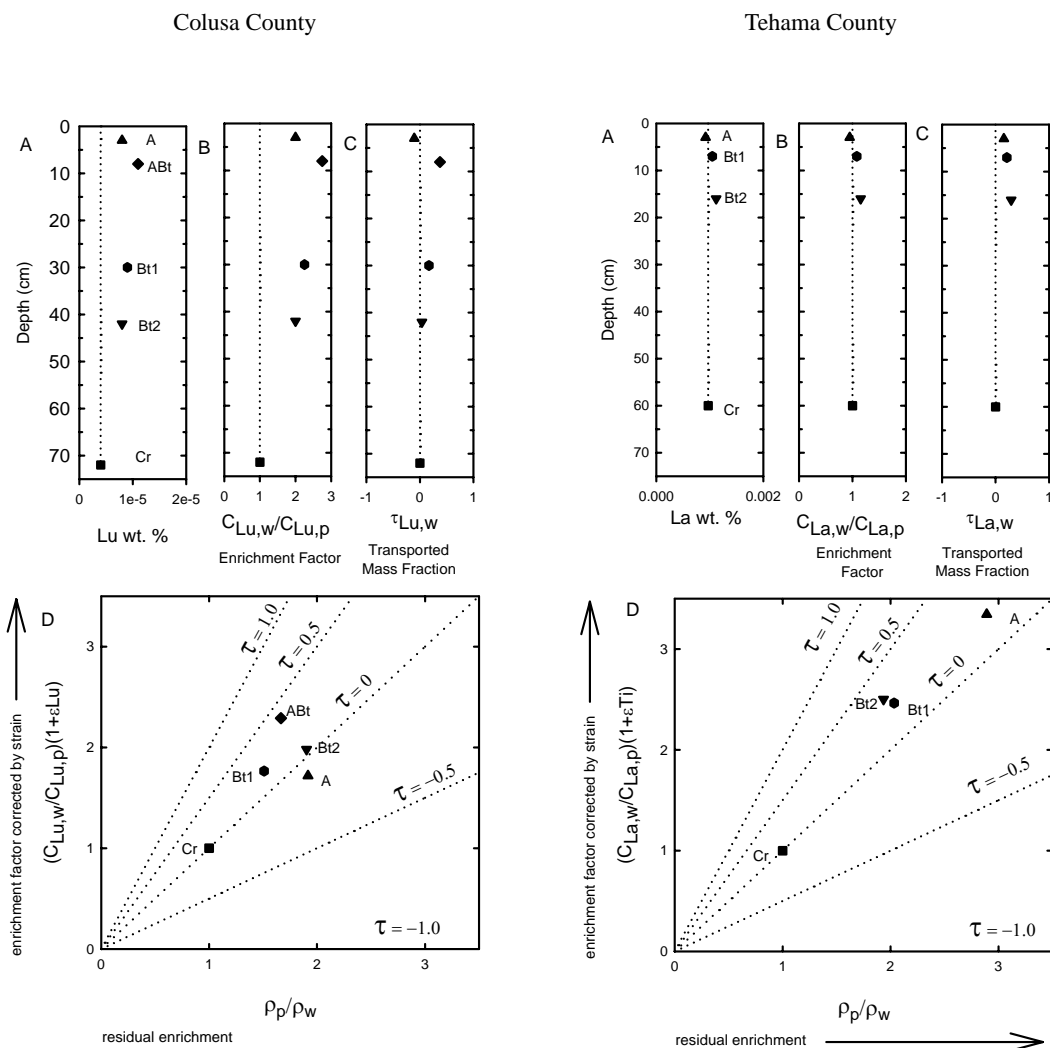


**Figure 4-37.** Depth plots of (A) weighted percent Lu, (B) enrichment factor, and (C) the transported mass fraction of Lu. (D) Plot of density ratio  $\rho_p/\rho_w$  representing the residual enrichment contribution vs. enrichment corrected by strain using Ti as the immobile element. Dotted vertical line (A, B & C) is visual indicator for parent material value. Dotted lines (D) represent  $\tau$ , the mass fraction added or subtracted from each sample at 0, 50 and 100%.

## 4.9 APPENDIX C

All of the REE's, and the element Sc graphed as (A) weight percent, (B) enrichment factor and (C) transported mass fraction with strain corrected my Nb. Dotted vertical lines in A to C serve as visual indicator for parent material value. (D) Graphic contributions of the components of closed system mass movement of the element across the sample volume boundaries (soil horizons) using Nb ( $\epsilon_{Nb,w}$ ) as the strain correcting element. Where dotted lines represent  $\tau$ , the mass fraction added or subtracted from each sample at 0, 50 and 100%.

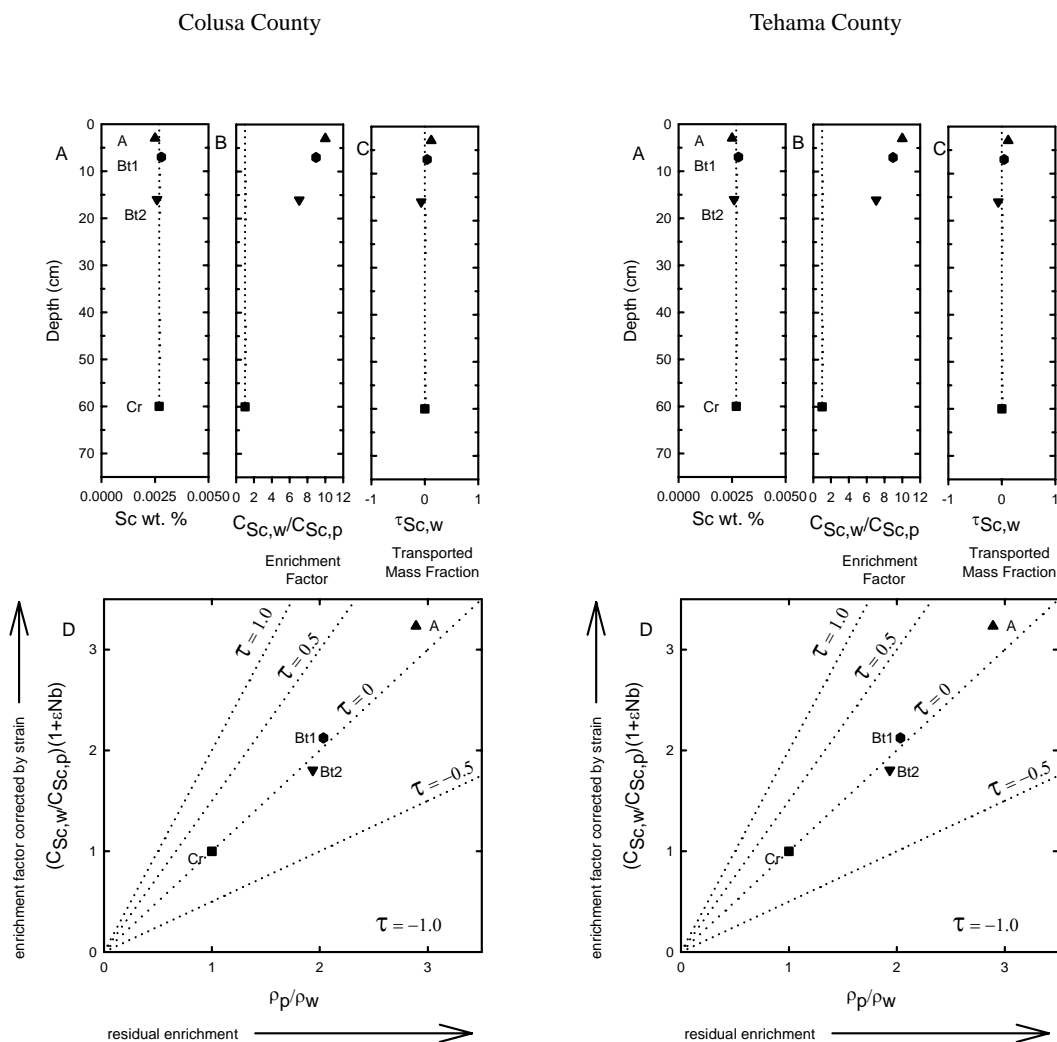


**Figure 4-38.** Depth plots of (A) weighted percent Sc, (B) enrichment factor, and (C) the transported mass fraction of Sc. (D) Plot of density ratio  $\rho_p/\rho_w$  representing the residual enrichment contribution vs. enrichment corrected by strain using Nb as the immobile element. Dotted vertical line (A, B & C) is visual indicator for parent material value. Dotted lines (D) represent  $\tau$ , the mass fraction added or subtracted from each sample at 0, 50 and 100%.

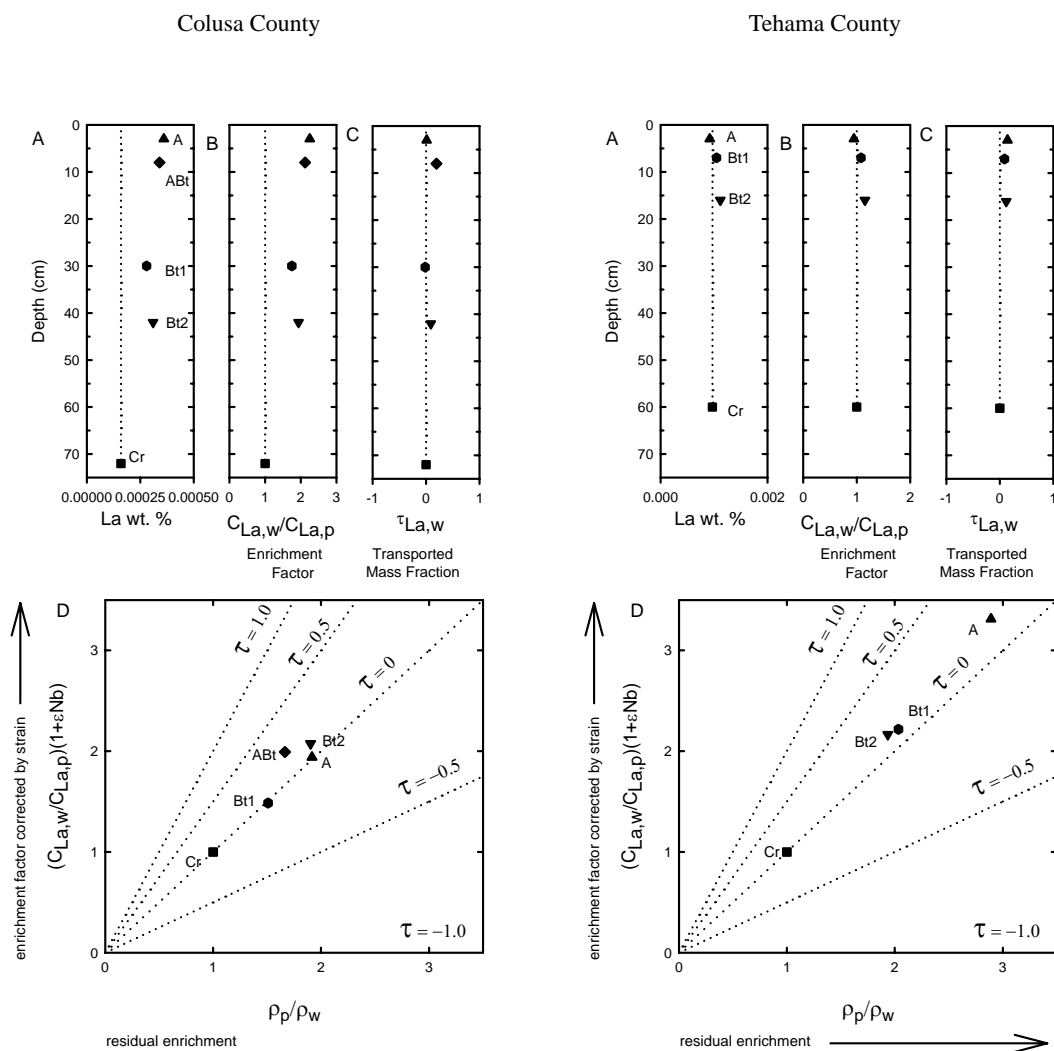


**Figure 4-39.** Depth plots of (A) weighted percent La, (B) enrichment factor, and (C) the transported mass fraction of La. (D) Plot of density ratio  $\rho_p/\rho_w$  representing the residual enrichment contribution vs. enrichment corrected by strain using Nb as the immobile element. Dotted vertical line (A, B & C) is visual indicator for parent material value. Dotted lines (D) represent  $\tau$ , the mass fraction added or subtracted from each sample at 0, 50 and 100%.

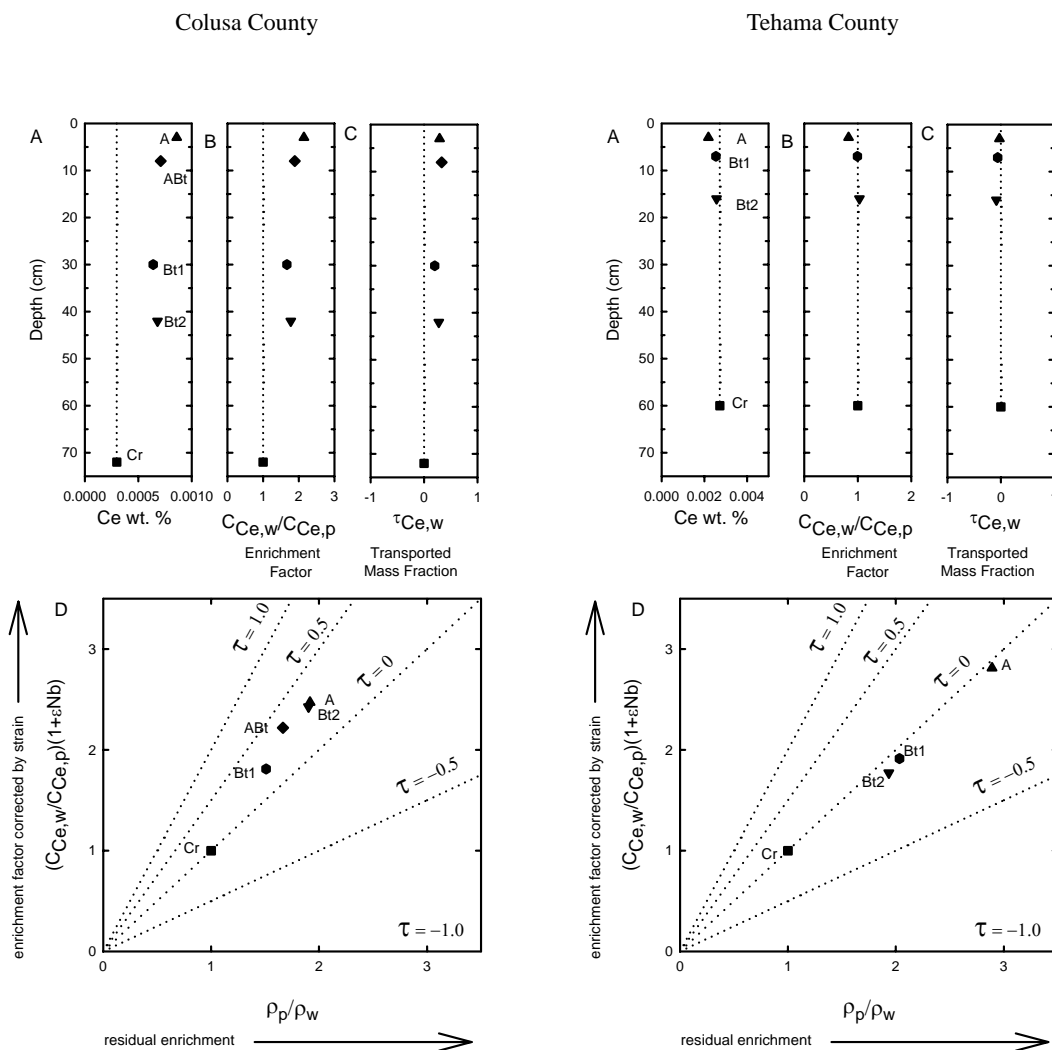


**Figure 4-40.** Depth plots of (A) weighted percent Ce, (B) enrichment factor, and (C) the transported mass fraction of Ce. (D) Plot of density ratio  $\rho_p/\rho_w$  representing the residual enrichment contribution vs. enrichment corrected by strain using Nb as the immobile element. Dotted vertical line (A, B & C) is visual indicator for parent material value. Dotted lines (D) represent  $\tau$ , the mass fraction added or subtracted from each sample at 0, 50 and 100%.

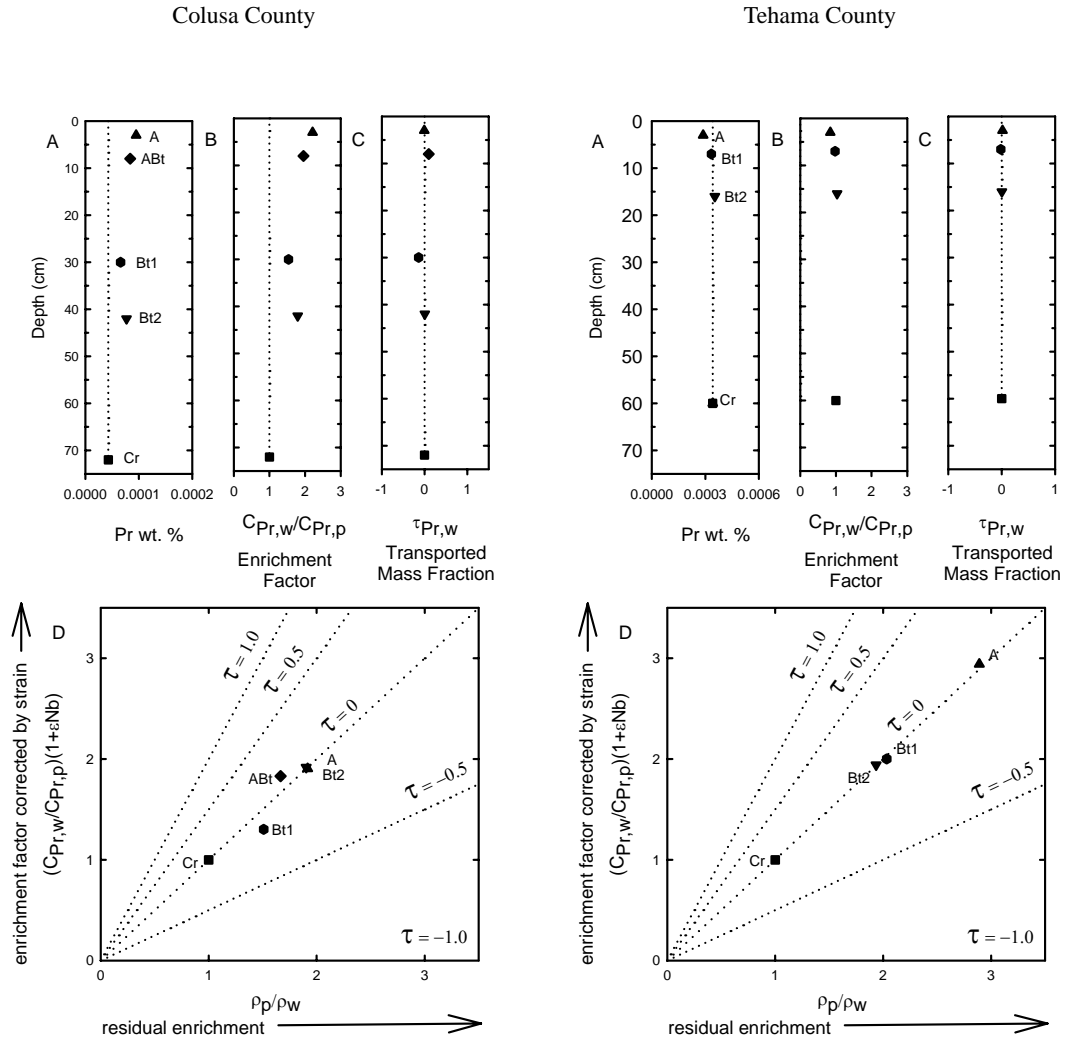


**Figure 4-41.** Depth plots of (A) weighted percent Pr, (B) enrichment factor, and (C) the transported mass fraction of Pr. (D) Plot of density ratio  $\rho_p/\rho_w$  representing the residual enrichment contribution vs. enrichment corrected by strain using Nb as the immobile element. Dotted vertical line (A, B & C) is visual indicator for parent material value. Dotted lines (D) represent  $\tau$ , the mass fraction added or subtracted from each sample at 0, 50 and 100%.

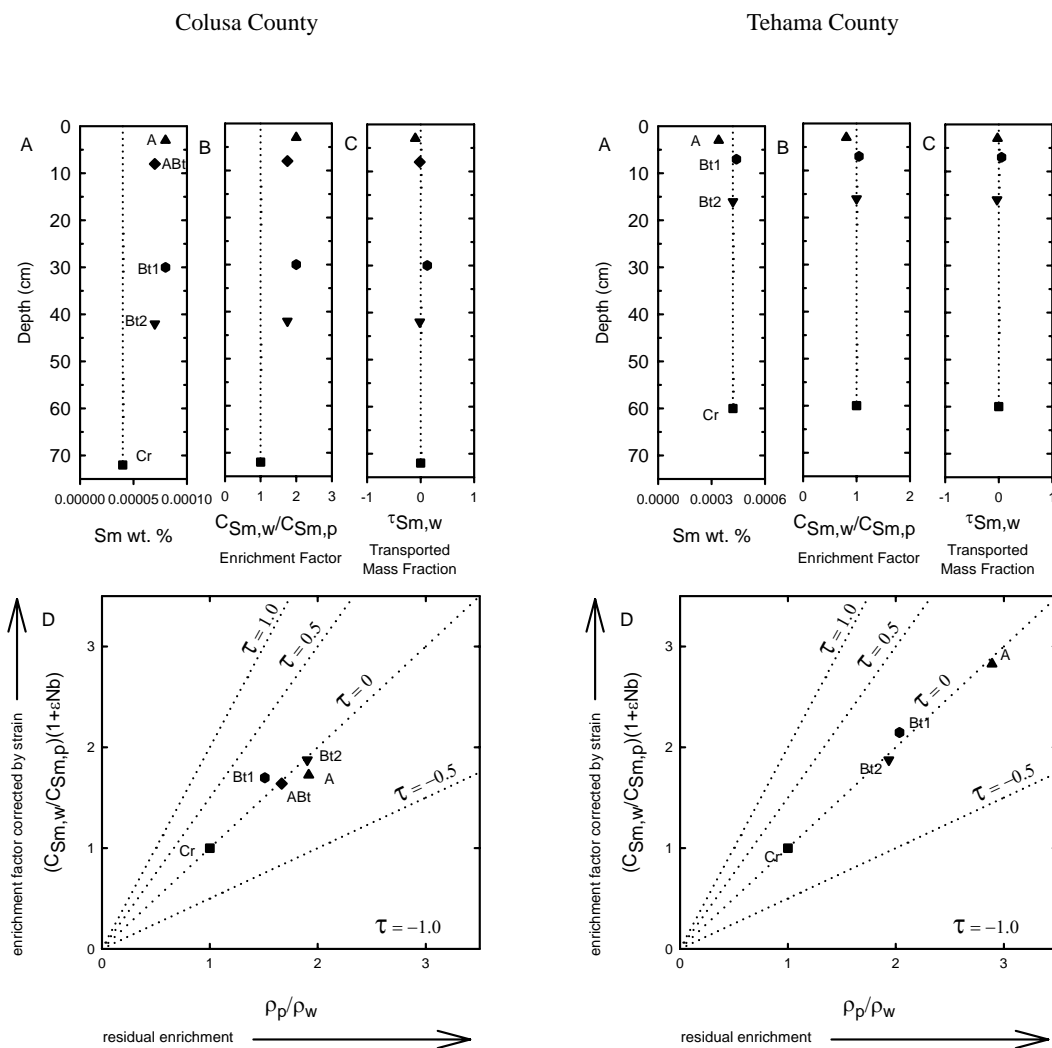


**Figure 4-42.** Depth plots of (A) weighted percent Sm, (B) enrichment factor, and (C) the transported mass fraction of Sm. (D) Plot of density ratio  $\rho_p/\rho_w$  representing the residual enrichment contribution vs. enrichment corrected by strain using Nb as the immobile element. Dotted vertical line (A, B & C) is visual indicator for parent material value. Dotted lines (D) represent  $\tau$ , the mass fraction added or subtracted from each sample at 0, 50 and 100%.

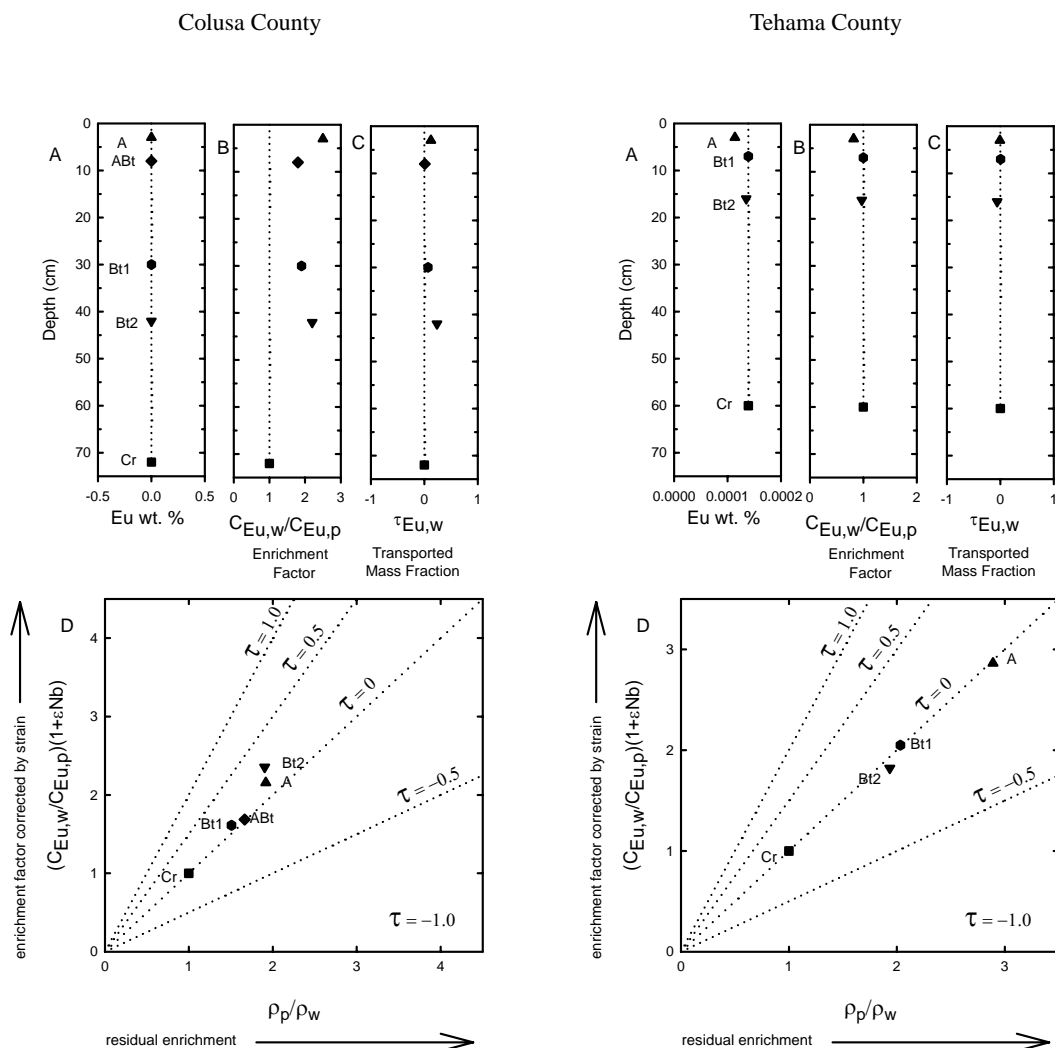


**Figure 4-43.** Depth plots of (A) weighted percent Eu, (B) enrichment factor, and (C) the transported mass fraction of Eu. (D) Plot of density ratio  $\rho_p/\rho_w$  representing the residual enrichment contribution vs. enrichment corrected by strain using Nb as the immobile element. Dotted vertical line (A, B & C) is visual indicator for parent material value. Dotted lines (D) represent  $\tau$ , the mass fraction added or subtracted from each sample at 0, 50 and 100%.



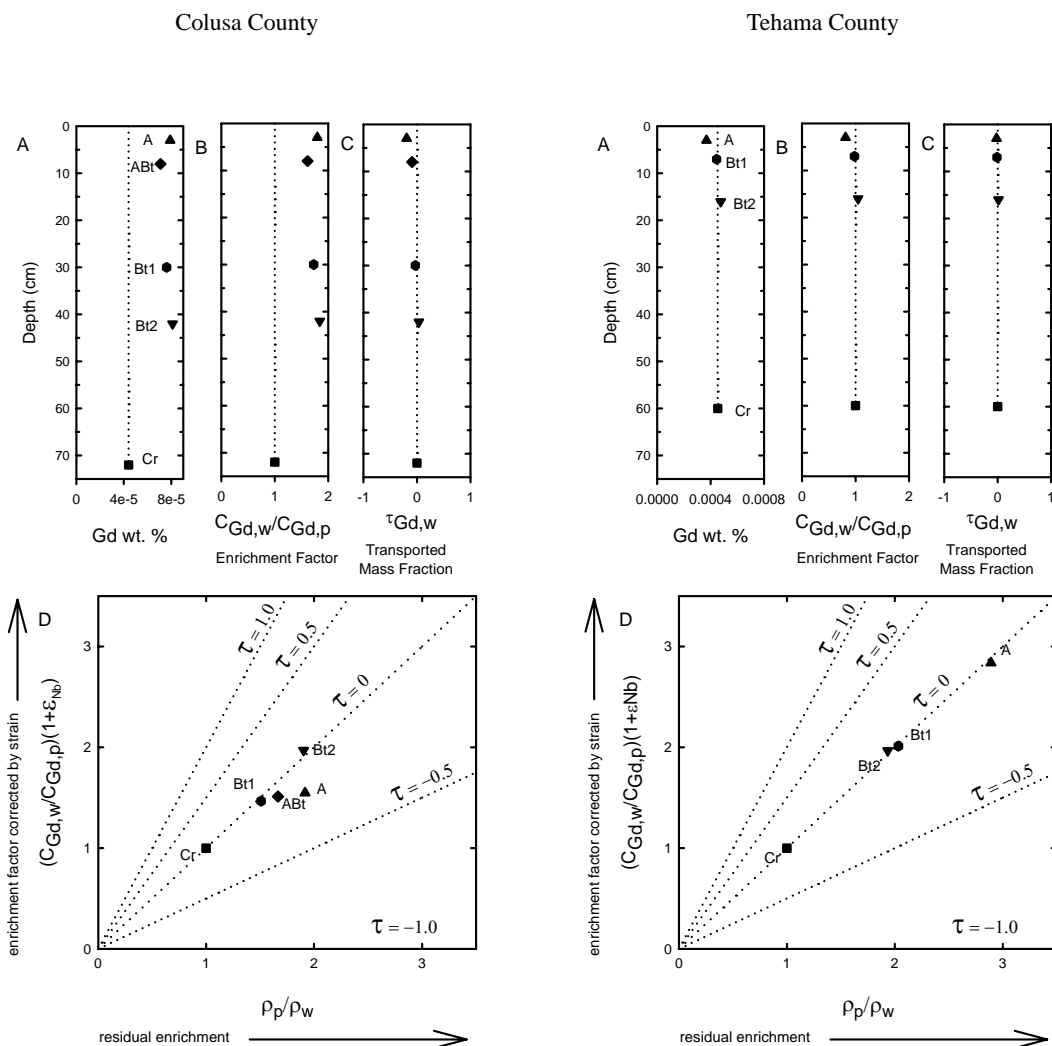


**Figure 4-44.** Depth plots of (A) weighted percent Gd, (B) enrichment factor, and (C) the transported mass fraction of Gd. (D) Plot of density ratio  $\rho_p/\rho_w$  representing the residual enrichment contribution vs. enrichment corrected by strain using Nd as the immobile element. Dotted vertical line (A, B & C) is visual indicator for parent material value. Dotted lines (D) represent  $\tau$ , the mass fraction added or subtracted from each sample at 0, 50 and 100%.

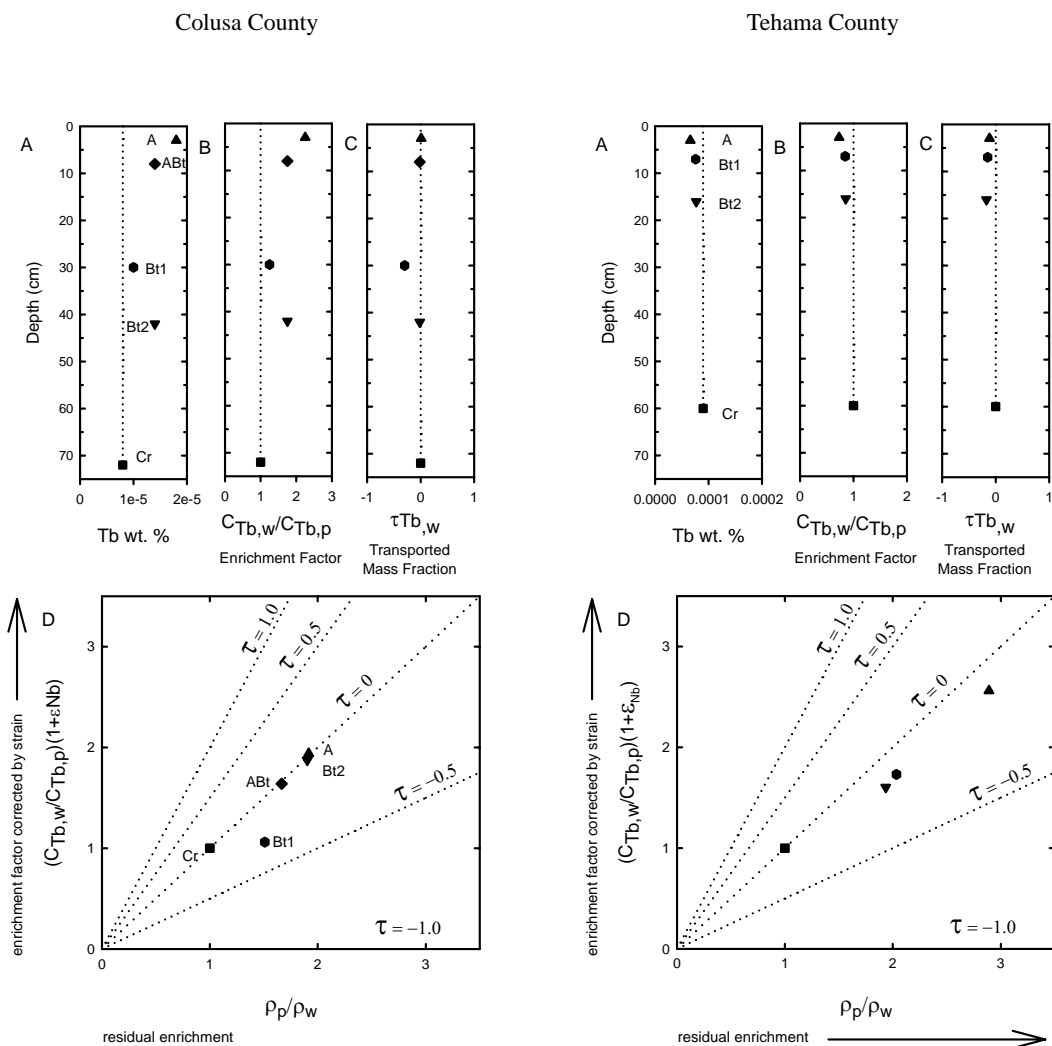


**Figure 4-45.** Depth plots of (A) weighted percent Tb, (B) enrichment factor, and (C) the transported mass fraction of Tb. (D) Plot of density ratio  $\rho_p/\rho_w$  representing the residual enrichment contribution vs. enrichment corrected by strain using Nb as the immobile element. Dotted vertical line (A, B & C) is visual indicator for parent material value. Dotted lines (D) represent  $\tau$ , the mass fraction added or subtracted from each sample at 0, 50 and 100%.

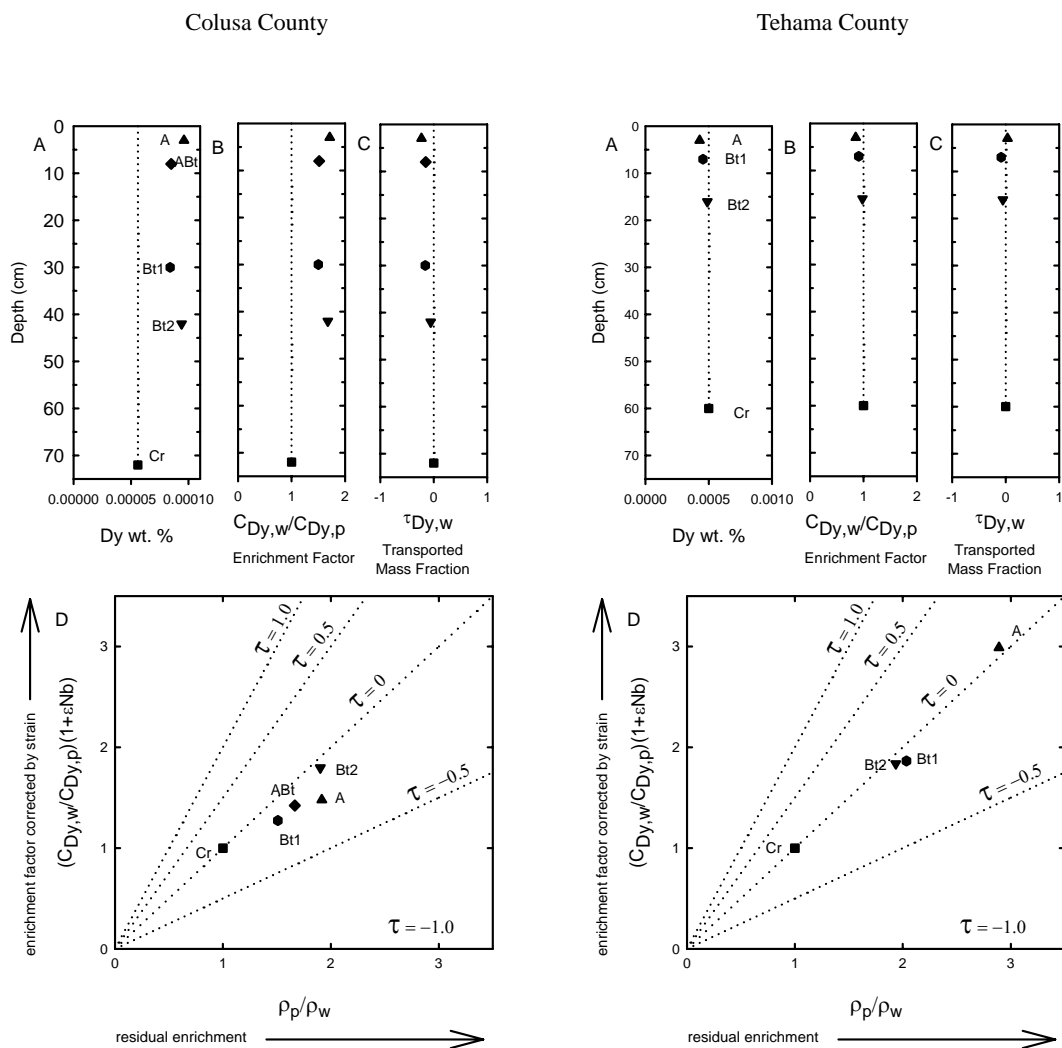


**Figure 4-46.** Depth plots of (A) weighted percent Dy, (B) enrichment factor, and (C) the transported mass fraction of Dy. (D) Plot of density ratio  $\rho_p/\rho_w$  representing the residual enrichment contribution vs. enrichment corrected by strain using Nb as the immobile element. Dotted vertical line (A, B & C) is visual indicator for parent material value. Dotted lines (D) represent  $\tau$ , the mass fraction added or subtracted from each sample at 0, 50 and 100%.

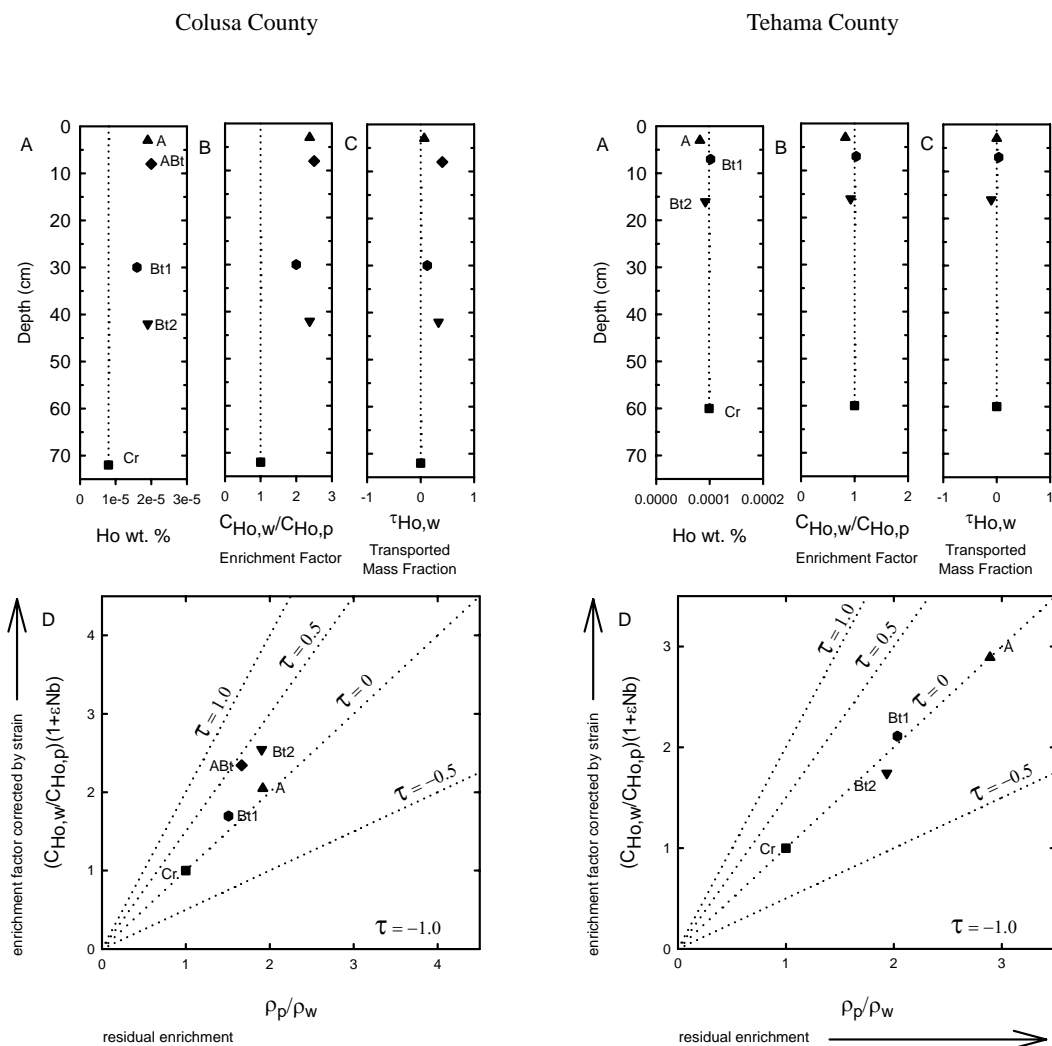


**Figure 4-47.** Depth plots of (A) weighted percent Ho, (B) enrichment factor, and (C) the transported mass fraction of Ho. (D) Plot of density ratio  $\rho_p/\rho_w$  representing the residual enrichment contribution vs. enrichment corrected by strain using Nb as the immobile element. Dotted vertical line (A, B & C) is visual indicator for parent material value. Dotted lines (D) represent  $\tau$ , the mass fraction added or subtracted from each sample at 0, 50 and 100%.

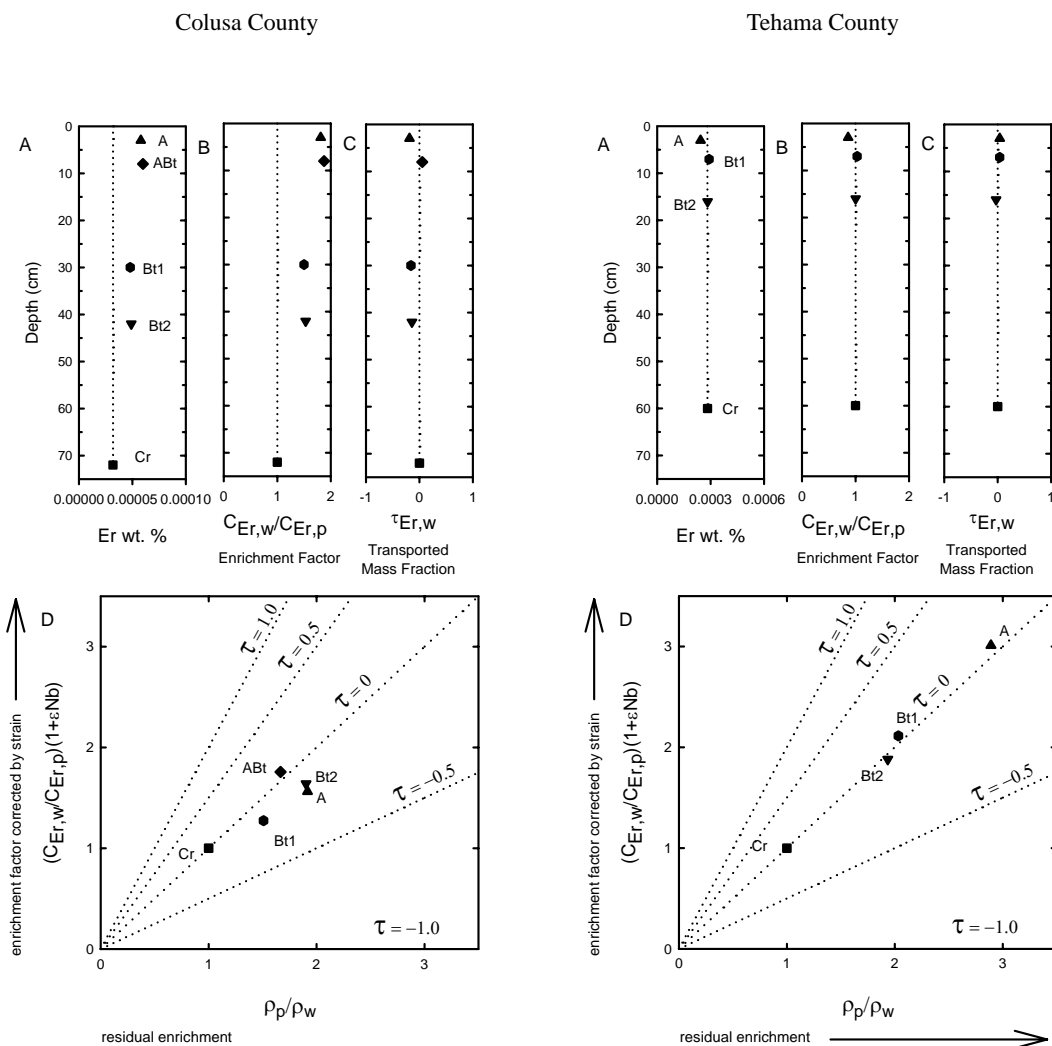


**Figure 4-48.** Depth plots of (A) weighted percent Er, (B) enrichment factor, and (C) the transported mass fraction of Er. (D) Plot of density ratio  $\rho_p/\rho_w$  representing the residual enrichment contribution vs. enrichment corrected by strain using Nb as the immobile element. Dotted vertical line (A, B & C) is visual indicator for parent material value. Dotted lines (D) represent  $\tau$ , the mass fraction added or subtracted from each sample at 0, 50 and 100%.

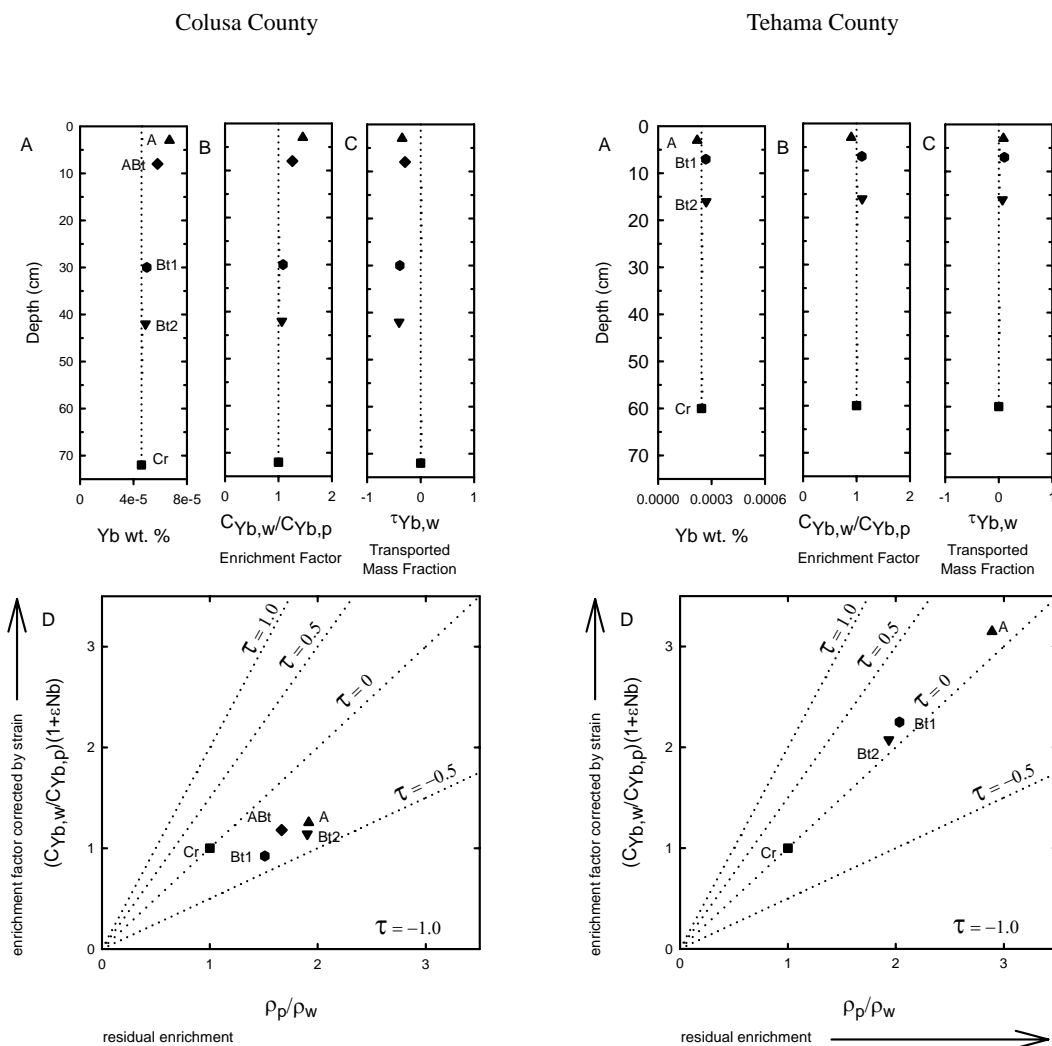


**Figure 4-49.** Depth plots of (A) weighted percent Yb, (B) enrichment factor, and (C) the transported mass fraction of Yb. (D) Plot of density ratio  $\rho_p/\rho_w$  representing the residual enrichment contribution vs. enrichment corrected by strain using Nb as the immobile element. Dotted vertical line (A, B & C) is visual indicator for parent material value. Dotted lines (D) represent  $\tau$ , the mass fraction added or subtracted from each sample at 0, 50 and 100%.

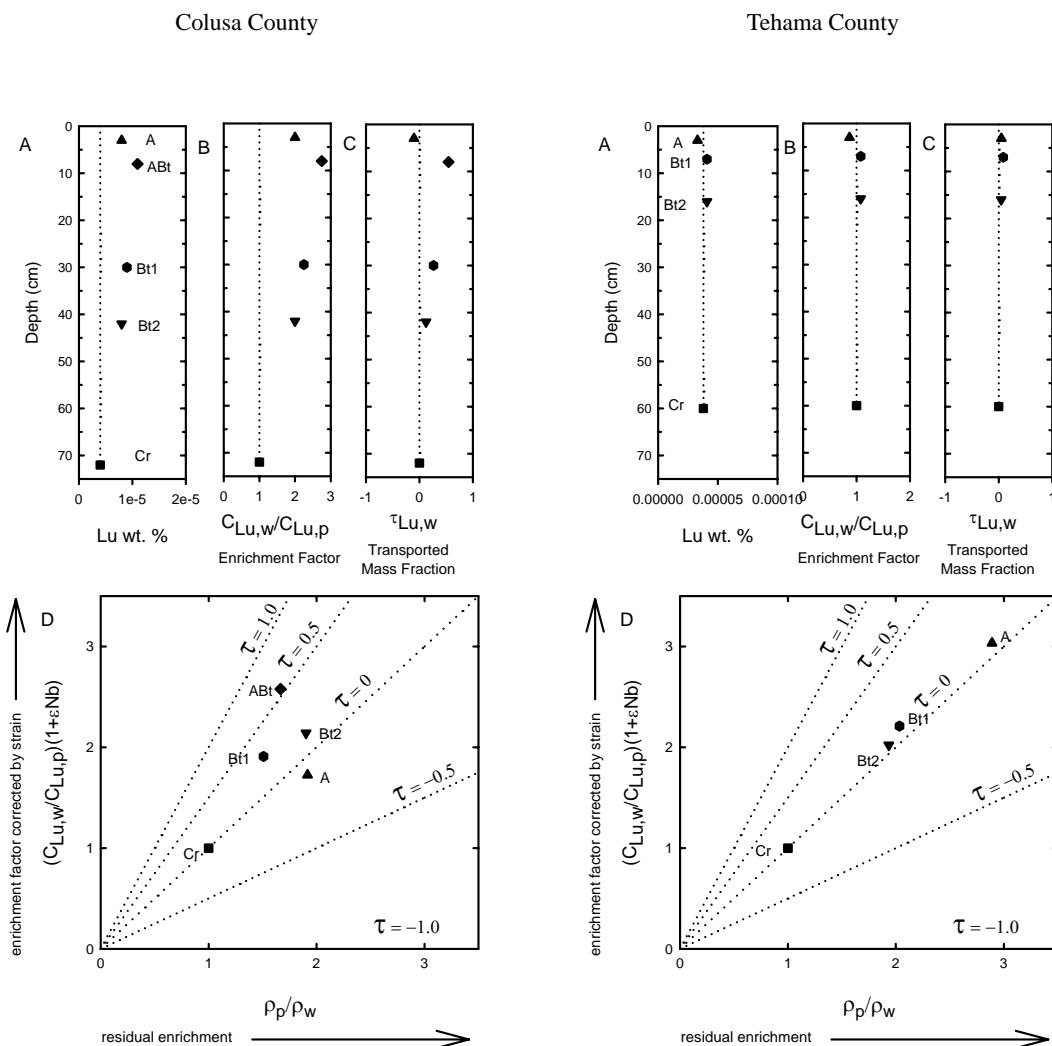


**Figure 4-50.** Depth plots of (A) weighted percent Lu, (B) enrichment factor, and (C) the transported mass fraction of Lu. (D) Plot of density ratio  $\rho_p/\rho_w$  representing the residual enrichment contribution vs. enrichment corrected by strain using Nd as the immobile element. Dotted vertical line (A, B & C) is visual indicator for parent material value. Dotted lines (D) represent  $\tau$ , the mass fraction added or subtracted from each sample at 0, 50 and 100%.

## 4.10 APPENDIX D

All of the REE's, and the element Sc graphed as (A) weight percent, (B) enrichment factor and (C) transported mass fraction with strain corrected by Zr. Dotted vertical lines in A to C serve as visual indicator for parent material value. (D) Graphic contributions of the components of closed system mass movement of the element across the sample volume boundaries (soil horizons) using Zr ( $\epsilon_{Zr,W}$ ) as the strain correcting element. Where dotted lines represent  $\tau$ , the mass fraction added or subtracted from each sample at 0, 50 and 100%.



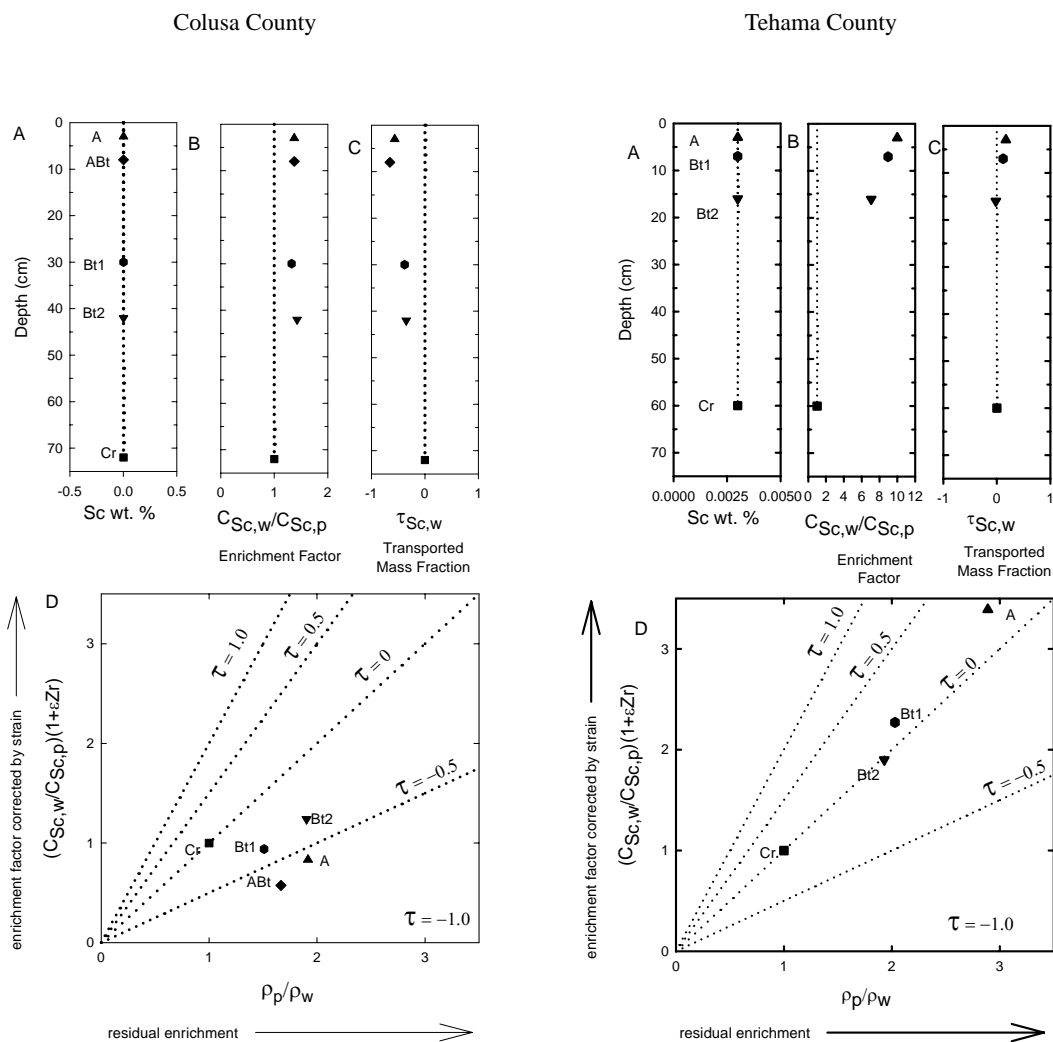


**Figure 4-51.** Depth plots of (A) weighted percent Sc, (B) enrichment factor, and (C) the transported mass fraction of Sc. (D) Plot of density ratio  $\rho_p/\rho_w$  representing the residual enrichment contribution vs. enrichment corrected by strain using Zr as the immobile element. Dotted vertical line (A, B & C) is visual indicator for parent material value. Dotted lines (D) represent  $\tau$ , the mass fraction added or subtracted from each sample at 0, 50 and 100%.

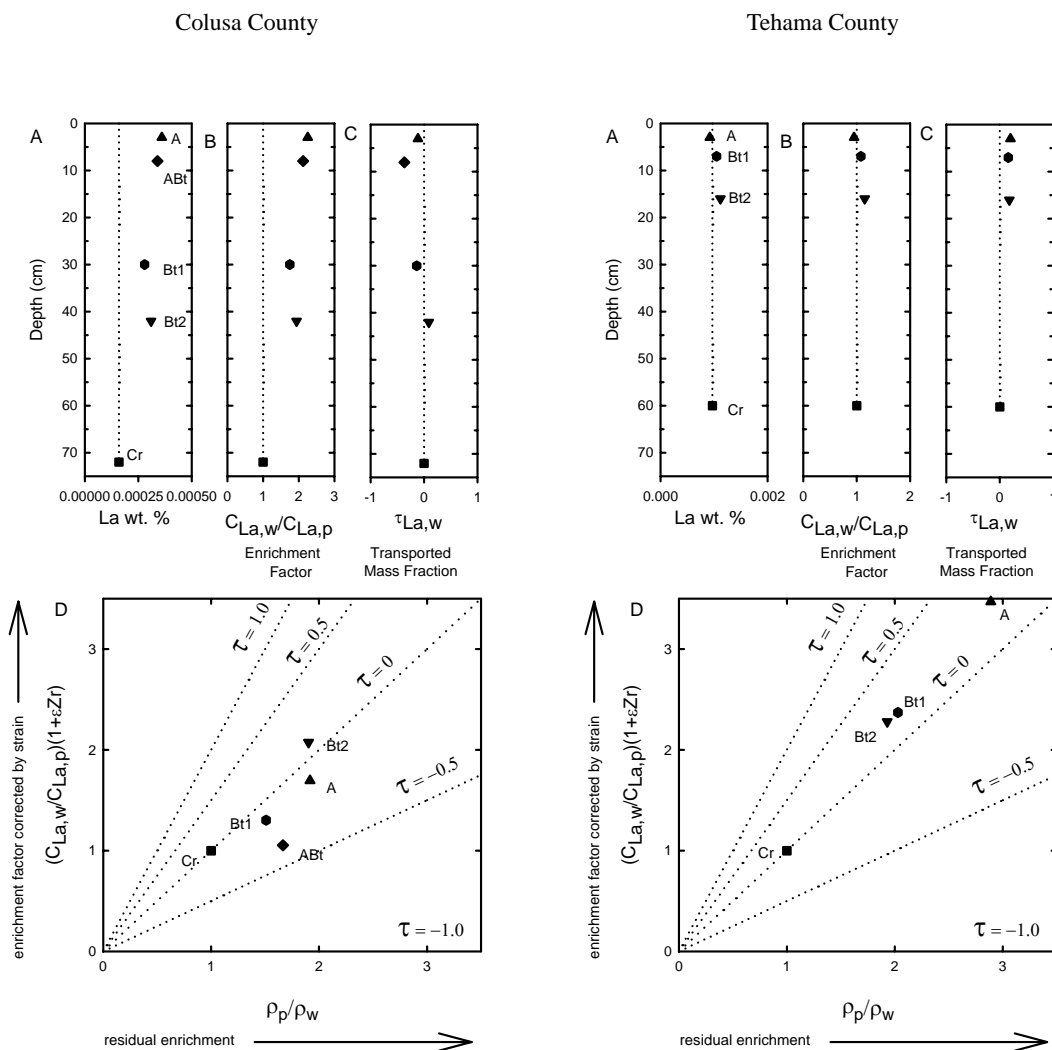


**Figure 4-52.** Depth plots of (A) weighted percent La, (B) enrichment factor, and (C) the transported mass fraction of La. (D) Plot of density ratio  $\rho_p/\rho_w$  representing the residual enrichment contribution vs. enrichment corrected by strain using Zr as the immobile element. Dotted vertical line (A, B & C) is visual indicator for parent material value. Dotted lines (D) represent  $\tau$ , the mass fraction added or subtracted from each sample at 0, 50 and 100%.

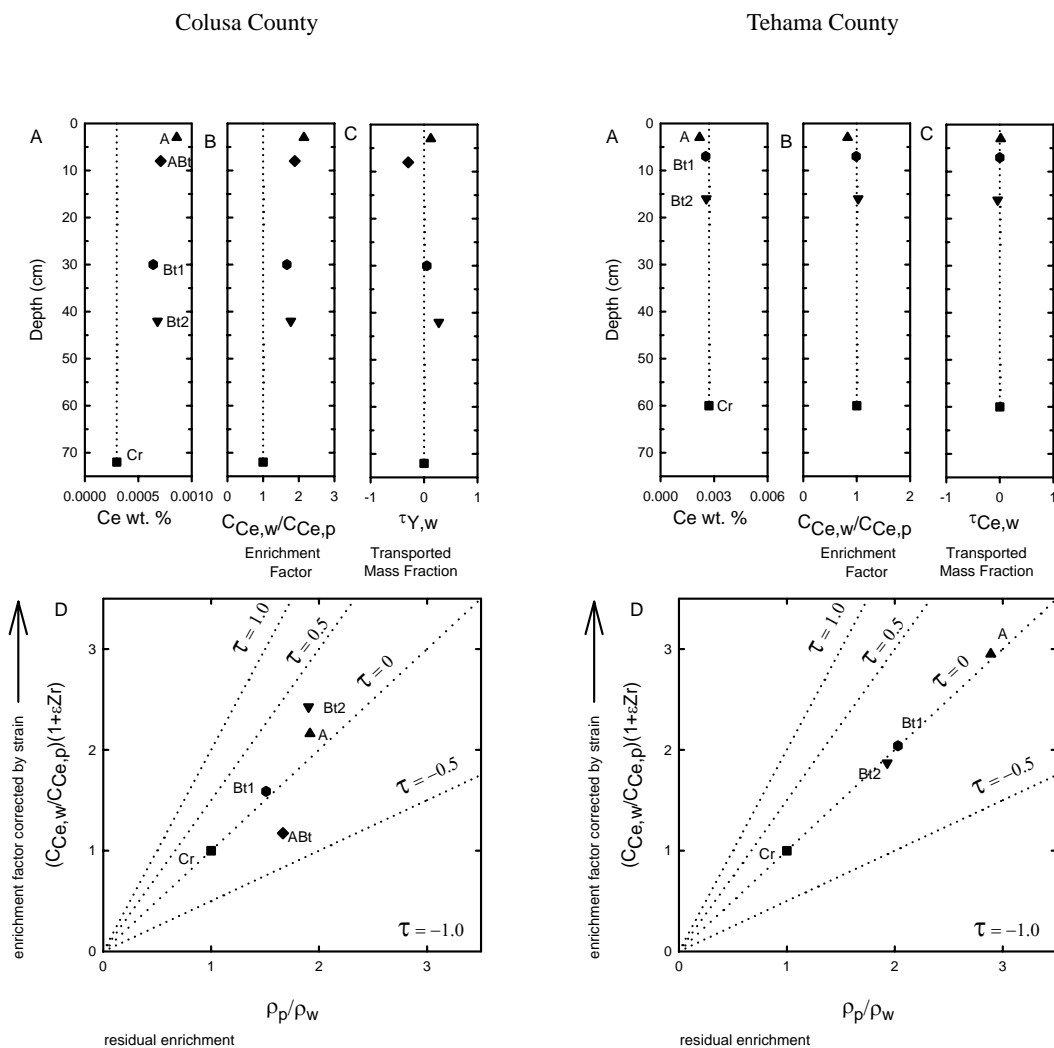


**Figure 4-53.** Depth plots of (A) weighted percent Ce, (B) enrichment factor, and (C) the transported mass fraction of Ce. (D) Plot of density ratio  $\rho_p/\rho_w$  representing the residual enrichment contribution vs. enrichment corrected by strain using Zr as the immobile element. Dotted vertical line (A, B & C) is visual indicator for parent material value. Dotted lines (D) represent  $\tau$ , the mass fraction added or subtracted from each sample at 0, 50 and 100%.

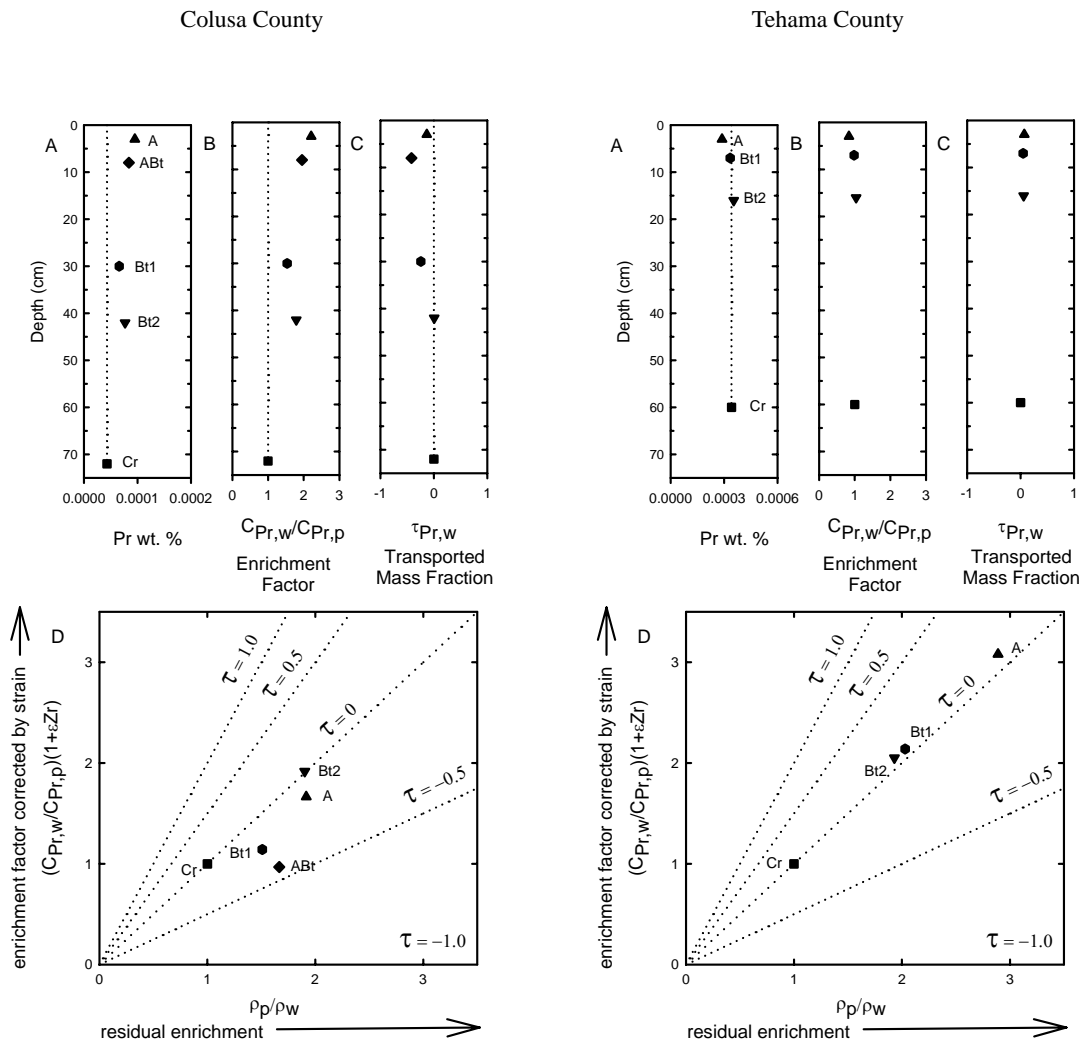


**Figure 4-54.** Depth plots of (A) weighted percent Pr, (B) enrichment factor, and (C) the transported mass fraction of Pr. (D) Plot of density ratio  $\rho_p/\rho_w$  representing the residual enrichment contribution vs. enrichment corrected by strain using Zr as the immobile element. Dotted vertical line (A, B & C) is visual indicator for parent material value. Dotted lines (D) represent  $\tau$ , the mass fraction added or subtracted from each sample at 0, 50 and 100%.

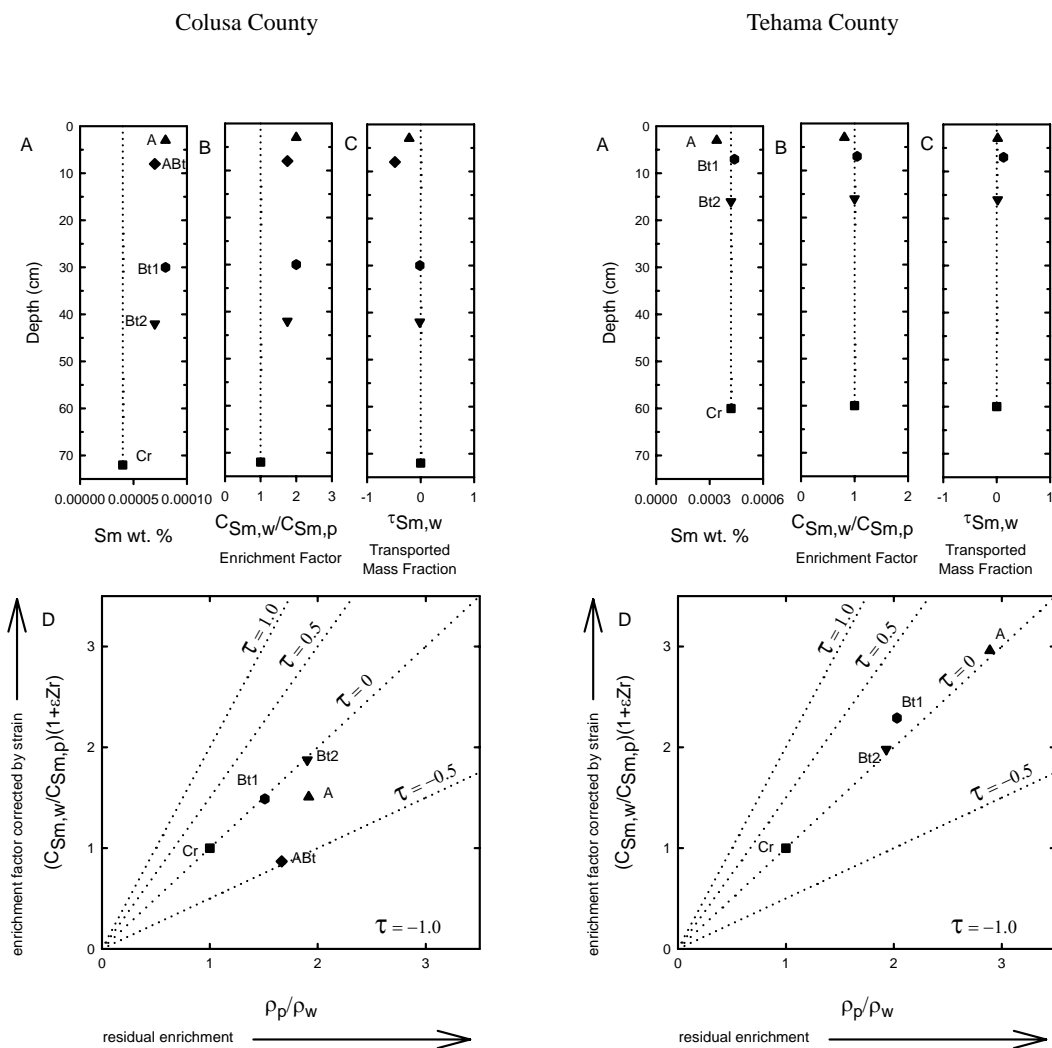


**Figure 4-55.** Depth plots of (A) weighted percent Sm, (B) enrichment factor, and (C) the transported mass fraction of Sm. (D) Plot of density ratio  $\rho_p/\rho_w$  representing the residual enrichment contribution vs. enrichment corrected by strain using Zr as the immobile element. Dotted vertical line (A, B & C) is visual indicator for parent material value. Dotted lines (D) represent  $\tau$ , the mass fraction added or subtracted from each sample at 0, 50 and 100%.

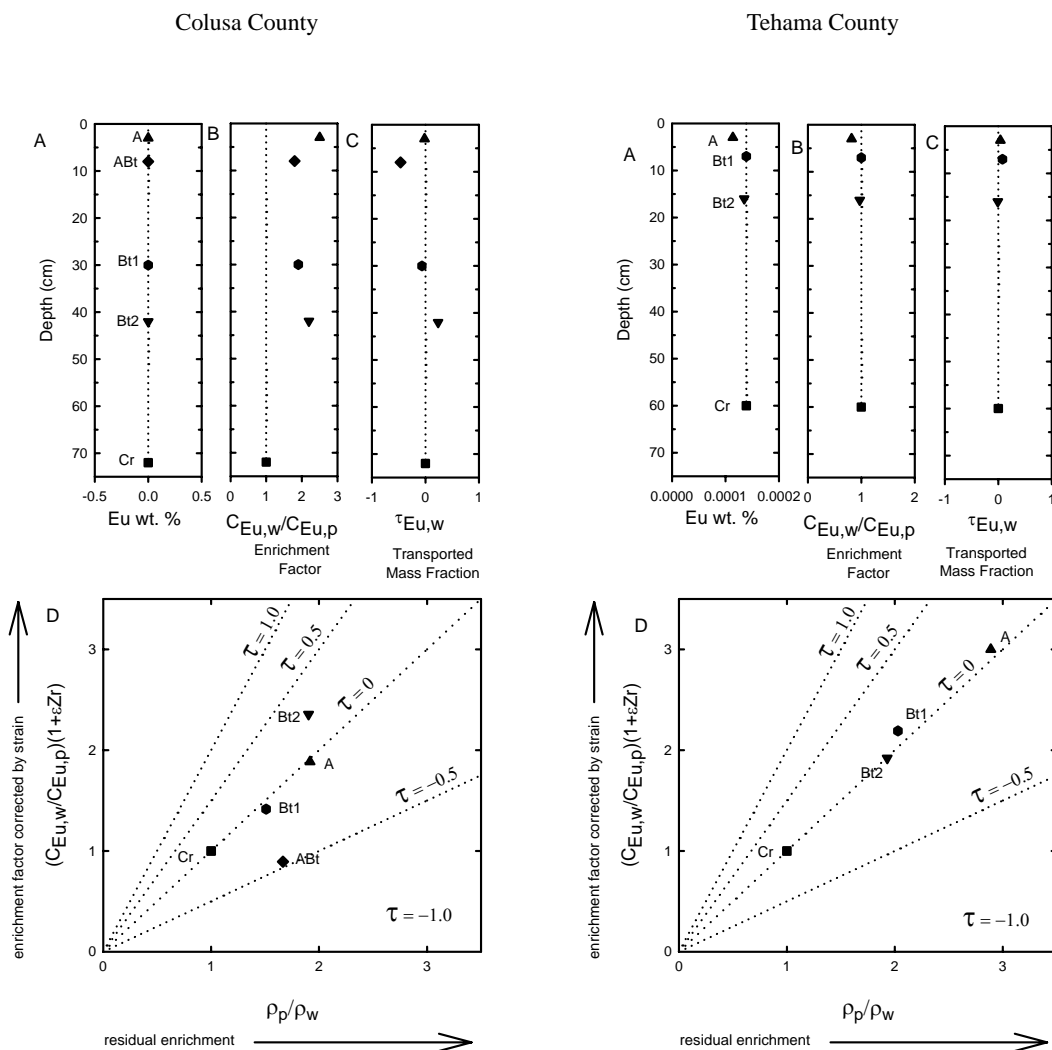


**Figure 4-56.** Depth plots of (A) weighted percent Eu, (B) enrichment factor, and (C) the transported mass fraction of Eu. (D) Plot of density ratio  $\rho_p/\rho_w$  representing the residual enrichment contribution vs. enrichment corrected by strain using Zr as the immobile element. Dotted vertical line (A, B & C) is visual indicator for parent material value. Dotted lines (D) represent  $\tau$ , the mass fraction added or subtracted from each sample at 0, 50 and 100%.

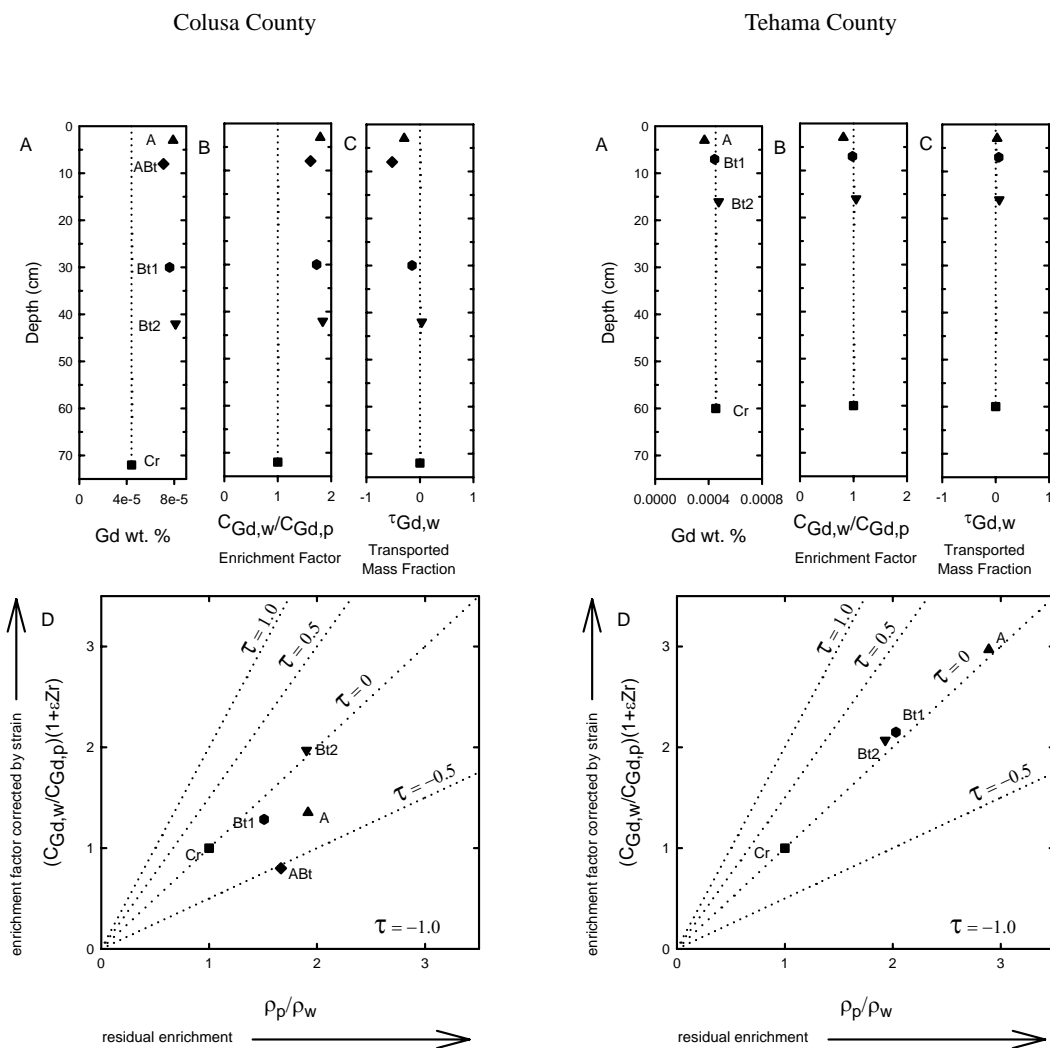


**Figure 4-57.** Depth plots of (A) weighted percent Gd, (B) enrichment factor, and (C) the transported mass fraction of Gd. (D) Plot of density ratio  $\rho_p/\rho_w$  representing the residual enrichment contribution vs. enrichment corrected by strain using Zr as the immobile element. Dotted vertical line (A, B & C) is visual indicator for parent material value. Dotted lines (D) represent  $\tau$ , the mass fraction added or subtracted from each sample at 0, 50 and 100%.

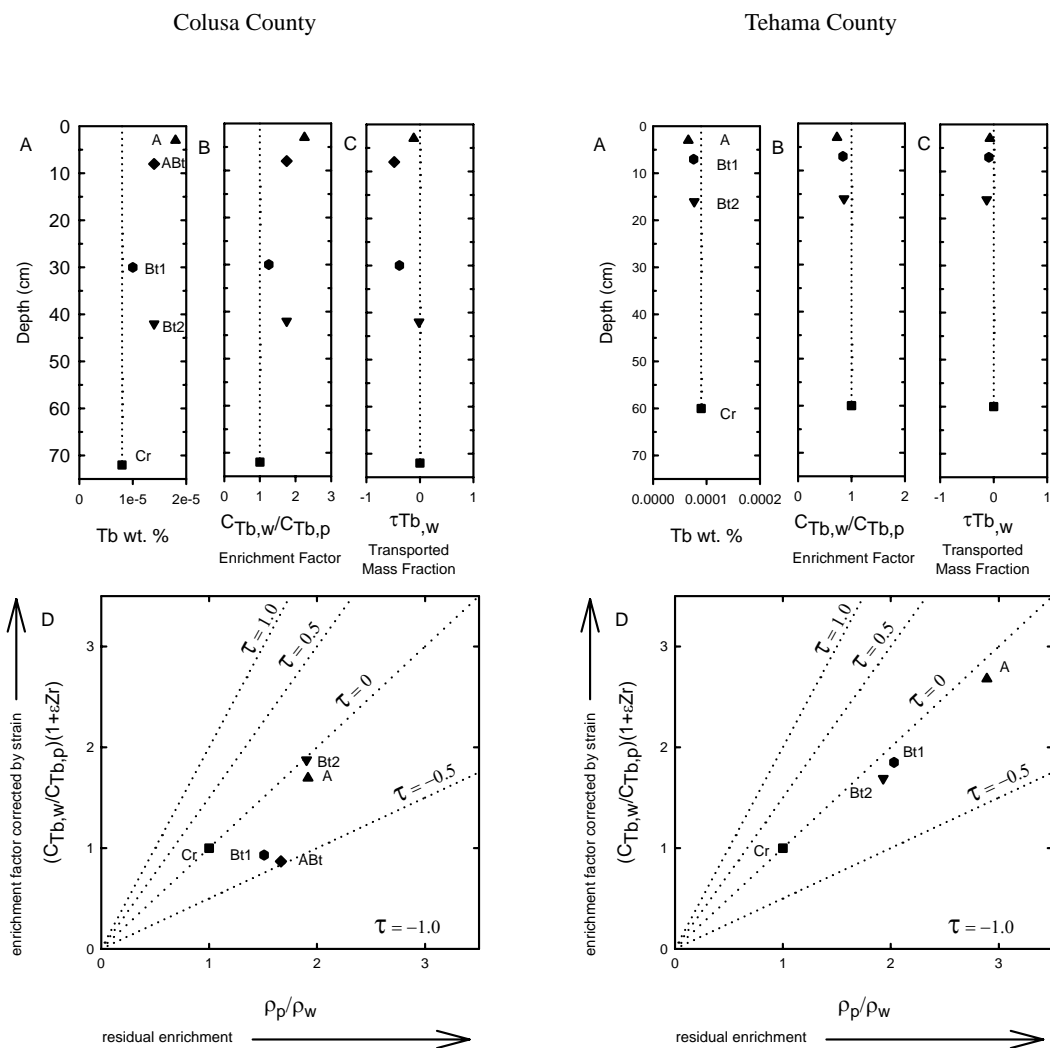


**Figure 4-58.** Depth plots of (A) weighted percent Tb, (B) enrichment factor, and (C) the transported mass fraction of Tb. (D) Plot of density ratio  $\rho_p/\rho_w$  representing the residual enrichment contribution vs. enrichment corrected by strain using Zr as the immobile element. Dotted vertical line (A, B & C) is visual indicator for parent material value. Dotted lines (D) represent  $\tau$ , the mass fraction added or subtracted from each sample at 0, 50 and 100%.



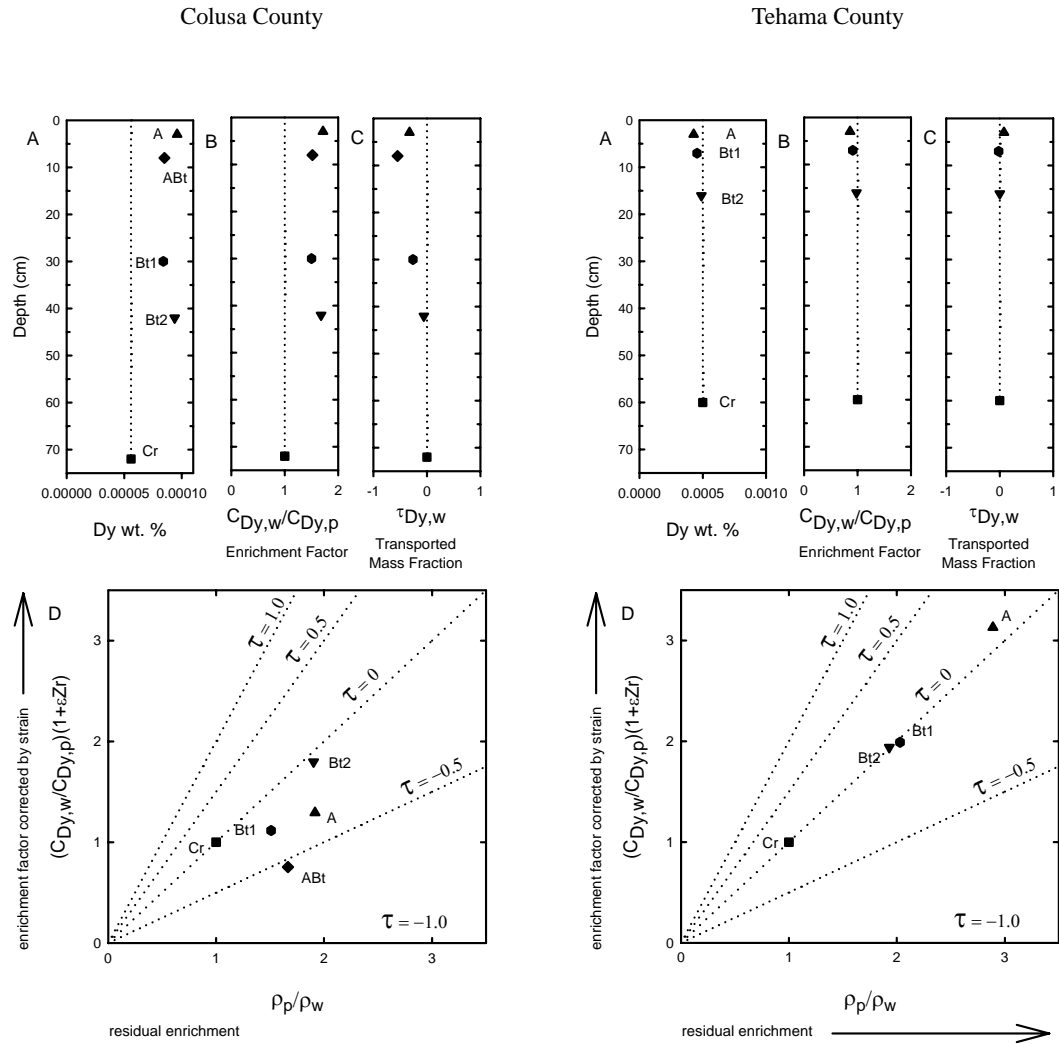


**Figure 4-59.** Depth plots of (A) weighted percent Dy, (B) enrichment factor, and (C) the transported mass fraction of Dy. (D) Plot of density ratio  $\rho_p/\rho_w$  representing the residual enrichment contribution vs. enrichment corrected by strain using Zr as the immobile element. Dotted vertical line (A, B & C) is visual indicator for parent material value. Dotted lines (D) represent  $\tau$ , the mass fraction added or subtracted from each sample at 0, 50 and 100%.

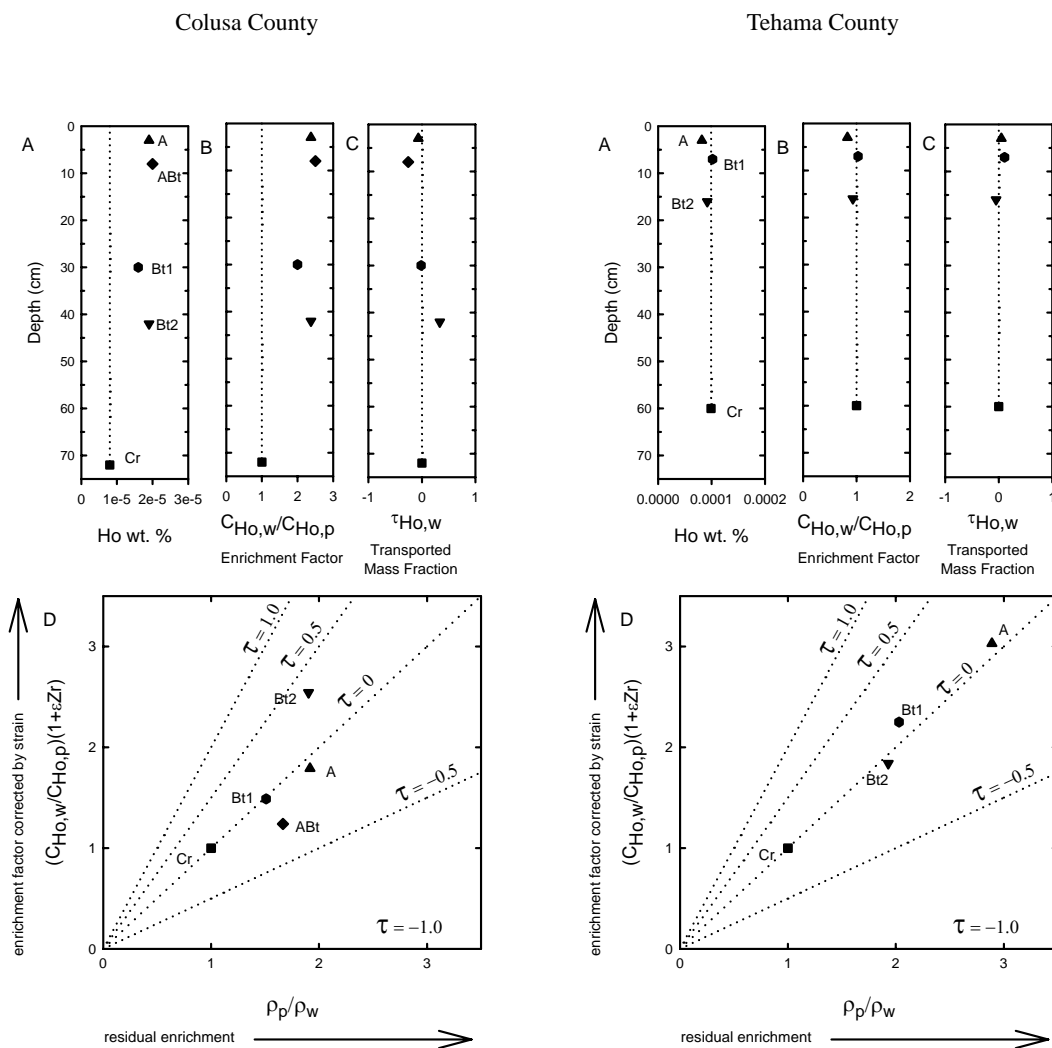


**Figure 4-60.** Depth plots of (A) weighted percent Ho, (B) enrichment factor, and (C) the transported mass fraction of Ho. (D) Plot of density ratio  $\rho_p/\rho_w$  representing the residual enrichment contribution vs. enrichment corrected by strain using Zr as the immobile element. Dotted vertical line (A, B & C) is visual indicator for parent material value. Dotted lines (D) represent  $\tau$ , the mass fraction added or subtracted from each sample at 0, 50 and 100%.

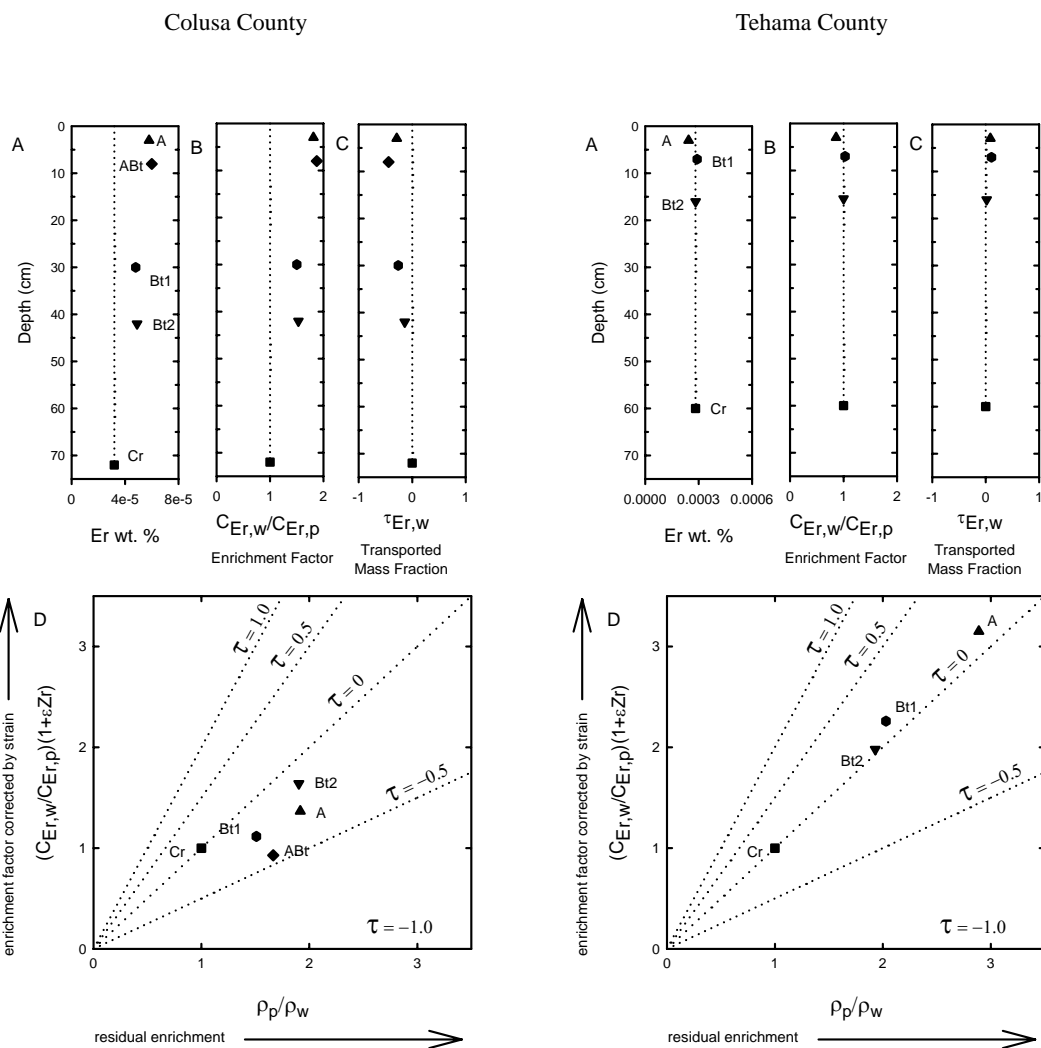


**Figure 4-61.** Depth plots of (A) weighted percent Er, (B) enrichment factor, and (C) the transported mass fraction of Er. (D) Plot of density ratio  $\rho_p/\rho_w$  representing the residual enrichment contribution vs. enrichment corrected by strain using Zr as the immobile element. Dotted vertical line (A, B & C) is visual indicator for parent material value. Dotted lines (D) represent  $\tau$ , the mass fraction added or subtracted from each sample at 0, 50 and 100%.

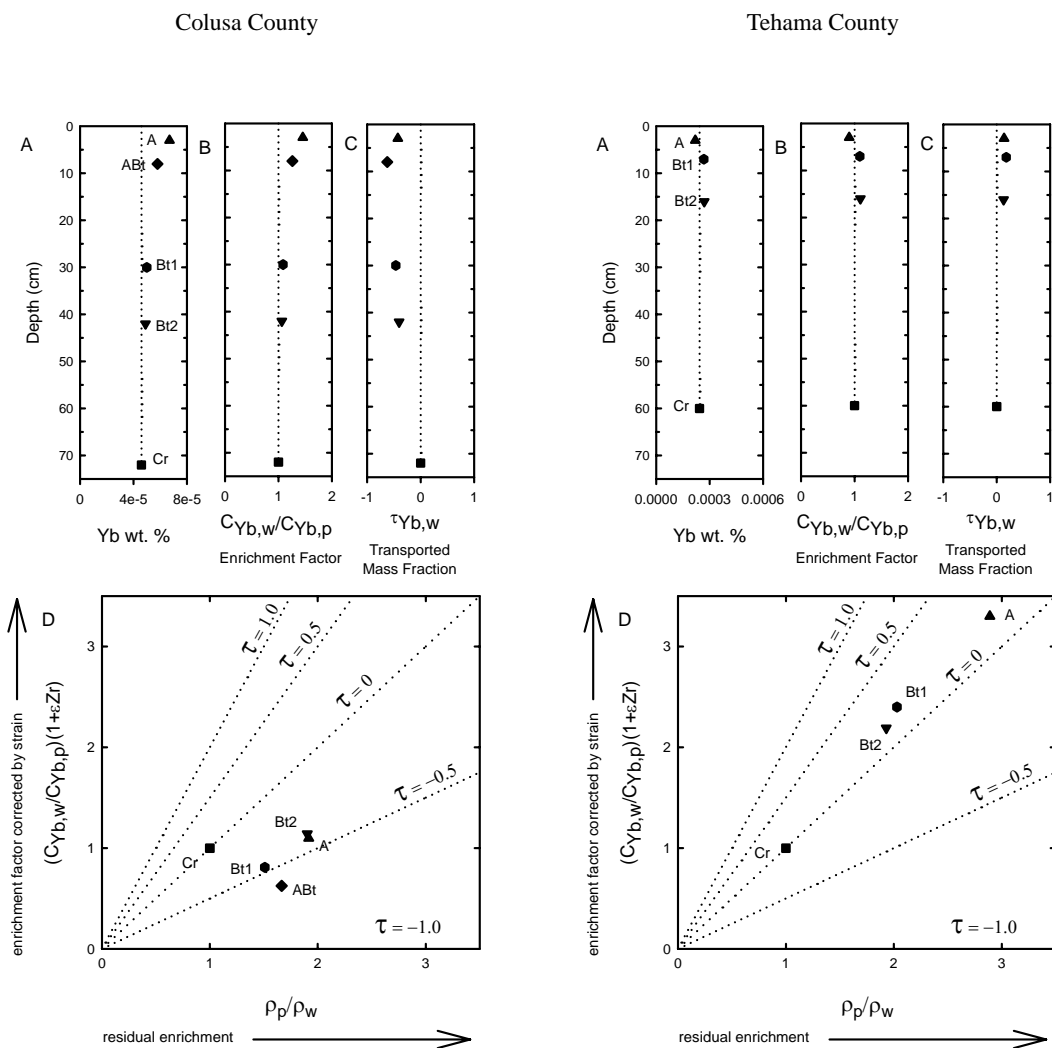


**Figure 4-62.** Depth plots of (A) weighted percent Yb, (B) enrichment factor, and (C) the transported mass fraction of Yb. (D) Plot of density ratio  $\rho_p/\rho_w$  representing the residual enrichment contribution vs. enrichment corrected by strain using Zr as the immobile element. Dotted vertical line (A, B & C) is visual indicator for parent material value. Dotted lines (D) represent  $\tau$ , the mass fraction added or subtracted from each sample at 0, 50 and 100%.

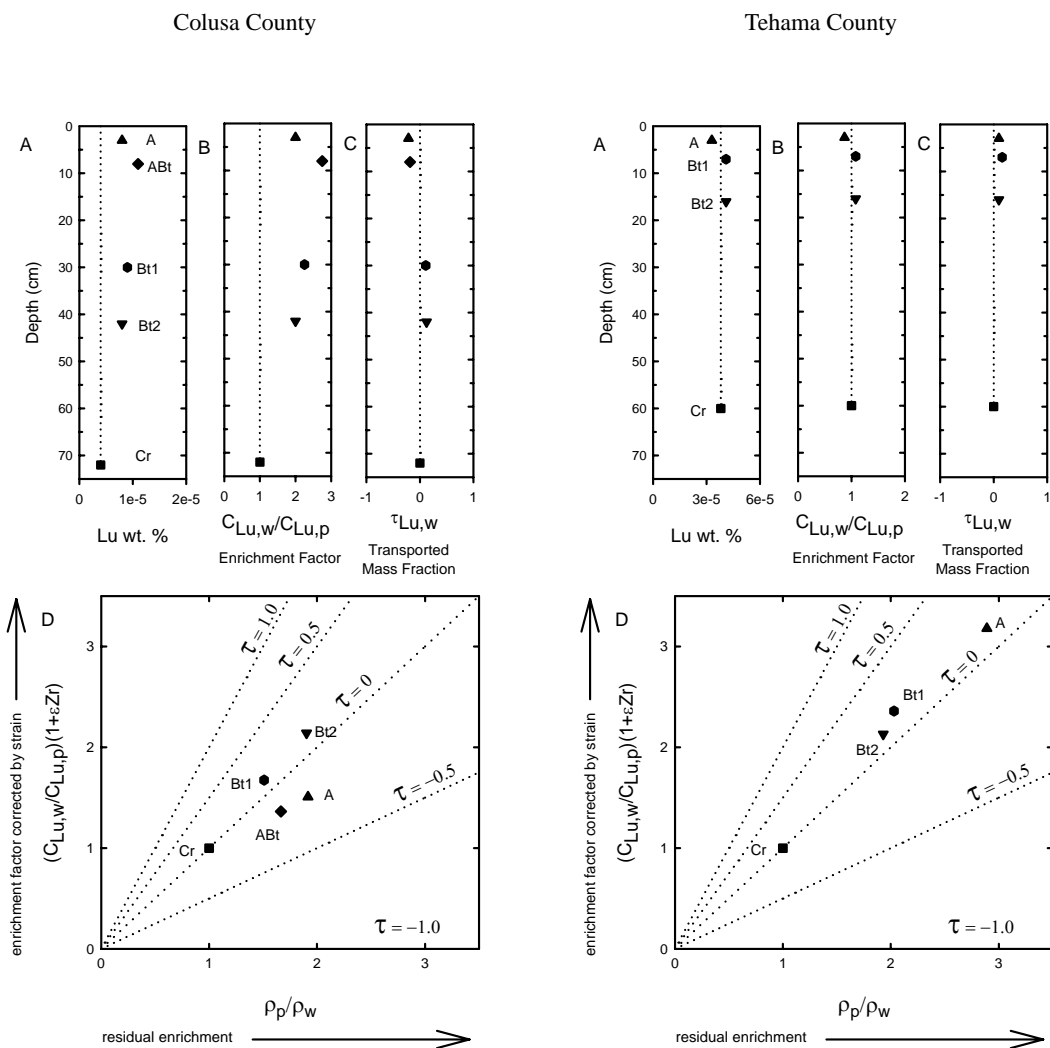


**Figure 4-63.** Depth plots of (A) weighted percent Lu, (B) enrichment factor, and (C) the transported mass fraction of Lu. (D) Plot of density ratio  $\rho_p/\rho_w$  representing the residual enrichment contribution vs. enrichment corrected by strain using Zr as the immobile element. Dotted vertical line (A, B & C) is visual indicator for parent material value. Dotted lines (D) represent  $\tau$ , the mass fraction added or subtracted from each sample at 0, 50 and 100%.

# **CHAPTER 5: FLUX OF ELEMENTS BY MASS BALANCE IN SOILS FROM THREE SERPENTINITIC LANDSCAPES**

## **5.1 INTRODUCTION**

Ultramafic rocks, of which serpentinite is a member, occupy <1% of the land surface of the earth, but they have long been the study of botanists, plant physiologists, phytochemists, plant geographers, and scientists from other disciplines. Landscapes dominated by serpentinite derived soil often support vegetation that stands in stark contrast (reduced vigor, smaller number of species, larger proportion of endemic species) to vegetation adjacent to landscapes dominated by non-serpentinite derived soils. The perceived difference has often been termed the “serpentine factor” and botanists often refer to “serpentine flora” (Brooks, 1987; Kruckeberg, 1985).

A primary component of the “serpentine factor” is the high Mg and low Ca condition that exists in these soils (Vlamiš and Jenny, 1948; Walker et al., 1955). High Mg and low Ca are generally inherited from the parent material, which is generally ultramafic. This may not always be true, however. Serpentinite mineralogical composition can include Ca bear-

ing minerals. Xenoliths such as rodingites and mafics can influence Ca availability on the “serpentinitic landscape” (McGahan, 2007).

Previous mineral weathering studies have determined that serpentinite dissolution from weathering is greater than for schist (Cleaves et al., 1974). Smectite is the primary secondary phyllosilicate in the soil and is solely in the clay size fraction (Wildman et al., 1968; Cleaves et al., 1974; Hargitt and Livesey, 1975; Driven et al., 1976; Ducloux et al., 1976; Senkayi, 1977; Istok and Harward, 1982; Rabenhorst et al., 1982; Graham et al., 1990; Bonifacio et al., 1997). The smectite composition tends toward nontronitic smectite (greater iron) in well drained landscape positions and saponitic smectite (greater Mg in the octahedral position) in imperfect or poorly drained landscape positions (Wildman et al., 1968; Driven et al., 1976; Ducloux et al., 1976; Senkayi, 1977). Chlorite is often a lithogenic derived component of the soil, but some researchers describe pedogenic chlorite as well (Hargitt and Livesey, 1975; Ducloux et al., 1976; Senkayi, 1977; Istok and Harward, 1982; Graham et al., 1990). Rabenhorst et al. (1982), however, attributed increasing chlorite with proximity to the surface to a concentration effect due to greater serpentine weathering.

Cleaves et al. (1974) derived mass flux utilizing a geochemical balance in a serpentinite watershed by allowing for reasonable secondary mineral formation and measured precipitation inputs. Driven et al. (1976) utilized stability diagrams to derive a weathering model and tested the model with measured elemental analysis, but the soil genesis conclusions were not possible because of the presence of many lithologic discontinuities. Brimhall and Dietrich (1987) explored mass balance at two ultramafic sites from bedrock upward through saprolite, but encountered evidence for colluviation in the soils.

During a survey of eleven soils formed on serpentinitic landscapes in California, three pedons were identified that were derived from contrasting parent materials: serpentinite, rodingite, and meta-gabbro. The differences in parent material mineralogy could affect release rates of elements that compose the minerals. The objectives of this study were to (1) identify the net gains and losses during weathering and soil formation of the soil elements Si, Al, Fe, Mg, and Ca of these three soils from serpentinitic landscapes and (2) identify pedogenic mineralogical alterations in these three profiles.

## **5.2 MATERIALS AND METHODS**

### **5.2.1 Field**

The study sites are in the California Coast Ranges physiographic region. All were mapped as Henneke soil series (Clayey-skeletal, magnesian, thermic Lithic Argixerolls), and the soil survey modal locations for Tehama, Colusa, and Napa Counties were chosen as a basis for site locations (Soil Survey Staff, 1999). The Henneke soil is a widely mapped soil series that is “soils formed in material weathered from serpentine and rocks of similar mineralogy” (Soil Survey Staff, 2005). The Tehama County site soil is derived from a rodingite. Rodingite is a massive, dense, buff to pink rock typically rich in grossular garnet and calcic pyroxene, and enveloped in serpentinite. It is formed by metasomatic alteration of a protolith that was next to or enveloped with the protolith to serpentinite. The Colusa County site soil is derived from serpentinite, and the Napa County site soil is derived from meta-gabbro. Pits were excavated by hand tools. Soils were described and sampled using conventional procedures (Soil Survey Division Staff, 1993). The soil pits were excavated on



summits above modal locations, in order to eliminate colluvial and alluvial influences, and were within the mapping polygon containing the Henneke series soil survey modal location. The soil moisture regimes are xeric and the temperature regimes are mapped as thermic. Volume of cobbles and stones were estimated in the field. Soils and gravels were sampled in conjunction with compliant cavity bulk density measurements (Soil Survey Staff, 2004).

### **5.2.2 Laboratory**

Soils were air dried, sieved to pass through a 2 mm sieve, and analyzed for particle size distribution by pipette method as described by Gee and Bauder (1986). Volume of coarse fraction gravels was determined directly by displacement of water. Displacement was performed after sieving compliant cavity bulk density samples to separate the gravels. The gravels were then soaked for 15 h in deionized water, washed to remove slaked soil material, and dried at 105°C for 15 h and weighed (Soil Survey Staff, 2004).

Three rocks from each parent material were ground with a agate mortar and pestle to pass a 140-mesh sieve. A sub-sample of approximately 10 g of the sieved < 2-mm soil material from each horizon was also ground and sieved to pass a 140-mesh sieve. Major elements were determined by ICP-emission spectrometry following a  $\text{LiBO}_2$  fusion and dilute nitric acid digestion. A sub-sample of approximately 10 g of the sieved < 2-mm soil material from each horizon was ground and sieved to pass a 140-mesh sieve. Major elements were determined by ICP-emission spectrometry following a  $\text{LiBO}_2$  fusion and dilute nitric acid digestion. A leachate of hot (95°C) Aqua Regia was analyzed by ICP-emission for precious and

base metals (Au, Ag, As, Bi, Cd, Cu, Hg, Mo, Ni, Pb, Sb, Se, Tl, Zn) (Sawhney and Stilwell, 1994).

## 5.2.3 Mass Balance Construction

The derivation and formulation of a soil mass balance model has been described in detail previously (Brimhall and Dietrich, 1987; Brimhall et al., 1988, 1991, 1992; Chadwick et al., 1990).

### 5.2.3.1 Basic conservation equations

The equation relating a chemical element,  $j$ , contained in the parent material is:

$$\left( \frac{(V_p \rho_p C(j, p))}{100} \right) + m_{(j, flux)} = \frac{(V_w \rho_w C(j, w))}{100} \quad \text{Equation 5-1.}$$

The left side of Equation 5-1 has two terms; the first term  $\left( \frac{(V_p \rho_p C(j, p))}{100} \right)$  is the mass, in grams, of the element  $j$ , contained in the parent material previous to weathering, subscripted as  $p$ . The term  $V$  is the volume in  $\text{cm}^3$ ,  $\rho$  the dry bulk density in  $\text{g cm}^{-3}$ , and  $C$  the chemical element concentration in weight percent. The second term  $m_{j, flux}$  is mass of element  $j$  introduced into or removed from the parent material volume. The right hand side of the Equation 5-1 is the mass of the element  $j$  contained in the fine earth fraction of the weathered volume of interest, subscripted  $w$ , and is also given as the product of the volume, dry bulk density, and weight percent concentration of the horizon of interest.

Volumetric changes that occur during pedogenesis are determined by adopting the classical definition of strain,  $\varepsilon$ , the ratio of the volume change in a process to the initial volume:

$$\varepsilon(i, w) = \frac{(V_w - V_p)}{V_p} = \left( \frac{V_w}{V_p} - 1 \right) \quad \text{Equation 5-2.}$$

where the subscript  $i$  refers to the strain determined by use of an immobile strain index element, and subscript  $w$  refers to strain due to weathering.

The element mass fraction,  $m_{j,flux}$ , added or removed from the system relative to the mass of element  $j$  originally in the parent material  $C_{j,p}\rho_p V_p$  is the open-chemical-system transport function,  $\tau_{j,w}$ :

$$\tau(j, w) = 100 \frac{m(j, flux)}{(C(j, p)\rho_p V_p)} \quad \text{Equation 5-3.}$$

### 5.2.3.2 Calculation of open-system mass transport

Equation 5-1, Equation 5-2, and Equation 5-3 can be used to give Equation 5-4 (Brimhall et al., 1988). The open-system-transport function,  $\tau_{j,w}$ , is the mass fraction added or subtracted, and is used to compute chemical gains and losses for each sample. It is computed directly from density and chemical composition data in combination with volume change values derived from the strain calculations:

$$\tau(j, w) = \left( \frac{\rho_w C(j, w)}{(\rho_p C(j, p))} (\varepsilon(i, w) + 1) - 1 \right) \quad \text{Equation 5-4.}$$

The open-system-transport function value of 0.0 indicates that the element has been immobile and was affected only by internal closed-chemical-system processes. These are resid-

ual effects due to changes in bulk density and strain effects due to changes in volume. A negative  $\tau_{j,w}$  value is a loss of element  $j$  mass, due to weathering, from that mass of element  $j$  originally present in the parent material. A positive value of  $\tau_{j,w}$  means that a mass of element  $j$  was added to the sample volume.

### 5.2.3.3 Determination of Strain

Calculation of the transport function for each element requires an estimate of strain (i.e., volume change). In soils, this can only be done by use of an immobile element. If we assume that an element like Y has been immobile it follows that the flux term ( $m_{j,flux}$ ) in Equation 5-3 is zero, and hence the open-system transport term  $\tau_{j,w}$  is assumed to be zero:

$$\varepsilon(i, w) = \left( \frac{\rho_p C(j, p)}{(\rho_w C(j, w))} - 1 \right) \quad \text{Equation 5-5.}$$

Correct application of the technique depends upon establishing the existence of a homogeneous parent material and immobility of at least one chemical species, typically Zr or Ti, for use as the index species,  $i$ , in strain determination. In Equation 5-5, strain results whenever a change in bulk density,  $\rho_w$ , is not compensated by an inversely proportional change in the concentration of the immobile element,  $C_{i,w}$ . Intense dissolution of minerals containing mobile elements leaves the weathered product enriched in immobile elements contained in chemically resistant minerals. Without a commensurate counteracting decrease in density, the calculated strain is negative, consistent with collapse, i.e., reduction in soil volume.

### 5.2.3.4 Calculation of gains and losses

By solving Equation 5-3 for  $m_{j,flux}$ , mass fluxes for each sample system can be calculated using the open-chemical-system transport function:

$$m_{(j, flux)} = \left( \frac{C(j, p)}{100} \rho_p V_p \right) (\tau_{(j, w)}) \quad \text{Equation 5-6.}$$

Within the first set of parentheses to the right side of the equation, the mass of element  $j$  contained in the parent material is given as the product of bulk density, volume, and concentration. By multiplying this original mass by the open-system transport function  $\tau_{j,w}$  we obtain the mass of  $j$  flux,  $m_{j,flux}$ , in  $g\ cm^{-3}$ .

The  $m_{j,flux}$  calculations give mass flux for a single sample of volume,  $V_p$ . A net mass flux for an entire soil profile to the depth investigated is possible if we express  $\tau_{j,flux}$  as a function of depth,  $Z$ , representing a profile thickness, and we can calculate the net mass flux  $\bar{m}_{(j, flux)}$ , to the depth,  $D_{j,w}$ .

$$\bar{m}_{(j, flux)}(g\ cm^{-2}) = \left( \rho_p \frac{C(j, p)}{100} \right) \left( \int_{(Z=0)}^{Z=(D_{j,w}) - CF} (\tau_{(j, w)z}) dZ \right) \quad \text{Equation 5-7.}$$

In Equation 5-7 the representative elementary volume term,  $V_p$  is expanded, from Equation 5-6 to be the product of a depth,  $D_{j,w}$  a horizon thickness, reduced by the coarse fraction contribution.

### 5.2.3.5 Contributions to chemical enrichment

Pedogenic changes can be expressed by the ratio of the chemical concentration of an element to its concentration in the parent material. This ratio, often called the enrichment factor,  $C_{j,w}/C_{j,p}$ , is derived from Equation 5-4:

$$\frac{C_{(j, w)}}{C_{(j, p)}} = \frac{\rho_p}{\rho_w} \times \frac{1}{(\varepsilon_{(i, w)} + 1)} \times (1 + \tau_{(j, w)}) \quad \text{Equation 5-8.}$$

The enrichment factor,  $C_{j,w}/C_{j,p}$ , of each sample volume is determined by three distinct processes: residual enrichment  $\rho_p/\rho_w$ , strain  $\frac{1}{(\varepsilon_{(i, w)} + 1)}$ , and mass transport,  $(1 + \tau_{j,w})$  with Equation 5-8.

For a closed system the mass transport of an immobile element is zero, and therefore, the open-system transport term  $\tau_{j,w}$  of the immobile element is assumed to be zero. Substituting zero for the open-system transport term  $\tau_{j,w}$  and rearranging Equation 5-8 allows separation for graphical treatment of the two contributions to closed system enrichment:

$$\frac{C_{(j, w)}}{C_{(j, p)}} (\varepsilon_{(i, w)} + 1) = \frac{\rho_p}{\rho_w} \quad \text{Equation 5-9.}$$

Residual enrichment of an element results from density changes, i.e., density decreases, due to dissolution and removal of mobile elements with a corresponding increase in porosity. On the other side of the equation is the enrichment factor, and here volume change that may be associated with the density changes are described by the strain term. Together, residual enrichment and enrichment corrected by strain describe “closed-system” contribution that results from mass movement of the element across the sample volume boundaries either soil horizons or pedons.

To graphically depict the open-system, transport Equation 5-8 is rearranged to Equation 5-10:

$$\frac{C(j, w)}{C(j, p)} (\varepsilon(i, w) + 1) = \frac{\rho_p}{\rho_w} (1 + \tau(j, w)) \quad \text{Equation 5-10.}$$

By substituting values of 0, 0.5, 1.0, -0.5, and -1.0 for the mass transport  $1 + \tau_{j,w}$  a series of lines are produced as guides to visualize the open-system transport. For example, the 0.0 line means any apparent enrichment or depletion is explained by residual enrichment and strain closed system transport with no mass transport across horizon boundaries. The 1.0 line means 100 percent enrichment has occurred due to mass transport. The -1.0 line means 100 percent depletion has occurred due to mass transport.

### 5.3 RESULTS AND DISCUSSION

Others have used rare earth elements (REEs) as immobile elements for assessing soil weathering (Aide and Smith-Aide, 2003). REEs are the lanthanum series excluding Pm and including Y and Sc. In a previous study (McGahan, 2007), a comparison of the potentiality immobile elements Zr, Ti, Y and Nb on two parent materials from serpentinitic landscapes (Tehama and Colusa Counties), Zr was determined to be mobile within the Colusa County soil profile, and therefore, not suitable to calculate strain. Ti, Y and Nb, were immobile. However, Nb was below detectable limits in the Napa County parent material precluding its use. For Napa County parent material the amount Ti content was only twice the detectable limit (0.012%), but Y was three times the detectable limit (0.00003%). Therefore, Y was used to calculate strain reported in this paper.

### 5.3.1 Tehama County

Tehama County fine earth fraction density generally decreased from the parent material with proximity to the surface, creating a large density ratio  $\rho_p/\rho_w$  (Fig. 5-1).

The soil strain profile had significant dilation that increased in magnitude with proximity to the surface (Fig. 5-2). Organic matter addition, faunal burrowing, root dilation, freeze-thaw, and mineral swelling (smectite) with hydration are among the mechanisms causing dilation (Chadwick et al, 1990; Brimhall et al, 1992).

The distribution of Si showed losses in weight % and enrichment factor that increased in magnitude with proximity to the surface. The transported mass fraction showed very slight losses in the Bt1 and Bt2 horizons, and a gain in the A horizon. The Si mass flux, integrated through the sampling depth for the fine earth fraction, was calculated to be  $-0.04 \text{ g cm}^{-2}$ . The Bt horizons components of transport, enrichment factor corrected by strain and residual enrichment, were roughly equivalent indicating closed system transport ( $\tau = 0$ ). The A horizon was Si enriched (Fig. 5-3). A Si enriched A horizon could indicate eolian additions, but there was no evidence of eolian additions in the sand and silt fractions when examined by polarizing light microscopy or x-ray diffraction.

With no evidence for an eolian source for the measured A horizon additions, we turn to the mineralogy to try to understand the Si distribution. There was no serpentine minerals in the profile. The parent material was a rodingite. XRD of crushed rock showed the Tehama County parent material mineralogy was composed of the ugrandite garnet grossularite (0.299 & 0.266 nm peaks), diopside (0.32 nm peak), hydroxy-interlayered-material (HIM) (1.4nm peak), and pumpellyite (0.29 nm peak). The HIM was characterized by a 1.4 nm

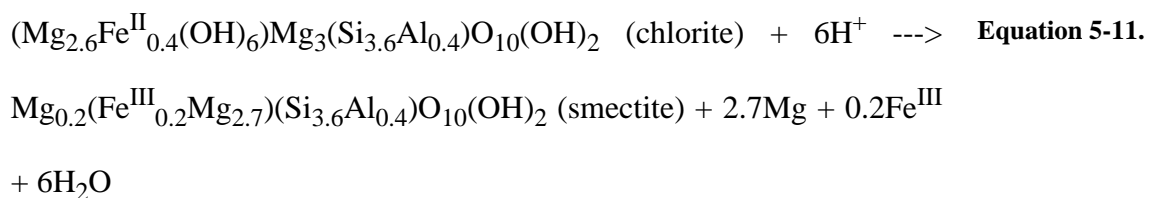


Mg-saturated peak, that collapsed with K-saturation and heating treatments which left a plateau of peaks between 1.4 nm and 1.0 nm. The silt fraction of the fine earth fraction had mineralogy similar to the parent material (Fig. 5-4).

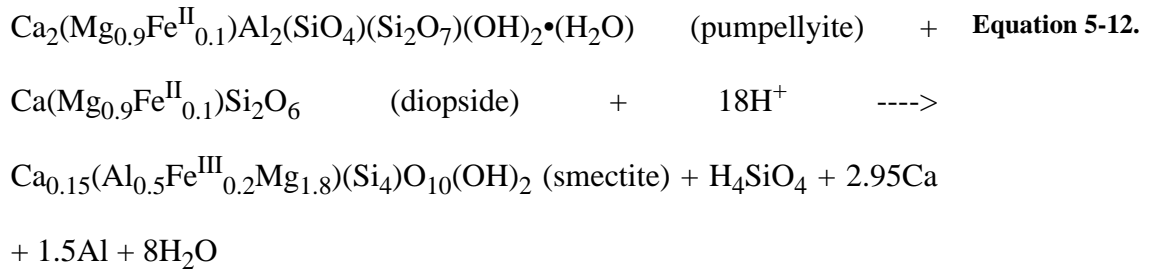
X-ray diffractograms of the clay fraction (Fig. 5-5) showed that the HIM persisted as a dominant mineral. The garnet peaks persisted, but were much less distinguishable with proximity to the surface. Diopside and pumpellyite peaks persist into the Bt2 horizon, but were indistinguishable in the Bt1 and A horizons.

Smectite (1.8 nm peak with Mg-saturation and glycerol solvation) was present in the clay fraction, and based on peak intensity, increased in importance with proximity to the surface (Fig. 5-5). Based on back scattered electron microscopy and energy dispersive x-ray spectroscopy the garnet was a greater component of the parent material mineralogy than the XRD diffractograms indicate (McGahan, 2007).

Thus, the mineral assemblage did not change greatly from the parent material to the sand and silt fraction of the soil. The Tehama County parent material garnet was most resistant to weathering, followed by HIM, with diopside and pumpellyite being the most weatherable primary minerals. The primary mineralogical alteration was the appearance of smectite in the clay fraction. It is likely that resistant garnet accumulation is responsible for the Si enrichment in the A horizon. Using chlorite as an analog to HIM, the idealized Equation 5-11 demonstrates that alteration of HIM to smectite is not expected to yield excess Si.



Similarly Si released during pumpellyite and diopside dissolution could be largely consumed by smectite formation (Equation 5-12).



The Mg distribution within the Tehama County profile showed gains in weight %, enrichment factor, and transported mass fraction that increased with proximity to the surface (Fig. 5-6). The Mg mass flux, integrated through the sampling depth for the fine earth fraction, was calculated to be  $0.48 \text{ g cm}^{-2}$  (Table 5-1). Magnesium enrichment increased with proximity to the surface. As discussed previously, dissolution of pumpellyite and diopside released Mg. The X-ray diffractograms of the clay fraction indicated that smectite became more prominent with proximity to the surface as Mg enrichment increased with proximity to the surface. Smectite formation undoubtedly is responsible for retention of some Mg, but certainly not responsible for enrichment. This result is puzzling. Enrichment of Mg was also calculated if either Ti or Nb were used as the strain calculating element. This parent material is an inclusion of rodingite in a landscape of serpentinite. While there was no evidence of eolian additions in the field or in any of the techniques we applied (XRD and Polarized Light Microscopy), it is possible that finely divided Mg as carbonates or evaporites have been added to the profile from neighboring/surrounding soils.

Distribution of Al within the Tehama County profile showed increasing losses in weight % and enrichment factor with proximity to the surface. The transported mass fraction plot

showed less Al loss than indicated by the weight % or enrichment factor. This was likely a result of less Al loss relative to other cations such as Ca. Furthermore, Al transported mass fraction losses did not increase with proximity to the surface commensurate with weight % or enrichment factor (Fig. 5-7). Attenuated Al losses were likely due to Al being incorporation into smectite, as smectite was a greater fraction of the clay mineralogy toward the surface. The mass flux, integrated through the sampling depth for the fine earth fraction, was calculated to be  $-0.42 \text{ g cm}^{-2}$  (Table 5-1).

The Fe distribution within the Tehama County profile showed gains in weight %, enrichment factor, and the transported mass fraction. The magnitude of gain increased with proximity to the surface (Figure 5-8). The mass flux, integrated through the sampling depth for the fine earth fraction, was calculated to be  $0.80 \text{ g cm}^{-2}$  (Table 5-1).

Fe was a constituent of diopside, pumpellyite, HIM, and garnet (McGahan, 2007). Pumpellyite dissolution would have resulted in Mg, Al and Si releases, but also small Fe releases. Diopside dissolution resulted in Mg and Si releases, but only small Fe releases. Trace minerals containing Fe, upon dissolution, also likely contributed to the Fe gains as the Fe oxidizes, precipitates and is conserved.

The parent material calcium content was greater for Tehama County than for Colusa or Napa Counties. Some of the parent material Ca was present in the relatively resistant grossularite. The more weatherable minerals diopside and pumpellyite also contained Ca. Dissolution of pumpellyite and diopside resulted in release of more Ca than Mg. Ca was not retained in the structural formation of secondary minerals. The Ca distribution within the Tehama County profile decreased in weight %, enrichment factor, and transported mass

fraction (Fig. 5-9). The Ca mass flux, integrated through the sampling depth for the fine earth fraction, was calculated to be  $-1.74 \text{ g cm}^{-2}$ . Some Ca was retained on the exchange complex, but most Ca released from dissolution of pumpellyite and diopside dissolution was apparently leached from the profile.

### **5.3.2 Colusa County**

The strain profile of the Colusa County soil had slight dilation in the Bt2 horizon and collapse in the overlying Bt1, ABt and A horizons. The pedon showed irregular decrease in density with proximity to the surface (Fig. 5-1). Distribution of Si showed losses in weight % and enrichment factor. The transported mass fraction showed Si-losses. The Si mass flux, integrated through the sampling depth for the fine earth fraction, was calculated to be  $-5.3 \text{ g cm}^{-2}$  (Fig. 5-11).

X-ray diffraction of the crushed rock of the Colusa County parent material showed that it was dominated by serpentine (0.72 nm and 0.36 nm peaks) with a minor component of chlorite (1.4 nm and 0.475 nm peaks that persisted with heating and did not expand with glycerol solvation) (Fig. 5-12). The silt fraction mineralogy was also dominated by serpentine with a minor component of chlorite. The 3rd order chlorite peak (0.475 nm) was slightly better defined than in the parent material diffractogram (Fig. 5-13).

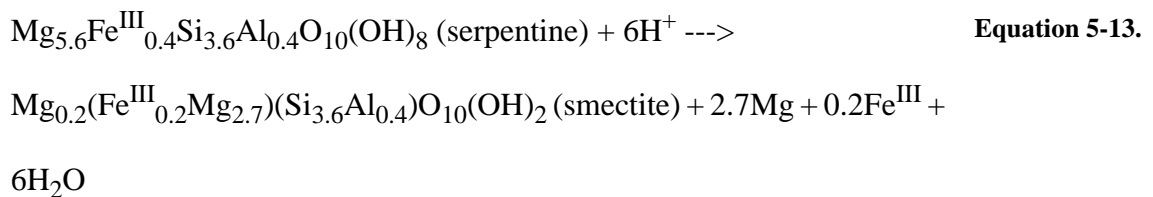
The soil clay mineralogy, by X-ray diffraction, was co-dominated by serpentine (0.72 nm and 0.36 nm peaks), vermiculite (1.4 nm peak that collapsed to 1.0 nm with K-saturation and heating treatments), and smectite in the Bt2 horizon. The Bt1, ABt and A horizon showed an increase in smectite peak size, respectively, and the presence of chlorite (1.4 nm

K- and Mg-saturated peak that did not collapse with K-saturation and heating treatments) (Fig. 5-14).

Considerable dissolution and leaching has apparently occurred in this profile. Alteration of serpentine to smectite was the dominant change in mineralogy with a subdominant alteration of chlorite or serpentine to vermiculite and then perhaps to smectite (Hargitt and Livesey, 1975; Ducloux et al., 1976; Senkayi, 1977; Istok and Harward, 1982). Mg distribution within the Colusa County profile showed gains in weight % and enrichment factor. The transported mass fraction showed Mg-losses (Fig. 5-15). The Mg mass flux, integrated through the sampling depth for the fine earth fraction, was calculated to be  $-2.01 \text{ g cm}^{-2}$  (Table 5-1).

The idealized formula for serpentine is  $\text{Mg}_6\text{Si}_4\text{O}_{10}(\text{OH})_8$ . However, isomorphous substitution of Fe and Al are possible with values as high as 24 % for Fe and 19% for Al (O'Hanley, 1996).

An alteration of serpentine to smectite should release Mg but little Si:



Similarly the alteration of chlorite to smectite (Equation 5-11) is not expected to release Si.

Silica, however, had nearly twice the transported mass fraction of Mg indicating that the alteration of serpentine to smectite was more complicated than the idealized equations above.

The Al distribution within the Colusa County profile showed minor gains in weight % and minor losses as enrichment factor. The transported mass fraction corrected by strain showed much larger Al-losses than weight % and enrichment factor would suggest (Fig. 5-16). The pH was moderately acidic to neutral (6.0 to 7.1) and not conducive to Al-mobility. While Al parent material content was lower than the Tehama County profile content, the % Al-loss was greater for the Colusa profile. Al-loss was not offset by Al-gains in the profile, and therefore, not explained by redistribution within the profile. Translocation out of the profile in association with organics was a possibility not explored in this study but seems unlikely. Colusa County Al mass flux, integrated through the sampling depth for the fine earth fraction, was calculated to be  $-0.86 \text{ g cm}^{-2}$  (Table 5-1).

Distribution of Fe within the Colusa County profile showed little change in weight % and enrichment factor (Fig. 5-17). The transported mass fraction showed Fe-losses greater than could be explained by dissolution of serpentinite even given a maximum Fe substitution amount. The mass flux, integrated through the sampling depth for the fine earth fraction, was calculated to be  $-3.9 \text{ g cm}^{-2}$  (Table 5-1).

It may be that the Fe loss from the profile is due to translocation out of the A and B horizons into the Cr horizon. This may be in association with smectite clay. Smectite increases in the clay fraction with depth in the profile based on relative clay X-ray diffractogram peak intensities. Wildman et al. (1968), Rabenhorst et al. (1982), and Graham et al. (1990) all suggested serpentine dissolution and smectite crystallization from soluble ions or gels as an explanation for this distribution. Lessivage of the fine clay fraction is also feasible. The Fe losses from the soil profile tends to strengthen this possibility as the Fe is not expected to be ionic. Analysis of the fine earth fractions was not performed nor were the clayey infillings

of the parent material cracks analyzed so we cannot offer conclusive evidence for leaching of Fe into the Cr horizon.

The parent material was very low in Ca (0.60 %). The Ca increased in weight % and enrichment factor, and the transported mass fraction showed gains (Fig. 5-18). The Ca mass flux, integrated through the sampling depth for the fine earth fraction, was calculated to be  $0.80 \text{ g cm}^{-2}$ .

As base cations both Mg and Ca are subject to leaching. We suggested that Mg leaching resulted upon serpentine dissolution. Losses were less than expected, probably due to Mg inclusion into smectite and chlorite. Ca inclusion into the smectite and chlorite does not occur. Because Ca content of the parent material was low, however, the accumulated Ca in the profile was likely strongly retained as a result of biocycling and cation exchange as has been proposed by others (Rabenhorst et al., 1982; Cleaves et al., 1974).

### **5.3.3 Napa County**

Distribution of Si within the Napa County profile showed gains in weight % and enrichment factor, but transported mass fraction showed Si losses (Fig. 5-20). Napa County strain profile showed considerable collapse (Fig. 5-19). The soil showed irregular decrease in density with proximity to the surface (Fig. 5-1). Napa County Si mass flux was calculated to be  $-2.73 \text{ g cm}^{-2}$  (Table 5-1).

Napa County parent material mineralogy was dominantly vermiculite (1.4 nm peak with Mg treatment collapsed to 1.0 nm with K treatment and heat) and plagioclase feldspar (0.630, 0.401, 0.374, 0.365, 0.336, 0.318, 0.293 nm peaks) (Fig. 5-21). A pyroxene XRD peak was not evident, but clino-pyroxene was identified by PLM (McGahan, 2007). The

silt fraction mineralogy, by x-ray diffraction, resembled the crushed rock with only a slight reduction in the intensity of the 1.4 nm vermiculite peak in the A horizon (Fig. 5-22).

The clay fraction based on x-ray diffraction contained smectite (1.4 nm Mg-treatment peak expansion to 1.8 nm with glycerol solvation). The plagioclase peaks were absent in the A horizon, and only a weak diffuse 3.18 nm plagioclase peak remained in the Bt horizon (Fig. 5-22).

Based on x-ray diffraction, desilication has likely resulted primarily at the expense of plagioclase. Increase in smectite peak intensity relative to vermiculite indicated a smectite increase with proximity to the surface. This coincided with reduced calculated losses of Si in the A horizon ( $-1.1 \text{ g cm}^{-2}$ ) compared to the Bt horizon ( $-1.63 \text{ g cm}^{-2}$ ) indicating some retention of Si with the formation of smectite

We asserted that formation of smectite in the Tehama County and Colusa County profiles attenuated the flux of Mg out of the profile by its inclusion into smectite and or chlorite. Mg distribution within the Napa County profile showed losses in weight % and enrichment factor. The transported mass fraction showed Mg-losses (Fig. 5-23). The Mg mass flux, integrated through the sampling depth for the fine earth fraction, was calculated to be  $-0.28 \text{ g cm}^{-2}$  (Table 5-1).

Distribution of Al and Fe within the Napa County profile showed gains in weight % and as enrichment factor, but losses when corrected for strain and residual enrichment (Fig. 5-24 and Fig. 5-25). Napa County Al mass flux, integrated through the sampling depth, was calculated to be  $-1.05 \text{ g cm}^{-2}$  (Table 5-1). The mass flux of Fe was calculated to be  $-0.99 \text{ g cm}^{-2}$  (Table 5-1). The loss of Fe from the A and Bt horizons could have been by leaching into the cracks of the R horizon. The smectite XRD peak intensities, however, do not increase



with depth as they did in the Colusa profile, therefore, the argument for lessivage of clay and Fe-oxides is less compelling.

Though quite different from the Colusa County parent material in mineralogical composition, the Napa County parent material was similar with respect to a low Ca content (0.01 %). Retention of Ca was likely also a result of biocycling (Fig. 5-26) (Cleaves et al., 1974; Rabenhorst et al., 1982; Graham et al., 1990).

## 5.4 SUMMARY

The objectives of this study were to determine net elemental gains and losses for soils formed on three serpentinite landscapes. These soils were formed from contrasting parent materials, and we wanted to identify pedogenic mineralogical alteration for these profiles. The three profiles had quite different mass flux (1 to 11 g cm<sup>-2</sup>) of the major soil elements (Si, Al, Fe, Mg and Ca) illustrating that soil formation on serpentinitic landscapes can have quite different elemental fluxes. Despite the parent material primary mineral assemblage differences, smectite formation was a major alteration product in all three profiles. Smectite formation likely attenuated Si losses in all profiles and Mg losses in two profiles.

Ca content increased in soils that had very low parent material Ca content. Biocycling is a likely mechanism for Ca retention when parent material content is very low and vegetation exists. When a parent material on the serpentinitic landscape has higher Ca content there is little need for retention via biocycling.

## 5.5 REFERENCES

- Aide, M., Smith-Aide, C. 2003. Assessing soil genesis by rare-earth elemental analysis. *Soil Sci. Soc. Am. J.* 67:1470–1476.
- Bonifacio, E., E. Zanini, V. Boero, M. Franchini-Angela. 1997. Pedogenesis in a soil catena on serpentine in north-western Italy. *Geoderma*. 75:33-51.
- Brimhall, G.H. and Dietrich, W.E. 1987. Constitutive mass balance relations between chemical composition, volume, density, porosity, and strain in metasomatic hydrochemical systems: results on weathering and pedogenesis. *Geochimica et Cosmochimica Acta* 51: 567-587.
- Brimhall, G.H., Lewis, C.J., Ague, J.J., Dietrich, W.E., Hampel, J., and Rix, P. 1988. Metal enrichment in bauxites by deposition of chemically mature aeolian dust. *Nature* 333: 819-824.
- Brimhall, G.H., Lewis, C.J., Ford, C., Bratt, J., Taylor, G. and Warren, O., 1991. Quantitative geochemical approach to pedogenesis: importance of parent material reduction, volumetric expansion, and eolian influx in laterization. *Geoderma* 51: 51-91.
- Brimhall, G.H., O.A. Chadwick, C.J. Lewis, W. Compston, I.F. Williams, K.J. Danti, W.E. Dietrich, M.E. Power, D. Hendricks, and J. Bratt. 1992. Deformational mass transport and invasive processes in soil evolution. *Science* 255: 695-702.
- Brooks, R.R. 1987. *Serpentine and its vegetation: a multidisciplinary approach* Dioscorides Press, Portland, OR.

- Chadwick, O.A., G.H. Brimhall, and D.M. Hendricks. 1990. From a black box to a gray box: a mass balance interpretation of pedogenesis. *Geomorphology* 3: 369-390.
- Cleaves, E.T., D.W. Fisher, and O.P. Bricker. 1974. Chemical weathering for serpentinite in the eastern piedmont of Maryland. *Geological Society of America Bulletin*. 85: 437-444.
- Dirven, J.M.C., J. van Schuylenborgh, and N. van Breemen. 1976. Weathering of serpentinite in Matanzas Province, Cuba: mass transfer calculations and irreversible reaction pathways. *Soil Sci. Soc. Am. J.* 40:901-907.
- Ducloux, J., A. Meunier, and B. Velde. 1976. Interlayered chlorite-vermiculite in soils developed on a small serpentinite body massif central, France. *Clay Minerals*. 11:121-135.
- Gee, G.W. and J.W. Bauder. 1986. Particle size analysis. In: A. Klute (ed), *Methods of soil analysis: Part 1 Physical and mineralogical methods*. American Society of Agronomy, Madison, WI., pp. 383-411.
- Graham, R.C., M.M. Diallo, and L.J. Lund. 1990. Soils and mineral weathering on phyllite colluvium and serpentinite in northwestern California. *Soil Sci. Soc. Am. J.* 54:1682-1690.
- Hargitt, R., and N.T. Livesey. 1975. Mineralogical and chemical properties of serpentinite soils in north-east Scotland. p. 655. *In Proceedings of the international clay conference-abstracts Mexico city, Mexico*. Applied Publishing. Wilmette Il. USA. July 16-23 1975.

- Istok, J.D. and M.E. Harward. 1982. Influence of soil moisture on smectite formation in soils derived from serpentinite. *Soil Sci. Soc. Am. J.* 46:1106-1108
- Jackson, M.L. 1985. *Soil chemical analysis - advanced course*. Revised 2nd edition, Parallel Press, Madison Wisconsin.
- Kruckeberg, A.R., 1985. *California serpentines: flora, vegetation, geology, soils, and management problems*. University of California Press, Berkeley.
- McGahan, D.G. 2007. *A survey of soils formed on serpentinitic landscapes in California*. Ph.D. diss. University of California Davis.
- O'Hanley, D.S. 1996. *Serpentinites: records of tectonic and petrological history*. Oxford University Press, New York.
- Rabenhorst, M.C., J.E. Foss, and D.S. Fanning. 1982. Genesis of Mayrland soils formed from serpentinite. *Soil Sci. Soc. Am. J.* 46: 607-616.
- Sawhney, B.L., and D.E. Stilwell. 1994. Dissolution and elemental analysis of minerals, soils and environmental samples, p. 49-82, *In* J. E. Amonette and L. W. Zelazny, eds. *Quantitative methods in soil mineralogy* SSSA Miscellaneous Publication. Soil Science Society of America, Madison, Wis., USA.
- Senkayi, A.L. 1977. *Clay mineralogy of poorly drained soils developed from serpentinite rocks*. Ph.D. diss. University of California Davis.

- Soil Survey Division Staff. 1993. Soil survey manual - agriculture handbook No. 18. U.S. Dept. of Agriculture: Supt. of Docs. U.S. G.P.O., Washington, DC.
- Soil Survey Staff. 1999. Soil Taxonomy: a basic system of soil classification for making and interpreting soil surveys. 2 ed. United States Department of Agriculture, Natural Resources Conservation Service, Washington, DC.
- Soil Survey Staff. 2004. Soil survey laboratory methods manual - soil survey investigations report no. 42. [Online WWW]. Available URL: <http://soils.usda.gov/technical/Imm/> [Accessed 7 February 2007].
- Soil Survey Staff., 2005. Official soil series descriptions [Online WWW]. Available URL: “<http://soils.usda.gov/technical/classification/osd/index.html>” [Accessed 7 February 2007].
- Vlams, J., and H. Jenny. 1948. Calcium deficiency in serpentine soils a revealed by absorbent technique. *Science* 107:549.
- Walker, R.B., H.M. Walker, and P.R. Ashworth. 1955. Calcium-magnesium nutrition with special reference to serpentine soils. *Plant Physiology* 30:214-221.
- Wildman, W.E., M.L. Jackson, and L.D. Whittig. 1968. Iron-rich montmorillonite formation in soils derived from serpentinite. *Soil Sci. Soc. of Am. J.* 32:7687-794.

**Table 5-1.** Colusa, Tehama, and Napa County mass flux,  $m_{jflux}$ , in  $g\ cm^{-2}$  of the fine earth volume when strain is calculated with Y.

	Tehama County				Colusa County					Napa County		
	A	Bt1	Bt2	total	A	ABt	Bt1	Bt2	total	A	Bt	total
<b>Si</b>	0.09	-0.05	-0.09	-0.04	-0.52	-0.64	-2.48	-1.65	-5.29	-1.10	-1.63	-2.73
<b>Al</b>	-0.05	-0.18	-0.19	-0.42	-0.09	-0.11	-0.41	-0.25	-0.86	-0.42	-0.63	-1.05
<b>Fe</b>	0.17	0.26	0.37	0.80	-0.39	-0.46	-1.84	-1.22	-3.91	-0.42	-0.58	-0.99
<b>Mg</b>	0.15	0.19	0.14	0.48	-0.25	-0.26	-0.80	-0.70	-2.01	-0.11	-0.17	-0.28
<b>Ca</b>	-0.24	-0.62	-0.88	-1.74	0.07	0.09	0.44	0.21	0.80	0.22	0.21	0.43

Colusa County coarse fraction was A=0.12, ABt=0.27, Bt1=0.27, Bt2=0.16.

Tehama County coarse fraction was A=0.43, Bt1=0.10, and Bt2=0.34.

Napa County coarse fraction was A=0.12 and Bt1=0.27.

## 5.6 FIGURES

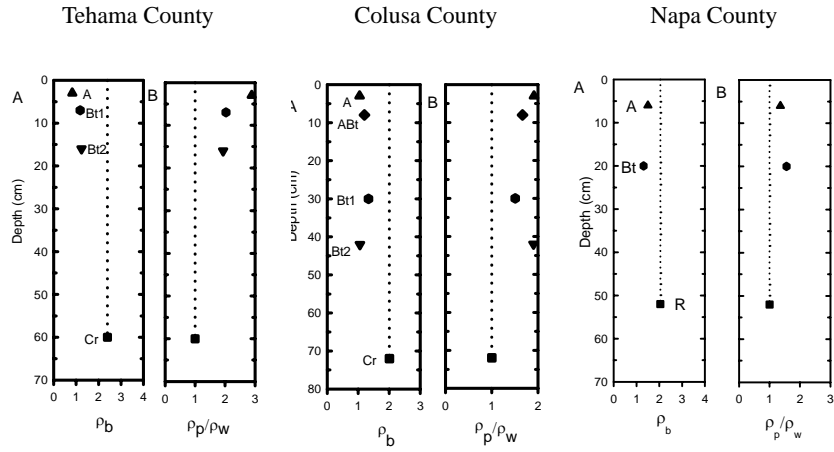


**Figure 5-1.** Depth plots of A) bulk density ( $\rho_b$ ), and B) density ratio (bulk density of parent material ( $\rho_p$ ) to bulk density of each horizon ( $\rho_w$ )). Dotted vertical line is visual indicator for parent material value.

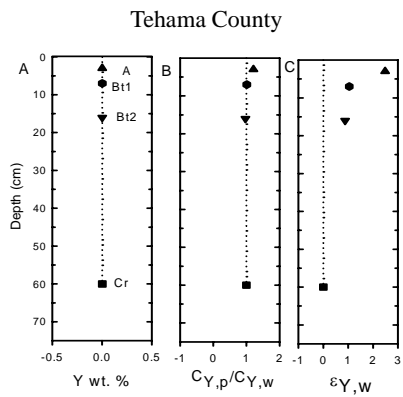


**Figure 5-2.** Tehama County depth plots (A) weight percent Y (B) the enrichment factor is the ratio of concentration Y in each horizon ( $C_{Y,w}$ ) to parent material ( $C_{Y,p}$ ). Together the weight percent and enrichment factor are used to calculate (C) strain,  $\epsilon_Y$ . Dotted vertical line is visual indicator for parent material value.

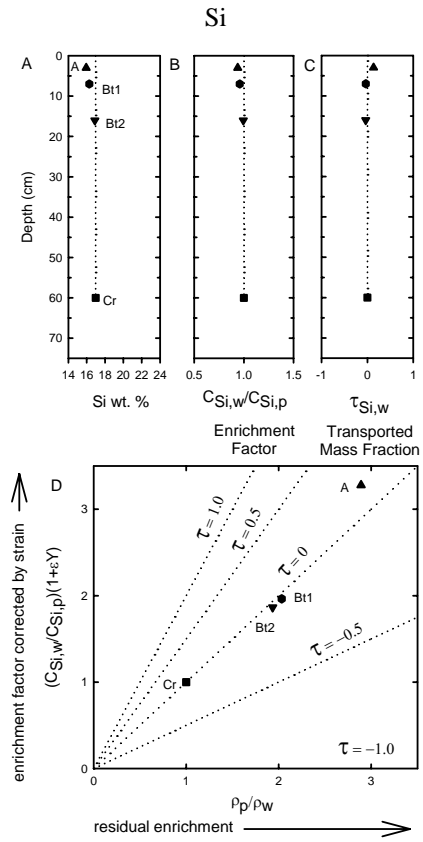


**Figure 5-3.** Si: Tehama County depth plots of (A) weight percent (B) enrichment factor, and (C) the transported mass fraction. (D) Plot of density ratio  $\rho_p/\rho_w$  representing the residual enrichment contribution vs. enrichment corrected by strain using Y as the immobile element. Dotted vertical lines in A, B and C are visual indicator for parent material value. Sloped dotted lines (D) represent  $\tau$ , the mass fraction added or subtracted from each sample at 0, 50 and 100%



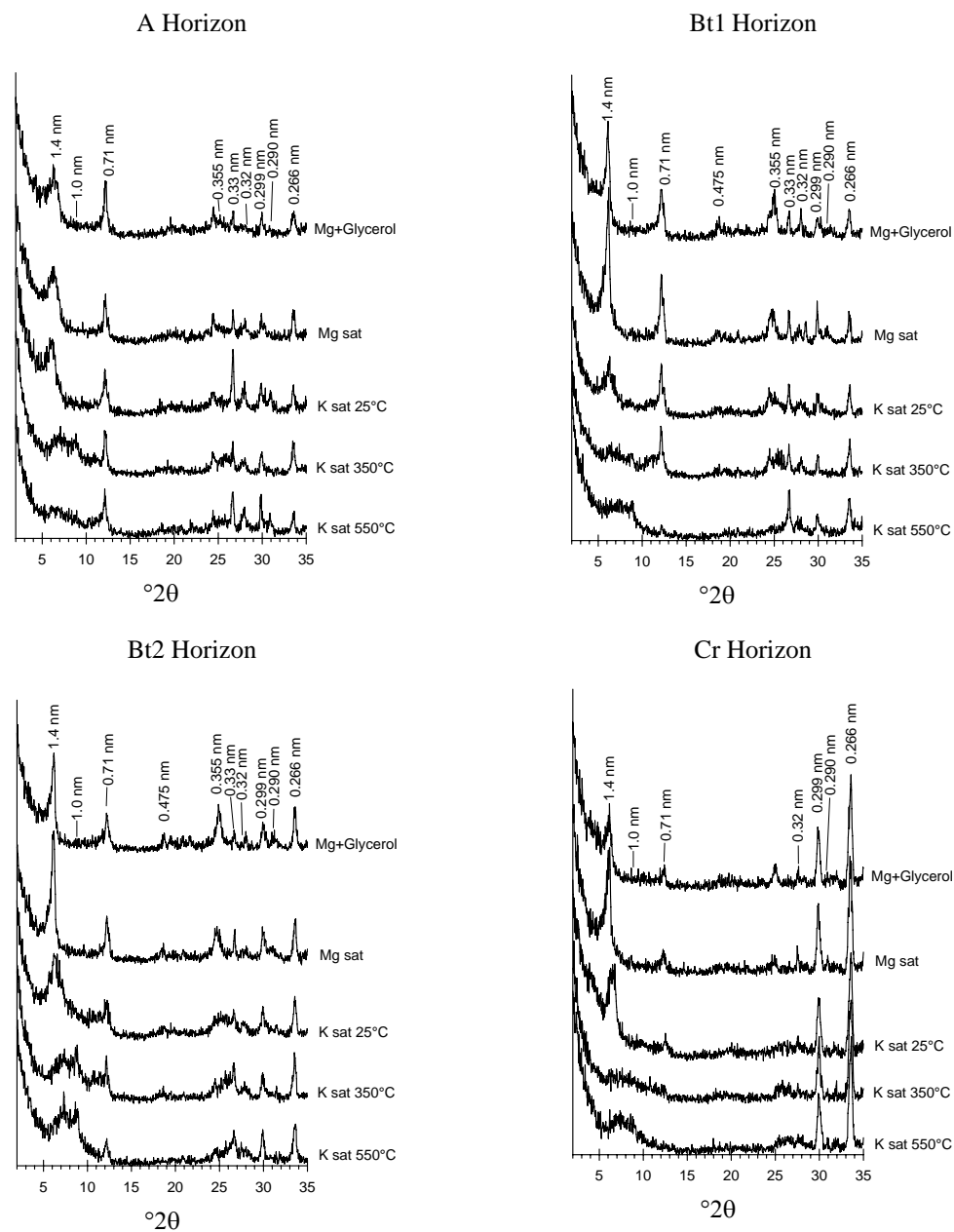


**Figure 5-4.** Tehama County Cr crushed rock and silt x-ray diffractograms. Hydroxy-interlayered-material (HIM) the 1.4 nm Mg-saturated peak that collapses incompletely to 1.0 nm with K-saturation and heating together with the reduction of a 0.355 nm (004) peak with K-saturation and heating; grossularite peaks at 0.299 & 0.266 nm; diopside 0.32 nm peak; pumpellyite 0.290 nm peak.

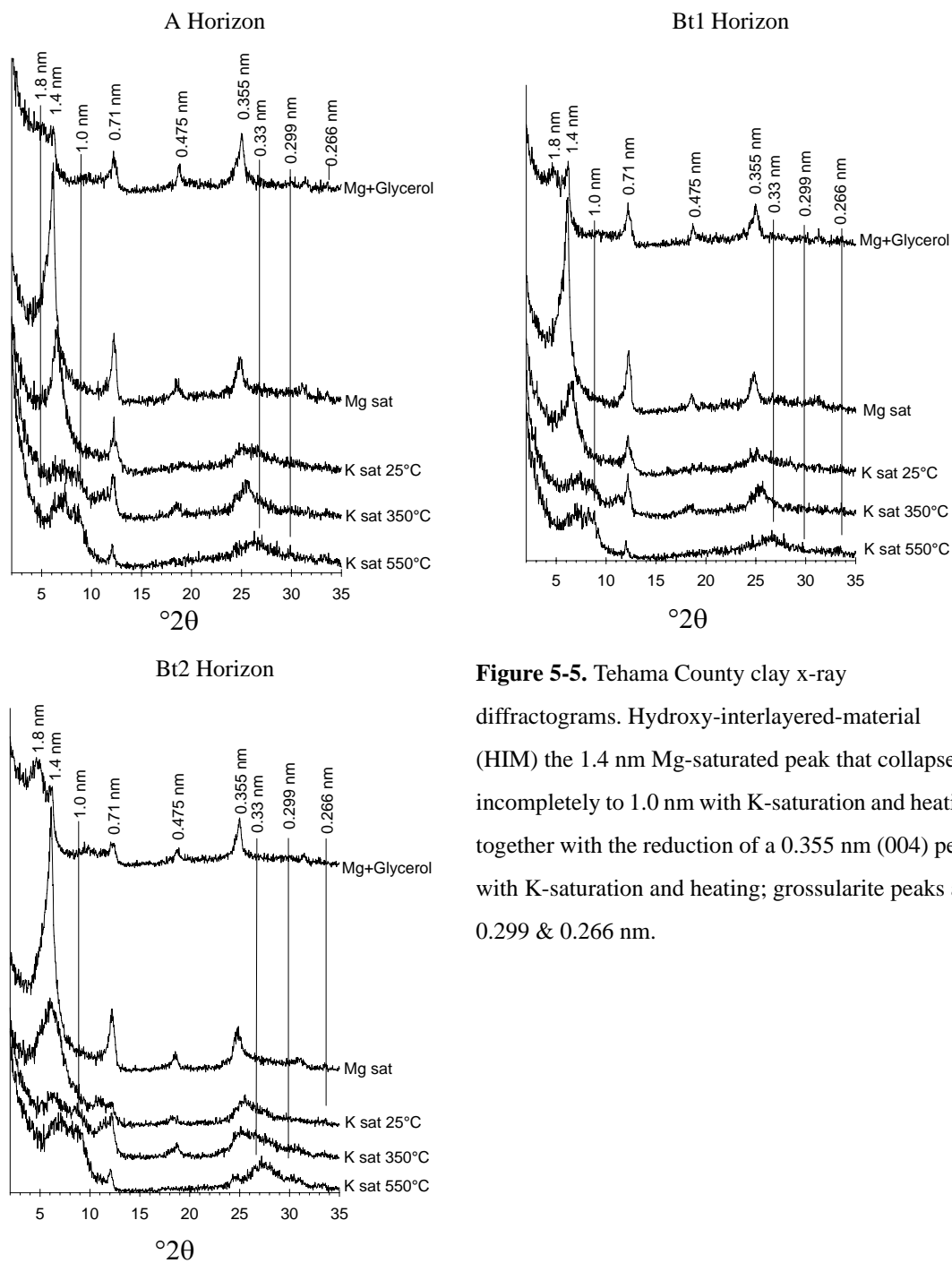


**Figure 5-5.** Tehama County clay x-ray diffractograms. Hydroxy-interlayered-material (HIM) the 1.4 nm Mg-saturated peak that collapses incompletely to 1.0 nm with K-saturation and heating together with the reduction of a 0.355 nm (004) peak with K-saturation and heating; grossularite peaks at 0.299 & 0.266 nm.

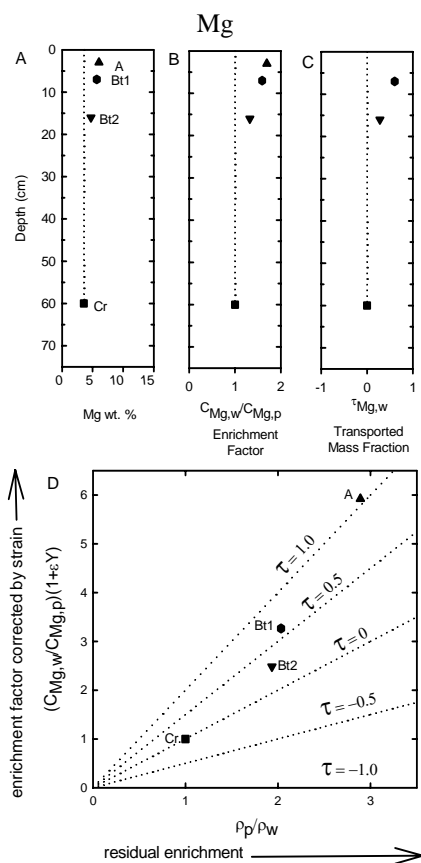


**Figure 5-6.** Mg: Tehama County depth plots of (A) weight percent (B) enrichment factor, and (C) the transported mass fraction. (D) Plot of density ratio  $\rho_p/\rho_w$  representing the residual enrichment contribution vs. enrichment corrected by strain using Y as the immobile element. Dotted vertical lines in A, B and C are visual indicator for parent material value. Sloped dotted lines, D, represent  $\tau$ , the mass fraction added or subtracted from each sample at 0, 50 and 100%

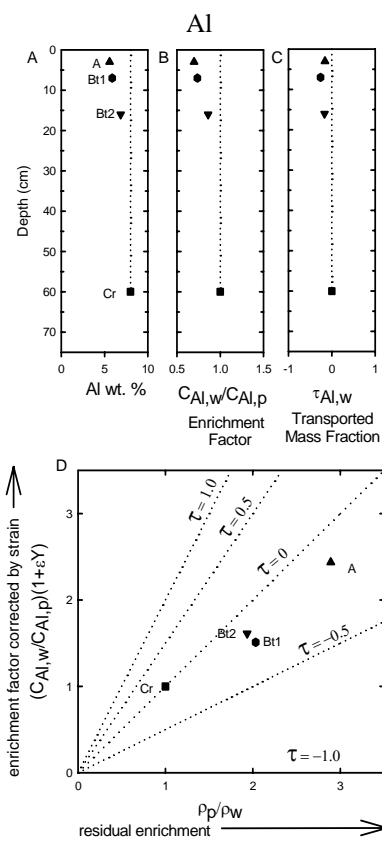


**Figure 5-7.** Al: Tehama County depth plots of (A) weight percent (B) enrichment factor, and (C) the transported mass fraction. (D) Plot of density ratio  $\rho_p/\rho_w$  representing the residual enrichment contribution vs. enrichment corrected by strain using Y as the immobile element. Dotted vertical lines in A, B and C are visual indicator for parent material value. Sloped dotted lines, D, represent  $\tau$ , the mass fraction added or subtracted from each sample at 0, 50 and 100%

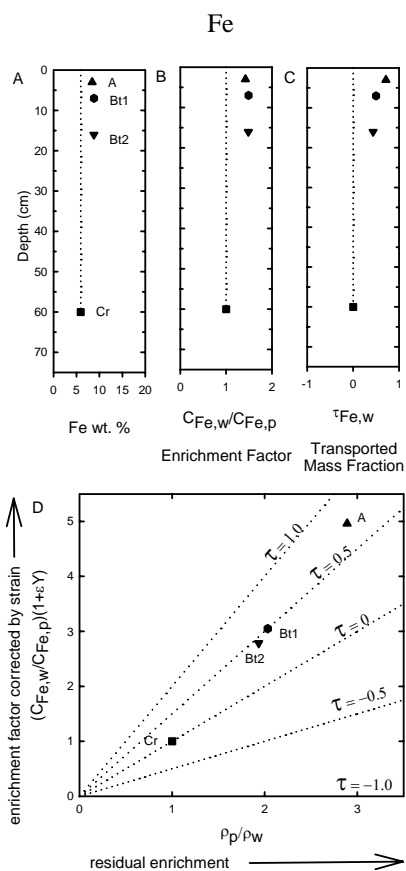


**Figure 5-8.** Fe: Tehama County depth plots of (A) weight percent (B) enrichment factor, and (C) the transported mass fraction. (D) Plot of density ratio  $\rho_p/\rho_w$  representing the residual enrichment contribution vs. enrichment corrected by strain using Y as the immobile element. Dotted vertical lines in A, B and C are visual indicator for parent material value. Sloped dotted lines, D, represent  $\tau$ , the mass fraction added or subtracted from each sample at 0, 50 and 100%.

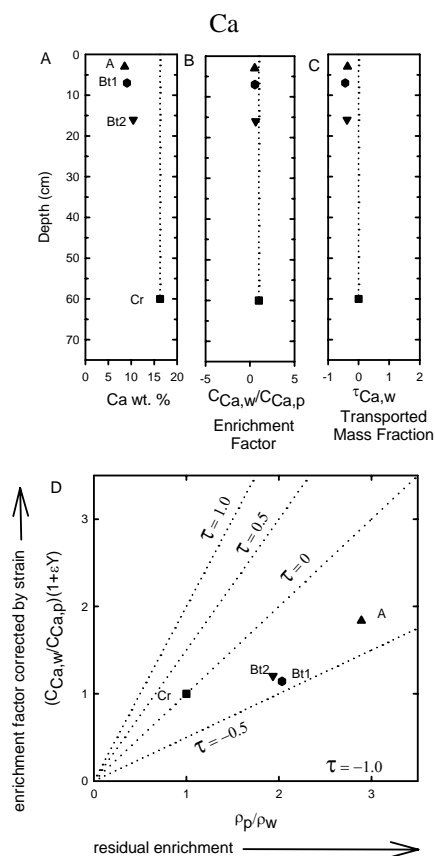


**Figure 5-9.** Ca: Tehama County depth plots of (A) weight percent (B) enrichment factor, and (C) the transported mass fraction. (D) Plot of density ratio  $\rho_p/\rho_w$  representing the residual enrichment contribution vs. enrichment corrected by strain using Y as the immobile element. Dotted vertical lines in A, B and C are visual indicator for parent material value. Sloped dotted lines, D, represent  $\tau$ , the mass fraction added or subtracted from each sample at 0, 50 and 100%.

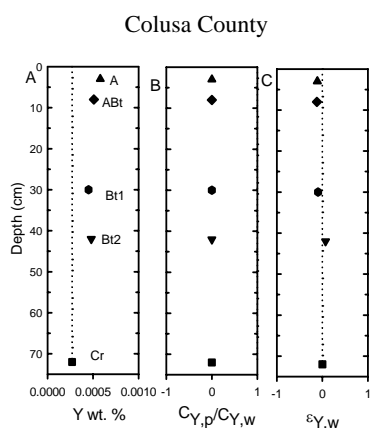


**Figure 5-10.** Colusa County depth plots (A) weight percent Y (B) the enrichment factor is the ratio of concentration Y in each horizon ( $C_{Y,w}$ ) to parent material ( $C_{Y,p}$ ). Together the weight percent and enrichment factor are used to calculate (C) strain,  $\epsilon_{Y,w}$ . Dotted vertical line is visual indicator for parent material value.

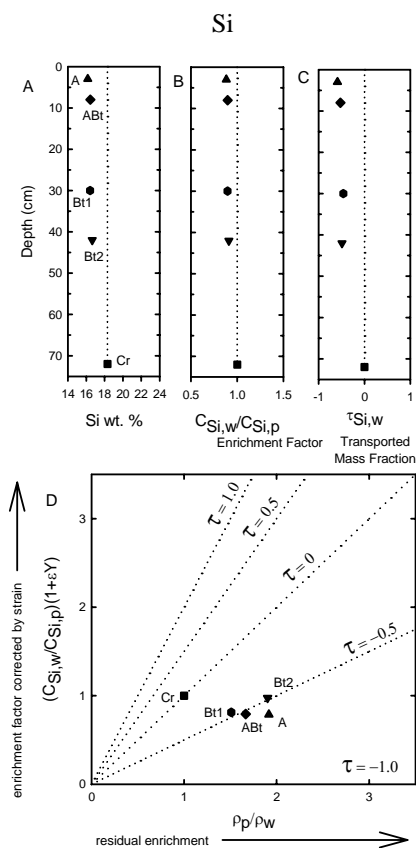


**Figure 5-11.** Si: Colusa County depth plots of (A) weight percent (B) enrichment factor, and (C) the transported mass fraction. (D) Plot of density ratio  $\rho_p/\rho_w$  representing the residual enrichment contribution vs. enrichment corrected by strain using Y as the immobile element. Dotted vertical lines in A, B and C are visual indicator for parent material value. Sloped dotted lines (D) represent  $\tau$ , the mass fraction added or subtracted from each sample at 0, 50 and 100%

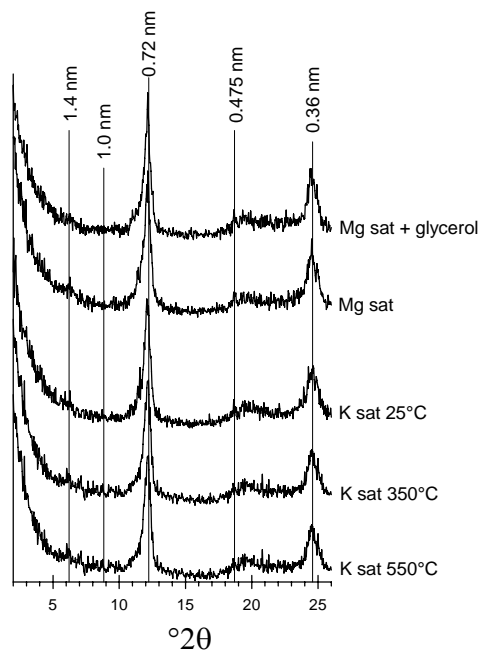


**Figure 5-12.** Colusa County Cr horizon rock x-ray diffractograms. Serpentine (0.72 nm and 0.36 nm peaks) with a minor component of chlorite (1.4 nm and 0.475 nm peaks that persist with heating and do not expand with glycerol solvation).

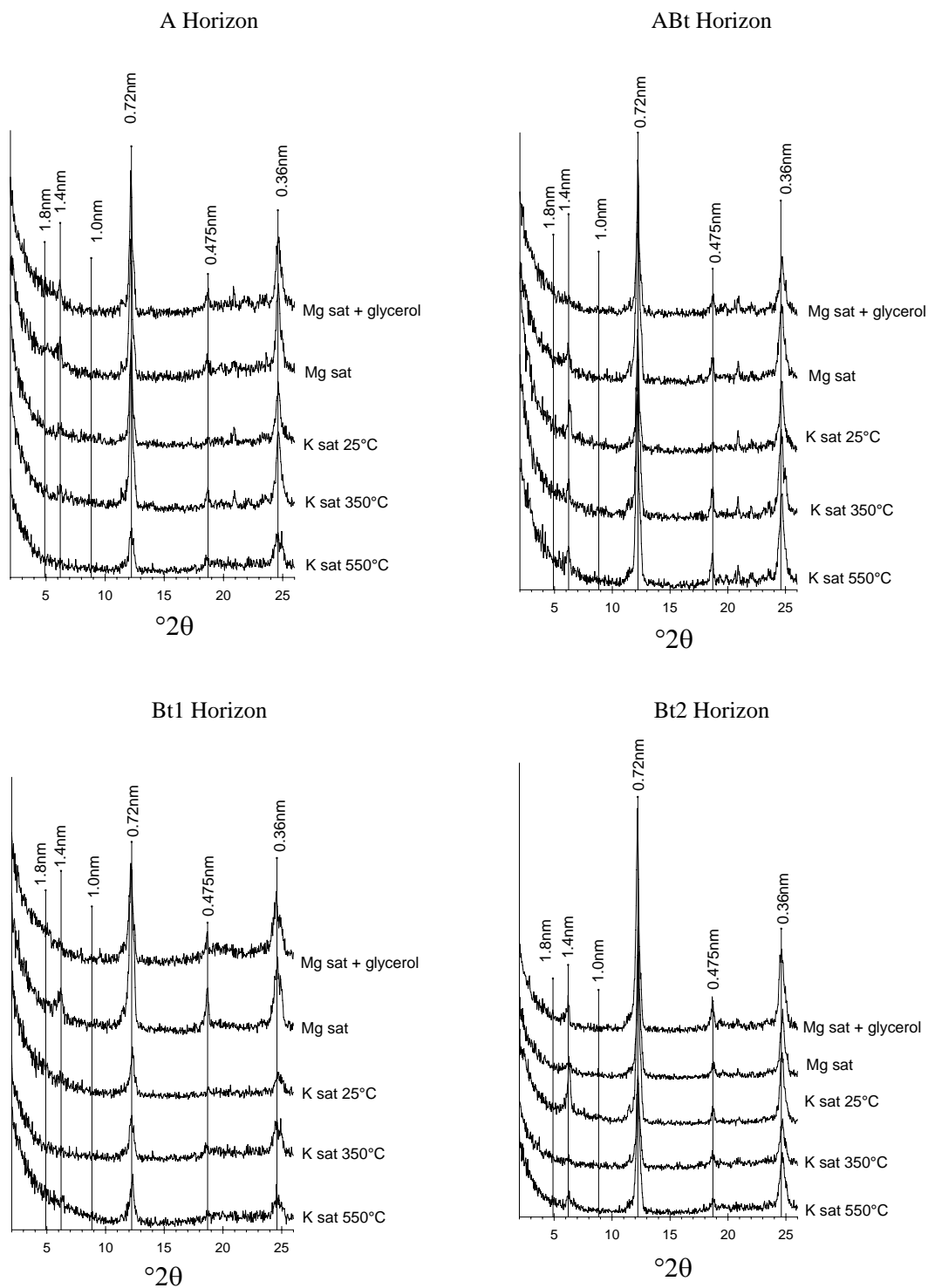


**Figure 5-13.** Colusa County silt x-ray diffractograms. Serpentine (0.72 nm and 0.36 nm peaks) with a minor component of chlorite (1.4 nm and 0.475 nm peaks that persist with heating and do not expand with glycerol solvation).

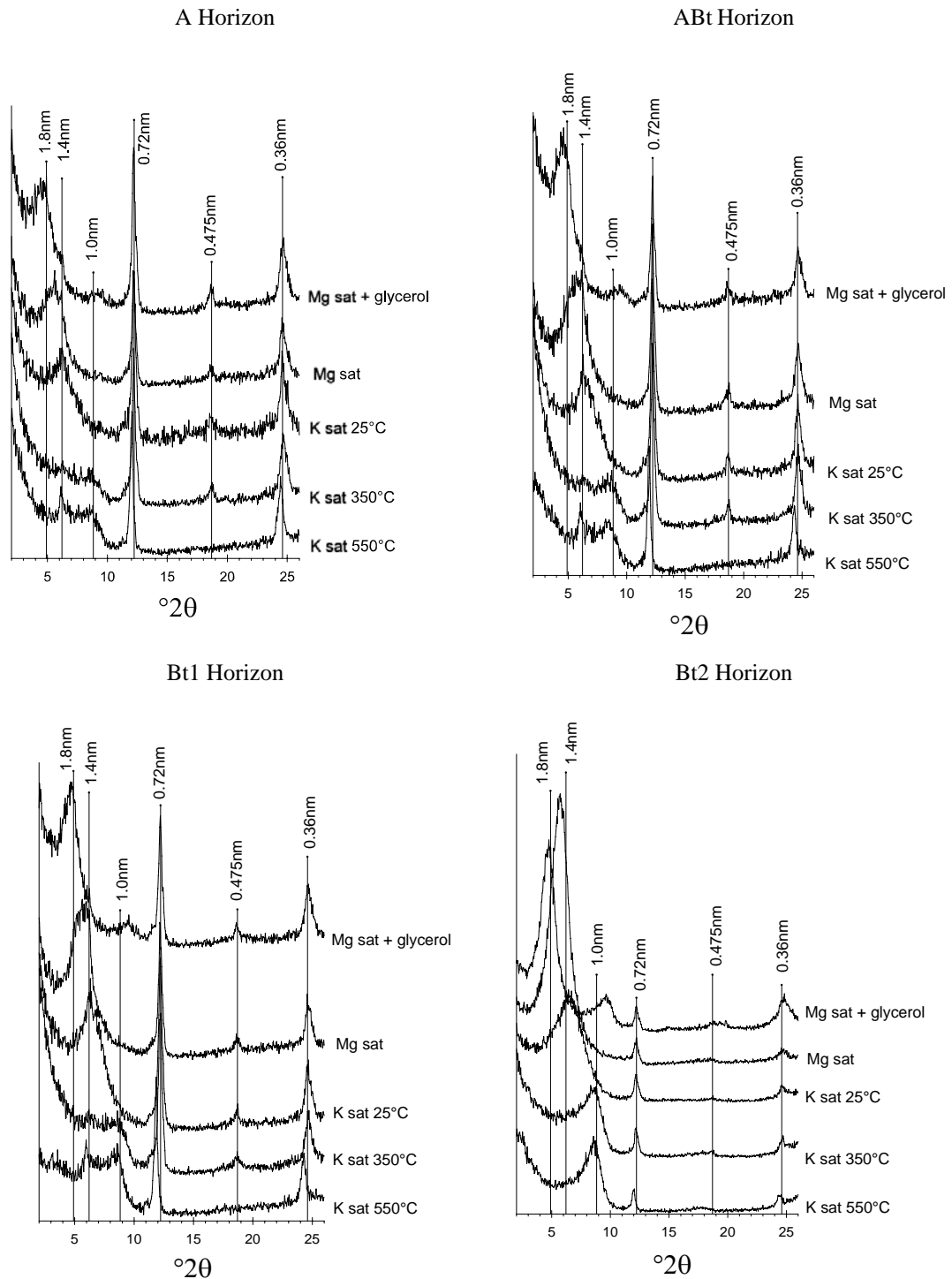


**Figure 5-14.** Colusa County clay x-ray diffractograms. Serpentine (0.72 nm and 0.36 nm peaks), chlorite (1.4 nm and 0.475 nm peaks that persist with heating and do not expand with glycerol solvation), vermiculite (1.4 nm peak that collapses to 1.0 nm with K-saturation and heating), and smectite (1.4 nm peak that expands to ~1.8 nm with Mg-saturation and glycerol solvation).



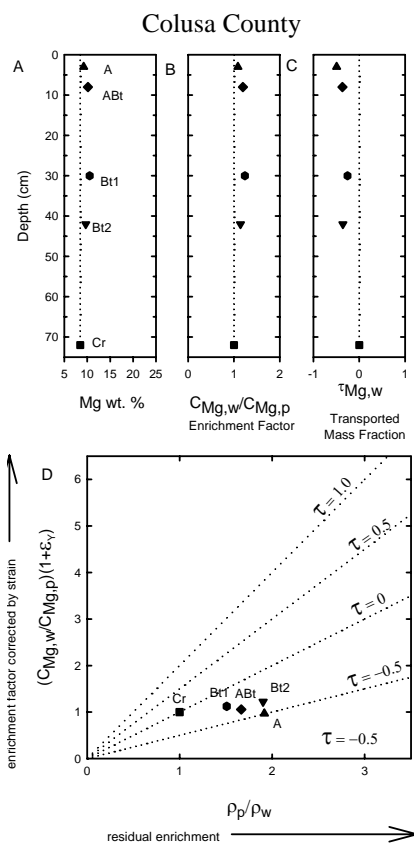


**Figure 5-15.** Mg: Colusa County depth plots of (A) weight percent (B) enrichment factor, and (C) the transported mass fraction. (D) Plot of density ratio  $\rho_p/\rho_w$  representing the residual enrichment contribution vs. enrichment corrected by strain using Y as the immobile element. Dotted vertical lines in A, B and C are visual indicator for parent material value. Sloped dotted lines, D, represent  $\tau$ , the mass fraction added or subtracted from each sample at 0, 50 and 100%.

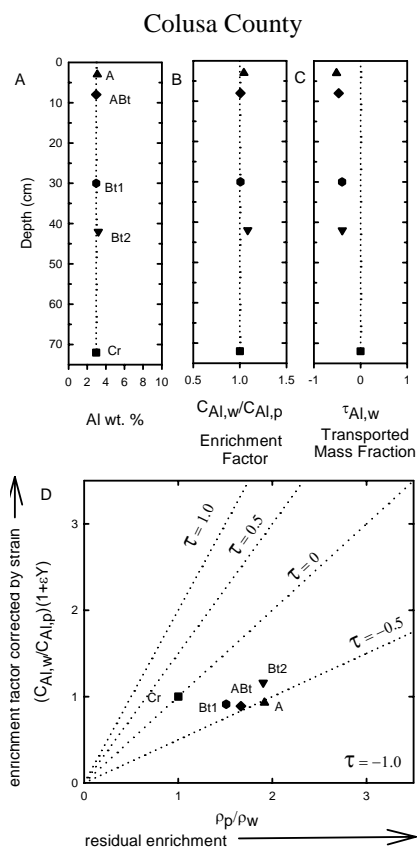


**Figure 5-16.** Al: Colusa County depth plots of (A) weight percent (B) enrichment factor, and (C) the transported mass fraction. (D) Plot of density ratio  $\rho_p/\rho_w$  representing the residual enrichment contribution vs. enrichment corrected by strain using Y as the immobile element. Dotted vertical lines in A, B and C are visual indicator for parent material value. Sloped dotted lines, D, represent  $\tau$ , the mass fraction added or subtracted from each sample at 0, 50 and 100%.

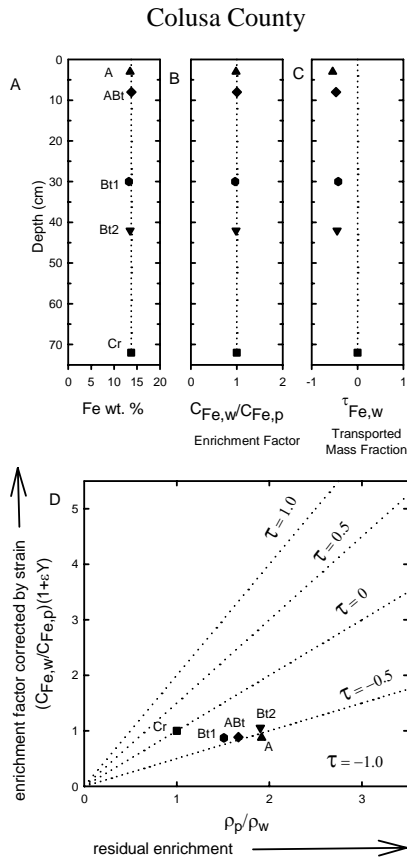


**Figure 5-17.** Fe: Colusa County depth plots of (A) weighted percent; (B) enrichment factor, and (C) the transported mass fraction (D) Plot of density ratio  $\rho_p/\rho_w$  representing the residual enrichment contribution vs. enrichment corrected by strain using Y as the immobile element. Dotted vertical lines in A, B and C are visual indicator for parent material value. Sloped dotted lines, D, represent  $\tau$ , the mass fraction added or subtracted from each sample at 0, 50 and 100%.

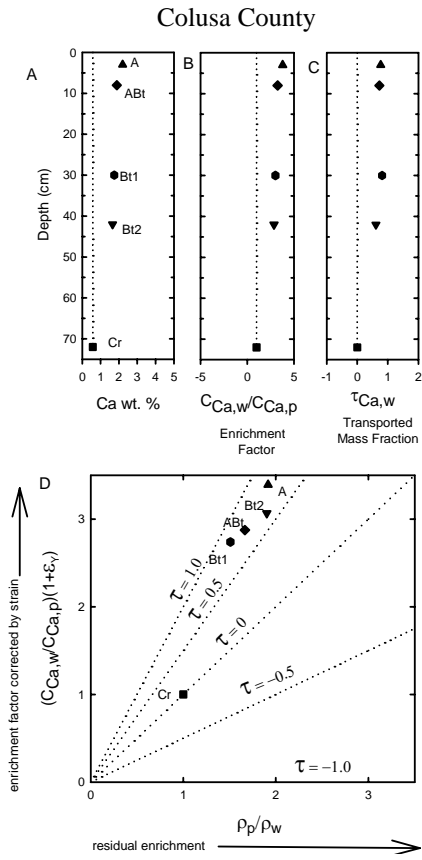


**Figure 5-18.** Ca: Colusa County depth plots of (A) weight percent (B) enrichment factor, and (C) the transported mass fraction. (D) Plot of density ratio  $\rho_p/\rho_w$  representing the residual enrichment contribution vs. enrichment corrected by strain using Y as the immobile element. Dotted vertical lines in A, B and C are visual indicator for parent material value. Sloped dotted lines, D, represent  $\tau$ , the mass fraction added or subtracted from each sample at 0, 50 and 100%.

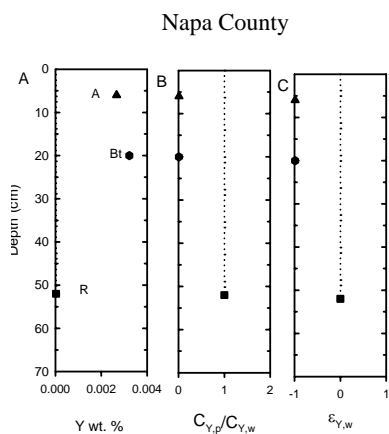


**Figure 5-19.** Napa County depth plots (A) weight percent Y (B) the enrichment factor is the ratio of concentration Y in each horizon ( $C_{Y,w}$ ) to parent material ( $C_{Y,p}$ ). Together the weight percent and enrichment factor are used to calculate (C) strain,  $\epsilon_Y$ . Dotted vertical line is visual indicator for parent material value.

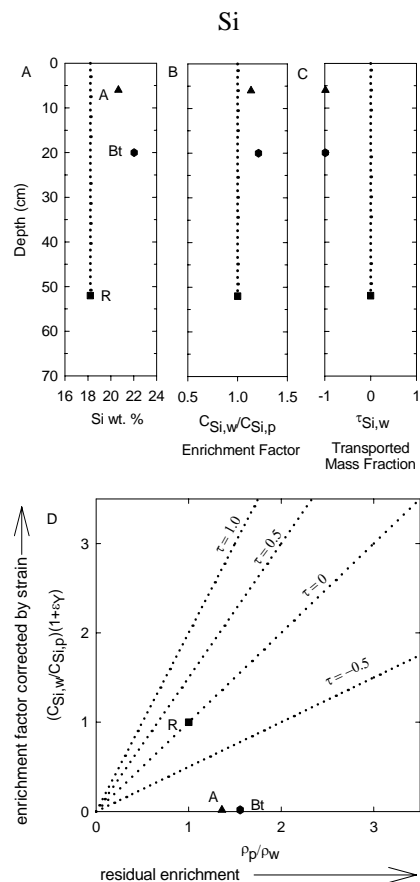


**Figure 5-20.** Si: Napa County depth plots of (A) weight percent (B) enrichment factor, and (C) the transported mass fraction. (D) Plot of density ratio  $\rho_p/\rho_w$  representing the residual enrichment contribution vs. enrichment corrected by strain using Y as the immobile element. Dotted vertical lines in A, B and C are visual indicator for parent material value. Sloped dotted lines (D) represent  $\tau$ , the mass fraction added or subtracted from each sample at 0, 50 and 100%

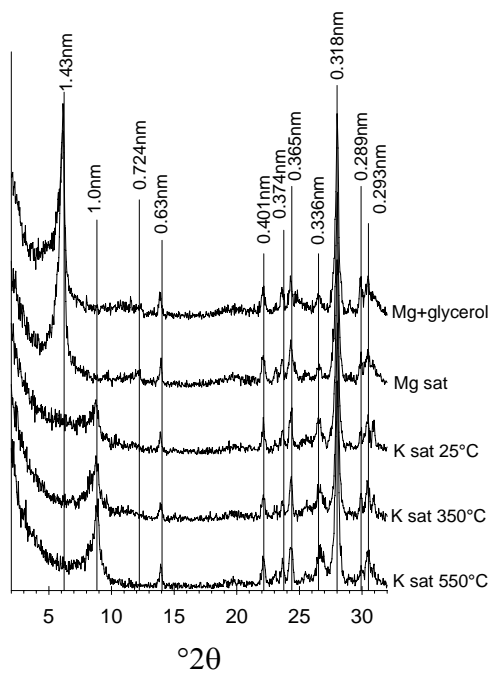


**Figure 5-21.** Napa County parent material x-ray diffractogram. Vermiculite 1.4 nm peak with Mg treatment collapsed to 1.0 nm with K-saturation treatment and heat; vermiculite peak also at 0.289. Plagioclase feldspar peaks at 0.630, 0.401, 0.374, 0.365, 0.336, 0.318, 0.293 nm.

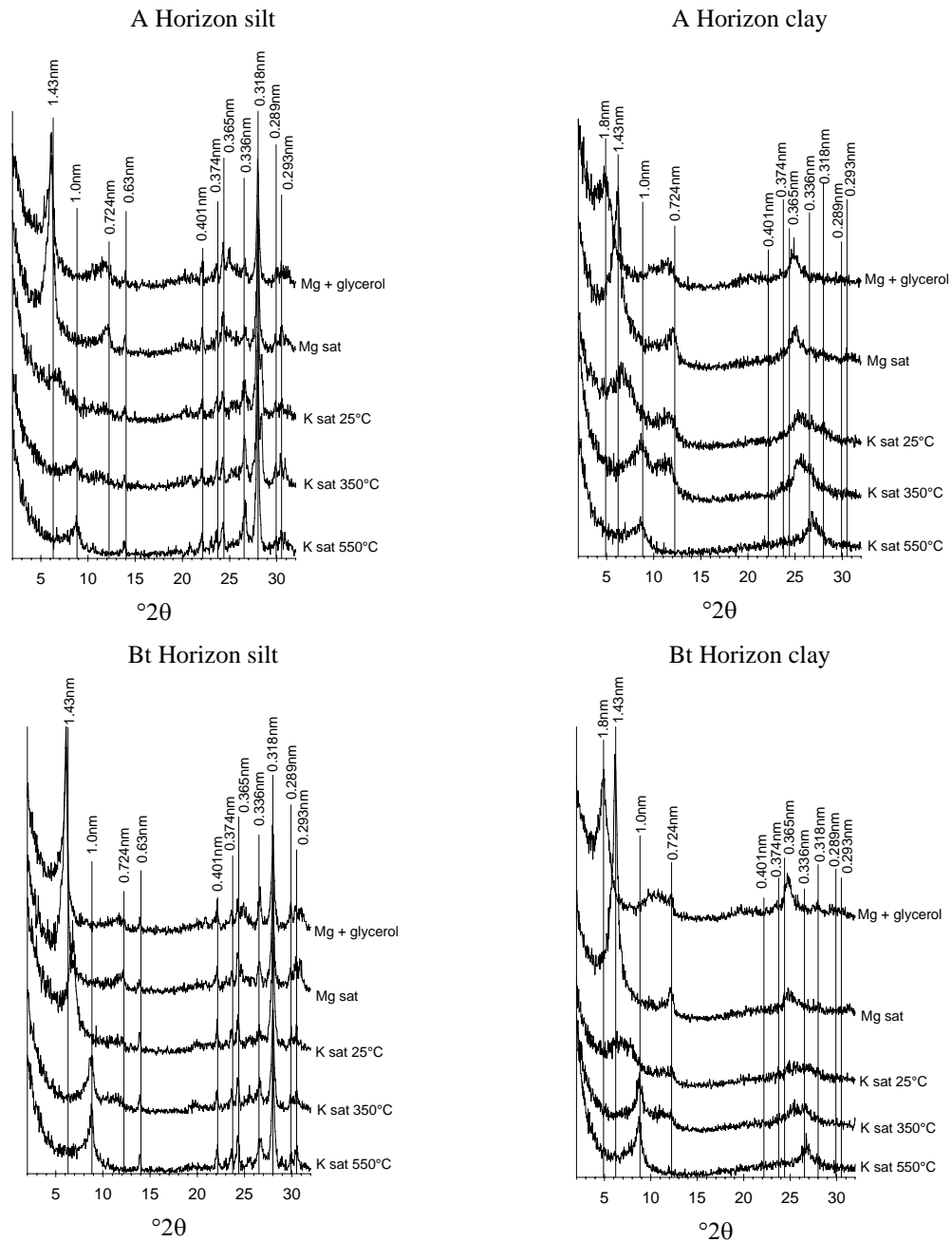


**Figure 5-22.** Napa County clay and silt x-ray diffractograms. Vermiculite 1.4 nm peak with Mg treatment collapsed to 1.0 nm with K-saturation treatment and heat; vermiculite peak also at 0.289. Plagioclase feldspar peaks at 0.630, 0.401, 0.374, 0.365, 0.336, 0.318, 0.293 nm. Clay x-ray diffractograms similar to crushed rock and silt with the addition of smectite 1.8 nm peak with Mg-treatment and glycerol solvation. Maximum peak intensity shift from vermiculite in the Bt horizon to smectite in the A horizon. Plagioclase peaks diminished respective to rock or silt fraction.

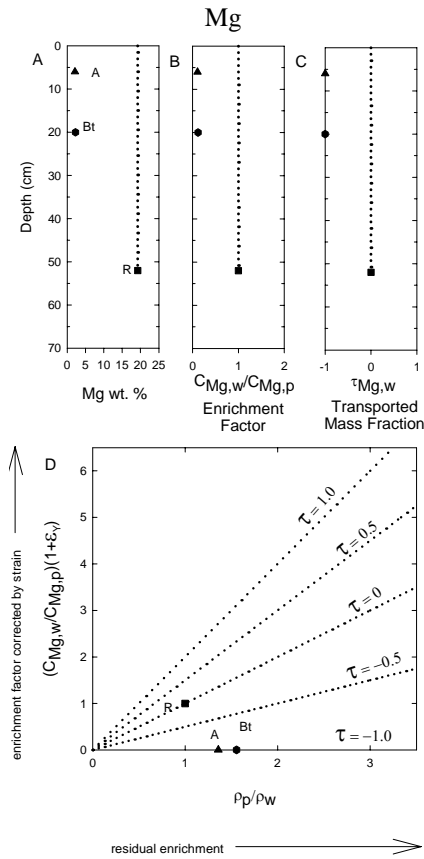


**Figure 5-23.** Mg: Napa County depth plots of (A) weight percent (B) enrichment factor, and (C) the transported mass fraction. (D) Plot of density ratio  $\rho_p/\rho_w$  representing the residual enrichment contribution vs. enrichment corrected by strain using Y as the immobile element. Dotted vertical lines in A, B and C are visual indicator for parent material value. Sloped dotted lines, D, represent  $\tau$ , the mass fraction added or subtracted from each sample at 0, 50 and 100%

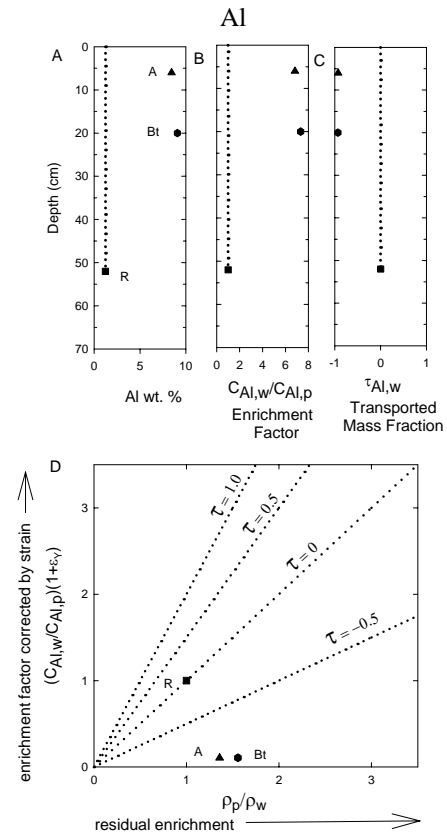


**Figure 5-24.** Al: Napa County depth plots of (A) weight percent (B) enrichment factor, and (C) the transported mass fraction. (D) Plot of density ratio  $\rho_p/\rho_w$  representing the residual enrichment contribution vs. enrichment corrected by strain using Y as the immobile element. Dotted vertical lines in A, B and C are visual indicator for parent material value. Sloped dotted lines, D, represent  $\tau$ , the mass fraction added or subtracted from each sample at 0, 50 and 100%

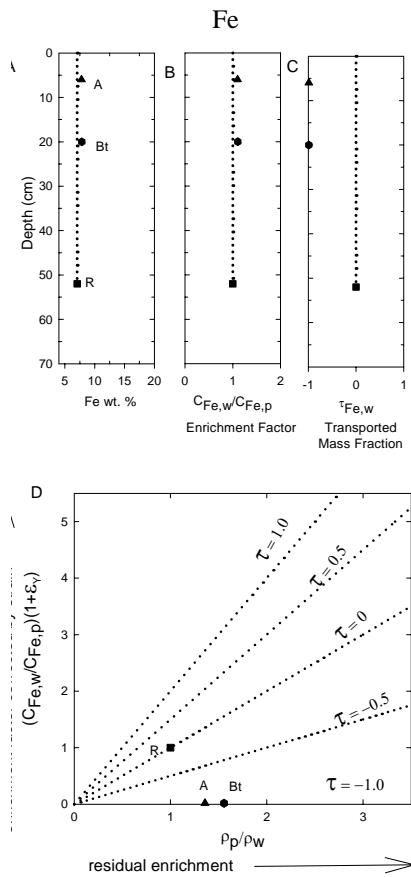


**Figure 5-25.** Fe: Napa County depth plots of (A) weight percent (B) enrichment factor, and (C) the transported mass fraction. (D) Plot of density ratio  $\rho_p/\rho_w$  representing the residual enrichment contribution vs. enrichment corrected by strain using Y as the immobile element. Dotted vertical lines in A, B and C are visual indicator for parent material value. Sloped dotted lines, D, represent  $\tau$ , the mass fraction added or subtracted from each sample at 0, 50 and 100%.

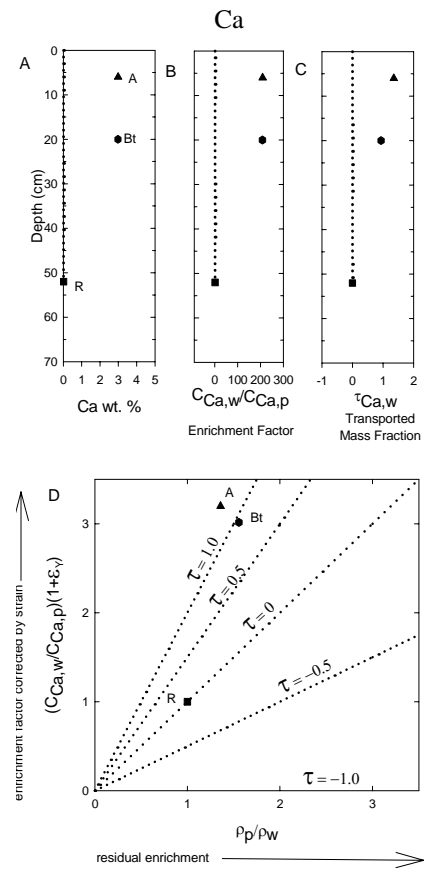


**Figure 5-26.** Ca: Napa County depth plots of (A) weight percent (B) enrichment factor, and (C) the transported mass fraction. (D) Plot of density ratio  $\rho_p/\rho_w$  representing the residual enrichment contribution vs. enrichment corrected by strain using Y as the immobile element. Dotted vertical lines in A, B and C are visual indicator for parent material value. Sloped dotted lines, D, represent  $\tau$ , the mass fraction added or subtracted from each sample at 0, 50 and 100%.

## 5.7 APPENDIX A

**Table 5-2.** Colusa, Tehama, and Napa County minor and trace element mass flux,  $m_{j,flux}$  in  $g\ cm^{-2}$  of the fine earth volume when strain is calculated with Y.

	Tehama County				Colusa County					Napa County		
	A	Bt1	Bt2	total	A	ABt	Bt1	Bt2	total	A	Bt	total
Na					0.29	0.40	1.74	1.02	3.45	0.36	0.44	0.80
K					0.01	0.01	0.04	0.02	0.07			
Ti	$-3.55 \times 10^{-4}$	-0.01	-0.02	$-2.54 \times 10^{-2}$	$3.06 \times 10^{-4}$	$6.46 \times 10^{-4}$	$7.43 \times 10^{-3}$	$2.48 \times 10^{-3}$	0.01	-0.01	-0.02	-0.04
P	$-9.42 \times 10^{-4}$	$-2.96 \times 10^{-3}$	-0.01	$-9.25 \times 10^{-3}$	$-4.20 \times 10^{-4}$	$-1.14 \times 10^{-3}$	$2.53 \times 10^{-3}$	$-2.20 \times 10^{-3}$	$-1.22 \times 10^{-3}$	$-2.78 \times 10^{-3}$	$-2.90 \times 10^{-3}$	$-5.69 \times 10^{-3}$
Mn	$3.38 \times 10^{-3}$	0.01	0.01	$1.47 \times 10^{-2}$	$-3.35 \times 10^{-3}$	$-3.96 \times 10^{-3}$	-0.01	-0.01	-0.03	-0.01	-0.01	$-1.27 \times 10^{-2}$
Cr	0.01	0.01	0.01	0.04	-0.01	-0.01	-0.04	-0.02	-0.09	$-1.55 \times 10^{-3}$	$-2.04 \times 10^{-3}$	$-3.60 \times 10^{-3}$
Ni	0.01	0.01	0.01	0.02	-0.01	-0.02	-0.06	-0.04	-0.13	$-5.67 \times 10^{-4}$	$-7.40 \times 10^{-4}$	$-1.31 \times 10^{-3}$
Sc	$1.31 \times 10^{-5}$	$1.04 \times 10^{-5}$	$-2.58 \times 10^{-5}$	$-2.34 \times 10^{-6}$	$-5.66 \times 10^{-5}$	$-6.24 \times 10^{-5}$	$-1.72 \times 10^{-4}$	$-1.55 \times 10^{-4}$	$-4.46 \times 10^{-4}$	$-2.05 \times 10^{-4}$	$-3.35 \times 10^{-4}$	$-5.40 \times 10^{-4}$
Be	$-1.64 \times 10^{-4}$	$-2.59 \times 10^{-4}$	$-4.32 \times 10^{-4}$	$-8.55 \times 10^{-4}$						0.00	$-7.46 \times 10^{-5}$	$-7.46 \times 10^{-5}$
Co	$3.55 \times 10^{-4}$	$6.34 \times 10^{-4}$	$7.50 \times 10^{-4}$	$1.74 \times 10^{-3}$	$-6.14 \times 10^{-4}$	$-8.12 \times 10^{-4}$	$-2.88 \times 10^{-3}$	$-1.71 \times 10^{-3}$	-0.01	$-2.36 \times 10^{-4}$	$-3.27 \times 10^{-4}$	$-5.63 \times 10^{-4}$
Cs					$-2.61 \times 10^{-7}$	$-7.59 \times 10^{-7}$	$1.42 \times 10^{-6}$	$1.06 \times 10^{-5}$	$1.10 \times 10^{-5}$			
Ga	$8.13 \times 10^{-6}$	$1.02 \times 10^{-5}$	$2.84 \times 10^{-5}$	$4.67 \times 10^{-5}$	$-1.98 \times 10^{-5}$	$-2.17 \times 10^{-5}$	$-9.63 \times 10^{-5}$	$-5.13 \times 10^{-5}$	$-1.89 \times 10^{-4}$	$-8.31 \times 10^{-5}$	$-1.25 \times 10^{-4}$	$-2.08 \times 10^{-4}$
Hf	$1.98 \times 10^{-6}$	$-1.56 \times 10^{-6}$	$4.23 \times 10^{-6}$	$4.65 \times 10^{-6}$								
Nb	$-8.75 \times 10^{-6}$	$-1.84 \times 10^{-5}$	$-2.35 \times 10^{-5}$	$-5.06 \times 10^{-5}$	$2.92 \times 10^{-7}$	$-6.90 \times 10^{-7}$	$3.44 \times 10^{-6}$	$0.00 \times 10+0$	$3.04 \times 10^{-6}$			
Rb					$2.04 \times 10^{-5}$	$1.53 \times 10^{-5}$	$1.24 \times 10^{-4}$	$3.28 \times 10^{-5}$	$1.93 \times 10^{-4}$	$-1.70 \times 10^{-5}$	$-1.09 \times 10^{-5}$	$-2.79 \times 10^{-5}$
Sn	$-7.35 \times 10^{-6}$	$-1.72 \times 10^{-5}$	$-2.89 \times 10^{-5}$	$-5.35 \times 10^{-5}$	$-2.81 \times 10^{-5}$	$-4.40 \times 10^{-5}$	$-1.35 \times 10^{-4}$	$-1.90 \times 10^{-5}$	$-2.26 \times 10^{-4}$	$-5.39 \times 10^{-6}$	$-1.49 \times 10^{-5}$	$-2.02 \times 10^{-5}$
Sr	$-1.62 \times 10^{-5}$	$-7.26 \times 10^{-5}$	$-1.43 \times 10^{-4}$	$-2.31 \times 10^{-4}$	$3.24 \times 10^{-4}$	$3.67 \times 10^{-4}$	$1.54 \times 10^{-3}$	$6.82 \times 10^{-4}$	$2.91 \times 10^{-3}$			
Ta	$-1.21 \times 10^{-6}$	$-8.14 \times 10^{-7}$	$-3.16 \times 10^{-6}$	$-5.19 \times 10^{-6}$								
Th	$3.57 \times 10^{-6}$	$4.39 \times 10^{-6}$	$3.83 \times 10^{-6}$	$1.18 \times 10^{-5}$	$-2.87 \times 10^{-6}$	$-3.24 \times 10^{-6}$	$-1.75 \times 10^{-5}$	$-1.06 \times 10^{-5}$	$-3.42 \times 10^{-5}$			
U	$2.56 \times 10^{-7}$	$8.89 \times 10^{-7}$	$-1.34 \times 10^{-7}$	$1.01 \times 10^{-6}$	$-3.56 \times 10^{-7}$	$-1.03 \times 10^{-6}$	$-5.80 \times 10^{-6}$	$-2.66 \times 10^{-6}$	$-9.85 \times 10^{-6}$			
V	$1.77 \times 10^{-4}$	$2.63 \times 10^{-4}$	$1.96 \times 10^{-4}$	$6.37 \times 10^{-4}$	$-1.90 \times 10^{-4}$	$-1.70 \times 10^{-4}$	$-8.28 \times 10^{-4}$	$-4.28 \times 10^{-4}$	$-1.62 \times 10^{-3}$	$-1.38 \times 10^{-3}$	$-1.86 \times 10^{-3}$	$-3.23 \times 10^{-3}$



**Table 5-2.** Colusa, Tehama, and Napa County minor and trace element mass flux,  $m_{j,flux}$ , in  $g\ cm^{-2}$  of the fine earth volume when strain is calculated with Y.

	Tehama County				Colusa County					Napa County		
	A	Bt1	Bt2	total	A	ABt	Bt1	Bt2	total	A	Bt	total
W	$-7.35 \times 10^{-7}$	$1.87 \times 10^{-8}$	$-1.34 \times 10^{-7}$	$-8.50 \times 10^{-7}$	$2.28 \times 10^{-7}$	$2.16 \times 10^{-6}$	$6.45 \times 10^{-6}$	$-6.32 \times 10^{-7}$	$8.20 \times 10^{-6}$	$-5.39 \times 10^{-7}$	0.00	$-5.39 \times 10^{-7}$
Zr	$-2.36 \times 10^{-5}$	$-6.96 \times 10^{-5}$	$-9.19 \times 10^{-5}$	$-1.85 \times 10^{-4}$	$2.49 \times 10^{-5}$	$1.46 \times 10^{-4}$	$1.79 \times 10^{-4}$	$0.00 \times 10^{+0}$	$3.50 \times 10^{-4}$	$-1.49 \times 10^{-4}$	$-2.61 \times 10^{-4}$	$-4.10 \times 10^{-4}$
La	$5.79 \times 10^{-6}$	$7.57 \times 10^{-6}$	$1.64 \times 10^{-5}$	$2.97 \times 10^{-5}$	$7.79 \times 10^{-7}$	$2.84 \times 10^{-6}$	$5.00 \times 10^{-6}$	$5.64 \times 10^{-6}$	$1.43 \times 10^{-5}$			
Ce	$-3.07 \times 10^{-6}$	$-1.40 \times 10^{-5}$	$-3.28 \times 10^{-5}$	$-4.99 \times 10^{-5}$	$1.21 \times 10^{-5}$	$1.26 \times 10^{-5}$	$6.14 \times 10^{-5}$	$3.78 \times 10^{-5}$	$1.24 \times 10^{-4}$			
Pr	$2.40 \times 10^{-7}$	$-4.83 \times 10^{-7}$	$1.34 \times 10^{-7}$	$-1.09 \times 10^{-7}$	$1.16 \times 10^{-7}$	$1.93 \times 10^{-7}$	$-1.96 \times 10^{-6}$	$1.13 \times 10^{-7}$	$-1.54 \times 10^{-6}$	$-4.72 \times 10^{-6}$	$-7.19 \times 10^{-6}$	$-1.19 \times 10^{-5}$
Nd	$9.06 \times 10^{-8}$	$1.15 \times 10^{-7}$	$-7.04 \times 10^{-6}$	$-6.83 \times 10^{-6}$	$-3.36 \times 10^{-6}$	$-4.76 \times 10^{-6}$	$-2.93 \times 10^{-5}$	$-2.06 \times 10^{-5}$	$-5.80 \times 10^{-5}$			
Sm	$-3.84 \times 10^{-7}$	$2.00 \times 10^{-6}$	$-1.87 \times 10^{-6}$	$-2.52 \times 10^{-7}$	$-2.56 \times 10^{-7}$	$-3.77 \times 10^{-7}$	$4.51 \times 10^{-6}$	$-2.21 \times 10^{-7}$	$3.66 \times 10^{-6}$			
Eu	$-5.38 \times 10^{-8}$	$8.67 \times 10^{-8}$	$-1.17 \times 10^{-6}$	$-1.14 \times 10^{-6}$	$1.91 \times 10^{-7}$	$-7.59 \times 10^{-8}$	$9.93 \times 10^{-7}$	$1.06 \times 10^{-6}$	$2.17 \times 10^{-6}$			
Gd	$-3.42 \times 10^{-7}$	$-4.13 \times 10^{-7}$	$1.02 \times 10^{-6}$	$2.61 \times 10^{-7}$	$-7.05 \times 10^{-7}$	$-8.65 \times 10^{-7}$	$9.50 \times 10^{-7}$	$5.82 \times 10^{-7}$	$-3.80 \times 10^{-8}$			
Tb	$-4.22 \times 10^{-7}$	$-1.16 \times 10^{-6}$	$-2.20 \times 10^{-6}$	$-3.78 \times 10^{-6}$	$3.52 \times 10^{-8}$	$-7.54 \times 10^{-8}$	$-1.13 \times 10^{-6}$	$-4.43 \times 10^{-8}$	$-1.21 \times 10^{-6}$			
Dy	$6.95 \times 10^{-7}$	$-3.60 \times 10^{-6}$	$-3.61 \times 10^{-6}$	$-6.52 \times 10^{-6}$	$-1.01 \times 10^{-6}$	$-1.35 \times 10^{-6}$	$-3.03 \times 10^{-6}$	$-1.06 \times 10^{-6}$	$-6.45 \times 10^{-6}$	$-2.84 \times 10^{-6}$	$-8.28 \times 10^{-6}$	$-1.11 \times 10^{-5}$
Ho	$1.60 \times 10^{-9}$	$3.23 \times 10^{-7}$	$-1.41 \times 10^{-6}$	$-1.08 \times 10^{-6}$	$1.06 \times 10^{-7}$	$4.50 \times 10^{-7}$	$1.23 \times 10^{-6}$	$1.29 \times 10^{-6}$	$3.07 \times 10^{-6}$			
Er	$4.80 \times 10^{-7}$	$9.60 \times 10^{-7}$	$-1.12 \times 10^{-6}$	$3.17 \times 10^{-7}$	$-4.06 \times 10^{-7}$	$-2.64 \times 10^{-8}$	$-1.58 \times 10^{-6}$	$-1.38 \times 10^{-6}$	$-3.39 \times 10^{-6}$	$-8.34 \times 10^{-6}$	$-1.39 \times 10^{-5}$	$-2.23 \times 10^{-5}$
Tm	$2.42 \times 10^{-7}$	$6.34 \times 10^{-7}$	$3.74 \times 10^{-7}$	$1.25 \times 10^{-6}$								
Yb	$8.91 \times 10^{-7}$	$2.24 \times 10^{-6}$	$2.50 \times 10^{-6}$	$5.63 \times 10^{-6}$	$-8.36 \times 10^{-7}$	$-1.19 \times 10^{-6}$	$-5.50 \times 10^{-6}$	$-3.97 \times 10^{-6}$	$-1.15 \times 10^{-5}$	$-9.62 \times 10^{-6}$	$-1.58 \times 10^{-5}$	$-2.54 \times 10^{-5}$
Lu	$7.62 \times 10^{-8}$	$2.85 \times 10^{-7}$	$2.45 \times 10^{-7}$	$6.06 \times 10^{-7}$	$-2.92 \times 10^{-8}$	$2.67 \times 10^{-7}$	$9.03 \times 10^{-7}$	$2.02 \times 10^{-7}$	$1.34 \times 10^{-6}$	$-1.18 \times 10^{-6}$	$-1.94 \times 10^{-6}$	$-3.12 \times 10^{-6}$
Ba	$1.81 \times 10^{-4}$	$3.31 \times 10^{-4}$	$3.45 \times 10^{-4}$	$8.56 \times 10^{-4}$	$5.83 \times 10^{-4}$	$6.17 \times 10^{-4}$	$2.70 \times 10^{-3}$	$1.05 \times 10^{-3}$	$4.95 \times 10^{-3}$	$-3.20 \times 10^{-4}$	$-3.79 \times 10^{-4}$	$-6.99 \times 10^{-4}$
Mo	$8.53 \times 10^{-8}$	$8.76 \times 10^{-7}$	$-4.45 \times 10^{-8}$	$9.17 \times 10^{-7}$	$-5.67 \times 10^{-7}$	$-6.90 \times 10^{-7}$	$-2.58 \times 10^{-6}$	$-1.77 \times 10^{-6}$	$-5.61 \times 10^{-6}$	$-5.34 \times 10^{-7}$	$-7.40 \times 10^{-7}$	$-1.27 \times 10^{-6}$
Cu	$-5.07 \times 10^{-6}$	$2.20 \times 10^{-5}$	$-6.85 \times 10^{-5}$	$-5.16 \times 10^{-5}$	$-2.91 \times 10^{-4}$	$-3.65 \times 10^{-4}$	$-5.32 \times 10^{-4}$	$-3.33 \times 10^{-4}$	$-1.52 \times 10^{-3}$	$-2.79 \times 10^{-4}$	$-3.80 \times 10^{-4}$	$-6.59 \times 10^{-4}$
Pb	$7.91 \times 10^{-5}$	$6.01 \times 10^{-5}$	$9.00 \times 10^{-6}$	$1.48 \times 10^{-4}$	$-1.09 \times 10^{-5}$	$-4.56 \times 10^{-5}$	$-7.97 \times 10^{-5}$	$-2.35 \times 10^{-5}$	$-1.60 \times 10^{-4}$	$-2.76 \times 10^{-5}$	$-1.78 \times 10^{-5}$	$-4.54 \times 10^{-5}$
Zn	$2.82 \times 10^{-5}$	$6.51 \times 10^{-5}$	$-8.55 \times 10^{-5}$	$7.87 \times 10^{-6}$	$-1.67 \times 10^{-4}$	$-2.25 \times 10^{-4}$	$-4.33 \times 10^{-4}$	$-2.78 \times 10^{-4}$	$-1.10 \times 10^{-3}$	$-3.36 \times 10^{-4}$	$-3.85 \times 10^{-4}$	$-7.22 \times 10^{-4}$
As					-0.01	-0.02	-0.06	-0.04	-0.14	$-3.72 \times 10^{-6}$	$-5.89 \times 10^{-6}$	$-9.61 \times 10^{-6}$
Cd	$1.71 \times 10^{-7}$	$1.25 \times 10^{-8}$	$-1.47 \times 10^{-6}$	$-1.29 \times 10^{-6}$	$-5.91 \times 10^{-6}$	$-7.68 \times 10^{-6}$	$-2.60 \times 10^{-5}$	$-1.97 \times 10^{-5}$	$-5.93 \times 10^{-5}$	$-1.06 \times 10^{-6}$	$-7.40 \times 10^{-7}$	$-1.80 \times 10^{-6}$
Sb					$-2.83 \times 10^{-7}$	$-3.45 \times 10^{-7}$	$6.45 \times 10^{-7}$	$-8.85 \times 10^{-7}$	$-8.69 \times 10^{-7}$			
Au	$5.23 \times 10^{-9}$	$5.28 \times 10^{-9}$	$-1.78 \times 10^{-9}$	$8.72 \times 10^{-9}$	$-4.07 \times 10^{-7}$	$-7.33 \times 10^{-7}$	$-3.22 \times 10^{-6}$	$-1.45 \times 10^{-6}$	$-5.82 \times 10^{-6}$	0.00	$-3.11 \times 10^{-8}$	$-3.11 \times 10^{-8}$

**Table 5-2.** Colusa, Tehama, and Napa County minor and trace element mass flux,  $m_{j,flux}$ , in  $g\ cm^{-2}$  of the fine earth volume when strain is calculated with Y.

	Tehama County				Colusa County					Napa County		
	A	Bt1	Bt2	total	A	ABt	Bt1	Bt2	total	A	Bt	total
Hg	$1.66 \times 10^{-7}$	$4.36 \times 10^{-7}$	$4.05 \times 10^{-7}$	$1.01 \times 10^{-6}$	$-7.28 \times 10^{-9}$	$-1.13 \times 10^{-8}$	$-3.06 \times 10^{-8}$	$-2.47 \times 10^{-8}$	$-7.39 \times 10^{-8}$	$-6.41 \times 10^{-7}$	$-4.46 \times 10^{-7}$	$-1.09 \times 10^{-6}$
Tl					$-3.70 \times 10^{-7}$	$-5.53 \times 10^{-7}$	$-1.78 \times 10^{-6}$	$-7.89 \times 10^{-7}$	$-3.49 \times 10^{-6}$			
Se	$-2.05 \times 10^{-6}$	$-4.32 \times 10^{-6}$	$-7.13 \times 10^{-6}$	$-1.35 \times 10^{-5}$								

Colusa County coarse fraction was A=0.12, ABt=0.27, Bt1=0.27, Bt2=0.16.

Tehama County coarse fraction was A=0.43, Bt1=0.10, and Bt2=0.34.

Napa County coarse fraction was A=0.12 and Bt1=0.27.

